# ABSTRACT

Title of Document:              SPATIAL MODELING AND UNIT
                                HYDROGRAPH DEVELOPMENT WITH
                                RADAR RAINFALL

                                *Stephanie Nicole Rew, Master of Science, 2009*

Directed By:                    Dr. Richard H. McCuen, Civil and
                                Environmental Engineering

Most hydrologic models use point rainfall data. Point data do not account for spatial characteristics of a storm. This research investigated the benefits of spatially- and temporally-varying rainfall data. Semivariogram analyses were made to assess the importance of the following storm characteristics: size, shape, type, and velocity. Rainfall and flow gage data from the aridlands Walnut Gulch Watershed and regional data were used. A model was developed to estimate transmission losses (TL) using hydrograph routing (temporally-varying data), then a procedure was developed to use radar rainfall data (spatially-varying data) to develop unit hydrographs (UH). Exponentially shaped UHs resulted from TLs. UHs developed from radar data agreed closely with Thiessen-averaged UHs developed from rain gage data, indicating that radar UHs better represented the overall watershed processes than a UH based on a single rain gage. Therefore, accurate UHs can be developed from radar data.

SPATIAL MODELING AND UNIT HYDROGRAPH DEVELOPMENT WITH
RADAR RAINFALL


By


Stephanie Nicole Rew


Thesis submitted to the Faculty of the Graduate School of the
University of Maryland, College Park, in partial fulfillment
of the requirements for the degree of
Master of Science
2009


Advisory Committee:
Dr. Richard H. McCuen, Chair
Dr. Kaye Brubaker
Dr. Allen Davis

# Dedication

I would like to dedicate this document to my family, for all of the love, support, and patience they have shown me, especially over the last eighteen months while I conducted this research.

# Acknowledgements

I would like to acknowledge several faculty members who have helped me along this path. First I would like to acknowledge my undergraduate advisor, Dr. Adel Shirmohammadi, and thank him for all the support and encouragement he offered me. Without him, I do not believe I would be an engineer today. I would also like to acknowledge my graduate advisor, Dr. Richard McCuen, for the help, encouragement, and advice he has given me on this research project and in general. I would also like to thank two professors in particular, Dr. Kaye Brubaker and Dr. Eric Seagren, for everything they have taught me in the last few years. Finally I would like to thank all the members of my committee for the time they have spent helping me to prepare and refine this document.

In regards to the research itself, there are also several people whose help I must gratefully acknowledge. I would like to thank the staff at the Southwest Watershed Research Center for providing data sets from the Walnut Gulch Experimental Watershed on their website, and for taking the time to answer questions when I did not understand something about the data. I would also like to thank everyone involved in the development of Hydro-NEXRAD, which made obtaining radar data for this research so easy. Special thanks go to the researchers at the University of Iowa, for all the time that they spent answering my questions about Hydro-NEXRAD and the data it provided.

# Table of Contents

# Table of Tables

# Table of Figures

# List of Abbreviations

ARS    Agricultural Research Service

C      channel routing coefficient

dBZ    decibels of radar reflectance

DEM    Digital Elevation Model

$f_c$    Horton's ultimate infiltration capacity

$f_o$    Horton's initial infiltration capacity

GIS    Geographic Information System

h      separation distance (semivariograms)

I      channel inflow

K      Horton's infiltration capacity decay coefficient

LI     lateral inflow to a stream

$L_I$    lateral inflow (used in equations)

$L_T$    transmission loss (used in equations)

O      channel outflow

pdf    probability density function

R      rainfall intensity

R      correlation coefficient

$R^2$    coefficient of determination

S      channel storage

Se/Sy  standard error ratio

STTL   Spatio-Temporal Transmission Loss model

TL     transmission losses

USDA United States Department of Agriculture

$\gamma(h)$     semivariogram

Z       radar reflectance

Z-R equation   reflectance-rainfall transformation equation or relationship

# CHAPTER 1

# INTRODUCTION

## *1.1. RESEARCH PROBLEMS IN ARIDLANDS HYDROLOGIC DESIGN*

### 1.1.1. Transmission Losses

Transmission losses are known to be a significant process in arid and semi-arid regions (Cornish, 1961; Keppel and Renard, 1962; Peebles *et al.*, 1981). Transmission losses can be defined as flow that infiltrates into the channel bed, which is thus removed from the surface floodwave. The result of transmission loss can be significant reductions in flow volume, peak flow, flow velocity, and flow rate (Jordan, 1977). In some scenarios losses may not even be noticed because the water lost is replaced by local inflow, or surface runoff from the watershed entering the channel between an upstream and a downstream flow gage.

Transmission losses are primarily a concern in arid and semi-arid regions because these streams tend to be ephemeral, flowing only in response to a rainfall event. In contrast, streams in more humid climates tend to have some baseflow constantly. The beds, banks, and floodplains of streams in arid regions are usually made up of coarse-textured alluvial material. These soils have high infiltration potential, and they tend to have very low moisture content in the time between flow events, leading to high potential for losses to infiltration (Keppel and Renard, 1962).

Hydrographs for arid and semi-arid regions also tend to have somewhat different characteristics than those for more humid regions. The typical hydrograph

1

consists of three stages: a rising limb, a peak, and then a receding limb. In arid

regions, there is typically a delay to the start of runoff due to transmission losses, then

a very rapid rise to the peak. The receding limb of a hydrograph in an arid region

also tends to be shorter than usual, which has also been attributed to transmission

losses (Peebles, 1981) that occur when the rainfall intensity drops below the

infiltration capacity of the channel bed.

## 1.1.2. Analyses That Involve Radar Rainfall

The rain gage is the traditional method for measuring rainfall. These are

placed in various locations around a region, so that rainfall can be measured at these

points. Rain gages are only capable of measuring point rainfall, so various estimation

methods must be used in order to derive regional characteristics of the rainfall.

Unfortunately, only a few rain gages are generally located within a region, resulting

in a low density rain gage network. With only a few rain gages, it can be quite

difficult to determine the spatio-temporal variation of a rainfall event over the

watershed area. Because of these challenges, many in the field of hydrology have

begun to consider either supplementing or completely replacing rain gage data with

radar data. Radar data are better able to characterize spatial variation of rainfall;

however, these data are not without their own challenges. Using both data sets, the

rain gage data and the radar data, may allow the strengths of each to decrease the

weaknesses of the other (Hoblit and Curtis, 2002).

One reason that radar data are not yet commonly used in hydrologic

applications is that the technology is still developing. While radar has been used in

many applications for a long time, the level of accuracy currently seen in weather

radar could be improved. Common sources of error include blockage of the radar beam due to ground clutter, atmospheric refraction, wind drift moving the rain drops horizontally between the time they are registered by the radar beam and the time they hit the ground, and evaporation of rain drops as they fall through the air. There is also potential for error in how the raw radar data are interpolated and analyzed to derive information about the rainfall intensity. Despite these errors, many people believe that radar data has great potential for use in hydrologic applications (Gerstner and Heinemann, 2008; Sharif *et al.*, 2004; Islam *et al.*, 2008).

### *1.1.1.1. Analysis of Spatial Data Problems Using Synthetic Data*

Synthetic data are often useful in the initial examination of research questions. Synthetic data can be designed to avoid the uncertainty that observed data are likely to include. It can be helpful to use synthetic data in an initial study to observe trends and draw conclusions. Similar studies can then be conducted using observed data to determine that the trends and conclusions identified remain true for observed data. Analyses investigating the benefit of spatial data sets are likely to be complex and the data themselves are likely to be complicated. Using synthetic data when initially addressing these questions will eliminate some of the complexity and allow preliminary conclusions to be drawn. Based on the outcome of the preliminary studies using synthetic data further studies can be conducted using real data sets to verify the preliminary findings.

### *1.1.1.2. Z-R Relationship*

A radar beam does not directly measure the rainfall intensity experienced over the watershed. Instead, the beam is reflected back off of the rain drops it encounters in the air and returned to the radar station. This reflectance measurement must be

related in some way to the rainfall amount in order to compute useful information such as the rainfall intensity (Gerstner and Heinemann, 2008). Due to many investigations, a power model equation, known as a reflectance (Z)-rainfall rate (R) equation, has been identified as the best method of transforming reflectance data (in $mm^6/m^3$) to a rainfall rate (mm/hr). The standard form of the equation is:

$$Z = AR^b \qquad\qquad\qquad (1\text{-}1)$$

where Z is reflectance ($mm^6/m^3$), R is rainfall rate (mm/hr), and *A* and *b* are coefficients.

A single, universal transformation equation has not been identified, so the choice of which equation to use can result in large errors in rainfall intensity measurements. This explains why the Z-R transformation equation is often mentioned as one of the largest sources of error in radar data. Many equations have already been developed for various climates and rainfall characteristics, but the National Weather Service has identified the following equation as being fairly widely applicable (Ulbrich and Miller, 2001):

$$Z = 300R^{1.4} \qquad\qquad\qquad (1\text{-}2)$$

It is used for most of the United States and for most rainfall types. For specific rainfall scenarios a few other equations are used by the National Weather Service. It is also possible, if radar and rain gage data are available for the same location, to calibrate a new, location specific Z-R transformation equation, if desired. The problem at this point is that the value of calibrating a Z-R relationship for a location of interest is not known.

### 1.1.3. Analysis of Factors Affecting the Semivariogram

Semivariograms are used to illustrate spatial or temporal variance in a dataset. They have been commonly used in hydrologic modeling applications as input to the kriging method, which is a method that can be used to predict rainfall for areas in which data are not present (Cheng *et al.*, 2007). Semivariograms are represented using the notation $\gamma(h)$, where h is a given separation distance, which is related to the size of the grid used in the calculations. Though using a regular grid is advantageous in calculating semivariograms, it is not absolutely necessary. The value of $\gamma(h)$ is typically plotted against h, with two characteristics influencing the shape of this plot. The first characteristic, the radius of influence, is the separation distance (h) at which point the semivariogram plot approaches a constant value. The second characteristic, the sill, is the portion of the semivariogram where $\gamma(h)$ is approximately equal to the sample variance (Hromadka *et al.*, 1993).

Rain gage data can be used to compute semivariograms; however, rain gages are rarely found in a grid pattern, and they are rarely found in sufficiently high densities in a given region to compute accurate values of the sill and radius of influence. These factors can make calculating semivariograms somewhat challenging, so another method of calculating semivariograms in order to make rainfall predictions could be desirable. One possible source of input data to be considered would be radar data. Radar data would provide more accurate spatial information about rainfall and would not face the problem of a low density of measurements over a watershed of interest. The objective of this research was to determine the effect that various storm characteristics would have on the calculated semivariogram.

5

### 1.1.4. Rain Gage Density Analyses

Rain gages are the traditional method of measuring rainfall. An individual rain gage measures rainfall at a specific point, thus the term point rainfall is used to describe these measurements. Many possible factors can cause a rain gage to incorrectly measure rainfall, including wind drift, blockage by trees or other structures located near the gage, and mechanical failure, among others. However, a major problem with rain gage measurements is that they often fail to reflect the spatial variability of rainfall. The accuracy of watershed-wide rainfall estimates derived from rain gages will depend on both the number of rain gages located within the watershed and also on their specific locations relative to each other. Larger numbers of rain gages within a watershed will better indicate spatial variations in the rainfall, and they will reduce the effect of inaccurate measurements due to an individual rain gage. The location of the rain gages relative to each other is equally important. A high number of rain gages clustered very close together in a large watershed will not provide a good indication of spatial variations in rainfall, whereas a network of gages spaced out across the entire watershed will provide a good understanding of any spatial characteristics of the rainfall (Sieck *et al.*, 2007).

### 1.1.5. Unit Hydrograph Analyses: Point vs. Spatial Rainfall Input Data

Unit hydrographs are frequently used tools in hydrologic analysis and design. A unit hydrograph can be defined as a hydrograph that results from exactly one inch of precipitation excess falling uniformly over a watershed during a specific time interval. The ultimate purpose of the unit hydrograph is to transform precipitation excess into direct runoff. The first step to deriving a unit hydrograph is to separate

losses.  Losses needed to be separated from runoff to obtain direct runoff, while initial

abstraction and losses need to be separated from precipitation to obtain precipitation

excess.  Two methods are commonly used to derive unit hydrographs.  The more

simple method, known as the rainfall-excess reciprocal method, divides each ordinate

of the direct runoff by the reciprocal of the precipitation excess in order to obtain the

ordinates of the unit hydrograph.  This ensures that the unit hydrograph ordinates will

sum to one.  The second option, known as the least squares analysis, is a regression

analysis that uses the precipitation excess and direct runoff to determine the optimum

values of unit hydrograph parameters.  A specific distribution must be assumed for

the unit hydrograph in order to use this method (McCuen, 2005).

Unit hydrographs are typically used in design to predict the watershed

response to a given storm event, e.g., the likely runoff that a hydrological design

would need to be able to accommodate.  The procedure is to calculate a unit

hydrograph and then convolve that with a particular design storm.  Convolution is a

mathematical operation that involves multiplication, translation, and then addition,

resulting in the ordinates of the direct runoff.  This provides information about the

runoff that would result from a given storm, which can then be used to properly size a

hydrologic design (McCuen, 2005).

Precipitation information is usually obtained from rain gages in deriving unit

hydrographs.  Unfortunately, rain gages can not often provide information about the

spatial characteristics of rainfall due to the fact that dense rain gage networks are rare,

so the ability to provide rainfall information from an alternate source could improve

the unit hydrograph derivation procedure.  The ideal choice would be radar data

because most of the United States falls within the coverage area of a radar station, and because it can easily provide more spatial information about rainfall.

## *1.2. GOALS AND OBJECTIVES*

### 1.2.1. Transmission Losses

Given the potential effect of transmission losses on the characteristics of a runoff hydrograph, channel characteristics might be a significant factor in the response of an aridlands watershed. As a unit hydrograph is used to reflect a watershed response, the effect of transmission losses on unit hydrographs is currently a need for hydrologic analysis and design in aridlands. One objective of this research was to develop a method to estimate transmission losses along a channel using a hydrograph method, rather than the typical flow volume reduction method (Lane *et al.*, 2007). Transmission losses must account for infiltration as a flow hydrograph is routed downstream.

### 1.2.2. Analyses Involving Radar Rainfall

The possibility of using radar rainfall data in hydrologic applications is still a fairly new idea that has not yet been thoroughly investigated. Synthetic data sets can be used to investigate the limitations of point rainfall data. With respect to this aspect of the research two objectives were addressed. First, the abilities of two averaging methods, the Thiessen polygon and the arithmetic averaging methods, to make regional rainfall estimates based on point rainfall data are investigated. Second, regional rainfall estimates derived using these averaging methods based on point data will be compared to a known, synthetic rainfall surface. This will illustrate the

failings of point rainfall data and provide evidence that adapting hydrologic models to use spatial rainfall is beneficial.

The most readily available spatial data set that could be used in hydrologic applications is radar data. After studies using synthetic data have provided evidence that spatial data could be beneficial to hydrologic application, studies investigating the potential of radar data to serve as input to hydrologic models should be studied. Since semivariograms are often used to estimate rainfall when point rainfall data are lacking, the possibility of using radar data as an input should be evaluated. In doing this, the effect of varying Z-R transformation equations could also be investigated. The objective of this research is to determine whether radar data could be used instead of rain gage data in calculating storm semivariograms, and to investigate the effect of varying the coefficients of the Z-R transformation equation. A final objective involving radar rainfall data is to assess the potential benefits of calibrating location-specific Z-R transformation equations. Typically the National Weather Service's standard equation is used; however, calibrating equations for a specific location or storm type could improve the accuracy of the rainfall predictions made using the radar data.

### 1.2.3. Analysis of Factors Affecting the Semivariogram

In order to demonstrate that spatial data are beneficial to hydrologic applications, it is necessary to address the limitations of point data. As previously mentioned, semivariograms are often used to interpolate rainfall when point data are not available. The objective of this part of the study was to investigate the factors that influence the calculation of a storm semivariogram and to determine which of

9

those factors have the most significant influence.  Four factors to be investigated are the shape, size, and velocity of the storm, and the storm type (peaked vs. uniform).

### 1.2.4. Rain Gage Density Analyses

One of the most serious limitations to rain gage density is the lack of high-density rain gage networks.  Semivariograms are used to predict rainfall when point data are not available for an area, but the accuracy of semivariograms based on a low-density rain gage network must be called into question.  The objective of this study is to investigate the effect of varying rain gage network densities on the calculation of a storm semivariogram.

Semivariograms are not the only hydrologic application that could be influenced by rain gage density.  Rain gage data can be used to make regional estimates of rainfall amounts using several averaging methods.  This study will investigate the effect that rain gage density has on the accuracy of regional rainfall estimates.

### 1.2.5. Unit Hydrograph Analyses: Point vs. Spatial Rainfall Input Data

Unit hydrographs are frequently used tools in hydrologic applications, but they are usually derived from rain gage measurements taken at a single rain gage.  As the purpose of the unit hydrograph is to predict the watershed response to a given storm event, it would seem that spatial data could be of great benefit in the unit hydrograph procedure.  Several topics related to the unit hydrograph procedure need to be investigated.  First, the limitations of point data in the unit hydrograph procedure must be evaluated.  The variation of unit hydrographs derived based on different rain gage hyetographs within the same area of the watershed should be

investigated.  A similar investigation should evaluate the level of variation present in

unit hydrographs derived based on rain gages located in different subareas of the

watershed.  Second, the ability of radar rainfall data to produce accurate unit

hydrographs should be investigated.  Finally, the impact of unit hydrograph variation

based on rainfall input on design calculations using the unit hydrograph should be

assessed.  The true level of significance of variations in unit hydrographs based on the

rainfall input used in the derivation process depends on the level of variation that

would exist in design calculations based on the unit hydrographs.

### 1.2.6. Summary of Research Objectives

- The overall goal of this research was to demonstrate the value of radar rainfall data to hydrologic applications

- The research objectives included:

    o Develop a channel routing-based transmission loss estimation method

    o Determine the benefit of calibrated radar-rainfall relationships

    o Evaluate storm factors influencing the calculated semivariogram

    o Evaluate the impact of rain gage density on regional rainfall estimates

    o Determine the benefit of using radar rainfall as input to unit hydrograph procedure

# CHAPTER 2

# LITERATURE REVIEW

## *2.1. TRANSMISSION LOSSES*

### 2.1.1. Infiltration

Infiltration has been found to be one of the most important hydrological processes in arid regions. Because many people have chosen to model transmission losses as infiltration losses the process of infiltration warrants further study. McCuen *et al*. (1981) examined possible methods for determining parameters for both the Green-Ampt infiltration equation and the Brooks-Corey procedure. Both of these equations are commonly used in determining infiltration losses; however, both require values for parameters that can be difficult to determine in areas where soil parameter measurements are not available. The main interest in this study was determining whether or not any trend existed in these parameters based on soil texture classes. This study determined that the parameters for these infiltration models do vary across the soil texture classes (McCuen *et al*., 1981).

Haws *et al*. (2004) also studied infiltration parameters, though this study focused on determining representative rates for field-scale rates. Determining these values can be difficult because soil can be extremely variable in the field. To determine these parameters steady-state infiltration was measured at a local scale, a hillslope scale, and a landscape scale. Data analyzed by geostatistical methods indicated that the sample variance decreased and the spatial correlation of infiltration

rates increased with depth. This study also showed that the typical infiltrometer ring method of measuring infiltration may not be sufficient to capture the spatial variability of infiltration properties (Haws *et al*., 2004).

Meadows *et al*. (2005) noted that typical methods of measuring infiltration properties in the lab tend to destroy the structure of the soil samples, which limits the ability to truly determine the infiltration properties. Also, most field methods produce average values, and do not fully capture the spatial variation within the field. In order to correct these problems, Meadows *et al*. developed a procedure that could determine the unsaturated hydraulic properties of a soil sample. The methods used in the laboratory under this procedure were then compared to infiltration tests conducted in the field. The laboratory methods developed were found to agree reasonably well with the field tests, with some differences possibly due to errors introduced in the field (Meadows *et al*., 2005).

Along with the Green-Ampt infiltration equation, Horton's infiltration equation is commonly used to model infiltration. Horton's equation states that:

$$f = f_c + (f_o - f_c)e^{-Kt} \tag{2-1}$$

In equation 2-1 f represents the infiltration capacity, $f_c$ represents the infiltration capacity of the soil after an extended wetting period, $f_o$ represents the initial infiltration capacity, K is a constant related to the decay of infiltration rate with time, which can be related to soil cover, and t represents time. This equation is most often used to construct infiltration-capacity curves for storm events, which are then used to determine rainfall excesses and losses. The parameters of this equation are a function

of surface texture and cover and both the initial and the ultimate infiltration capacities tend to be higher for sandy soils than other soil types (McCuen, 2005).

Horton's equation as presented above only applies when the rainfall excess is greater than the infiltration capacity, as the infiltration capacity then decreases at maximum capacity. However, when the rainfall excess is less than the infiltration capacity, the decrease in capacity occurs at a different rate. To determine this rate the mass-infiltration method can be used. The equation for this method is:

$$F = f_c t + \frac{(f_o - f_c)}{K}(1 - e^{-Kt})$$ (2-2)

In equation 2-2 F represents the total mass of water infiltrated at time t, and the rest of the parameters were explained with Horton's equation (2-1). This equation can be used to generate a mass-infiltration curve. The infiltration capacity (f) can be computed for any value of F from the mass infiltration curve. The infiltrated volume F, assumed to be equal to the total rainfall volume up to some point in time t, can be computed when the rainfall volume is less than infiltration capacity, and then the infiltration capacity itself can be calculated (McCuen, 2005).

## 2.1.2. Sealing of the Surface Soil

A common problem in arid environments is soil crusting or sealing, in which the top layer of soil has a greater density and shear strength than the lower soil layers, as well as finer pores and lower hydraulic conductivity. This surface seal can impact the ability of the soil to infiltrate water, which has already been declared to be a major hydrologic process in these climates. Carmi and Berliner (2008) studied the factors that influence the generation of runoff under natural rain conditions. The factors that were considered in the study were permeability of the crust, the roughness of the

14

crust, the soil salt content, and the time between rain events. Two treatments were evaluated, in the first treatment a crust built up over a long period of time, while the second treatment involved a complete destruction of any crust prior to the start of the experiment. The effects caused by the differences in treatment were evident only for the first two rainfall events, and thereafter did not cause differences in runoff generation. Roughness was shown to increase more markedly on plots that initially had a crust destroyed than the plots on which a long-term crust had developed. For most of the plots runoff was found to be similar between the two treatments; however, a few of the plots that had their crusts destroyed exhibited much higher runoff than the others. The results of this study indicated that the saturated hydraulic conductivity of the upper soil layer was not related to the generation of runoff from the plot. Results also showed a greater correlation between runoff and rainfall intensity as the time between rainfall events decreased (Carmi and Berliner, 2008).

Ben-Hur and Lado (2008) also evaluated the effect of soil surface sealing on infiltration rates. The interest of this study was in wetting conditions that would be experienced in the field, while many previous studies had focused on fast (and in some cases unrealistic) wetting conditions. The effects of various initial wetting conditions were therefore evaluated, along with interactions between the initial wetting condition and the formation of surface seals, infiltration rate, runoff, and soil loss. It was found that increases in soil wetting increased aggregate disaggregation, which increased seal formation, runoff, and soil loss. It was also seen that higher clay content made soil aggregates stronger and thus led to lower seal formation, runoff,

and soil loss. Also, the wetting rate was seen to be more influential to soil loss than to runoff generation (Ben-Hur and Lado, 2008).

## 2.1.3. Accounting for Transmission Loss by Volume Loss

Much of the research conducted into transmission losses so far has focused on accounting only for the loss in volume of flow, and in some cases accounting for the reduction in peak flow. Several of these papers are presented in the discussion below. Keppel and Renard (1962) measured transmission losses in two streams located in Walnut Gulch, the experimental watershed located near Tucson, Arizona. They provided a description of the observations made in the arid climate of Arizona to aid researchers as they began to understand the importance of transmission losses. Keppel and Renard found that a shorter rise time was common in the downstream hydrograph compared to the upstream hydrograph, and that the volume of runoff measured at the downstream station was often much less than that at the upstream station (Keppel and Renard, 1962).

Jordan (1977) recognized the importance that a comprehensive understanding of transmission losses could have to all types of hydrologic modeling, and attempted to develop general relations that could be used to estimate transmission losses when little observed data were available. He calculated the volume of flow at upstream and downstream gaging stations from discharge records when flow was known to be due mainly to surface flow. Ultimately Jordan was able to develop an equation to calculate volume loss over the length of a stream section and also an equation to predict volume loss in the first mile of that stream section. He believed that the

second equation would be more useful in comparing transmission losses between different events and streams (Jordan, 1977).

Walters (1990) noted that most of the research into transmission losses had been applied to arid regions in the United States and developed regression equations that could be applied to transmission losses in Saudi Arabia. He based his work on that of Jordan (1977); developing several equations that could be used to estimate transmission losses, one of which estimated losses only for the first mile of the stream, allowing for better comparison between different streams. He also took into account the influence that antecedent moisture could have on the infiltration process responsible for transmission losses, which had not previously been examined in detail (Walters, 1990).

The 2007 edition of the National Engineering Handbook included a chapter on transmission losses. The methods were developed to account for transmission losses both when measured flow data were and were not available. These methods allow prediction equations for outflow volume to be developed given a set of observed data, and they allow prediction equations for peak flow rate to be developed. Stated disadvantages to this method include a lack of hydrograph routing, no consideration of attenuation due to storage, and no consideration for the influence of antecedent moisture condition (Lane *et al.*, 2007).

## 2.1.4. Accounting for Transmission Loss by Hydrograph Routing

As discussed above, the majority of research into transmission losses has focused on accounting for transmission losses on a volume basis, rather than accounting for the losses as the flow is routed through the channel. There have been

a few studies focusing on accounting for losses through the duration of the routing procedure. Cornish (1961) acknowledged that classical routing methods could not be used in arid climates due to the assumption in those methods of constant flow volume. Cornish studied and reported on the characteristics and properties of flow in a channel that were revealed by inflow and outflow hydrographs for a channel subject to transmission losses. After studying these characteristics and properties, he was able to develop a technique for channel routing that could be used for river forecasting. Two routing methods were studied, a Verdigris-routing method and a modified Kohler routing method. Both methods were found to give acceptable and similar results, though the Kohler method was noted to be the faster, simpler method. Cornish concluded this study by providing an example calculation proving that the channel bed material was capable of absorbing the volume of water found to have been lost in the observed flow records (Cornish, 1961).

Moench *et al*. (1974) used a convolution integral that was already accepted to represent the interactions between a stream and groundwater when little information about the aquifer itself was available. The convolution integral enables computation of variations in both transmission losses and base flow in a channel on a continuous basis, which is much closer to reality than merely calculating volume of loss. This technique also utilized the unit response method, which is based on the superposition of individual responses, to route the hydrograph in this example. The results of this study indicate how necessary it is to account for transmission losses and base flow when evaluating discrepancies between observed and modeled flow, though in

general fairly good agreement was found between the observations and the values predicted by the model (Moench *et al.*, 1974).

## *2.2. RAIN GAGE MEASUREMENTS*

### 2.2.1. Temporal and Spatial Sampling

Meselhe *et al.* (2009) evaluated the response of a conceptual lumped hydrologic model (HEC-HMS) and a physically based distributed hydrologic model (MIKE SHE) to changes in temporal and spatial rainfall sampling. This research was conducted in the Goodwin Creek experimental watershed in northern Mississippi, which has a network of 30 rain gages and 14 flow gages. To evaluate the effects of temporal rainfall sampling both models were run using rain gage data on a 15 minute time step, then on a 30 minute time step, a 1 hour time step, 2 hour time step, and a 6 hour time step. To evaluate the effects of spatial rainfall sampling both models were run using all 30 of the available rain gages, then 20 of the rain gages, 10 of the rain gages, 5 of the rain gages, 2 rain gages, and 1 of the rain gages. Unsurprisingly, the distributed model (MIKE SHE) was found to perform better, in terms of reproducing observed hydrographs and fitting peak discharges, than the conceptual lumped model, and it was also found to be more sensitive to both the temporal and spatial rainfall sampling schemes. The overall conclusion of this research was that coarse sampling, whether it is temporally or spatially coarse, can introduce significant errors in hydrologic model predictions (Meselhe *et al.*, 2009).

## 2.3. RADAR RAINFALL

### 2.3.1. Sources of Error in Radar Data

Many sources of error exist in radar rainfall data. Many studies have been conducted to determine the best methods to correct these errors. Chumchean *et al*. (2006a) determined four main sources of error in radar rainfall measurements and attempted to determine the relative importance of these sources. The sources of error cited in this paper were variability in the vertical profile of reflectivity, error in measuring the radar reflectivity, error in the conversion from reflectivity to rainfall rate, and finally error in using rain gages (points) to represent mean-aerial rainfall over a radar pixel during the calibration of radar data with rain gage data. Chumchean *et al*. determined that rain gages were not able to represent mean-aerial rainfall with high accuracy and that radar reflectivity measurement errors were due to radar beam spreading with distance from the radar. Two mean field bias-adjustment methods were developed and tested in this study, one involving the estimation of bias at each time step using sample observations and the other involving a Kalman filter to estimate bias. It was found that both methods were able to decrease error in radar rainfall as levels of error correction were added (Chumchean *et al.*, 2006a).

Chumchean *et al*. (2006b) addressed the errors in the measurement of reflectivity and in the conversion from reflectivity to rainfall rate. The study developed a statistical basis that could be used to correct residual errors in the radar data. To do this radar data were compared to rain gage data, and a Kalman filter was used to update the bias and error variance used in the procedure. This study aimed to determine the number of rain gages necessary for accurate results and to determine

differences in the bias due to storm types.  The research concluded that larger

numbers of rain gages led to more representative results, and that biases could not be

corrected using this procedure for convective events; however, for climatological and

stratiform events the Kalman filter procedure could be used to correct biases in the

radar data (Chumchean *et. al*, 2006b).

Islam *et al*. (2008) acknowledged that radar data were still less accurate than

rain gage data when rainfall values needed to be estimated in a quantitative manner.

The goal of this particular study was, therefore, to evaluate several methods that

could be used to bring radar rainfall data and rain gage data into closer agreement

with each other.  The specific objectives included adding a space-time interpolator to

radar scans, adding a wind-drift correction scheme, and adding an attenuation

correction scheme.  It was determined that a 10-minute scan interval may not be

frequent enough to truly capture the spatio-temporal variation in rainfall rates, thus

leading to the desire for the space-time interpolator.  The problem of wind-drift was

addressed by a Lagrangian-based trajectory algorithm that could calculate the

displacement of precipitation between the radar scan height and the ground.  Finally,

the attenuation correction algorithm developed previously by Wexler and Altas

(1963) was added to the procedure.  These correction schemes were then tested on six

storms occurring in 2000 in the city of Winnipeg (Islam *et al.*, 2008).

## 2.3.2. Error and Bias Correction of Radar Data

Various sources of error have been cited in the literature to explain the

frequent inaccuracies of radar rainfall estimates.  Prior to the work of Seo *et al*.

(1999) the focus of error correction was to minimize error variance.  Seo *et al*.

proposed a procedure that could be used at the National Weather Service (NWS) River Forecast Center (RFC) and the Weather Forecast Offices (WFO) to adjust bias in radar data based on the operational experience and existing procedures in those offices. The emphasis was to create a procedure that was unbiased, intuitive, and parsimonious, rather than just focusing on minimizing the errors. To achieve the intuitive and parsimonious goals in this procedure a simple Kalman filtering method, recursive estimation via exponential smoothing, was chosen for use. Radar-rain gage pairs were used to determine mean field bias in order to validate the procedure. Overall this procedure was shown to be unbiased in the long run and it was found to perform well under a wide variety of conditions related to rain gage network density and radar calibration (Seo *et al.*, 1999).

Jordan *et al.* (2000) explained that the main resistance to using radar data in hydrology was due to concern about errors in radar precipitation measurement. Their study examined the statistical properties of error related to the radar rainfall data sampling strategy. They believed that this would be the first step in the design of hydrological models that could withstand the significant amount of measurement noise that existed in radar data. They determined that errors of larger magnitude existed in a five-minute precipitation sampling scheme than in a ten-minute sampling scheme. They also concluded that spatial averaging of precipitation estimates was not an efficient means to reduce errors related to poor temporal sampling schemes. It was also determined that a time integration process generally led to a smaller mean standard error. A final conclusion drawn from the study was that parameters

controlling error distributions increased for hourly rainfall accumulations compared to instantaneous accumulations (Jordan *et al*., 2000).

Sharif *et al*. (2002) used simulation rather than observed data to examine the propagation of error in radar rainfall.  An atmospheric model was used to simulate a convective storm and generate radar data.  To determine the effect of radar errors on hydrologic predictions they also modeled runoff over the land surface using Horton's equation.  To compare the radar rainfall estimates to "true" rainfall measurements the watershed total rainfall volume ratio, the root-mean-square error in the simulated hydrograph, the total runoff volume ratio, and the runoff peak discharge ratio were evaluated.  The results of the study indicated that errors related to the radar measurement range and the orientation of the radar were amplified in the modeled runoff, and that errors in radar calibration could either reduce or amplify range and orientation errors.  The errors in predicted runoff were found to be relatively small within a range of 70-km from the radar, but they increased steadily beyond this range.  From the study Sharif *et al*. (2002) concluded that range and orientation related error could not be addressed adequately in calculating only storm total volumes and that orientation errors could be reduced by either decreasing the resolution or reducing the width of the radar beam.

Sharif *et al*. (2004) attempted to understand the effects that the distance between a radar station and a watershed can have on radar rainfall estimates for that watershed.  They were particularly interested in the effects on the average rainfall volume for the watershed, the peak discharge in runoff from the storm event, the runoff volume, and the root-mean-square error of the runoff hydrograph.  Again

Sharif *et al.* worked with simulated data rather than real data, in this case using a radar simulator to create radar-rainfall estimates that were used as input to a physically-based, infiltration-excess hydrologic model. Statistical analyses were performed to determine relationships between rainfall volume errors, runoff volume errors, peak discharge errors, and their range effect. From the study Sharif *et al.* determined that the relationship between peak discharge errors and the runoff volume errors were not dependent on the radar range or the magnitude of rainfall error; however, errors in the rainfall volume were found to be amplified during the transformation between radar reflectivity and rainfall estimates. They again concluded that errors began to increase significantly beyond a range of 80-km (Sharif *et al.*, 2004).

Wood *et al.* (2000) further investigated the accuracy of radar rainfall estimates calibrated with rain gage data. The method of calibrating the radar data in this case involved combining a single rain gage with a radar estimate, allowing the calibration factor to vary in time. The study assessed the ability of a single rain gage and a radar station to estimate rainfall at several important spatial scales. The dynamic calibration factor described above was compared to a static calibration, which is not allowed to vary in time, and a hybrid calibration factor. At short distances from the radar the hybrid calibration factor was allowed to vary in time and at larger distances the hybrid calibration factor more closely resembled a static calibration factor. The results of this study showed that the hybrid calibration factor performed better than rain gages, uncalibrated radar estimates, and statically calibrated radar estimates for most of the rain gages in the study watershed. These results can be used to draw

conclusions as to the rain gage network density required in combination with a radar station to improve the ability to accurately predict flood events (Wood *et al.*, 2000).

Borga *et al.* (2002) identified three categories of radar errors: miscalibration of radar system and lack of electronic stability of the radar, the radar detection environment, and fluctuations in the atmosphere. They investigated possible processing scenarios that could correct for systematic and range-dependent radar errors. The focus in range dependent errors was within 30 to 70-km from the radar station, which is within the range that Sharif *et al.* (2002 and 2004) reported to lead to acceptable accuracy. The results of the study, however, indicated that a range smaller than 70-km can affect the accuracy of radar rainfall estimates. The combined adjustment technique using rain gage-based radar adjustments utilized was shown to reduce the overall error in rainfall estimates over the study watershed, implying that homogeneity in the accuracy of radar rainfall estimates with respect to range and scanning elevation is necessary in order to apply gage-based adjustment of radar data (Borga *et al.*, 2002).

### 2.3.3. Rain Gage-Adjusted Radar Rainfall Measurements

Many people believe that combining radar data and rain gage data could help eliminate many of the errors and biases in radar data discussed above, and that merging the two datasets could reduce the limitations of both. There are equally as many potential sources of error in rain gage data as there are in radar data. Sieck *et al.* (2007) evaluated several sources or rain gage error, focusing on rain gage location, rain gage calibration, and correction for wind effects. The purpose of this research was to illustrate the difficulties that could be encountered in obtaining acceptably

accurate rain gage data, and to prevent future users from blindly accepting rain gage

data without considering the potential inaccuracies.  The research was conducted in

the Goodwin Creek experimental watershed in Mississippi, which had a network of

43 rain gages.  They examined rainfall data for two storms, and between those events

they found a total of eight rain gages reporting suspicious or inaccurate data.  Rain

gages located above the ground surface were compared to rain gages located in pits at

the ground surface.  The above-ground rain gages were found to catch less rainfall

than the in-ground rain gages, which is likely a direct result of wind effects.

In evaluating the necessity of calibration of rain gages Sieck *et al.* determined

that type of rain gage (such as tipping bucket or weighing rain gage) influenced the

necessity of calibration, and that accuracy of rainfall measurements made even after

calibration was completed was dependent on the rainfall intensity.  Wind forces

raindrops to fall at an angle, which will be some function of the speed of the wind and

the diameter of the raindrop), so wind tends to cause above-ground rain gages to

catch less rainfall than rain gages at the ground surface.  In this study tipping bucket

rain gages were seen to have an undercatch of 2 to 6% compared to in-ground rain

gages, while weighing bucket rain gages were found to have an undercatch of 1.5 to

3.5%.  Sieck *et al.* (2007) concluded that properly installing and maintaining rain

gages, as well as frequently calibrating them, is necessary for accurate rain gage

measurements.  Calibration at a variety of rainfall intensities improves the effects of

calibration.  Location of the rain gage is very important to data accuracy, and placing

several rain gages close together can provide redundancy in data that is necessary for

quality control.  Finally, the wind effect influences the catch of above-ground rain

gages; however, it is still difficult to exactly quantify the effect of wind on rain gage catch (Sieck *et al.*, 2007).

Westcott *et al*. (2008) compared rain gage data and radar data on a daily and a monthly time basis over three years in the Midwestern United States. They determined that radar data and rain gage data tended to agree to within approximately 25%. They also found that as actual precipitation totals increased the radar precipitation estimates tended to be equal to or smaller than the rain gage estimates; however, when precipitation totals were lower, the radar estimates tended to be larger than the gage estimates. This study concluded that a multi-sensor (including radar and rain gage data) improved precipitation estimates on a daily basis over radar data alone (Westcott *et al*., 2008).

Hoblit *et al*. (2003) attempted to create a seamless radar map over the state of Florida while using gage-adjusted radar precipitation estimates. The purpose of this was to eliminate discontinuities that occur in radar estimates when two radar stations have overlapping ranges. The rain gage data were used to improve the accuracy of the radar estimates. A spatial adjustment algorithm was used to adjust the radar data to the gage data after a uniform radar-rain gage ratio was found to be insufficient. The spatial adjustment method adjusted each radar pixel based on a weighted average of ratios from nearby gages and did not actually force the radar data to exactly match the gage data at each gage location. This algorithm was found to slightly warp the gage-adjusted radar data so that rainfall estimates were generally close to the rain gage estimates without compromising the spatial signature of the radar data (Hoblit *et al*., 2003).

Vieux *et al.* (2009) compared rain gage rainfall data, raw radar data, and rain gage corrected radar data as input dataset to the model Vflo. They were interested in determining how the initial parameter estimates and input datasets influenced the ability of the model to predict runoff. Rainfall data from two typhoon events and two heavy convective storm events were used as input to the model. The results of this research indicate that rain gage-adjusted radar data, which has been corrected for bias, provides more accurate runoff predictions than either raw rainfall data or rain gage data. Raw radar data was found to underestimate peak discharges, while rain gage data was found to produce inconsistent results (Vieux *et al.*, 2009).

## 2.3.4. Accounting for Spatial Variability of Rainfall

A major advantage to radar data over rain gage data is the ability to better show the spatial variability of rainfall events. Arnaud *et al*. (2002) studied the sensitivity of hydrological models to the spatial distribution of rainfall. They were especially interested in determining how spatial variability influenced flood prediction ability. Three models using different methods of predicting runoff were evaluated in this study. The three models were applied to four hypothetical homogeneous watersheds, with the sensitivity of the model being determined by the differences between the observed peak flow distributions. It was found that differences in the flows increased the most for larger watersheds because the variability in rainfall increases over the watershed. Based on the results of this study Arnaud *et al*. (2002) concluded that the calibration of these hydrologic models can be severely affected when spatially averaged rainfall is used rather than the actual rain fields.

Cheng *et al*. (2007) studied the spatial and temporal effects of rainfall in Taiwan. Ordinary kriging was used to examine the efficiency and the accuracy of rainfall events with particular attention paid to events in which rain gage data were missing. The accuracy of various weighting procedures was evaluated under conditions of missing data and complete data sets. Spatial variation of the rainfall was described by semivariograms while the kriging, co-kriging, and block kriging methods were used to interpolate the rainfall. When data were missing, block kriging was found to most accurately estimate the rainfall distribution, and overall the results showed the interpolation processes to represent the observed rainfall well. This implies that the rainfall interpolation process used can be used to create a spatio-temporal rainfall input for hydrologic models (Cheng *et al*., 2007).

## 2.3.5. Runoff Simulations Using Radar Data

Runoff simulation and prediction is one aspect of hydrology that could be greatly improved by the use of radar rainfall estimates. Peters and Easton (1996) believed that improved techniques of predicting runoff could result from the wide availability of radar data. They developed an adaptation to the Clark runoff model that could model translation and linear storage attenuation of surface runoff. The rainfall excess from storm events was lagged to the watershed of the outlet based on grid cells and a runoff hydrograph for the event was calculated. The hydrographs created by this model provided a reasonably good fit to the observed event hydrographs. Peters and Easton (1996) concluded that, if a storm with large spatial variability were modeled using this method, large differences between the modeled

and observed hydrographs could result because of the grid-based calculation of losses and translation of rainfall excess.

Vieux *et al*. (2005) also evaluated a runoff simulation method, with their interest lying in predicting runoff more accurately in urban environments. A distributed model that used the spatial resolution of radar data was developed and led to the discovery that the spatial resolution influenced the prediction accuracy of the model. This phenomenon was found to scale with the size of the watershed being studied. The model developed was a physics-based hydrologic model, the results of which indicated that fairly accurately provide real-time rainfall-runoff prediction was possible. The data provided could be used to more accurately predict floods for specific locations (Vieux *et al*., 2005).

### 2.3.6. Effects of Storm Type and Movement

It has long been suspected that the type of storm event can influence radar rainfall estimates, and movement of a storm has also been found to affect rainfall estimates. March *et al*. (1979) developed regression equations that related storm rainfall depth to both watershed topography and storm type. Equations were developed for six different storm types, as well as one equation that considered all of the storm types. Results of this study showed that equations considering storm type as a variable did not more accurately predict rainfall, compared to the rainfall measured by rain gages, for specific sites than equations that did not consider storm type (March *et al*., 1979).

Lee and Huang (2007) considered storm movement to be one of the more important factors responsible for spatial and temporal rainfall variability. They were

interested in determining the effect of storm movement on equilibrium discharge.

Two conceptual models were developed representing different watershed geometries

and using algorithms based on the kinematic-wave theory to model runoff. The

results of this study indicated that, when storms move downstream across the

watershed, the runoff can reach an equilibrium condition, despite the fact that the

storm length is shorter than the watershed length and the rainfall duration is less than

the time to equilibrium runoff for a stationary uniform storm. According to Lee and

Huang (2007) this is contradictory to conventional hydrologic design, in which the

storm duration must be equal to the equilibrium time in order to attain the maximum

discharge.

## 2.3.7. Reflectance-Rainfall (Z-R) Relationship

### 2.3.7.1. Sensitivity to Z-R Relationship

The relationship between reflectivity Z and rainfall rate R began to be

investigated thoroughly by Marshall and Palmer in the late 1940's. Research into this

relationship has indicated that a power law of the form:

$$Z = AR^b \qquad\qquad (2\text{-}3)$$

where Z is the radar reflectance in decibels of reflectivity, R is the rainfall intensity as

measured by a rain gage, and A and b are coefficients, is the correct form for this

relationship. Marshall *et al*. (1947) conducted experiments to verify the theoretical

finding that the power reflected from raindrops was proportional to Z. This

experiment utilized radar data as well as filter papers showing raindrop distributions.

The filter papers determined the value of Z, which corresponded to the measurements

of the radar, and the rainfall rate used during the experiment was known. This

allowed Marshall *et al*. (1947) to determine that the relationship:

$$Z = 190R^{1.72} \tag{2-4}$$

applied to the data used in this experiment.

Marshall and Palmer (1948) continued their work examining the distribution

of raindrops. They again compared the distribution of raindrops on filter paper with

radar readings. Using this data they were able to develop relationships between drop

diameter and number of drops, the mass or rainwater per unit volume of space and the

reflectivity, and the reflectivity and the rainfall rate. They confirmed the equation

from their previous paper, that:

$$Z = 190R^{1.72} \tag{2-5}$$

Since the work of Marshall and Palmer, the National Weather Service (NWS)

has determined a standard relationship between Z and R that can be applied in most

rainfall situations across the country. This relationship is:

$$Z = 300R^{1.4} \tag{2-6}$$

Ulbrich and Miller (2001) wished to evaluate the degree to which variations in

the coefficients *A* and *b* affects the accuracy of radar measurements. They also

wished to determine if inaccuracies due to the Z-R relationship could explain the

often large discrepancies between radar data and rain gage data for the same region.

Raindrop size distribution was determined using a Joss drop disdrometer, and radar

and rain gage data were obtained for regions in upstate South Carolina. The first

stage of this experiment found that the standard equation stated previously was

adequate, but only when adjustments had been made for calibration errors. They

found, as many others have, that when adjustments were made to take into account storm type, accuracy in radar measurements, as compared to the disdrometer measurements, can be improved. Ultimately Ulbrich and Miller determined that while adjusting *A* and *b* can lead to some improvement in the accuracy of radar measurements, the improvement is minor compared to errors caused by calibration offset of the radar, but when adjustments for this calibration offset have been made, good agreement was found between radar and rain gage data (Ulbrich and Miller, 2001).

Habib *et al*. (2008) also examined errors in the Z-R relationship; however, they considered the errors with respect to the sensitivity of runoff simulations. They used a physically based, continuous-mode distributed hydrological model to predict runoff during rainfall events. They were most interested in the variation in Z-R relationships at different temporal scales, so they determined appropriate relationships for different temporal scales. The experiment was performed using both disdrometer data and radar data. Habib *et al*. concluded that the method that was used to derive parameters of the Z-R relationship was largely responsible for the sensitivity of runoff simulations. When event-specific relationships were used along with bias removal procedures and minimization of random errors fairly accurate hydrographs resulted.

### *2.3.7.2. Dynamic Z-R Relationship*
Gerstner and Heinemann (2008) listed a slightly different set of error sources in radar rainfall measurement. This list of errors included attenuation of the radar beam, ground clutter, beam occlusion, and the relationship between reflectivity and rainfall rate (Z-R relationship) utilized. The purpose of this research was to develop a

statistical objective analysis method to improve the accuracy of rainfall data in order that radar data could eventually come to replace rain gage data. In order to conduct this research, an algorithm was developed to identify different types of precipitation (stratiform versus convective). After this algorithm had identified the precipitation type, the Z-R relationship was applied to determine the rainfall rates, and then a bias correction was applied. Once this was done, the modified statistical objective analysis scheme was applied to adjust the radar data to more closely match the rain gage measurements. The algorithm to determine storm type was deemed reasonably accurate, and the statistical objective analysis was able to reduce errors, compared to rain gage measurements, in radar rainfall data in 75% of the tested cases.

## 2.4. UNIT HYDROGRAPHS

### 2.4.1. History and Evolution of the Unit Hydrograph

Clark developed his unit hydrograph (UH) technique in order to better define the relationship between unit hydrographs and flood routing and to then use this relationship to derive more accurate unit hydrographs. Kull *et al*. (1998) detailed the history of the UH from Clark's work to ModClark, a program developed by the Hydrologic Engineering Center (HEC) to integrate data from new technologies into the UH procedure. After detailing this history, the authors then provided a demonstration of the ModClark program in the Salt River Basin, Missouri, in order to demonstrate the ability of this program to work with the existing HEC-1 method, and to utilize data from Digital Elevation Models (DEMs) and radar rainfall data, as well as other data sources (Kull *et al*., 1998).

Hoblit and Curtis (2002) further demonstrated the use of ModClark and other HEC programs in their attempt to integrate radar rainfall data and hydrologic models. In their study, they used the abilities of ModClark to characterize the variation in rainfall rates within the watershed and to route runoff through the various sub-watersheds based on the location of the rainfall within the watershed. This will increase the ability of the model to place the correct amount of rainfall at the correct location in the watershed at the correct moment in time, an ability which is lacking when rain gage data are used (Hoblit and Curtis, 2002).

Many watershed do not have rain gages or flow gages that can be used for deriving unit hydrographs from rainfall and runoff data. In these ungaged watersheds synthetic unit hydrograph procedures can be used to develop necessary unit hydrographs. There are many methods available for deriving synthetic unit hydrographs, including Snyder's Method and the NRCS (SCS) Method, but assuming the form of a probability density function (pdf) for the unit hydrograph has become popular. Bhunya *et al.* (2007) evaluated four pdfs for use in deriving synthetic unit hydrographs. The pdfs evaluated were the two-parameter Gamma, the three-parameter Beta, the two-parameter Weibull, and the one-parameter Chi-square distribution. Analytical and numerical schemes were used to determine values for the various distribution parameters, and then observed data were used to validate the synthetic unit hydrographs. The Beta and Weibull distributions were found to be more flexible than the Gamma and Chi-square distributions, due to the fact that they can have either positive or negative skew. This allowed them to more accurately fit the observed hydrographs. A disadvantage to using a pdf to develop a unit

hydrograph is that a unit hydrograph recession limb must have some point where the flow equals zero. With the exception of the Beta distribution, all of the pdfs considered approach zero asymptotically. Bhunya *et al.* (2007) concluded that each of the four pdfs produced more accurate unit hydrographs that the current methods of computing synthetic unit hydrographs (Snyder's method, NRCS (SCS) method, and Gray's Method), and that the Beta and Weibull distributions were the most accurate of the pdfs. The Beta distribution has been found to approximate the Gamma distribution, and the Chi-square distribution is also similar to the Gamma distribution, so the final conclusion reached was that the three-parameter Beta distribution, where two parameters are non-dimensional shape parameters and the third parameter is a scale parameter, would be the best pdf to use in calculating synthetic unit hydrographs.

### 2.4.2. Digital Elevation Model and GIS Technology

As mentioned in the discussion of the development of the program ModClark considerable technology has been developed since the original development of the UH procedure, much of which could provide very useful hydrologic information. Noto and La Loggia (2007) attempted to use some of these technological developments to aid in modeling hydrological processes with a distributed UH procedure. A Geographic Information System (GIS) provided a digital elevation model (DEM) of the watershed, which was used to determine the flow paths for runoff water, as well as watershed morphology and land use. This knowledge of the watershed enabled the time-area curve to be computed by the program. The watershed was separated into cells, and the total watershed response was calculated as

36

the sum of the responses from each cell. Cell response was determined by a process of channel flow and linear reservoir routing (Noto and La Loggia, 2007).

Cleveland *et al*. (2008) also attempted to use watershed topographical information to develop unit hydrographs. The procedure that they developed estimated UH parameters by analyzing the distribution of raindrop arrival time. Information about the slope of the watershed provided by a DEM was used to determine flow paths and speeds of the raindrops, and a particle tracking program was used to generate the arrival time distribution. A unit hydrograph was then fit to the arrival time distribution. This procedure was evaluated on 126 watersheds in Texas, and was determined to be a reasonable approach, though it was acknowledged to be very computationally demanding (Cleveland *et al*., 2008).

### 2.4.3. Arid Region Unit Hydrograph Procedure

The method for developing unit hydrographs in arid regions must be somewhat different from that for non-arid regions due to the differences in climate. Sen has conducted multiple studies into the development of UHs for Saudi Arabia. Sen (2007) noted that infiltration effects were not considered in the UH procedure; however, infiltration is a major hydrologic process in arid climates. Sen, therefore, developed an equation that could be used to produce a UH that would account for the condition of the soil and sub-soil prior to the wetting event. The method developed was actually an adaptation of the commonly used Snyder's method.

Sen (2008) addressed the problem of data scarcity in arid region hydrology and noted that traditional methods of hydrological modeling would not work in these regions due to the differences in climate. Sen again modified Snyder's UH method,

this time to develop hydrographs for ungaged watersheds.  The hydrograph calculated

using the method is similar to the Natural Resources Conservation Service (NRCS)

dimensionless UH; however, for arid regions more values along the recession limb

were deemed necessary (Sen, 2008).

# CHAPTER 3

# DATA SOURCES

## *3.1. WALNUT GULCH EXPERIMENTAL WATERSHED*

      The Walnut Gulch Experimental Watershed, located near Tucson, Arizona, in the San Pedro River Basin, was chosen as the study area for this research because it is heavily gaged and because data are readily available through the United States Department of Agriculture's Southwest Watershed Research Center website. Walnut Gulch is part of the United States Department of Agriculture (USDA) Agricultural Research Service (ARS) Southwest Watershed Research Center. The Walnut Gulch Experimental Watershed is approximately 149 km$^2$ in area, and the watershed elevation ranges from 1220 m to 1950 m above mean sea level (Goodrich *et al.,* 2008), with much of the watershed ranging in elevation from 1220 m to 1500 m above mean sea level. The minimum daily temperatures in Walnut Gulch range from approximately 0 °C to 15 °C and the maximum daily temperatures range from approximately 25°C to 45 °C (Keefer *et al.*, 2008). The watershed consists of 16 large subwatersheds within the boundaries of the Walnut Gulch Experimental Watershed, each of which contains a number of rain gages as well as at least one flow gage at the outlet (Anon., 2007). Precipitation and flow gages have been in place in the watershed since 1953. The average annual precipitation between the years of 1956 and 2006 was measured to be approximately 316 mm, more than half of which occurs during the summer monsoon season (July through September) (Goodrich *et al.,* 2008). The streams located within the watershed are ephemeral, dry

approximately 99% of the time (Anon., 2007). Runoff is usually in response to thunderstorm events, and the events are generally fairly short, with peak flows arriving very quickly (Stone *et al.,* 2008). All data sets, including rain gage and flow gage data sets, are available on the internet (Southwest Watershed Research Center, 2008).

### 3.1.1. Rain Gage Data

Digitally recording rain gages have been used to monitor precipitation in Walnut Gulch since 1999. A network of 88 weighing-type recording rain gages currently operates in the watershed. This gives a gage density of approximately 0.6 gages/km$^2$, which is among the most dense rain gage networks in the world. The weighing-type rain gages used were developed by the scientists working at the Southwest Watershed Research Center. Using an electronic strain gage, the weighing-type rain gages convert the weight of rainfall in the bucket to a voltage, then a linear relationship between voltage and rainfall depth is used to calculate the rainfall depth in a given time period. Rain gage data are available through the Southwest Watershed Research Center's website, which was given previously. The data sets include the rain gage number recording the rainfall, the date of the event, the time the event started, the number of minutes elapsed between the start of the rainfall and a given measurement, the cumulative depth of rainfall measured, and the rainfall intensity at the time of a given measurement. Rainfall data for a variety of storm events were utilized in several portions of this research (Goodrich *et al.,* 2008).

### 3.1.2. Flow Gage Data

The Walnut Gulch Experimental Watershed has a total of 30 flow gages. Eleven of these are on large (2.27 to 149 km$^2$) subwatersheds, eight are on medium (0.35 to 1.60 km$^2$) subwatersheds, and eleven are on small (0.0018 to 0.59 km$^2$) subwatersheds. A specific type of flume has been developed in response to the ephemeral nature of Walnut Gulch streams. Walnut Gulch supercritical flumes were used to measure flow on the larger watersheds, while Smith supercritical flumes were used to measure flow over the smaller watersheds. These special flumes are necessary because the runoff is very high in sediment. A potentiometer attached to the stilling well of the flume is used to measure flow depth, and the known geometry of the flume is used to determine the flow velocity and rate. Flow in medium-sized watersheds is measured using a stock pond. The change in water level in the stock pond is measured, and a stage-volume relationship developed from the pond topography is used to determine the flow. As with the rain gages, digital flumes have been in use since 1999. The record of runoff for Walnut Gulch is the longest flow record for a semiarid watershed in the world. As with rain gage data, flow gage data was obtained for the USDA Walnut Gulch Experimental Watershed website (Stone *et al.,* 2008).

## *3.2. RADAR DATA*

Radar data for the San Pedro River Basin was obtained from the Hydro-NEXRAD system. This is an internet service, developed by a group of researchers from the University of Iowa, Princeton University, the National Oceanographic and Atmospheric Administration, the National Climatic Data Center, and UCAR's

Unidata Program Center. The University of Iowa is currently providing most of the service support. The goal of this service is to make it easier for hydrologists to access radar data, so that this data can be better utilized in hydrologic applications. This service allows users to request a variety of radar data products for a given time period either for a specific radar station or for a specific watershed. The website for this service is www.hydronexrad.net.

Radar data can be downloaded from Hydro-NEXRAD in either ASCII or Arc-ASCII format. This provides a text file of radar readings (in decibels of reflectance) for the watershed or radar station chosen by the user. An added benefit of the Arc-ASCII files is that they can be loaded into ArcGIS. This allows to user to examine the radar data along with a map of the watershed or area in question. This method was used to identify radar pixels specifically corresponding to the area of the Walnut Gulch watershed. The radar data and a map showing the boundary of Walnut Gulch Experimental Watershed were viewed in ArcGIS simultaneously. From this the position of the pixels covering Walnut Gulch could be identified in the text files that contain radar data. The locations of rain gages and flow gages could also be added to the map of Walnut Gulch in ArcGIS, which helped determine which rain and flow gages would be associated with which radar pixels in later portions of the research. When radar data for the desired storm events were downloaded, it was important to note that radar data were recorded in Coordinated Universal Time (UTC), while the rain and flow gage data were recorded in local time. Therefore, the radar data were seven hours ahead of the rain and flow gage data, which needed to be accounted for when choosing the desired radar data.

# CHAPTER 4

# TRANSMISSION LOSSES

## *4.1. INTRODUCTION*

Transmission losses (TL) have been proven to be a significant hydrologic

process in arid and semi-arid climates.  Jordan (1977) defines transmission losses as

water that is part of the streamflow at one location, but which has been lost through

channel infiltration prior to reaching some location downstream.  This could lead to a

significant reduction in flow volumes, velocities, and rates, depending on the

magnitude of local inflow from the drainage area between the two locations and the

infiltration characteristics of the channel.  The ability to estimate TL is necessary for

applications such as flood routing and forecasting, floodplain delineation, and for

predicting ground-water recharge (Jordan, 1977).

Transmission losses are a key concern in arid and semi-arid regions especially

because ephemeral streams, or streams that flow only in response to storm or

snowmelt events, generally predominate in these regions.  The beds, banks, and

floodplains of these streams are generally composed of coarse-textured alluvial

materials.  High intake rates and low moisture contents characterize such alluvium

and can lead to significant decreases in downstream flow volumes (Keppel and

Renard, 1962).  Because ephemeral streams do not contain flow most of the time their

hydrographs have different characteristics than streams with continuous flow.  The

hydrograph for an ephemeral stream is often characterized as having an initial delay

in the start of flow followed by a very rapid rise to peak flow and a receding limb of

short duration, due in part to transmission losses (Peebles *et al*., 1981). The relatively steep rise occurs because the initial part of the runoff is lost to TL so the initial runoff at the downstream section is the result of the peak flow portion of the runoff hydrograph from the upstream section.

## *4.2. METHODS AND MATERIALS*

### 4.2.1. Purpose of Research

Much of the research on transmission losses to date has involved reducing the total volume of flow by some appropriate factor and possibly evaluating the reduction of the peak flow. Few studies have attempted to account for TL as the streamflow is routed along the channel. While it is true that transmission losses do reduce the volume and peak flow of a flood event, this approach does not allow the spatio-temporal variation of TL to be understood. The objective of this research was to develop a hydrograph routing method that could estimate the volume of TL at each point along the channel and each time increment of the flow hydrograph. The model was tested and calibrated using flow gage data from Walnut Gulch Experimental Watershed, located near Tucson, Arizona. Both storm-to-storm variation and reach-to-reach analyses were made.

### 4.2.2. Flow Gage Data

Flow gage data were obtained from the United States Department of Agriculture (USDA) Agricultural Research Service (ARS) Southwest Watershed Research Center website. Study reaches were identified as lengths of stream between an upstream and a downstream flow gage. Six potential reaches were identified for

use in this research, the lengths of which varied from 2400 m to 8100 m. Based on images from GoogleEarth a rectangular cross-section was assumed for each reach. The watershed area draining into the upstream flow gage was also necessary input information. The six drainage areas ranged in size from 227 ha to 12723 ha. Ultimately flow gage data from eighteen events were determined to be acceptable for use in this study. Data were downloaded as Microsoft Excel files, converted to text files, filtered of unnecessary information, and then underwent several pre-processing steps prior to use.

### 4.2.3. Data Conversion

As mentioned previously, the raw data were obtained from Walnut Gulch Experimental Watershed. Flow data for selected events were downloaded from the USDA ARS Southwest Watershed Research Center website. The data were not separated by gage, but were grouped by event, the gages had not been recording on a constant time interval, and few of the gage flow records for one event began at the same time. For use in modeling TL the desired data format included pairs of upstream and downstream flow gages, a constant recording time interval, and the same start time for each upstream and downstream flow gage pair. Several pre-processing programs were developed to convert the data into the desired format.

The first step, separating the data by gage and converting the data to text files, was done by hand. Each flow event was examined, and separate files were created for each gage that recorded flow during that event. The number of ordinates in the flow record was noted, and then the Excel files were converted to text files. Occasionally two flow events were recorded on the same day; in these flow events,

only one event was chosen, based on event duration, magnitude of flow, and the number of gages recording flow at that time.

After individual text files had been created for each gage registering flow in each event, the data were converted to a constant time interval. A preprocessing program was developed that read in the original text files and interpolated flow values for any missing data points. The output files from this program had a constant reporting time interval of one minute, which was chosen because it seemed to be the dominant reporting interval in the raw data. A simple linear interpolation scheme was used to fill in flow values that were missing from the raw data. A few flow gages had the ability to report data every fifteen seconds, though even these gages had missing data that needed to be interpolated. As it was believed that there would be little change in flow rates over the course of fifteen seconds, the preprocessing program also deleted these extra values from the record.

The next step in the data preparation was to combine the individual flow gage records into upstream and downstream gage pairs and to make sure both the upstream and downstream gage records started at the same time. First, a map of Walnut Gulch Experimental Watershed including flow gage locations and the stream network was examined to determine appropriate gage pairings. It was determined that in some cases multiple upstream gages would feed into the same downstream gage. In combining two upstream gages, several problems needed to be overcome. First, one of the flow gage records needed to be adjusted so that both gages had the same flow start time, and second, the two records needed to be added together. A program was developed that could input two individual data files, add the appropriate number of

zeros to the file with the later start time, and then add the two records together. This created one upstream flow record.

Once an upstream flow record was obtained, another preprocessing program was needed to combine the upstream flow record and the downstream flow record into one text file. This program also needed to be able to account for differences in the start time of the two files. A second program was developed that could add the appropriate number of zeros to either the upstream or downstream record, whichever had the later start time, and then create one file that contained the upstream and then the downstream hydrograph. The output file from this preprocessing program was then ready to be input into the program that was developed to model transmission losses, which will be described next.

## 4.2.4. Spatio-Temporal Transmission Loss Model

The final step was to develop a program that could model transmission losses in a channel. The purpose of this program was to route the upstream flow, using the Convex routing method, through the channel reach while infiltrating, using Horton's equation and the mass-infiltration equation, the appropriate amount of that flow into the channel bed. The overall model developed in this study combines lateral inflow (LI), TL, and channel routing into one algorithm. Figure 4-1 shows a pictorial representation of the model. The stream (shown as the black rectangular box with blue lines indicating the water surface) is modeled as having a rectangular cross-section, with a number of equally sized cells. Each cell has a rectangular land area of equal size (shown as the green rectangles attached to the stream) contributing lateral inflow to the stream. Transmission losses are modeled as flowing out of the bottom

47

of the stream (represented by blue arrows) into a box located below the stream (brown rectangular box) representing the infiltration capacity.

Runoff enters the stream either as flow from the upstream contributing area or LI into the stream section between the upstream and downstream gages. Both the upstream flow and LI are represented as time-dependent hydrographs rather than total storm volumes. During the first time step LI is introduced to each cell and streamflow from the watershed that contributes runoff to the upper gage enters the first or uppermost cell. Transmission losses are computed for each cell based on this initial amount of water in the storage of each stream cell. Next the streamflow is routed one time step through the channel. During each subsequent time step both upstream inflow and LI are added and streamflow is routed to the next downstream cell. Transmission losses are computed based on the amount of water storage in each cell. The outflow from the most downstream cell for each time step represents the computed downstream hydrograph.
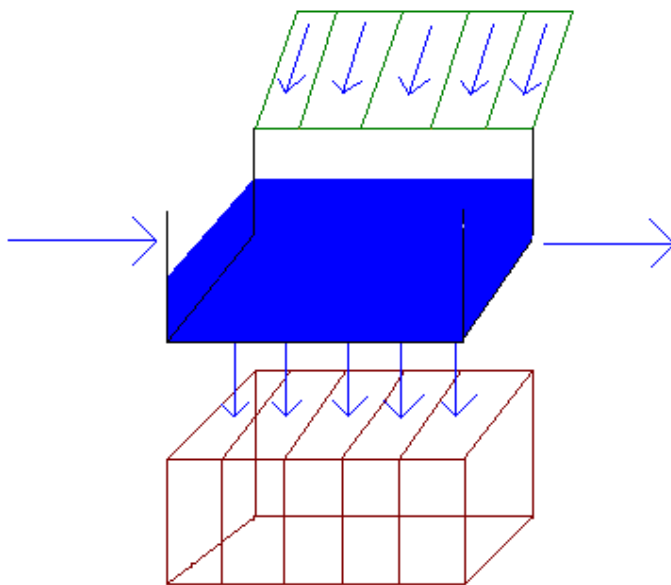


**Figure 4-1: Diagram of Transmission Loss Model**

### 4.2.5. Modeling of Transmission Losses

Transmission losses were modeled using the mass-infiltration method which uses Horton's infiltration equation:

$$f = f_c + (f_o - f_c)e^{-Kt} \tag{4-1}$$

where $f_c$ is the ultimate infiltration capacity (capacity after a long period of wetting), $f_o$ is the initial infiltration capacity (capacity at beginning of storm event when soil is dry), and K is a constant that describes the decay of the infiltration capacity with time. Parameters $f_c$, $f_o$, and K reflect channel soil properties. Because it is common in arid and semi-arid regions for the infiltration capacity to be greater than the amount of water available in the runoff for infiltration, the mass-infiltration method was used. This method can be applied to cases where the water supply is less than the infiltration capacity, which in this case would mean that not all of the storage capacity below the channel was filled. When the storage volume in a cell is greater than the infiltration capacity, the infiltration capacity decreases at the maximum rate for that time step, which can be found by Horton's equation. However, when the runoff volume is less than the infiltration capacity, the decrease in capacity occurs at a lower rate, and therefore must be modeled differently in order to accurately estimate the volume of losses. The mass infiltration method calculates the total mass of water infiltrated using the integral of Equation 4-1:

$$F = f_c t + \frac{(f_o - f_c)}{K}(1 - e^{-Kt}) \tag{4-2}$$

in which F is the cumulative mass of water infiltrated at a given time, t from the beginning of the storm event, and $f_c$, $f_o$, and K are defined as in Horton's equation (4-1) (McCuen, 2005).

## 4.2.6. Streamflow Routing

The routing model with transmission loss included was based on the continuity of mass, which is the standard form for most hydrologic routing methods:

$$I + L_I - L_T - O = \frac{dS}{dt} \tag{4-3}$$

in which I is the inflow to the channel either at the upstream section or local inflow, O is the outflow in the channel at the downstream section, $L_T$ is the transmission loss between the two sections, $L_I$ is lateral inflow, S is the storage within the reach, and t is time. Transmission losses were estimated using F from equation 4-2 for a given time period. Equation 4-3 was applied through subsections, or cells, of the channel so that the spatio-temporal distribution of the TL could be computed. The outflow from each cell was computed numerically by solving for the outflow of Equation 4-4:

$$O = I + L_I - L_T - \frac{dS}{dt} \tag{4-4}$$

The inflow and transmission losses are added to and subtracted from the storage and the outflow from any cell is proportional to the storage:

$$O = CS \tag{4-5}$$

in which C is the routing coefficient and the outflow is transformed from a flow rate to a volume. As the surface storage of water increases in a channel cell, the outflow will increase according to the value of C. However, as the storage in a cell increases, the TL also increases, which decreases the amount of storage.

Unless LI, which is the runoff into the stream reach from the land between the two sections, occurred, TL should decrease as the runoff hydrograph moves downstream because TL reduce the storage as the flood wave moves downstream.

Even if transmission losses did not occur, translation and attenuation of the hydrograph would occur, which spreads the flood hydrograph over time. With less storage at any point because of transmission losses, the pressure head decreases. Because TL decrease the volume of surface water stored in each cell, the streamflow will have a greater head at upstream sections when compared with downstream cell sections. As the head decreases as the floodwave moves downstream, the TL lessens.

When lateral inflow is present, the transmission loss hydrograph may or may not attenuate as the distance downstream increases. The characteristics of the TL hydrograph as well as the outflow hydrograph will depend on the volume and timing of the LI relative to the volume and timing of the upstream hydrograph. If the volume of LI replaces the lost TL volume, then the downstream hydrograph will not show the attenuation from the TL and routing. Both the TL and downstream hydrographs may increase because the LI will increase the storage in each cell of the channel. Thus, the outflow from the stream reach will be difficult to analyze.

## 4.2.7. Detailed Model Description

In addition to a data file that contains an upstream and downstream flow-gage pair for a runoff event, physical information about the channel was input to the Spatio-Temporal Transmission Loss (STTL) Model. This physical information includes the number of stream cells, the width of the cells, the length of the cells, and the area of the watershed draining into the upstream gage. Information about the stream segments, including width and length, as well as watershed area, was derived from GIS. Initial estimates for $f_o$, $f_c$, K, and C were also input. A routing time increment, determined based on the raw flow data, was also necessary input

information, and a percentage of lateral inflow to the channel could be specified. In this program lateral inflow was accounted for as the specified percentage multiplied by the upstream hydrograph as a simplifying assumption.

After the input information was entered, initial step sizes were entered for each of the infiltration and routing parameters ($f_o$, $f_c$, K, and C). The program then used a numerical optimization scheme to determine the optimum value for each parameter. The goal in optimizing these parameters was to determine values that provided the lowest possible standard error ratio and bias for the model. As initial estimates for the infiltration parameters, the means of the values provided by Bedient *et al*. (2008) for various types of sandy soil were used ($f_o$ = 329.5 mm/hr, $f_c$ = 49.75 mm/hr, and K = 17.41 $hr^{-1}$). The initial routing coefficient was set at 0.2 as large storage attenuation effects were expected. After the program had determined the optimum parameters for the conditions being modeled, those values were used to model the infiltration and routing of the runoff, then an output file comparing the modeled runoff to the observed runoff and detailing the bias and goodness-of-fit statistics calculated for that model was produced.

## *4.3. RESULTS AND DISCUSSION*

### 4.3.1. Model Goodness-of-Fit Results

Tables 4-1 and 4-2 present the input information and model results for nine runoff events between various gage pairs. It is important to note that LI was not added to every event. Lateral inflow was added on a case-by-case basis, when it appeared that the addition of LI could improve upon the goodness-of-fit statistics. The Walnut Gulch data files did not indicate whether or not LI occurred. The ratio of

52

the downstream-to-upstream volumes ranged from 12% to 65%. In general, the

relative biases were more negative for low values of the ratio of the downstream to

upstream volumes of flow. As an example, the model of the flow event of August 4,

2007, which had a volume ratio of 0.1161, had a bias of -40%, a standard error ratio

greater than 0.8, and a correlation coefficient of less than 0.6. To a lesser extent this

was also evident in the event that occurred on June 17, 2000, for which the volume

ratio was 0.2259 and the model had a relative bias of approximately -10%, a standard

error ratio greater than 0.45, and a correlation coefficient of 0.89. In general, as the

volume ratio approached 0.5, the relative biases lessened to less than -10%, the

standard error ratios improved to less than 0.5, and the correlation coefficients

increased to greater than 0.9. In the process of optimizing the model parameters for

these events, improvement in one goodness-of-fit statistic (bias or standard error)

occurred with a simultaneous loss of accuracy in the other statistic (standard error or

bias, respectively). To further evaluate the performance of the STTL Model several

graphs comparing the observed and predicted downstream flow events were created.

These figures are presented in Appendix A.

**Table 4-1: Model Input Information**

| Date of Event | 7/20/07 | 8/05/99 | 8/11/06 | 8/06/07 | 8/04/07 | 8/17/07 | 6/17/00 | 8/04/07 | 7/20/07 |
|---|---|---|---|---|---|---|---|---|---|
| Gage Pair | 6→2 | 6→2 | 6→2 | 6→2 | 6+3→2 | 6+3→2 | 4→3 | 4→3 | 2→1 |
| Upstream Volume ($*10^5$ $m^3$) | 1.4041 | 0.4954 | 2.3352 | 1.582 | 2.4977 | 3.8837 | 0.1473 | 0.0856 | 0.9416 |
| Downstream Volume ($*10^5$ $m^3$) | 0.6663 | 0.2647 | 1.258 | 0.7777 | 0.2901 | 2.4091 | 0.0333 | 0.0560 | 0.5695 |
| Downstream Volume/ Upstream Volume | 0.4745 | 0.5343 | 0.5389 | 0.4916 | 0.1161 | 0.6203 | 0.2259 | 0.6547 | 0.6048 |
| Channel Length (m) | 5574 | 5574 | 5574 | 5574 | 5308 | 5308 | 2400 | 2400 | 8096 |
| Lateral Inflow (%) | 10 | 0 | 0 | 0 | 0 | 0 | 0 | 10 | 30 |

**Table 4-2: Results of Model**

| Date of Event | 7/20/07 | 8/05/99 | 8/11/06 | 8/06/07 | 8/04/07 | 8/17/07 | 6/17/07 | 8/04/07 | 7/20/07 |
|---|---|---|---|---|---|---|---|---|---|
| Gage Pair | 6→2 | 6→2 | 6→2 | 6→2 | 6+3→2 | 6+3→2 | 4→3 | 4→3 | 2→1 |
| Predicted Downstream Volume ($*10^5$ m$^3$) | 0.6305 | 0.2407 | 1.1606 | 0.7186 | 0.1740 | 2.3055 | 0.0302 | 0.0539 | 0.5814 |
| $f_o$ (mm/hr) | 425 | 5834 | 1500 | 2674 | 2064 | 2747 | 550 | 280 | 494 |
| $f_c$ (mm/hr) | 69.3 | 49.3 | 10.0 | 9.1 | 294.0 | 150.0 | 522.1 | 73.6 | 36.0 |
| $f_o/f_c$ | 6.13 | 11.84 | 150.00 | 293.80 | 7.02 | 18.32 | 1.05 | 3.80 | 13.71 |
| k (hr$^{-1}$) | 0.352 | 34.370 | 1.850 | 4.447 | 0.010 | 1.575 | 0.027 | 4.182 | 4.820 |
| C | 0.051 | 0.076 | 0.116 | 0.198 | 0.098 | 0.132 | 0.099 | 0.091 | 0.050 |
| Relative Bias | -0.054 | -0.091 | -0.078 | -0.076 | -0.400 | -0.043 | -0.094 | -0.039 | 0.021 |
| $S_e/S_y$ | 0.501 | 0.369 | 0.425 | 0.322 | 0.823 | 0.195 | 0.454 | 0.366 | 0.758 |
| R | 0.866 | 0.930 | 0.906 | 0.947 | 0.571 | 0.981 | 0.893 | 0.932 | 0.655 |
| $R^2$ | 0.751 | 0.864 | 0.820 | 0.897 | 0.326 | 0.962 | 0.798 | 0.868 | 0.430 |

## 4.3.2. Analysis of Fitted Parameters

In evaluating the results for both the reach-to-reach and the storm-to-storm events a large variation in the TL parameters $f_o$, $f_c$, and K occurred, while the routing coefficient varied little, from 0.05 to 0.2. In general, the values of $f_o$ and C were positively correlated, as shown in Figure 4-2. If the soils were relatively dry, then the initial infiltration capacity was high and a relatively large value of C was needed to ensure that too much transmission loss did not occur. Generally, the routing coefficient C was lower when lateral inflow was included, i.e. mean values of 0.064 versus 0.120. A smaller routing coefficient tends to reduce the peak outflow because the water is kept in channel storage for a longer period of time, which has the additional effect of increasing TL.

The values determined for Horton's decay coefficient K varied significantly between events. The K values ranged from 0.01 to 34.37 hr$^{-1}$, with most of the values falling between 1.5 and 4.8 and a median value of 1.85 hr$^{-1}$. Because K is the rate at which the transmission loss rate drops from the initial capacity $f_o$ to the ultimate rate $f_c$, a large value of K would indicate a very rapid decline from the initial to the ultimate infiltration rate. The value of K will vary with the shape of the upstream hydrograph. When calibrating a relatively flat hydrograph with low volumes at the

start of the storm, the TL capacity does not drop rapidly. Thus, a low K is expected. For a rapidly rising upstream storm hydrograph, the capacity will drop quickly, which produces a large value of K. It would not be unexpected to see such a sudden drop off in infiltration rate in an arid region where a high initial infiltration rate would lead to a rapid decrease in infiltration capacity. The flow event which had a K value of 0.01 also had the poorest goodness-of-fit statistics of any of the events. This event also had very high infiltration rate parameters, which would imply that the channel experienced high TL during this event. Because the modeled TL would be so large, the model would predict a very low runoff volume, which led to a large negative bias.
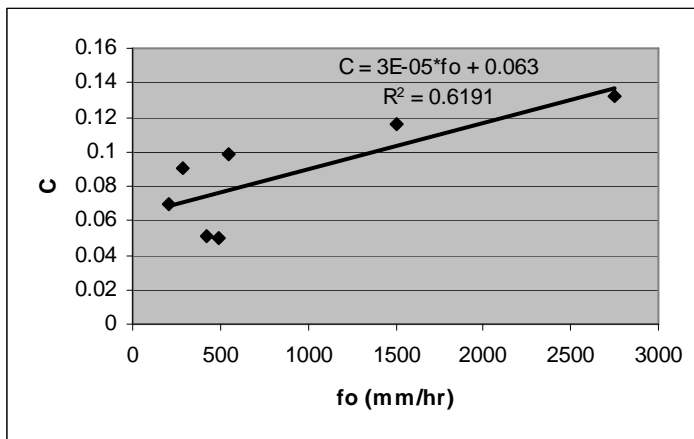


**Figure 4-2: Relationship Between $f_o$ and C Values Determined by STTL Model**

## 4.3.3. Storm-to-Storm Variation

Variation in the model parameters between storms for the same gage pair were examined for two purposes. First, one objective was to determine if one set of parameters could apply to that region of the watershed under multiple storm conditions. Second, another objective was to identify the data characteristics that influenced the ability of the model to fit the measured data. For instance, could a particularly high or low antecedent moisture condition explain a given set of model results? If this was found to be the case, a set of guidelines could be developed to

help model users find the correct parameter values for the conditions that they wished to model.

The first step was to assess the storm-to-storm variation of the coefficients. For the six storm events that occurred at either gage 6 into 2 or gages 6 and 3 into 2 the range of parameter values, the mean parameter values, the standard deviations of the parameter values, and the coefficients of variation were computed.  The initial infiltration capacity ($f_o$) was found to range from 425 mm/hr to 2747 mm/hr.  The mean of this was 1666 mm/hr, and the standard deviation was 1008 mm/hr.  This resulted in a coefficient of variation of 0.61.  For the ultimate infiltration capacity ($f_c$) the range was 9.1 mm/hr to 294 mm/hr, with a mean of 97 mm/hr and a standard deviation of 110 mm/hr, which yields a coefficient of variation of 1.13.  The decay coefficient (K) ranged from 0.01 hr$^{-1}$ to 34.37 hr$^{-1}$, with a mean of 7.1 hr$^{-1}$, and a standard deviation of 13.45 hr$^{-1}$.  The coefficient of variation for K was 1.89.  The routing coefficient (C) ranged from 0.051 to 0.198, with a mean of 0.112 and a standard deviation of 0.051, resulting in a coefficient of variation of 0.455.  The higher the coefficient of variation the more variable the results are for a given parameter.

In evaluating the storm-to-storm variation it appears that the decay coefficient and the ultimate infiltration coefficient have the highest variability.  These values could not likely be transferred to another event without causing serious inaccuracies.  The variation in initial infiltration capacity is also fairly high, indicating that these values should not be transferred to other events.  The variation in routing parameter,

however, may be low enough to apply the mean values to other events without causing significant inaccuracies.

Without examining the rainfall data for a given time period prior to these flow events it is difficult to quantify the exact reasons for the variation in infiltration parameters between storms. The high storm-to-storm variation in the three parameters of Horton's equation can likely be explained by differences in antecedent moisture conditions, which would influence the initial infiltration rate during an event. It is also possible that differences in rainfall characteristics such as intensity and duration could explain some of this variation in infiltration parameters. For instance, a high intensity storm would likely produce high runoff and little infiltration, while a low intensity storm would result in high infiltration and little runoff. Similarly a long duration storm may completely satisfy the infiltration capacity of the channel and cause high runoff towards the end of the storm, while a short duration storm may never completely satisfy the infiltration demand, in which case most of the flow could become TL.

### 4.3.4. Site-to-Site Variation

Site-to-site variation in model parameters was examined to determine whether or not one set of parameters could be valid for the entire watershed. In the nine studies conducted and presented in Tables 1 and 2, three stream sections were studied. To compare the variation between the sites, average values of each parameter were determined for the sites where multiple events had been studied (i.e., gages 6 into 2 or gages 6 and 3 into 2, and gage 4 into 3). These averages were assumed to be representative of that particular site. This yielded one set of

parameters for each of the three sites in question. The initial infiltration capacities ($f_o$) ranged from 280 mm/hr to 1666 mm/hr, with a mean of 858 mm/hr and a standard deviation of 701 mm/hr, which yields a coefficient of variation of 0.82. The ultimate infiltration capacities ($f_c$) ranged from 36 mm/hr to 522 mm/hr, with a mean of 137 mm/hr, a standard deviation of 137 mm/hr, and a coefficient of variation of 1. The decay coefficients (K) ranged from 0.027 $hr^{-1}$ to 7.101 $hr^{-1}$, with a mean of 4.67 $hr^{-1}$, a standard deviation of 2.5 $hr^{-1}$, and a coefficient of variation of 0.54. The routing coefficients (C) range from 0.05 to 0.132, with a mean of 0.086, a standard deviation of 0.032, and a coefficient of variation of 0.37. The site-to-site variation shows that the initial and ultimate infiltration capacities have the highest variation, and therefore should not be transferred to other sites on the watershed. The decay coefficient also had a fairly high coefficient of variation and is likely too variable to be transferred from one location to another. However, the routing coefficient had a fairly low variability, and could likely be transferred throughout the watershed without introducing undue error.

The site-to-site variation can likely be explained by variations in soil properties. A detailed soil map of Walnut Gulch Experimental Watershed shows the large variation in soil types from one portion of the watershed to the next. The different soil types will have different infiltration properties, which would lead to differences in the infiltration parameters determined in the model. Reasoning similar to that presented for the storm-to-storm variation can also apply to site-to-site variation. Differences in both antecedent moisture conditions and storm characteristics are also a possible explanation for site-to-site variation. Previous

storms may have affected different portions of the sites in the watershed differently, leading to different antecedent moisture conditions in different portions of the watershed. Also variations in storm characteristics such as intensity or duration across the watershed would influence the infiltration parameters at different locations.

### 4.3.5. Effects of Lateral Inflow

A significant volume of lateral inflow can mask the effect of transmission losses. With no LI, the volume and peak of the upstream hydrograph should decrease as the flood wave moves downstream. However, as the volume of LI increases, the water volume reduction due to TL will be offset such that a decrease in volume and peak at the downstream section may not be evident from the measured flow. The runoff entering the stream as LI may approximately match the water infiltrated from the channel as TL. If the only measurements are the upstream and downstream hydrographs, the effects of TL and LI may not be evident.

The shape, volume, and peak of the downstream hydrograph depend on the corresponding characteristics of the upstream hydrograph, the TL characteristics of the channel bed, and the magnitude and timing of any LI to the channel. Lateral inflow can also have a significant effect on the distribution of TL along the channel, not just the characteristics of the downstream hydrograph. Lateral inflow into a channel subsection occurs before streamflow from the upper gage is routed to the cells, thus satisfying a portion of the TL demand of that cell. As the infiltration demand of a cell decreases, a higher percentage of the streamflow ultimately routed to the cell will remain in surface storage and be routed to the next cell. This increases both the volume and the peak flow of the downstream hydrograph.

Figure 4-3 shows the effect that LI has on the distribution of TL along a channel. The same scenario was modeled four times for the July 20, 2007, event, with increasing amounts of lateral inflow. The control run, with no LI, demonstrates that, as the flow travels downstream, the volume of TL decrease because streamflow is less and, therefore, from a physical standpoint, the pressure head is lower. This lower head means that storage in the cells along the reach will cause water to infiltrate at a lower rate than from the cells upstream. As LI is added, the head in each cell increases such that a higher volume of water infiltrates into the downstream cells than they could infiltrate when lateral inflow was not present. As Figure 4-3 shows, as the volume of LI added to the stream increases, the downstream cells are able to infiltrate larger volumes of water, leading to increasing TL volumes. The total TL of Figure 4-3 indicate that, when the LI is about 20% of the volume of the upstream hydrograph, the lateral inflow volume offsets the volume of transmission losses such that the measured downstream hydrograph would suggest that TL were not a factor. Table 4-3 illustrates the effects that LI can have on the downstream hydrograph volume, the predicted downstream hydrograph peak, and the downstream-to-upstream volume ratio for the same modeling scenarios as shown in Figure 4-3.

The assumption of LI affects both the TL hydrograph and the accuracy of the model calibration. Measurements of lateral inflow are generally not available, so the actual volume and distribution of LI is generally not known. However, LI can affect the characteristics of the downstream hydrographs, so an incorrect assumption can cause the calibration to yield inaccurate parameter estimates and poor goodness of fit.

The magnitude of LI could be estimated using a standard computer program such as TR-20 if desired, but again, without the presence of gages along the stream bank, there is no method of determining LI that is completely accurate.

To better understand the effect that LI has on the results of the STTL model, including the model parameter estimates and the goodness-of-fit statistics, the August 5, 1999, event was modeled three times. First the scenario was modeled with no LI, to serve as a control, then the scenario was modeled with 10% LI, and finally the scenario was modeled with 30% LI. Table 4-4 provides a summary of these results. The final infiltration parameter values showed significant variation with amount of lateral inflow. With increasing amounts of LI, the initial infiltration rate ($f_o$) decreased and the ultimate infiltration rate ($f_c$) increased, to the point that the difference between the two values is quite small. A clear trend is not evident for the variation in K values in this situation, as K was a less sensitive parameter; however, it is quite clear that the presence of LI influences the final parameter values. The routing coefficient did not change significantly with the addition of LI; however, the decreasing trend is logical as explained earlier.

In actual situations, the amount of LI is not known, so an assumption must be made. The amount assumed will influence both the goodness-of-fit statistics and the model parameters. When LI occurs, less water needs to be removed from storage in the stream to satisfy the infiltration demand, so the routing coefficient decreases. The goodness-of-fit statistics for the scenario in which 30% lateral inflow was added are poorer than statistics from the other cases because in this situation 30% lateral inflow is too high, and the model is being forced to overpredict the flow. A lower amount of

LI, such as 15% or 20%, would probably have had somewhat better goodness-of-fit

statistics; however, 30% lateral inflow was chosen in this case to show the effect that

a larger than necessary amount of LI could have on model results.
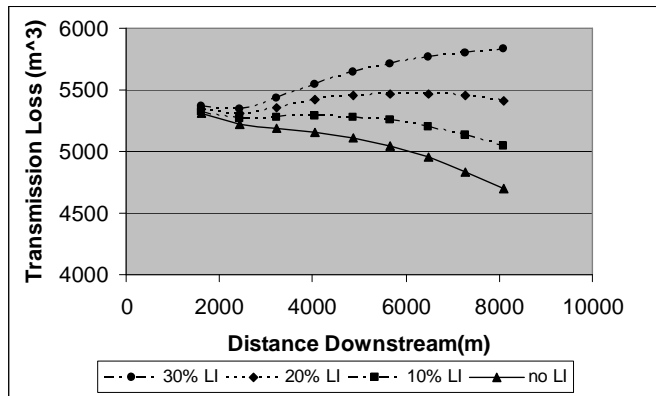


**Figure 4-3: Effect of Lateral Inflow on Transmission Loss Distribution**

**Table 4-3: Effect of Lateral Inflow on Model Results**

|  | 0% LI | 10% LI | 20% LI | 30% LI |
|---|---|---|---|---|
| Computed Downstream Volume ($*10^5$ $m^3$) | 0.4380 | 0.4818 | 0.5256 | 0.5695 |
| Predicted Downstream Peak Flow ($m^3/s$) | 215 | 250 | 283 | 313 |
| Downstream Volume/ Upstream Volume | 0.6047 | 0.6047 | 0.6048 | 0.6048 |

**Table 4-4: Comparison of One Event with Varying Amounts of Lateral Inflow**

|  | 0% LI | 10% LI | 30% LI |
|---|---|---|---|
| $f_o$ | 584 | 200 | 74 |
| $f_c$ | 49 | 59 | 66 |
| k | 34.37 | 7.974 | 29.90 |
| C | 0.0764 | 0.0697 | 0.0500 |
| Relative Bias | -0.0906 | -0.0826 | 0.0819 |
| $S_e/S_y$ | 0.3694 | 0.3695 | 0.4860 |
| R | 0.9296 | 0.9296 | 0.8746 |
| $R^2$ | 0.8642 | 0.8641 | 0.7648 |

## 4.3.6. Advantages of Spatio-Temporal Transmission Loss Model

The Spatio-Temporal Transmission Loss (STTL) model, which was

developed to account for TL in arid climates, has several advantages. First, the model

is based on physical principles. A channel routing method based on the continuity of

mass and storage is utilized. Most other methods only account for the total volume of TL based on the reduction in hydrograph volume and peak flow. Because channel routing was used and the channel was divided into multiple cells, the model allows for TL to be evaluated in both time and space. The model uses an established infiltration method to account for losses into the channel. Therefore, the values determined for the infiltration parameters and the routing coefficient have a physical basis.

Second, the STTL model can allow for the presence of LI. As demonstrated previously, the presence or absence of LI can have a significant effect on the distribution of TL with distance downstream and on the parameters and the accuracy of the fit. Third, the volume of TL can be determined at any point along the length of the reach. This can be done by using multiple cells, and then fitting an equation to the TL distribution provided in the model output. Fitting an equation based on predictions for each of the cells allows the calculation of transmission loss at any point in the stream, as opposed to providing transmission loss estimates only at certain locations based on the cell size. Fourth, this method could easily be adapted to allow for variation of the infiltration parameters along the length of the stream. This would be highly advantageous when studying a long stream reach or a watershed that had high variability in soil characteristics.

### 4.3.7. Comparison to Lane's Model

The NRCS method of Lane *et al*. (2007) is currently the most widely used method of computing volumes of TL. The STTL method has much in common with Lane's method of computing TL for arid environments. Both calculate a volume of

TL based on upstream and downstream flow records, and both can take into account the effect that LI can have on the streamflow. Both methods can predict the change in downstream flow volume and peak that will result from TL. Despite these similarities, however, a number of differences exist between the methods.

The STTL method and the method developed by Lane rely on different underlying theories. Lane used a differential equation as the basis for his model, while the STTL method is based on the principles of channel routing and Hortonian infiltration. As a result of this, the parameters (three infiltration parameters and a routing coefficient) have a physical meaning. Further, the use of four parameters in this method, as opposed to two parameters used in Lane's method, increases the flexibility of this model as compared to Lane's model.

Another key difference between the models is when and how the models approach zero. To predict TL along the length of a channel, Lane's model uses an exponential decay model that approaches zero as distance down the channel increases. In contrast, TL in the STTL model approaches zero only when $f_c$ (the ultimate infiltration capacity) is very small. The routing coefficient C also influences the decay in this model. The use of the downstream hydrograph is a third key difference between the two models. Lane's model uses end-of-channel volumes to calibrate its coefficients, while the STTL model uses the hydrograph ordinates. Using the hydrograph in this model means that the shape of the hydrograph will influence the parameter values.

In order to calibrate Lane's model, linear least squares is used between multiple events. Also, only upstream and downstream volumes of the total

streamflow are required.  The regression parameters determined from the linear least squares analysis determine the exponential decay value for the model.  The linear least squares regression model requires that that multiple storm events be analyzed to determine parameter values.  The STTL model, on the other hand, is able to determine parameter values using only one storm event.  This is especially advantageous when data are sparse.  However, because more data are used, the calibration process is more involved than the calibration process for Lane's method.

A final important difference between the STTL model and Lane's model is the ability to calculate TL at intermediate points.  Lane's model provides a regression equation that could calculate the TL at any point along the channel.  In comparison, the STTL model can only calculate TL at intermediate locations along the channel if multiple cells are used in the model.  Transmission losses would then be calculated for each cell.  Alternatively, if multiple cells are used, an equation could be fit to the points given that define the spatial distribution of the TL.  With an equation fitted to the TL distribution, then TL could be calculated for any point along the channel.

Another program was written and used to compare the STTL method to Lane's method.  This new program took the same data that was used in testing the STTL method and computed results based on Lane's method.  Figures 4-4, 4-5, and 4-6 illustrate the varying degrees of agreement in results between the STTL method and Lane's method.  The flow event occurring on August 17, 2006, gave almost perfect agreement in calculated downstream volume between the methods.  However, the event occurring on August 11, 2006, showed an overprediction in downstream volume, meaning an underprediction of TL, by Lane's method.  Conversely, the event

occurring on August 5, 1999, showed an underprediction of downstream volume, and thus an overprediction of TL, by Lane's method as compared to the STTL method. The differences between the results of the two models for the August 5, 1999, event required further investigation. As reported in Table 4-2, this event had the highest K value of any event modeled, which was believed to account for the difference between the model results. The hydrograph for this event was found to have a double peak and a rapid, steeply sloped rise time, which may have influenced the K value. Because the STTL model is based on one hydrograph and Lane's model is based on regression of five total streamflow volumes, this difference between the results of the two methods for an event with an unusual hydrograph is not unexpected.
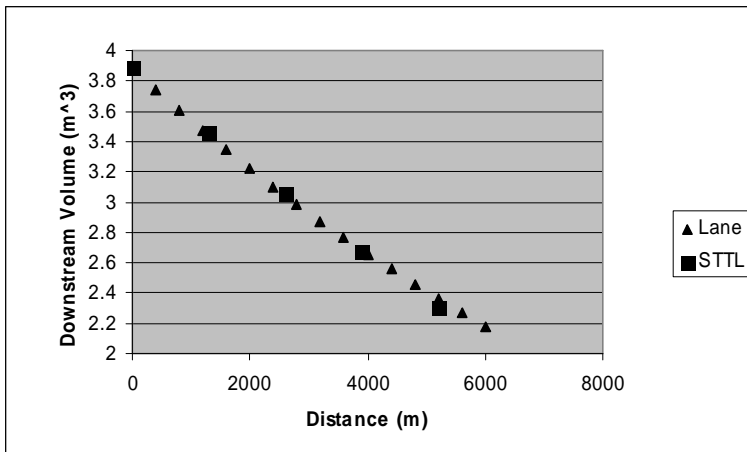


**Figure 4-4: Good Agreement Between Lane and STTL Methods for 8/17/2006**
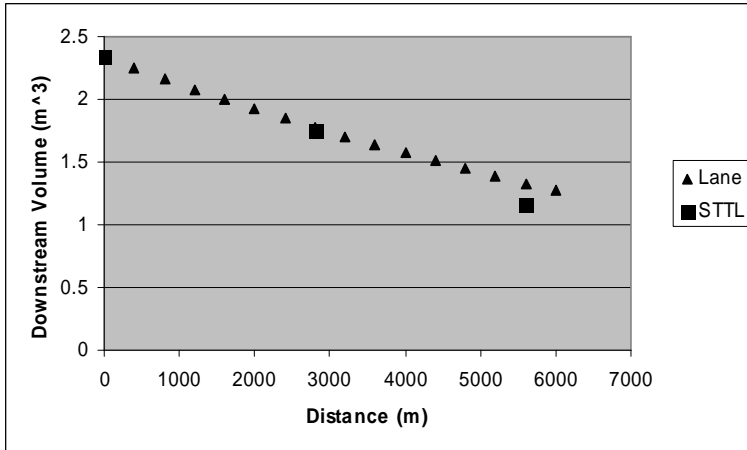
**Figure 4-5: Moderate Agreement Between Lane and STTL Methods for 8/11/2006**
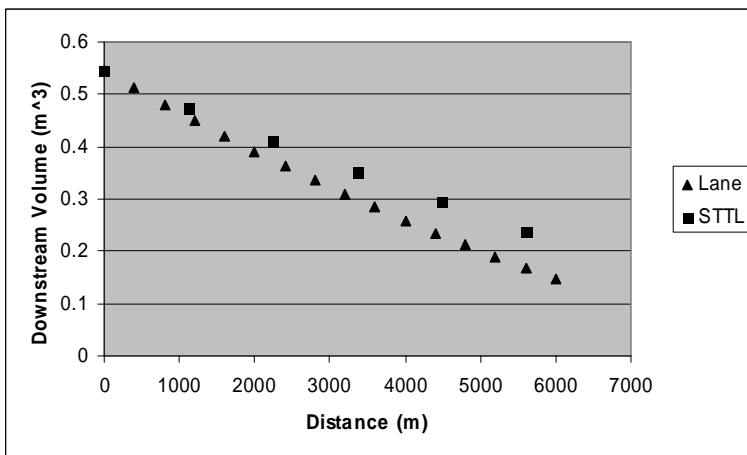


**Figure 4-6: Poor Agreement Between Lane and STTL Models for 8/5/1999**

## 4.4. CONCLUSIONS

A model was developed with the ability to estimate transmission losses along a channel reach while routing the floodwave through the channel. The three Hortonian infiltration parameters ($f_o$, $f_c$, and K), as well as a routing coefficient (C) were optimized using the nonlinear least-squares method, and then used to model streamflow routing and TL into the channel bed material. The model also allows the addition of LI from the watershed surrounding the stream reach into the channel. The Walnut Gulch Experimental Watershed located near Tucson, Arizona, was chosen as the location for this study because it is heavily gaged and because data are easily

67

available.  Flow gage data for several combinations of upstream and downstream flow gages were collected and used to calibrate and test this model.  Analyses of both storm-to-storm variation and site-to-site variation were made, in the hope of determining an average parameter set that would apply under many conditions throughout the watershed.  Unfortunately it was seen that the variation in parameters was so high that average parameters could not be accurately used to predict TL.  However, when the numerical optimization scheme was used to determine appropriate parameter values for each storm event and for each stream reach, the model was seen to perform well, with acceptable bias and goodness-of-fit statistics in nearly all of the test cases.

The STTL model allows for analyses of TL based on flow hydrographs, rather than just total flow volumes.  Thus, the model parameters are sensitive to more than just the total volume under the hydrograph, with the model parameters reflecting how TL vary with time and along the lengths of the channel.  This method is also based on the physical processes of Hortonian infiltration and channel routing.  The model allows for the input of LI into the channel reach, and TL could fairly easily be determined for any point along the channel.  Also, this model would be fairly easy to adapt to allow for variation in parameters along the channel.

Further research is still needed in many areas to more accurately predict TL in arid and semi-arid climates.  A method for estimating LI when such measurements are not readily available would help improve the accuracy of transmission loss predictions.  If information about antecedent soil moisture condition or antecedent precipitation could be collected it could be related to the infiltration parameters $f_o$, $f_c$,

and K.  Knowledge of the storm event antecedent moisture condition in combination with knowledge about storm characteristics could aid in explaining the variations seen in both site-to-site and storm-to-storm analyses.  Similarly, measures of soil porosity and its variation along a channel reach could help explain variations in the optimum infiltration parameters determined by the model.

# CHAPTER 5

# ANALYSES THAT INVOLVE RADAR RAINFALL

## *5.1. INTRODUCTION*

The traditional method for measuring rainfall is the rain gage.  Rain gages, however, only measure point rainfall, so an estimation method is necessary in order to derive spatial rainfall characteristics.  According to Chumchean *et al*. (2003), the accuracy of rain gage data in representing average rainfall over a large area is quite low.  Deriving spatial characteristics of rainfall can be especially difficult when a low rain gage density exists in a watershed, as is often the case.  Due to these problems associated with rain gage data, as well as other potential inaccuracies in rain gage data, many hydrologists have begun to consider the idea of either replacing or supplementing rain gage data with radar measurements.  According to Hoblit and Curtis (2002) merging radar and rain gage data would combine the strengths of each data set while reducing the weaknesses associated with each of them.   Radar data has the ability to provide spatial characteristics of rainfall events much more easily than rain gage data; however, the technology is still being improved and sources of error are still being identified and reduced or eliminated.  According to Krajewski and Smith (2002) radar-rainfall data has great potential for use in runoff and flood forecasting models, which should soon be realized in application.  A few applications in which they believe that radar data could be useful include design of flood control structures, control of urban storm water systems, water supply forecasting,

groundwater recharge assessment, and non-point source pollution assessment (Krajewski and Smith, 2002).

### 5.1.1. Errors and Problems Existing in Radar Data

Many sources of error in radar data have been identified. Gerstner and Heinemann (2008) identified several sources of error related to the radar beam itself and to interpretation of the radar readings. The radar beam itself could be attenuated by heavy rainfall, ground clutter could interfere with the beam, or beam occlusion could occur. Radar data does not provide information about rainfall directly. Rather, the radar beam is reflected off of raindrops in the air and the scatter of the beam that is reflected back to the radar station is measured. A relationship between this reflectance and rainfall rate is used to transform the radar readings to useful information about the rainfall. This equation is called the reflectance (Z) – rainfall rate (R) relationship. Many Z-R relationships are possible, and the choice of equation can influence the amount of rainfall that was measured. Therefore the choice of Z-R equation is a potential source of error in radar measurements (Gerstner and Heinemann, 2008). They conclude that, while these errors remain strong, radar data can not currently take the place of rain gage data in hydrological applications.

Sharif *et al.* (2004) also discussed the relationship between reflectance and rainfall rate as a source of error in radar data. They state that no unique relationship exists between the two, making accurate conversion between them difficult. They also suggest other reasons for inaccuracies in radar measurements, including the curvature of the earth and atmospheric refraction caused by the height of the radar beam increasing with distance away from the radar station. This means that, as the

distance between the radar station and the location being measured by the radar increases, the radar beam is measuring at a higher distance above the ground surface. Because of this, for large enough distances away from the radar station it cannot be assumed that the radar rainfall readings are representative of the rainfall falling at the ground. Many processes, including wind drift and evaporation, could alter the rainfall between the location of the radar measurement and the ground surface. Sharif *et al.* (2004) cite a study done by Kitchen and Jackson (1993) that claims that the range effect described above could be one of the major causes of observed underestimation of rainfall accumulation by radar.

Islam *et al.* (2008) specifically discussed the errors that wind could cause in radar rainfall measurements. They state that wind gusts could cause rainfall to drift and be horizontally displaced by up to several kilometers between the point in the air at which the radar measured the rainfall and the point at which the rainfall hits the ground. If raindrops do not fall directly vertically, but rather drift some distance horizontally, there will be a mis-match between radar data and corresponding rain gage data. If rain gage data were being used to calibrate radar data or check for accuracy this could cause significant problems. However, Islam *et al.* (2008) believed that with the addition of an algorithm to correct for wind drift the agreement between radar and rain gage data could be much improved.

Young (2008) compared radar and rain gage data for an area in Mississippi to quantify their differences. He examined the long-term bias in radar data, as well as the correlation between the rain gage and radar data for multiple time periods. In plotting this data, he observed a high degree of scatter between the rain gage and

radar data, indicating that good agreement between the two data sets, which should essentially be measuring the same rainfall, did not exist. In examining the bias between the two data sets, he found that during the cold season an overall bias of -39% existed, while during the warm season the overall bias was only -32%. This finding of under-prediction of rainfall by the radar data has also been found in many other studies.

Despite the many sources of errors and problems with radar data, there still exists great potential for radar data to be utilized in hydrological applications in the future. As stated earlier, the radar data can much more easily provide spatial information about rainfall events, saving the expense of a dense rain gage network. When some of the error sources discussed above, including accounting for wind drift, beam occlusion, and the use of improper Z-R relationships, have been reduced, radar data will likely be a valuable tool to hydrologists.

## *5.2. ANALYSIS OF SPATIAL DATA PROBLEMS USING SYNTHETIC DATA*

### 5.2.1. Introduction

It is often helpful to set up analyses using synthetic data prior to analyzing observed data. In this case, synthetic data were analyzed to draw conclusions about the smoothing effect that various point rainfall averaging methods could have compared to true spatial rainfall data. Both the arithmetic averaging method and the Thiessen polygon method were investigated for averaging point rainfall measurements. Preliminary conclusions about the effect of pixel size, area associated with each rain gage, amount of rainfall, and rainfall pdf on the estimated rainfall

averages for a pixel were also made. The conclusions from this preliminary study could then be used to guide more detailed investigations into the accuracy of radar data compared to rain gage data.

The overall goal of this analysis was to assess the interaction of pixel size and the spatial extent of storm rainfall. This goal is assessed using a simulation approach so that relevant variation can be controlled. The specific objectives used to meet this goal were: (1) to show the effect of storm peakedness within a pixel on the variance reduction of Thiessen and arithmetic average storm rainfall methods; (2) to examine the effect of storm magnitude on variance reduction with the averaging methods; and (3) to evaluate the effect of the randomness of rainfall rates on observations made from the previous analyses.

A simulation program was developed that could compute the arithmetic and Thiessen polygon rainfall averages for a given pixel from two rain gages. This program allowed the user to specify the number of simulations, the minimum rainfall depth and the slope of the rainfall depth surface, the distribution of error in the rainfall, and the fraction of the pixel area assigned to each rain gage. Rainfall was computed as the sum of systematic and nonsystematic components. The systematic component was a linear model with a user specified slope, including zero. The nonsystematic variation could be generated from any one of five distribution functions with user specified parameters. Based on the user specified mean and slope, the rainfall depth surface was assumed to vary linearly over the pixel. The program output provided the mean and standard deviation of the rainfall depth

74

measured at each gage, as well as the mean and standard deviation of the rainfall

averages computed by both the arithmetic method and the Thiessen polygon method.

## 5.2.2. Effect of Pixel Size Variation

### 5.2.2.1. Methods and Materials

Over the spatial extent of a rainfall event, the depth is expected to vary. As

the area increases, the variation in depth should increase. To show spatial variation in

the rainfall depth, the slope of the rainfall depth surface was changed to simulate

change in the size of the pixel. An increased slope yields greater variation in rainfall,

which simulated a larger spatial area, while a decreased slope simulated a more

uniform rainfall that is expected over a smaller pixel. The first analysis investigated

whether or not the size of the pixel influenced the amount of smoothing done by the

rainfall depth averaging methods. Four scenarios were set up to evaluate this

analysis, with only the slope of the rainfall depth surface varying between them.

Slopes of 1.5, 3, 4.5, and 6 were evaluated in the study. The minimum depth of

rainfall simulated was 2 mm, and a normal pdf with a mean of 2 and a standard

deviation of 0.4 was used for the random component of the rainfall depth.

### 5.2.2.2. Results and Discussion

All averaging methods smooth data. For example, moving average filtering is

used to smooth hydrologic time series. The arithmetic average and Thiessen polygon

methods are commonly used for spatial averaging of rainfall data. The smoothing of

rainfall data reduces the variation, i.e., the standard deviation, while preserving the

mean. While variance reduction is at times desirable, in other cases it can mask a

relationship with another variable. In the case of radar rainfall data and point rain

gage data, smoothing of the spatial estimates of the point measurements could mask

75

the correlation between spatially distributed radar rainfall estimates and areal estimates based on point measurements.

The results of the simulation analyses were evaluated in terms of loss of variation between the areal averaged gage-measured rainfall depths and the calculated average rainfall depths. The standard deviations of the rainfall depths at the gages were considered to reflect the true variation in the rainfall depth, while the standard deviations of the arithmetic and Thiessen polygon averaging methods represented the variation in areal averaged rainfall depth. The standard deviation of rainfall depth measurements reported for a rain gage was subtracted from the Thiessen polygon standard deviation and the arithmetic average standard deviation. The rain gage standard deviations were subtracted from the averaging method standard deviations so that a negative difference would emphasize the loss in variation due to smoothing by the averaging method.

The first analysis investigated the effect that cell size has on the average rainfall depth by varying the slope of the rainfall depth surface in the program. A greater slope yields a more peaked rainfall event which reflects a greater pixel size. The results of this study are presented in Table 5-1, and the summary of loss of variation is presented in Table 5-2. In examining Table 5-2, it is evident that the Thiessen polygon method has a smaller loss of variation than the arithmetic averaging method. Specifically, the standard deviations for the Thiessen estimates are much closer to the gage estimates than are the arithmetic average estimates, which is evident from the smaller differences in Table 5-2. This means that the Thiessen

polygon method is smoothing the rainfall depth results less than the arithmetic method when the average rainfall for a pixel is calculated based on two rain gages.

It is interesting to note here that in some cases the Thiessen polygon method had a standard deviation higher than the standard deviation for one of the rain gages, resulting in a positive difference between the two. For instance, the difference between the Thiessen polygon standard deviation and the standard deviation for rain gage 1 was -0.078 for a rainfall surface slope of 1.5, but the difference was 0.028 for a rainfall surface slope of 6. This does not imply that the Thiessen method introduces variation in these scenarios. Instead, it reflects the fact that the rainfall depth surface for one rain gage is greater than the other gage, and thus has a higher standard deviation. The Thiessen method averages the rainfall depth based on the values at the two gages, therefore when one gage has a significantly higher standard deviation than the other, it is expected that the Thiessen polygon standard deviation will be higher than the standard deviation of the gage receiving the lower rainfall amount.

It is also interesting to note that while the difference between the Thiessen polygon method standard deviations and the rain gage standard deviations become less negative as the slope of the rainfall surface increases, the difference between the arithmetic method standard deviations and the rain gage standard deviations becomes more negative as the rainfall surface slope increases. For instance, the difference between the arithmetic standard deviation and the standard deviation of rain gage 1 is -0.132 for a slope of 1.5, but the difference is -0.279 for a slope of 6. This indicates that the absolute smoothing of the arithmetic averaging method increases as the variability of the rainfall surface increases. However, when computing the ratios of

the standard deviations of the arithmetic method to the standard deviations of the rain

gages, it is seen that the ratio is relatively constant. The ratio of the standard

deviation of the arithmetic method to the standard deviation of rain gage 1 for a

rainfall surface slope of 1.5 is 0.711 while the ratio is 0.705 for a rainfall surface

slope of 6. This indicates that while the absolute smoothing increases with increasing

storm variability, the relative smoothing remains constant as the storm variability

increases.

**Table 5-1: Results of Analysis of Changing Pixel Size, where Arith. Means Arithmetic, and Std. Dev. Means Standard Deviation**

| Slope | Gage 1 Mean | Gage 1 Std. Dev. | Gage 2 Mean | Gage 2 Std. Dev. | Thiessen Mean | Thiessen Std. Dev. | Arith. Mean | Arith. Std. Dev. |
|---|---|---|---|---|---|---|---|---|
| 1.5 | 4.37 | 0.45 | 5.12 | 0.45 | 4.75 | 0.37 | 4.75 | 0.32 |
| 3 | 4.74 | 0.58 | 6.25 | 0.58 | 5.50 | 0.55 | 5.50 | 0.42 |
| 4.5 | 5.12 | 0.76 | 7.38 | 0.75 | 6.25 | 0.76 | 6.25 | 0.54 |

**Table 5-2: Summary of Loss of Variation in Averaging Methods for Changing Pixel Size, where Arith. Means Arithmetic and Std. Dev. Means Standard Deviation**

| Slope | Std. Dev. Thiessen-Gage 1 | Std. Dev. Arith.-Gage 1 | Std. Dev. Thiessen-Gage 2 | Std. Dev. Arith.-Gage 2 |
|---|---|---|---|---|
| 1.5 | -0.078 | -0.132 | -0.074 | -0.127 |
| 3 | -0.035 | -0.171 | -0.030 | -0.166 |
| 4.5 | 0.000 | -0.222 | 0.005 | -0.217 |
| 6 | 0.028 | -0.279 | 0.034 | -0.273 |

## 5.2.3. Effect of Rain Gage Area

### *5.2.3.1. Methods and Materials*

Each rain gage within a pixel represents an area within the pixel. A gage near

the boundary of the pixel likely reflects less of the rainfall occurring over the spatial

extent of the pixel than would a gage in the center of the pixel. If one of two gages

represents a relatively large area, then taking the arithmetic average of the two gage

estimates would place too much weight on the less representative gage measurement.

Therefore, it was believed that the portion of the pixel area represented by a rain gage

would influence the amount of smoothing seen in the average rainfall depth

calculations.  The simulation program allowed the user to specify a fraction of the

pixel in which the first gage was located, with the rest of the area assigned to the

second gage.  Seven scenarios were modeled in this case, with the fraction assigned to

the first gage varying from 0.2 to 0.8.  This study was also conducted once with a

rainfall depth surface slope of 0 and a second time with a slope of 3.  A slope of 0

indicated a uniform storm, while a slope of 3 would have linearly increasing rainfall

between the two gages.  Again 2 mm of rainfall were simulated as the minimum

rainfall depth, and a normal pdf with a mean of 2 and a standard deviation of 0.4 was

used to provide the random component of the rainfall depth.

### 5.2.3.2. Results and Discussion

The second analysis evaluated the effect of varying the amount of pixel area

associated with each rain gage.  The results of the analyses with a slope of 0 are

presented in Table 5-3, and a summary of loss of variation due to the averaging

methods is presented in Table 5-4.  Table 5-5 contains the results of the analyses with

a slope of 3, and Table 5-6 contains the corresponding summary of loss of variation.

From the values in Tables 5-4 and 5-6, it is clear that the Thiessen polygon averaging

method generally loses less variation than the arithmetic averaging method, meaning

that less smoothing will result from using the Thiessen polygon averaging method

than from using the arithmetic averaging method.  The differences between the two

methods are more dramatic when the rainfall depth varies more over the pixel.  For

instance, when the rainfall surface was uniform and rain gage 1 had 70% of the pixel

area assigned to it the difference in standard deviations of the Thiessen polygon

method and rain gage 1 was -0.105, while for the same scenario when there was

variability in the rainfall surface the difference between the standard deviations of the

Thiessen method and gage 1 was -0.180.  When the gages represent different areas,

taking the average essentially amounts to assigning an incorrect weight to each gage

estimate.  A slope of 0 results in a uniform storm with no difference in rainfall

between the two gages.  Thus, differences in the variations are expected to be smaller

in this case.

It is again interesting to note that when the rainfall surface varied the standard

deviations calculated for the Thiessen polygon averaging method were in some cases

higher than the standard deviations calculated for one of the two rain gages.  For

instance, when the rainfall surface had a slope to it the difference in standard

deviations between the Thiessen method and rain gage 1 was 0.071, while the

difference in standard deviations between the Thiessen method and rain gage 2 was -

0.174.  This is again due to one of the rain gages receiving a higher amount of rainfall

than the other because of the sloping rainfall surface.

**Table 5-3: Results of Analyses for Varying Fraction of Area Associated with Each Rain Gage with a Slope of 0, where Arith. Means Arithmetic, and Std. Dev. Means Standard Deviation**

| Area Fraction | Gage 1 Mean | Gage 1 Std. Dev. | Gage 2 Mean | Gage 2 Std. Dev. | Thiessen Mean | Thiessen Std. Dev. | Arith. Mean | Arith. Std. Dev. |
|---|---|---|---|---|---|---|---|---|
| 0.2 | 4.00 | 0.399 | 4.00 | 0.394 | 4.00 | 0.299 | 4.00 | 0.280 |
| 0.3 | 4.00 | 0.399 | 4.00 | 0.394 | 4.00 | 0.295 | 4.00 | 0.280 |
| 0.4 | 4.00 | 0.399 | 4.00 | 0.394 | 4.00 | 0.292 | 4.00 | 0.280 |
| 0.5 | 4.00 | 0.399 | 4.00 | 0.394 | 4.00 | 0.291 | 4.00 | 0.280 |
| 0.6 | 4.00 | 0.399 | 4.00 | 0.394 | 4.00 | 0.291 | 4.00 | 0.280 |
| 0.7 | 4.00 | 0.399 | 4.00 | 0.394 | 4.00 | 0.293 | 4.00 | 0.280 |
| 0.8 | 4.00 | 0.399 | 4.00 | 0.394 | 4.00 | 0.297 | 4.00 | 0.280 |

**Table 5-4: Summary of Loss of Variation Due to Averaging for Varying Areas Associated with Each Rain Gage with a Slope of 0, where Arith. Means Arithmetic, and Std. Dev. Means Standard Deviation**

| Area Fraction | Std. Dev. Thiessen-Gage 1 | Std. Dev. Arith.-Gage 1 | Std. Dev. Thiessen-Gage 2 | Std. Dev. Arith.-Gage 2 |
|---|---|---|---|---|
| 0.2 | -0.100 | -0.119 | -0.095 | -0.114 |
| 0.3 | -0.104 | -0.119 | -0.099 | -0.114 |
| 0.4 | -0.107 | -0.119 | -0.102 | -0.114 |
| 0.5 | -0.108 | -0.119 | -0.103 | -0.114 |
| 0.6 | -0.107 | -0.119 | -0.102 | -0.114 |
| 0.7 | -0.105 | -0.119 | -0.101 | -0.114 |
| 0.8 | -0.102 | -0.119 | -0.097 | -0.114 |

**Table 5-5: Results of Analyses for Varying Fraction of Area Associated with Each Rain Gage with a Slope of 3, where Arith. Means Arithmetic, and Std. Dev. Means Standard Deviation**

| Area Fraction | Gage 1 Mean | Gage 1 Std. Dev. | Gage 2 Mean | Gage 2 Std. Dev. | Thiessen Mean | Thiessen Std. Dev. | Arith. Mean | Arith. Std. Dev. |
|---|---|---|---|---|---|---|---|---|
| 0.2 | 4.30 | 0.433 | 5.80 | 0.792 | 4.92 | 0.539 | 5.05 | 0.454 |
| 0.3 | 4.45 | 0.474 | 5.95 | 0.718 | 5.11 | 0.545 | 5.20 | 0.433 |
| 0.4 | 4.60 | 0.526 | 6.10 | 0.648 | 5.31 | 0.549 | 5.35 | 0.420 |
| 0.5 | 4.74 | 0.586 | 6.25 | 0.581 | 5.50 | 0.551 | 5.50 | 0.415 |
| 0.6 | 4.89 | 0.653 | 6.40 | 0.521 | 5.69 | 0.549 | 5.65 | 0.420 |
| 0.7 | 5.04 | 0.723 | 6.55 | 0.469 | 5.88 | 0.544 | 5.80 | 0.433 |
| 0.8 | 5.19 | 0.798 | 6.70 | 0.428 | 6.07 | 0.538 | 5.94 | 0.455 |

**Table 5-6: Summary of Loss of Variation for Varying Fractions of Pixel Area Associated with Each Rain Gage with a Slope of 3, where Arith. Means Arithmetic, and Std. Dev. Means Standard Deviation**

| Area Fraction | Std. Dev. Thiessen-Gage 1 | Std. Dev. Arith.-Gage 1 | Std. Dev. Thiessen-Gage 2 | Std. Dev. Arith.-Gage 2 |
|---|---|---|---|---|
| 0.2 | 0.106 | 0.021 | -0.253 | -0.338 |
| 0.3 | 0.071 | -0.041 | -0.174 | -0.285 |
| 0.4 | 0.024 | -0.106 | -0.098 | -0.228 |
| 0.5 | -0.035 | -0.171 | -0.030 | -0.166 |
| 0.6 | -0.104 | -0.233 | 0.028 | -0.101 |
| 0.7 | -0.180 | -0.290 | 0.075 | -0.035 |
| 0.8 | -0.260 | -0.343 | 0.110 | 0.027 |

## 5.2.4. Effect of Varying Amount of Rainfall

### 5.2.4.1. Methods and Materials

The third analysis investigated the effect that increasing the minimum rainfall depth had on the average rainfall depths. The minimum rainfall depths used were 1 mm, 2 mm, 5 mm, 10 mm, and 15 mm. This analysis was done twice, first with a

slope of 0 and then with a slope of 3. A slope of 0 represented a uniform storm with no systematic variation between the gages, while a slope of 3 had increasing rainfall across the pixel. Again a normal pdf was used with a mean of 2 and a standard deviation of 0.4 to provide the random component of the rainfall depth.

### 5.2.4.2. Results and Discussion

The third analysis considered the impact that varying amounts of rainfall could have on the calculated average rainfall depth values. Table 5-7 presents the full results of this analysis for a rainfall surface with a slope of 0 and Table 5-8 presents the summary of loss of variation associated with each of the averaging methods. Table 5-9 then presents the results of the same analysis for a slope of 3, and Table 5-10 presents the summary of loss of variation for this scenario. The results of this analysis again suggest that the Thiessen polygon averaging method results in somewhat less smoothing than the arithmetic averaging method. For example, the difference in standard deviations between the Thiessen method and rain gage 1 for a minimum rainfall depth of 5 mm was -0.108, while the difference in standard deviations between the arithmetic method and rain gage 1 was -0.119 when the rainfall depth surface had no variability. The difference between these two values is not significant.

For slopes of both 0 and 3 it would appear that the amount of rainfall does not have an effect. The loss in variation is essentially constant, with some slight random variation, regardless of the amount of rainfall. As table 5-10 shows, the difference in standard deviations between the Thiessen method and rain gage 1 varied from -0.106 to -0.108 for minimum rainfall depths varying from 1 mm to 15 mm, and the

differences in standard deviations between the arithmetic method and rain gage 1

varied from -0.119 to -0.121 for the same depths.

**Table 5-7: Results of Analysis of Varying Rainfall Amounts with a Slope of 0, where Std. Dev. Means Standard Deviation, and Arith. Means Arithmetic**

| Minimum Rainfall Depth (mm) | Gage 1 Mean | Gage 1 Std. Dev. | Gage 2 Mean | Gage 2 Std. Dev. | Thiessen Mean | Thiessen Std. Dev. | Arith. Mean | Arith. Std. Dev. |
|---|---|---|---|---|---|---|---|---|
| 1 | 3.00 | 0.399 | 3.00 | 0.394 | 3.00 | 0.291 | 3.00 | 0.280 |
| 2 | 4.00 | 0.399 | 4.00 | 0.394 | 4.00 | 0.291 | 4.00 | 0.280 |
| 5 | 7.00 | 0.399 | 7.00 | 0.394 | 7.00 | 0.291 | 7.00 | 0.281 |
| 10 | 12.00 | 0.399 | 12.00 | 0.394 | 12.00 | 0.293 | 12.00 | 0.280 |
| 15 | 17.00 | 0.399 | 17.00 | 0.396 | 17.00 | 0.292 | 17.00 | 0.278 |

**Table 5-8: Summary of Loss of Variation of Averaging Methods for Varying Rainfall Amounts with a Slope of 0, where Arith. Means Arithmetic, and Std. Dev. Means Standard Deviation**

| Minimum Rainfall Depth (mm) | Std. Dev. Thiessen-Gage 1 | Std. Dev. Arith.-Gage 1 | Std. Dev. Thiessen-Gage 2 | Std. Dev. Arith.-Gage 2 |
|---|---|---|---|---|
| 1 | -0.108 | -0.119 | -0.103 | -0.113 |
| 2 | -0.108 | -0.119 | -0.103 | -0.114 |
| 5 | -0.108 | -0.119 | -0.103 | -0.114 |
| 10 | -0.106 | -0.119 | -0.101 | -0.114 |
| 15 | -0.107 | -0.121 | -0.104 | -0.118 |

**Table 5-9: Results of Analysis of Varying Rainfall Amounts with a Slope of 3, where Std. Dev. Means Standard Deviation and Arith. Means Arithmetic**

| Minimum Rainfall Depth (mm) | Gage 1 Mean | Gage 1 Std. Dev. | Gage 2 Mean | Gage 2 Std. Dev. | Thiessen Mean | Thiessen Std. Dev. | Arith. Mean | Arith. Std. Dev. |
|---|---|---|---|---|---|---|---|---|
| 1 | 3.74 | 0.586 | 5.25 | 0.581 | 4.50 | 0.551 | 4.50 | 0.415 |
| 2 | 4.74 | 0.586 | 6.25 | 0.581 | 5.50 | 0.551 | 5.50 | 0.415 |
| 5 | 7.74 | 0.586 | 9.25 | 0.581 | 8.50 | 0.552 | 8.50 | 0.456 |
| 10 | 12.74 | 0.586 | 14.25 | 0.580 | 13.50 | 0.552 | 13.50 | 0.415 |
| 15 | 17.74 | 0.587 | 19.25 | 0.581 | 18.50 | 0.552 | 18.50 | 0.412 |

**Table 5-10: Summary of Loss of Variation for Varying Rainfall Amounts with a Slope of 3, where Arith. Means Arithmetic, and Std. Dev. Means Standard Deviation**

| Minimum Rainfall Depth (mm) | Std. Dev. Thiessen-Gage 1 | Std. Dev. Arith.-Gage 1 | Std. Dev. Thiessen-Gage 2 | Std. Dev. Arith.-Gage 2 |
|---|---|---|---|---|
| 1 | -0.035 | -0.171 | -0.030 | -0.166 |
| 2 | -0.035 | -0.171 | -0.030 | -0.166 |
| 5 | -0.035 | -0.170 | -0.029 | -0.165 |
| 10 | -0.034 | -0.171 | -0.029 | -0.165 |
| 15 | -0.035 | -0.175 | -0.030 | -0.170 |

## 5.2.5. Effect of Probability Distribution Function

### 5.2.5.1. Methods and Materials

The final factor investigated was the effect of the choice of pdf of the random variation on the computed average rainfall depths for the pixel.  The program allowed the user to choose from a uniform pdf, a normal pdf, an exponential pdf, a gamma pdf, and an extreme value pdf.  Five scenarios were set up, one for each of the above mentioned pdfs.  When using the uniform pdf the parameters to be specified are the lower bound and the upper bound.  Values of 1.5 and 5, respectively, were chosen for these parameters.  In simulations using the normal pdf the mean and standard deviation were the parameters to be specified.  As with the previous analyses, a mean of 2 and a standard deviation of 0.4 were chosen.  The exponential pdf required specification of only one parameter.  This parameter was set to 2.5 for this analysis.  The gamma pdf needed both a scale and a shape parameter.  Values chosen for these parameters were 2.5 and 3 respectively.  The extreme value pdf also required that two parameters, the location parameter and the scale parameter, be specified.  Again values of 2.5 and 3, respectively, were chosen.  A minimum rainfall depth of 2 mm was simulated.  While the results of these analyses are not directly comparable because of the differences in the pdfs, it was an interesting question to examine.

### 5.2.5.2. Results and Discussion

The final analysis compared the smoothing effects for several different rainfall pdfs. Table 5-11 presents the results of these analyses, while Table 5-12 presents the summary of loss of variation for each of the averaging methods. Due to differences in the different pdfs it is difficult to truly compare these results; however some general conclusions can be reached. In every case the Thiessen polygon averaging method smoothes the results less than the arithmetic averaging method, as seen in Table 5-12. For example, for the exponential pdf the difference in standard deviations between the Thiessen method and rain gage 1 was -0.634, while the difference in standard deviations between the arithmetic method and rain gage 1 was -0.708. The normal pdf, which was used in all of the previous analyses, has the smallest difference in loss of variation between the two averaging methods, with a loss of variation of -0.108 for the Thiessen averaging method and a loss of variation of -0.119 for the arithmetic averaging method, while the exponential, gamma, and extreme value pdfs have significantly higher differences between the averaging methods. If one of these pdfs were to be used further then it would clearly be to the best advantage to use the Thiessen polygon averaging method rather than the arithmetic averaging method to maintain as much of the original variation as possible. However, the differences between the Thiessen polygon and the arithmetic averaging methods are significantly lower for the normal and uniform pdfs, indicating that the arithmetic method could be used without excessive loss of variation in an analysis using either of these pdfs, because the parameters were set to have lower variation and therefore fewer extreme rainfall values.

**Table 5-11: Results for with Varying PDFs, where Std. Dev. Means Standard Deviation and Arith. Means Arithmetic**

| PDF | Gage 1 Mean | Gage 1 Std. Dev. | Gage 2 Mean | Gage 2 Std. Dev. | Thiessen Mean | Thiessen Std. Dev. | Arith. Mean | Arith. Std. Dev. |
|---|---|---|---|---|---|---|---|---|
| Uniform | 5.26 | 1.011 | 5.24 | 1.015 | 5.25 | 0.745 | 5.25 | 0.717 |
| Normal | 4.00 | 0.399 | 4.00 | 0.394 | 4.00 | 0.291 | 4.00 | 0.280 |
| Exponential | 4.48 | 2.505 | 4.53 | 2.566 | 4.51 | 1.871 | 4.51 | 1.796 |
| Gamma | 9.49 | 4.347 | 9.61 | 4.382 | 9.56 | 3.213 | 9.55 | 3.087 |
| Extreme Value | 3.44 | 2.646 | 3.39 | 2.651 | 3.42 | 1.947 | 3.41 | 1.873 |

**Table 5-12: Summary of Loss of Variation for Varying PDFs, where Arith. Means Arithmetic, and Std. Dev. Means Standard Deviation**

| PDF | Std. Dev. Thiessen-Gage 1 | Std. Dev. Arith.-Gage 1 | Std. Dev. Thiessen-Gage 2 | Std. Dev. Arith.-Gage 2 |
|---|---|---|---|---|
| Uniform | -0.266 | -0.294 | -0.270 | -0.298 |
| Normal | -0.108 | -0.119 | -0.103 | -0.114 |
| Exponential | -0.634 | -0.708 | -0.695 | -0.770 |
| Gamma | -1.134 | -1.260 | -1.169 | -1.295 |
| Extreme Value | -0.699 | -0.772 | -0.704 | -0.777 |

## 5.2.6. Conclusions

Analyses were conducted to determine the influence that several factors had on the loss of variation in rainfall estimates caused by using averaging methods. The averaging methods compared were the Thiessen polygon method and the arithmetic method. It was acknowledged that any averaging method would lead to smoothing, or loss of variation, in the rainfall estimates calculated as compared to the true rainfall values. The impact of four factors on the degree of smoothing was investigated. The first was the storm variability, as measured by the slope of the storm surface, and then the amount of watershed area represented by each of two rain gages was investigated. Next varying the amount of rainfall observed over the watershed was investigated, and the final factor was using different probability density functions to represent the

random variation added to the rainfall estimates to represent the lack of perfect correlation between real data sets.

One consistent trend was discovered in investigating the four factors described. In all cases the Thiessen averaging method was seen to result in a smaller amount of smoothing, and therefore less loss of variation as compared to the true data, than the arithmetic method. In examining the results of the investigation into the effects of storm variation two conclusions were reached. First, the difference between the variation in the Thiessen averages and the true data decreased as the storm variability increased. The opposite was true for the arithmetic averages, as the storm variability increased the difference between the variability of the average value and the true value was observed to increase. The second conclusion reached was that though the absolute smoothing increased with increasing storm variability, the relative smoothing remained fairly constant as the storm variability increased.

The results of the gage area investigation showed that the amount of watershed represented by each of the rain gages was most important for a highly variable storm, as would be expected. Rain gage measurements would likely be less accurate for a highly variable storm, and thus any rainfall estimates made using the rain gage data would be a less accurate representation of the true rainfall. Varying the amount of rainfall observed over the watershed was not observed to influence the loss of variation in rainfall estimates made using averaging methods. Finally, the results of the analysis of varying probability distribution functions were somewhat inconclusive, as the different functions are difficult to compare to each other. It was determined; however, that the differences in variation between the Thiessen polygon

averaging method and the arithmetic averaging method were less severe when using a normal or uniform probability distribution function as compared to the exponential, gamma, and extreme value distributions.

## 5.3. Z-R RELATIONSHIPS

### 5.3.1. Introduction

As mentioned previously, radar data does not measure rainfall intensity directly. Instead, the radar beam is reflected off of raindrops in the air and back to the radar station to be measured. In order to obtain useful information about the rainfall intensity a relationship between this reflectance and rainfall rate is used. This relationship transforms the radar readings to rainfall intensity. This equation is called the reflectance (Z) – rainfall rate (R) relationship. A unique Z-R relationship does not exist, and the choice of equation used can influence the amount of rainfall that was measured. This lack of a unique relationship between the radar reflectivity and the rainfall intensity experienced can result in potentially significant errors in converting radar data to rainfall measurements (Gerstner and Heinemann, 2008). The Z-R equation is usually of the form:

$$Z = AR^b \tag{5-1}$$

The National Weather Service uses one standard equation for most of the United States. This equation is applicable to most of the climates and types of rainfall experienced in the United States. This standard equation (Ulbrich and Miller, 2001) is:

$$Z = 300R^{1.4} \tag{5-2}$$

## 5.3.2. Effect of Varying Z-R Relationship on Semivariograms – Trial 1

### 5.3.2.1. Introduction

Semivariograms are used to illustrate spatial variance in data sets. Semivariograms are easiest to evaluate when measurements are made on a grid, where the grid lines are a distance h apart. The notation $\gamma(h)$ is used to represent the semivariogram for a separation distance h, related to the grid size, and they tend to be plotted as $\gamma(h)$ versus h. To determine the shape of the semivariogram two characteristics are important. The separation distance where the semivariogram begins to approach a constant value is called the radius of influence. This value occurs when a semivariogram approaches the sample variance. The second characteristic is the sill. The sill is the portion of the semivariogram where $\gamma(h)$ is approximately the sample variance (Hromadka, 1993). Semivariograms will be discussed in more detail in chapter 6. This experiment evaluated the effect that the Z-R transformation equation used to convert radar data to rainfall rate data had on the storm semivariogram.

### 5.3.2.2. Methods and Materials

The first experiment conducted to determine the effect that the Z-R transformation equation had on the storm semivariogram used several different Z-R relationships to determine the rainfall rate for the same measured reflectance values. Watershed 1, which was a synthetic 60-km by 48-km with a total of 208 rain gages was used with a synthetic storm, identified for future use as storm 2. This storm had ellipses with major axes of 0-km at the center, 5-km, 12-km, 19-km, and 28-km. Rather than a rainfall depth, a reflectance value, in decibels of reflectance, which is a log scale, was input to the program for each ellipse. The reflectance values used were

55-dBZ at the center, then 45-dBZ, 30-dBZ, 20-dBZ, and 5-dBZ. The program then

converted these values into true reflectance values from the decibel scale used by the

radar, and calculated a semivariogram for the reflectance values.

After calculating the true reflectance values the program converted those

values into rainfall rate values using the given Z-R relationship. Finally the program

multiplied each rainfall rate value by a time increment of 5 minutes, which is the

standard time interval of radar scans. A semivariogram was then computed for the

rainfall depths. Five different commonly used Z-R relationships (Collier, 1996;

Morin *et al.*, 2006) were compared in this experiment. Those relationships were:

$$Z = 300R^{1.4} \tag{5-3}$$

$$Z = 655R^{1.4} \tag{5-4}$$

$$Z = 500R^{1.5} \tag{5-5}$$

$$Z = 250R^{1.5} \tag{5-6}$$

$$Z = 200R^{1.6} \tag{5-7}$$

As with all of the semivariogram analysis experiments the relative bias, standard error

ratio, correlation coefficient, sill value, and radius of influence were recorded for

comparison.

### 5.3.2.3. Results and Discussion

The results of trial 1, shown in Tables 5-13 through 5-15, indicate that the

choice of Z-R transformation equation can significantly affect the computation of the

semivariogram. Table 5-13 shows the results of a semivariogram computed from

reflectance data before a transformation was applied. Obviously the transformation

equation did not cause any change to occur in this data as there was change was not

evident in the semivariogram parameters as the transformation equation varied. This

semivariogram was computed in order to compare any trends in the data to trends

found in semivariograms computed from rainfall depth information. In comparing

Table 5-13 to Tables 5-14 and 5-15 it is obvious that the sill values are significantly

different when reflectance data is used versus rainfall depth data, but the radius of

influence does not seem to be significantly different between the two data types.

**Table 5-13: Semivariogram Calculated for Reflectance Data**

| Z-R Equation | Maximum Separation Distance (km) | Sill ($*10^{10}$ mm2) | Radius of Influence (km) | Relative Bias | Standard Error Ratio | R |
|---|---|---|---|---|---|---|
| $Z=300R^{1.4}$ | 28 | 0.25 | 29 | -0.011 | 0.138 | 0.992 |
| $Z=300R^{1.4}$ | 32 | 0.18 | 18 | -0.002 | 0.909 | 0.990 |
| $Z=655R^{1.4}$ | 28 | 0.25 | 29 | -0.011 | 0.138 | 0.992 |
| $Z=655R^{1.4}$ | 32 | 0.18 | 18 | -0.002 | 0.909 | 0.990 |
| $Z=500R^{1.5}$ | 28 | 0.25 | 29 | -0.011 | 0.138 | 0.992 |
| $Z=500R^{1.5}$ | 32 | 0.18 | 18 | -0.002 | 0.909 | 0.990 |
| $Z=250R^{1.5}$ | 28 | 0.25 | 29 | -0.011 | 0.138 | 0.992 |
| $Z=250R^{1.5}$ | 32 | 0.18 | 18 | -0.002 | 0.909 | 0.990 |
| $Z=200R^{1.6}$ | 28 | 0.25 | 29 | -0.011 | 0.138 | 0.992 |
| $Z=200R^{1.6}$ | 32 | 0.18 | 18 | -0.002 | 0.909 | 0.990 |

**Table 5-14: E-W Semivariograms of Rainfall Depths Calculated from Reflectance Data Using Varying Z-R Transformation Equations**

| Z-R Equation | Maximum Separation Distance (km) | Sill (mm2) | Radius of Influence (km) | Relative Bias | Standard Error Ratio | R |
|---|---|---|---|---|---|---|
| $Z=300R^{1.4}$ | 24 | 801.7 | 37 | 0.004 | 0.053 | 0.999 |
| $Z=300R^{1.4}$ | 28 | 629.8 | 27 | 0.010 | 0.157 | 0.980 |
| $Z=300R^{1.4}$ | 32 | 490.3 | 20 | 0.009 | 0.818 | 0.653 |
| $Z=655R^{1.4}$ | 24 | 262.6 | 37 | 0.003 | 0.053 | 0.999 |
| $Z=655R^{1.4}$ | 28 | 206.4 | 27 | 0.010 | 0.157 | 0.980 |
| $Z=655R^{1.4}$ | 32 | 160.8 | 20 | 0.009 | 0.818 | 0.653 |
| $0.500R^{1.5}$ | 24 | 238.8 | 41 | 0.006 | 0.063 | 0.998 |
| $Z=500R^{1.5}$ | 28 | 173.0 | 27 | 0.014 | 0.187 | 0.985 |
| $Z=500R^{1.5}$ | 32 | 136.0 | 21 | 0.011 | 0.801 | 0.671 |
| $Z=250R^{1.5}$ | 24 | 602.7 | 41 | 0.006 | 0.063 | 0.998 |
| $Z=250R^{1.5}$ | 28 | 435.9 | 27 | 0.014 | 0.187 | 0.985 |
| $Z=250R^{1.5}$ | 32 | 342.8 | 21 | 0.011 | 0.801 | 0.671 |
| $Z=200R^{1.6}$ | 24 | 519.6 | 16 | 0.001 | 0.938 | 0.516 |
| $Z=200R^{1.6}$ | 28 | 334.2 | 47 | 0.008 | 0.078 | 0.998 |
| $Z=200R^{1.6}$ | 32 | 264.8 | 27 | 0.017 | 0.213 | 0.981 |

**Table 5-15: N-S Semivariograms of Rainfall Depths Calculated from Reflectance Data Using Varying Z-R Transformation Equations**

| Z-R Equation | Maximum Separation Distance (km) | Sill (mm2) | Radius of Influence (km) | Relative Bias | Standard Error Ratio | R |
|---|---|---|---|---|---|---|
| $Z=300R^{1.4}$ | 20 | 1145.7 | 49 | 0.007 | 0.076 | 0.998 |
| $Z=300R^{1.4}$ | 24 | 615.4 | 24 | 0.017 | 0.207 | 0.983 |
| $Z=300R^{1.4}$ | 28 | 469.1 | 18 | 0.013 | 0.589 | 0.620 |
| $Z=655R^{1.4}$ | 20 | 355.0 | 46 | 0.008 | 0.075 | 0.998 |
| $Z=655R^{1.4}$ | 24 | 201.7 | 24 | 0.017 | 0.207 | 0.983 |
| $Z=655R^{1.4}$ | 28 | 153.8 | 18 | 0.012 | 0.859 | 0.620 |
| $Z=500R^{1.5}$ | 20 | 377.5 | 60 | 0.011 | 0.094 | 0.997 |
| $Z=500R^{1.5}$ | 24 | 168.5 | 23 | 0.020 | 0.240 | 0.977 |
| $Z=500R^{1.5}$ | 28 | 129.7 | 18 | 0.015 | 0.845 | 0.637 |
| $Z=250R^{1.5}$ | 20 | 1048.5 | 66 | 0.010 | 0.094 | 0.997 |
| $Z=250R^{1.5}$ | 24 | 424.5 | 23 | 0.020 | 0.240 | 0.977 |
| $Z=250R^{1.5}$ | 28 | 326.9 | 18 | 0.015 | 0.845 | 0.637 |
| $Z=200R^{1.6}$ | 20 | 1501.3 | 125 | 0.012 | 0.111 | 0.995 |
| $Z=200R^{1.6}$ | 24 | 324.4 | 23 | 0.023 | 0.267 | 0.971 |
| $Z=200R^{1.6}$ | 28 | 252.0 | 18 | 0.017 | 0.831 | 0.651 |

Tables 5-14 and 5-15 show the effect that the Z-R transformation equation has on both the East-West and the North-South semivariograms. Five commonly used Z-R relationships were examined in this trial, but they do not vary in any systematic way that allows data trends to be evident. What is evident, however, is that the choice of transformation equation used can have significant influence on the fitted sill and radius of influence. This indicates that calibration of a transformation equation for a specific location would be necessary to obtain an accurate semivariogram. In most weather radar applications, however, calibration of the Z-R relationship is not done, and one or two standard equations are applied to most of the area of the United States of America.

### 5.3.3. Effect of Varying Z-R Relationship on Semivariograms – Trial 2

*5.3.3.1. Introduction*

The previous evaluation of the effect of Z-R equation on the storm semivariogram considered several commonly used Z-R equations. This did not allow for evaluation of the *A* and *b* coefficients individually. The purpose of this research was to determine the effect of each coefficient individually on the calculated storm semivariogram.

*5.3.3.2. Methods and Materials*

The second experiment used to study the effects of the Z-R relationship on the semivariogram was designed to consider the effect of each coefficient individually. Therefore four Z-R relationships were used, which may or may not be relationships commonly accepted, but which spanned the range of commonly used values. The Z-R relationships used were:

$$Z = 200R^{1.4} \tag{5-8}$$

$$Z = 200R^{1.6} \tag{5-9}$$

$$Z = 600R^{1.4} \tag{5-10}$$

$$Z = 600R^{1.6} \tag{5-11}$$

These relationships varied the *A* and *b* values individually and thus were able to provide insight into the effect each coefficient had on the computed semivariogram. Watershed 1 and storm 2 were used as they were in trial 1, and as always the relative bias, standard error ratio, correlation coefficient, sill, and radius of influence were compared among the fitted semivariograms.

### 5.3.3.3. Results and Discussion

Because the Z-R relationships examined in trial 1 did not vary in a systematic way firm conclusions about the effect of the coefficients *A* and *b* individually could not be drawn. In order to determine the individual effect of the coefficients a second study was conducted. The results of this study are presented in Tables 5-16 and 5-17. From these tables it is obvious that neither of the coefficients has any significant effect on the radius of influence. An increase in either of the coefficients, however, leads to a decrease in the sill values. This result is expected because the standard form of the equation calculates reflectance based on rainfall rate, so to calculate rainfall rate based on reflectance the equation must be solved for R, and the reciprocals of *A* and *b* must be used. When *A* or *b* increase their reciprocals decrease, which explains the corresponding decrease in sill. This study again illustrates the effect the choice of Z-R relationship can have on the semivariogram, which reinforces the idea that the Z-R relationship must be calibrated in order to obtain an accurate semivariogram.

**Table 5-16: E-W Semivariogram for Varying Z-R Transformation Equations**

| Z-R Equation | Maximum Separation Distance (km) | Sill (mm2) | Radius of Influence (km) | Relative Bias | Standard Error Ratio | R |
|---|---|---|---|---|---|---|
| $Z=200R^{1.4}$ | 24 | 1428.9 | 37 | 0.004 | 0.053 | 0.999 |
| $Z=200R^{1.4}$ | 28 | 1123.8 | 27 | 0.010 | 0.157 | 0.990 |
| $Z=200R^{1.4}$ | 32 | 875.0 | 20 | 0.009 | 0.818 | 0.653 |
| $Z=200R^{1.6}$ | 24 | 512.0 | 46 | 0.009 | 0.078 | 0.998 |
| $Z=200R^{1.6}$ | 28 | 334.2 | 27 | 0.017 | 0.213 | 0.981 |
| $Z=200R^{1.6}$ | 32 | 264.8 | 21 | 0.013 | 0.785 | 0.687 |
| $Z=600R^{1.4}$ | 24 | 297.8 | 37 | 0.004 | 0.053 | 0.999 |
| $Z=600R^{1.4}$ | 28 | 233.9 | 27 | 0.010 | 0.157 | 0.990 |
| $Z=600R^{1.4}$ | 32 | 182.2 | 20 | 0.009 | 0.818 | 0.652 |
| $Z=600R^{1.6}$ | 24 | 128.4 | 45 | 0.009 | 0.078 | 0.998 |
| $Z=600R^{1.6}$ | 28 | 84.7 | 27 | 0.017 | 0.213 | 0.981 |
| $Z=600R^{1.6}$ | 32 | 67.1 | 21 | 0.013 | 0.785 | 0.687 |

**Table 5-17: N-S Semivariogram for Varying Z-R Transformation Equations**

| Z-R Equation | Maximum Separation Distance (km) | Sill (mm2) | Radius of Influence (km) | Relative Bias | Standard Error Ratio | R |
|---|---|---|---|---|---|---|
| $Z=200R^{1.4}$ | 20 | 1974.6 | 47 | 0.008 | 0.076 | 0.998 |
| $Z=200R^{1.4}$ | 24 | 1098.4 | 24 | 0.017 | 0.207 | 0.983 |
| $Z=200R^{1.4}$ | 28 | 837.5 | 18 | 0.013 | 0.859 | 0.620 |
| $Z=200R^{1.6}$ | 20 | 1501.3 | 125 | 0.012 | 0.111 | 0.996 |
| $Z=200R^{1.6}$ | 24 | 324.4 | 23 | 0.023 | 0.267 | 0.971 |
| $Z=200R^{1.6}$ | 28 | 252.0 | 18 | 0.017 | 0.831 | 0.651 |
| $Z=600R^{1.4}$ | 20 | 401.5 | 46 | 0.008 | 0.075 | 0.998 |
| $Z=600R^{1.4}$ | 24 | 228.6 | 24 | 0.017 | 0.207 | 0.983 |
| $Z=600R^{1.4}$ | 28 | 174.3 | 18 | 0.013 | 0.859 | 0.620 |
| $Z=600R^{1.6}$ | 20 | 386.9 | 127 | 0.012 | 0.111 | 0.995 |
| $Z=600R^{1.6}$ | 24 | 82.1 | 23 | 0.023 | 0.237 | 0.971 |
| $Z=600R^{1.6}$ | 28 | 63.8 | 18 | 0.017 | 0.831 | 0.651 |

## 5.3.4. Conclusions

Two studies were conducted to examine the effect of using radar reflectance data rather than rain gage data to compute a semivariogram.  To do this rainfall reflectance was measured, and then a Z-R transformation equation was used to convert the reflectance data to rainfall intensity, and then rainfall depth data.  A unique Z-R equation does not exist, and the choice of equation used was seen to significantly influence the semivariogram calculated.  The sill values were found to be much more affected than the radius of influence values when radar reflectance data rather than rainfall depth data were used.  In fact, any increase in either the *A* or *b* coefficient values was found to decrease the sill value.  This finding led to the conclusion that it would be necessary to calibrate a Z-R equation for a specific location in order to calculate an accurate semivariogram.

## 5.3.5. Visual Comparison Between Radar and Rain Gage Data

### 5.3.5.1. Introduction

In order to make use of radar and rain gage data for future research into the relationship between reflectance and rainfall rate, and into the use of spatial data as input to the unit hydrograph procedure, it was important to understand how the radar data related to the rain gage data. Several methods were used to develop this understanding, including a visual comparison using plots of both data sets and calculating the correlation between the radar data and the rain gage data. Ideally the visual inspection would reveal common patterns or trends to the data sets, such as rising and peaking at corresponding times. The correlation analysis would ideally show a high degree of correlation, indicating a strong relationship between the various data sets.

### 5.3.5.2. Methods and Materials

In order to visually compare the radar data and the rain gage data, both data sets needed to be obtained. The Hydro-NEXRAD database used to obtain radar data provides five possible radar scan elevations, at 0.5°, 1.5°, 2.5°, 3.5°, and 4.5° tilt angles. Because which of these elevation scans would provide optimum coverage of the Walnut Gulch Experimental Watershed was unknown, all five were obtained for two storm events, occurring on August 13, 2006, and July 20, 2007. The rain gage data were obtained from the Agricultural Research Services' website for both of these storms. Then five of the sixteen radar pixels covering the Walnut Gulch area were chosen for use in several analyses in an effort to get a thorough sample of the watershed. The pixels chosen for this comparison were pixels 1, 4, 7, 10, and 16, as described below as they appear in Figure 5-1. The squares of varying gray colors are

the pixels, and the dots within the watershed boundary are the rain gages. The top

left-most pixel, which contains the watershed outlet, is identified as pixel 1, while the

top right-most pixel, which has only two rain gages within it, is identified as pixel 7.

Pixels 2 through 6 are located between these two pixels. The second row of pixels

can be identified, moving from left to right, as pixels 8 through 13. The pixels in the

bottom row are identified as pixels 14, 15, and 16, again moving from left to right.

The final preparation step was to identify which rain gages were located within the

boundaries of the pixels chosen for this study.
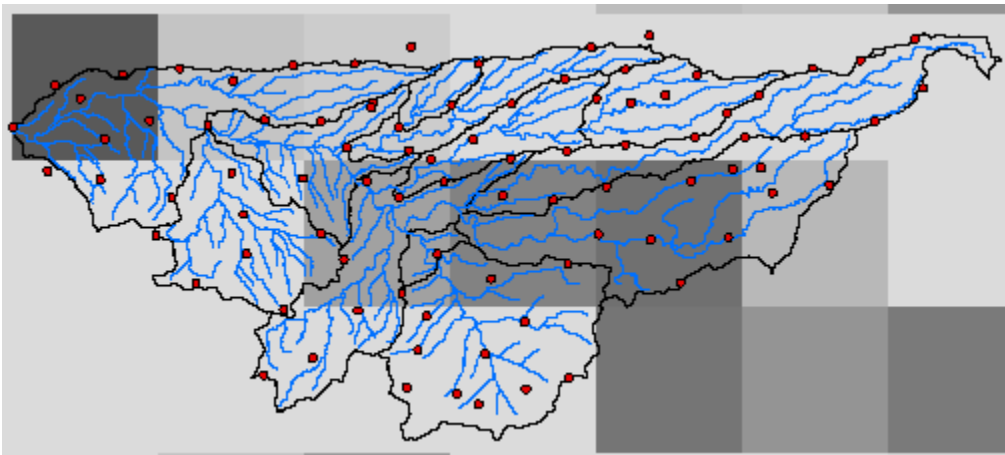


**Figure 5-1: Map of Walnut Gulch Experimental Watershed Boundaries, Including the Locations of Rain Gages and the Radar Pixels Associated with the Watershed**

Once all of the data sets had been identified and obtained, they could be

plotted against each other for comparison. The five radar scan elevations were

plotted on one graph in order to assess the degree of variation between the scan

heights. The rain gages were also plotted together, as either one figure or two figures,

depending on the number of rain gages. Pixels 1 and 16 had six rain gages each, and

pixels 4 and 10 had eight rain gages each. After plotting six and eight rain gages on

one graph, it was observed that the graphs were cluttered and difficult to read;

therefore two plots that contained half of the total number of rain gages were made

for each of the pixels.  Pixel 7, on the other hand, only contained two rain gages, which were plotted on one graph without difficulty. The plot(s) that contained rain gage data associated with each pixel were then compared to the plot that contained the radar scan elevation data, to determine what similarities existed between the data sets.  Perfect agreement between the radar data and rain gage data was not expected, as the two do not actually measure exactly the same thing; however the desired outcome was to detect general trends shared between the two data sets.

### 5.3.5.3. Results and Discussion

Figures 5-2, 5-3, and 5-4 and Figures 5-5, 5-6, and 5-7 provide a visual comparison between the radar data for each of the five possible scan elevations and the eight rain gages located within the bounds of the pixel for two different storms. The pixel identified as pixel 10 on the map was chosen for demonstration purposes, because reasonable agreement was seen between the radar and rain gage data for one storm, while less agreement was seen for the other storm.  The rain gage data for each storm are presented on two separate graphs because including data from eight rain gages on one plot resulted in a cluttered and difficult to read graph.

In examining the three plots associated with the storm on August 13, 2006, (Figures 5-2, 5-3, and 5-4) the agreement between the radar data and the rain gage data appears moderate at best.  However, it is important to note that the radar data are presented in decibels of reflectance (dBZ), which is a log scale.   The initial peak seen in the radar data for scans 2 through 5 (Figure 5-2) is mirrored in the rain gage data (Figures 5-3 and 5-4) fairly well; however, the rest of the data do not agree so well.  For the duration of the storm comparatively little variation in the radar reflectivity readings is evident, which should indicate little variation in the rainfall

intensities.  However, in the rain gage data, a large decrease in rainfall intensity is clearly seen.  After this decrease only small variation in the measured rainfall intensities is evident; however, the radar data seem to imply that the intensities being measured should be higher.  Also, a clear nonlinearity to the data is visible in the radar reflectivity readings, which is not well reflected in the rain gage data.  Better agreement is observed when the radar data are transformed from decibels of reflectance (dBZ) to reflectance (Z), but these graphs show such a large variation in the reflectance values that they are impractical to plot.

The three plots associated with the storm on July 20, 2007, (Figures 5-5, 5-6, and 5-7) show somewhat better agreement between the radar data (dBZ) and the rain gage data.  Again the first peak of the storm agrees well between the radar readings and the rain gage readings.  Then the radar measurements decrease somewhat, which is also seen in the rain gage measurements.  The decrease does again seem more severe in the rain gage data than it does in the radar data.  The more severe decrease in magnitude of the rain gage data can be explained by the fact that the radar data measures decibels of reflectance, rather than reflectance directly.  Decibels of reflectance are measured by radar stations rather than reflectance because variations over orders of magnitude are possible in reflectance.  A conversion equation, which will be discussed in more detail later, is used to convert the radar measurements from decibels of reflectance to reflectance in order to use the radar data for hydrologic and meteorological purposes.  Therefore, the rainfall measurements in decibels of reflectance mask the true severity of the changes in rainfall intensity.  In actuality, reasonable agreement does exist between the radar reflectance data and the rain gage

99

data; however, it is not practical to plot this information due to the large variation in reflectance values.

A final point of comparison between the radar and rain gage data is the nonlinearity evident in the data sets. Similar to the storm event on August 13, 2006, the radar reflectivities for the storm event on July 20, 2007, (Figure 5-5) increase and then decrease again in a nonlinear pattern. While the rain gage measurements (Figures 5-6 and 5-7) remain at a much lower level than that seen at the beginning of the storm, the nonlinearity evident in the data is seen in all of the rain gage records. While the radar measurements do not indicate that there should have been such a decrease in the intensity of rainfall between the beginning and end of the storm as is seen in the rain gage measurements, the rain gages more accurately match the trends of the radar data than was seen in the storm from August 13, 2006.
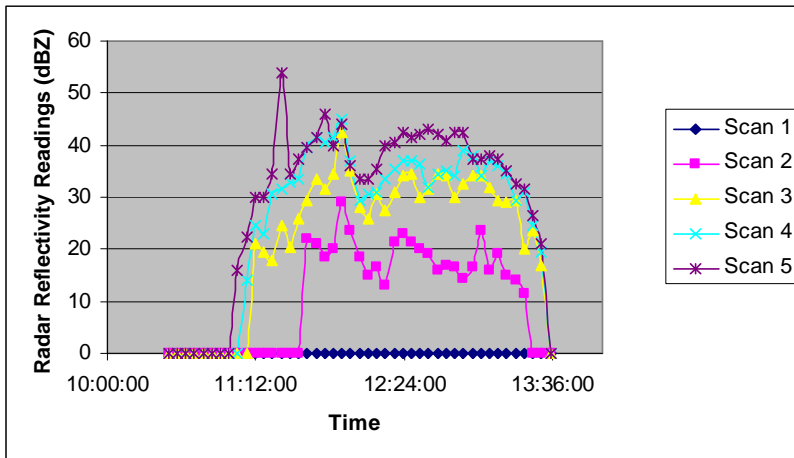


**Figure 5-2: Radar Reflectivity Readings for Scan Elevations for Pixel 10 for 8-13-06 Event**
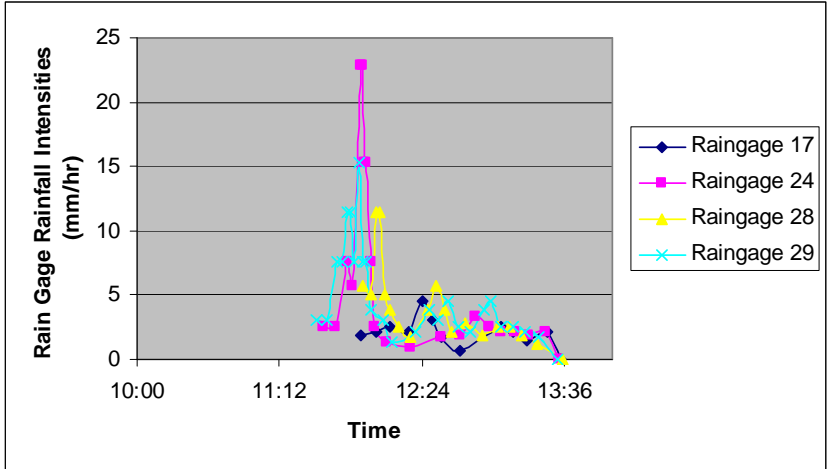
**Figure 5-3: Four Rain Gages Located Within Pixel 10 for 8-13-06 Event**
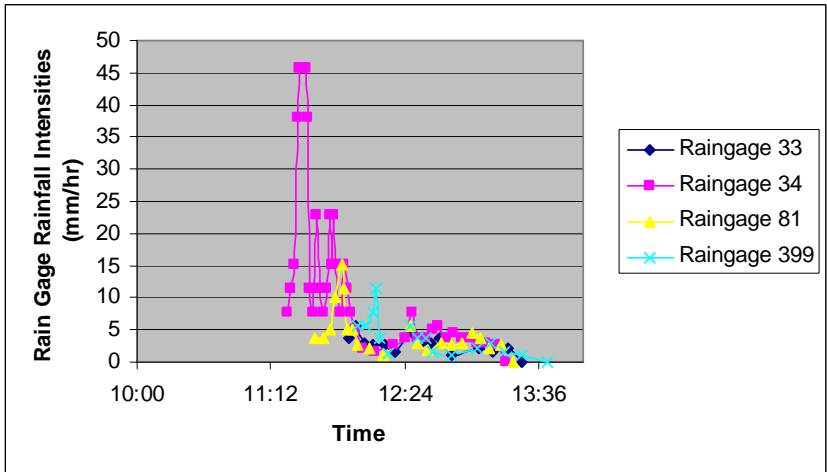


**Figure 5-4: Four Rain Gages Located Within Pixel 10 for Storm on 8-13-06**
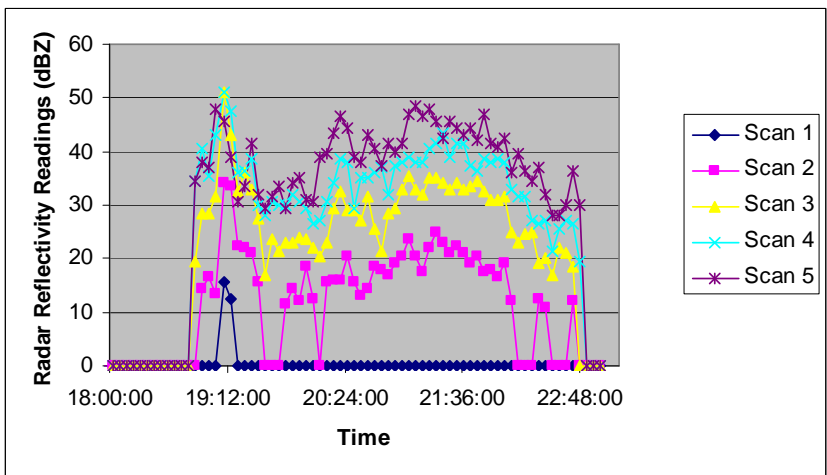


**Figure 5-5: Radar Reflectivity Readings for Scan Elevations for Pixel 10 for 7-20-07 Event**
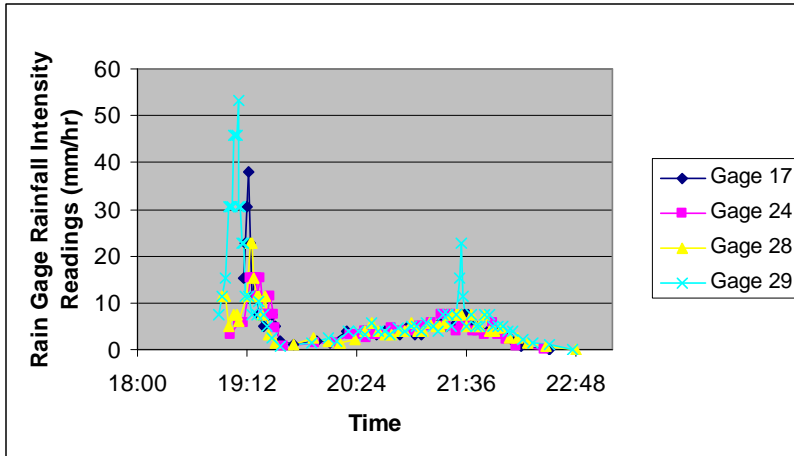
**Figure 5-6: Four the Rain Gages Located Within Pixel 10 for 7-20-07 Event**
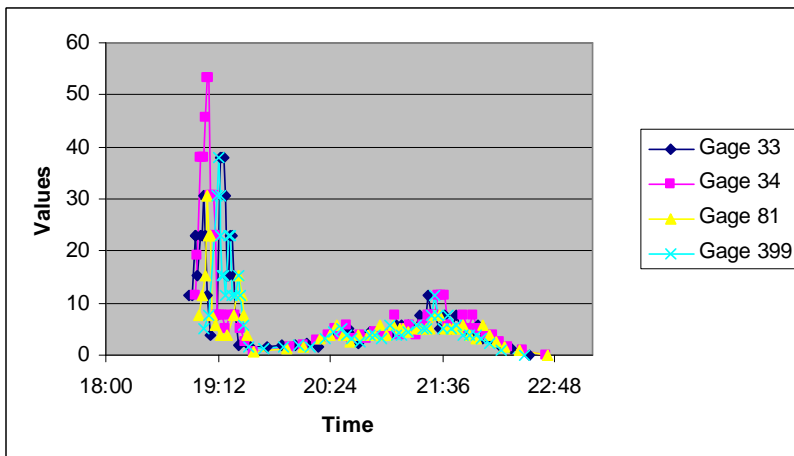


**Figure 5-7: Four Rain Gages Located Within Pixel 10 for 7-20-07 Event**

## 5.3.6. Cross-Correlation of Radar and Rain Gage Data

### *5.3.6.1. Introduction*

The results of the visible comparison of the radar data and the rain gage data

warranted further investigation.  The visual comparison did not provide convincing

evidence that a reasonably strong relationship existed between the two data sets.

Therefore, the cross-correlation analyses between the radar and rain gage data sets

was made for radar scan elevations 2 through 5 and every rain gage in the five sample

pixels chosen.

### 5.3.6.2. Methods and Materials

A cross-correlation program was used to compute the correlation between each radar scan and each rain gage in the pixel. The correlation was calculated between the data sets for nine different time lags: -4 (which means that the rain gage data was four time steps ahead of the radar data), -3, -2, -1, 0 (which means that the radar and rain gage data were on the same time step), 1, 2, 3, and 4 (which means that the radar data was four time steps ahead of the rain gage data). It was assumed that only a positive lag made physical sense because the radar measurements were taken while the rain was in the atmosphere, and the rain gage measurements were taken when the rain reached the ground surface. Therefore the radar would have to measure a given set of raindrops in the air before the rain gage could measure those same raindrops on the ground. The correlation results for each time lag were compared to determine the optimum time lag for each radar and rain gage combination.

The correlations were computed for two scenarios, described later, which differed in how zero values were dealt with. First the correlations were computed for the raw data sets, in which the radar measurements were taken in decibels of reflectance. Some alteration was necessary because the radar data sets and the rain gage data sets needed to be the same lengths in order to compute the correlations. Adjustments were also necessary to temporally align the data sets. The radar measurements were taken at a fairly constant time increment of approximately every four minutes and twelve seconds. The rain gage measurements, however, were taken at non-constant intervals depending on the intensity of rainfall. Therefore, rain gage measurements could occur as frequently as every minute, or there could be as much as an hour or more between readings. To calculate the correlations between the data

sets it was necessary to have one rain gage reading for every one radar reading. At points when rain gage readings came more frequently than radar readings an average rainfall intensity was calculated for the extra time steps, while the intensity of rainfall was assumed to be constant when the time between rain gage readings was greater than the time between radar readings. Once adjusted data sets had been created using this procedure, the correlations between the data sets could be calculated.

The final step involved eliminating zero values from the data sets. Because these data sets were eventually going to be used to calibrate the Z-R relationships between the radar and rain gage data, which use a power law, zero values could not be included in the data sets. Two different methods were used to eliminate zero values in the data sets. For scenario 1, a zero value that was present in a data record for either the radar or the rain gage data record was completely deleted. In the second scenario, zero values were eliminated by adding a small number, insignificant to the magnitude of the radar and rain gage measurements, to each measurement. A value of 0.001 was chosen for this purpose. This resulted in any values that had been zero in the original data set becoming 0.001, which could be logarithmically transformed for use in the power model.

### 5.3.6.3. Results and Discussion

The results of the cross-correlation analysis for the storm on August 13, 2006, are presented in Tables 5-18 through 5-22. Each table presents the cross-correlation result for each rain gage and radar scan level for one of the sample pixels used in this analysis. For instance, Table 5-18 contains the cross-correlation results for each of the four radar scan elevations for each of the six rain gages located within pixel 1. Tables 5-23 through 5-27 present the results of the analysis for the storm on July 20,

104

2007. Again, each table presents the cross-correlation results for each of the four radar scan elevations for all of the rain gages located within a specific pixel. The correlations calculated for the same pixels appear to be relatively similar for the different storms. The highest correlations are seen in the pixels located closest and farthest, pixels 1 and 16, respectively, from the radar station located near Tucson, Arizona, while the pixels in the middle of the watershed have consistently lower correlations. While it makes sense that pixel 1 would have high correlation, since it is closest to the actual radar, the reason for the high correlation of pixel 16 compared to the three pixels in the center of the watershed is unclear. The variations in elevation of the pixels could be responsible for this.

Wide variation in correlation is seen between the rain gages and radar scans in the sample pixels, ranging from excellent correlations of up to approximately 95% to poor correlations as low as 0.7%. However, overall acceptable correlation is seen between each radar scan elevation and at least one rain gage. In some cases, a time lag of 1 to 4 time steps, meaning that the rain gage data was between 1 and 4 time steps ahead of the rain gage data, gave the optimum correlation between the data sets. This indicates that a time delay of several minutes is necessary to properly align the radar and rain gage data sets to allow the raindrops measured by the radar to reach the rain gage at the ground surface.

For this analysis, each lag unit corresponded to a time delay of 5 minutes. A rough mathematical estimation was done to determine whether or not these lag values made physical sense. The Walnut Gulch Experimental Watershed is located from approximately 50 km to approximately 70 km away from the radar station in Tucson,

Arizona. Therefore, for scan level 2, for which the angle of the radar beam was 1.5°, the radar beam was measuring the air between 1.31 km and 1.83 km above ground. Assuming the rain drops were falling at terminal velocity, found to be approximately 6.5 m/s (Foote and Du Toit, 1969), it would take between 3.36 minutes and 4.69 minutes for these raindrops to reach the ground surface.

A similar analysis was completed for scan level 5. For scan level 5, for which the angle of the beam was 4.5°, the radar beam was measuring the air between approximately 3.94 and 5.51 km above the ground surface. From these heights, falling at terminal velocity, the raindrops would take approximately 10.1 minutes to 14.13 minutes to reach the ground. Based on these calculations, lags of 1, 2, or 3 time units do make physical sense. It should also be considered that the raindrops may not actually be falling at terminal velocity. For instance, updrafts in the atmosphere could force the droplets to move in a jerky pattern, periodically being forced in the upward direction by wind. Also, the terminal velocity used in these calculations assumes a raindrop diameter of approximately 2mm. If the droplets were significantly smaller than this they would be falling more slowly, and therefore take longer to reach the ground.

The purpose of this analysis was to determine whether or not a relationship existed between the radar data and the rain gage data. Because the visual inspection discussed above did not provide convincing evidence that a strong relationship existed between the two data sets, it was reassuring to see reasonable correlation values result from this analysis. The correlation results found in this analysis indicate that some relationship between the radar data and the rain gage data exists, meaning

that the two data sets can safely be used to derive Z-R relationships for the Walnut

Gulch Experimental Watershed.

**Table 5-18: Cross-Correlation Results for Rain Gages and Radar Scans in Pixel 1 for the 8-13-06 Event**

| Gage | Scan 2 | Scan 3 | Scan 4 | Scan 5 |
|---|---|---|---|---|
| 1 | 0.7715 | 0.8061 | 0.7812 | 0.8641 |
| 2 | 0.7812 | 0.8547 | 0.9215 | 0.8522 |
| 4 | 0.6968 | 0.7002 | 0.6143 | 0.6526 |
| 5 | 0.8185 | 0.8962 | 0.9447 | 0.9185 |
| 8 | 0.7949 | 0.7545 | 0.8114 | 0.8725 |
| 92 | 0.7855 | 0.802 | 0.8554 | 0.8809 |

**Table 5-19: Cross-Correlation Results for Rain Gages and Radar Scans in Pixel 4 for the 8-13-06 Event**

| Gage | Scan 2 | Scan 3 | Scan 4 | Scan 5 |
|---|---|---|---|---|
| 31 | 0.4356 | 0.5764 | 0.5133 | 0.6086 |
| 32 | 0.2655 | 0.4274 | 0.5019 | 0.0142 |
| 38 | 0.5228 | 0.6347 | 0.6672 | 0.5522 |
| 39 | 0.1635 | 0.2886 | 0.0525 | 0.1308 |
| 43 | 0.5322 | 0.6639 | 0.5612 | 0.4524 |
| 44 | 0.174 | 0.2363 | 0.1628 | 0.0071 |
| 71 | 0.2265 | 0.3735 | 0.4228 | 0.0807 |
| 87 | 0.4638 | 0.6014 | 0.6218 | 0.3682 |

**Table 5-20: Cross-Correlation Results for Rain Gages and Radar Scans in Pixel 7 for the 8-13-06 Event**

| Gage | Scan 2 | Scan 3 | Scan 4 | Scan 5 |
|---|---|---|---|---|
| 69 | 0.582 | 0.6088 | 0.4458 | 0.3895 |
| 70 | 0.495 | 0.6125 | 0.494 | 0.3976 |

**Table 5-21: Cross-Correlation Results for Rain Gages and Radar Scans in Pixel 10 for the 8-13-06 Event**

| Gage | Scan 2 | Scan 3 | Scan 4 | Scan 5 |
|---|---|---|---|---|
| 17 | 0.6069 | 0.4814 | 0.3194 | 0.1285 |
| 24 | 0.4697 | 0.4995 | 0.6041 | 0.3342 |
| 28 | 0.6325 | 0.6777 | 0.5722 | 0.3228 |
| 29 | 0.5714 | 0.567 | 0.7052 | 0.469 |
| 33 | 0.6668 | 0.6942 | 0.5073 | 0.3318 |
| 34 | 0.339 | 0.285 | 0.2571 | 0.4816 |
| 81 | 0.506 | 0.5223 | 0.6125 | 0.4343 |
| 399 | 0.5383 | 0.5971 | 0.5459 | 0.1448 |

**Table 5-22: Cross-Correlation Results for Rain Gages and Radar Scans in Pixel 16 for the 8-13-06 Event**

| Gage | Scan 2 | Scan 3 | Scan 4 | Scan 5 |
|---|---|---|---|---|
| 36 | 0.9359 | 0.7319 | 0.6612 | 0.5416 |
| 37 | 0.8302 | 0.7591 | 0.6664 | 0.5716 |
| 42 | 0.8079 | 0.6601 | 0.5949 | 0.5816 |
| 47 | 0.9503 | 0.8169 | 0.7323 | 0.552 |
| 48 | 0.91 | 0.7424 | 0.7403 | 0.6367 |
| 100 | 0.6981 | 0.7749 | 0.6512 | 0.454 |

**Table 5-23: Cross-Correlation Results for Rain Gages and Radar Scans in Pixel 1 for the 7-20-07 Event**

| Gage | Scan 2 | Scan 3 | Scan 4 | Scan 5 |
|---|---|---|---|---|
| 1 | 0.7272 | 0.6839 | 0.646 | 0.5953 |
| 2 | 0.7475 | 0.6865 | 0.6434 | 0.6013 |
| 4 | 0.6369 | 0.5425 | 0.4943 | 0.4429 |
| 5 | 0.66 | 0.6483 | 0.605 | 0.5609 |
| 8 | 0.6569 | 0.6322 | 0.6426 | 0.659 |
| 92 | 0.7176 | 0.6247 | 0.5879 | 0.5485 |

**Table 5-24: Cross-Correlation Results for Rain Gages and Radar Scans in Pixel 4 for the 7-20-07 Events**

| Gage | Scan 2 | Scan 3 | Scan 4 | Scan 5 |
|---|---|---|---|---|
| 31 | 0.3499 | 0.3328 | 0.3846 | 0.262 |
| 32 | 0.4879 | 0.3535 | 0.3601 | 0.256 |
| 38 | 0.216 | 0.4563 | 0.4175 | 0.1471 |
| 43 | 0.1145 | 0.5665 | 0.5214 | 0.2637 |
| 44 | 0.1603 | 0.0092 | 0.0843 | 0.2582 |
| 71 | 0.5749 | 0.5043 | 0.4521 | 0.3164 |
| 87 | 0.4284 | 0.3484 | 0.3629 | 0.2075 |

**Table 5-25: Cross-Correlation Results of Rain Gages and Radar Scans in Pixel 7 for the 7-20-07 Event**

| Gage | Scan 2 | Scan 3 | Scan 4 | Scan 5 |
|---|---|---|---|---|
| 69 | 0.5023 | 0.5127 | 0.451 | 0.4761 |
| 70 | 0.5041 | 0.5005 | 0.4337 | 0.4146 |

**Table 5-26: Cross-Correlation Results for Rain Gages and Radar Scans in Pixel 10 for the 7-20-07 Events**

| Gage | Scan 2 | Scan 3 | Scan 4 | Scan 5 |
|---|---|---|---|---|
| 17 | 0.7566 | 0.7594 | 0.7545 | 0.6005 |
| 24 | 0.743 | 0.8229 | 0.7825 | 0.4855 |
| 28 | 0.5894 | 0.714 | 0.744 | 0.5667 |
| 29 | 0.3564 | 0.4631 | 0.5685 | 0.3828 |
| 33 | 0.5144 | 0.6423 | 0.6816 | 0.4314 |
| 34 | 0.3645 | 0.4641 | 0.5504 | 0.4085 |
| 81 | 0.4732 | 0.542 | 0.6188 | 0.5623 |
| 399 | 0.6742 | 0.7237 | 0.6866 | 0.3995 |

**Table 5-27: Cross-Correlation Results for Rain Gages and Radar Scans in Pixel 16 for the 7-20-07 Event**

| Gage | Scan 2 | Scan 3 | Scan 4 | Scan 5 |
|------|--------|--------|--------|--------|
| 36   | 0.8784 | 0.5525 | 0.4607 | 0.4464 |
| 37   | 0.9093 | 0.5582 | 0.472  | 0.4441 |
| 42   | 0.8784 | 0.5668 | 0.4662 | 0.4201 |
| 47   | 0.8909 | 0.5753 | 0.4605 | 0.4219 |
| 48   | 0.6421 | 0.413  | 0.2575 | 0.2189 |
| 100  | 0.8927 | 0.5609 | 0.4385 | 0.404  |

### 5.3.6.4. Conclusions

Before radar data can be used to provide rainfall data in hydrologic analyses it is important to determine that the radar is capable of providing accurate rainfall information. If radar data is going to be transformed into rainfall intensity data, then some relationship should exist between the radar data and the corresponding rain gage data that measures rainfall data at the ground. Visual comparison of the two data sets did not provide convincing evidence that such a relationship existed; therefore the cross-correlation between the two data sets was computed. While wide variation was seen in the correlation values between the radar data sets and each of the rain gage data sets located within a given pixel, overall acceptable correlation (at least greater than 0.5) was seen the radar data and the rain gage data. Since reasonable correlation was seen in general between the two data sets it was concluded that enough of a relationship existed in order to use the radar data for hydrologic analyses. Therefore, equations could be developed to transform the radar data into rainfall intensity data, for later use in hydrologic models.

## 5.3.7. Calibration of Z-R Equations Using Radar and Rain Gage Data

### 5.3.7.1. Introduction

Once it was established that acceptable correlation between the radar data and the rain gage data existed, relationships between the radar reflectance values and the

rain gage measurements could be calibrated. This was done using regression between the two data sets. The National Weather Service, which operates a series of weather radar stations across the country, uses one standard equation for most locations. This equation, which has been found to be valid for much of the United States, is:

$$Z = 300R^{1.4} \qquad\qquad (5\text{-}12)$$

In some locations a second equation is available that is applicable to very specific rainfall types. However, it seems logical that rainfall in an arid or semi-arid region, such as Walnut Gulch, Arizona, could be significantly different from rainfall in a more humid region, such as Miami, Florida. Therefore, the possible effects of calibrating a relationship between rain gage and radar measurements for a specific location were investigated.

### 5.3.7.2. Research Objectives

In order to develop relationships between rain gage measurements and radar measurements specific to the Walnut Gulch area, regression was used. Because the radar measurements would ultimately be used to predict the rainfall rates, the rain gage record (criterion variable) was regressed on the radar record (predictor variable). Determining the level of variability in coefficients of the Z-R equations developed for the Walnut Gulch watershed was one objective of this study. Therefore, the variability in coefficients developed for the same radar pixel and the variability in coefficients developed for radar pixels in different portions of the watershed were investigated. These will reflect both within-pixel variation and between-pixel variation of the coefficients of the Z-R relationship. The variability of the coefficients for the same rain gage under different storm conditions was also considered. This analysis does make the assumption that the rain gage data are

accurate. In actuality, neither rain gage nor radar data are completely accurate. If

measures of the probability density function of rain gage and radar data were

available, an uncertainty analysis could be conducted to assess the effect of

inaccuracies in these data sets. Other objectives included determining the effect that

accounting for the optimum lag determined by the cross-correlation analysis had on

the equation coefficients, comparing both the coefficients and the performance of the

equations developed to those of the standard equation mentioned previously, and

investigating the sensitivity of rainfall predictions to the coefficient values.

### 5.3.7.3. Regression of Z-R Equations

Regression analyses were performed between the five radar pixels discussed

in the visual comparison and cross-correlation sections of this analysis and 15 of the

rain gages located within the boundaries of those pixels. To investigate the variability

in coefficients for the same pixel all eight of the rain gages located in pixel 10 and

both of the rain gages located in pixel 7 were analyzed. To examine the variability in

coefficients for different portions of the watershed, in addition to the ten rain gages

already analyzed, two rain gages from pixel 1, two rain gages from pixel 4, and one

rain gage from pixel 16 were chosen at random for analysis. As firm conclusions had

not been reached as to the radar scan elevations that were most suitable for hydrologic

analysis over the watershed, the data sets for scans 2, 3, 4, and 5 over each of the five

pixels were analyzed. The data sets for scan 1 were not analyzed because they

consisted almost entirely of zero values, most likely due to radar blockage in the

mountainous terrain. The data from the storms occurring on both August 13, 2006,

and July 20, 2007, were again used. Data files that contained a radar data set and a

rain gage data set from one of the rain gages located within the radar pixel boundaries were created for each of the 15 rain gages used in this analysis.

The data obtained directly from the radar could not be used in these analyses, as the radar reports values in decibels of reflectance.  The purpose of this study was to determine the relationship between the rain gage data and reflectance ($mm^6/m^3$), not the rain gage data and decibels of reflectance.  Therefore, the raw radar data measured in decibels needed to be transformed into reflectance values measured in $mm^6/m^3$ using the equation:

$$Z = 10^{dBZ/10}$$
5-13)

where Z is reflectance and dBZ is decibels of reflectance.  A regression program fitted a power model to each data set.  The log-transformed power model (Equation 5-1) produced biased predictions; therefore the intercept value of each of the calibrated Z-R equations had to be adjusted so predictions would be unbiased.

Ultimately three scenarios were evaluated for each rain gage and radar data set combination for both of the storm events.  The first scenario developed regression equations based on the data sets in which all zero values had been deleted.  The second scenario used the data sets in which a value of 0.001 had been added to each data record to eliminate zero values, but the optimum lag found in the cross-correlation analysis had not been accounted for in order to develop the regression equations.  The third scenario used the data sets in which 0.001 had been added to every data record to eliminate zero values, and the optimum lag had been accounted for in order to develop the regression equations.  After using regression on each of the

fifteen rain gages chosen for both storms under all three of the above-mentioned scenarios, a large number of Z-R equations had been fitted.

Several criteria were used to evaluate the Z-R equations that were calibrated. The goodness-of-fit statistics, including the standard error ratio and the correlation coefficient, were examined for each scenario. Then the calibrated equations were used to make rainfall intensity predictions. These predictions were compared to the rain gage data, which was assumed to contain the true rainfall rates. By subtracting the rain gage measurements from the radar rainfall predictions made by the calibrated Z-R equations the error in the predictions could be calculated. The calibrated equations developed for each of the four radar scan elevations were compared to the corresponding rain gage record in this manner.

The next step of this analysis was to determine whether or not calibrating location-specific Z-R relationships could improve the accuracy of rainfall predictions made for the study area. To determine this, the calibrated equations were compared to the standard equation (5-12) that is used at most of the radar stations in the United States. Rainfall predictions were calculated using the standard equation with the various radar data sets instead of the calibrated equations. The errors in the rainfall predictions made by the standard equation were compared with the errors calculated using the calibrated equations developed for the study area.

### 5.3.7.4. Results of Regression of Z-R Equations

The Z-R equations calibrated using the Walnut Gulch data were analyzed in a variety of ways. The goodness-of-fit statistics were compared for the same rain gage and radar combinations among the various scenarios. The rainfall intensity predictions calculated by the calibrated Z-R equations were compared to their

respective rain gage data records, and the errors in the rainfall intensity predictions were compared. Several statistical tests were performed to evaluate the prediction errors. Statistical tests were used to compare the errors of the four equations derived for the four radar scan elevations for one pixel and rain gage combination and to compare the prediction errors made using the equations calibrated for a given radar scan elevation to prediction errors made using the standard equation. Finally, equations with average coefficients were developed using the Z-R equations calibrated for both storms for each pixel and rain gage combination and the goodness-of-fit statistics and the errors calculated using these average equations were also examined.

**5.3.7.4.1. Comparison of Methods to Remove Zeros from Data Sets**

Removing measurements of zero from the radar and rain gage data sets was necessary in order to develop power equations to relate the data sets. Several methods were used to remove these zeros values. The first of these was to simply delete any data records including a zero value. The second was to add a small number, insignificant in comparison with the data values, such as 0.001, to all data records.

The best regression results seemed to be obtained when all zero recordings were deleted from the data set. Table 5-28 illustrates this for the storm event occurring on August 13, 2006, by comparing the goodness-of-fit statistics for the equation derived from rain gage 5 and pixel 1, using the third radar scan elevation. In this instance, deleting the zero values led to a decrease in the standard error ratio of 40%, and an increase in the coefficient of determination of nearly 60%, as compared

to the statistics when 0.001 was added to all data records. This finding was not entirely unexpected. In deleting the zero values, many of the zero values were removed from the data set, while adding 0.001 to every data value retained a lot of very small rainfall values in the data sets. The addition of the low values forced the equation fit to the data to take a different form than when the zero values were deleted. When the zero values were not deleted, they were given too much weight in the data set, and the resulting equation was forced to fit a number of very low rainfall values. The equations developed when the zero values were censored fit the moderate to high rainfall values that were observed, and thus better represent the actual rainfall that was observed.

**Table 5-28: Comparison of Goodness-of-Fit Statistics When Zeros Values are Deleted vs. When 0.001 Added to All Data Values for Storm on 8-13-06**

|                | Se/Sy | R     | $R^2$ | A     | b     |
|----------------|-------|-------|-------|-------|-------|
| 0.001 Added    | 1.151 | 0.000 | 0.000 | 0.001 | 0.865 |
| Zeros Deleted  | 0.637 | 0.786 | 0.619 | 0.146 | 0.350 |

**5.3.7.4.2. Effect of Accounting for Optimum Lag in Data Sets**

Because the radar beam measures rainfall while it is in the air and the rain gage measures rainfall at the ground surface, a time lag of several minutes may be necessary in order to temporally align the radar and rain gage data sets. The optimum time lag for each combination of radar scan elevation and rain gage data was identified in the cross-correlation analysis discussed previously. In order to properly account for the lag, a value of 0.001 had to be added to all data records to eliminate zero values, rather than deleting those zero values. To account for the lag, the data sets were adjusted in time by the number of time steps indicated by the optimum lag value. So if the optimum lag value for a given combination of data sets was found to be two, then the rain gage data was adjusted to be two time steps behind the radar

data, as explained in the section describing the cross-correlation analysis. Two scenarios were modeled. First 0.001 was added to all data values, but the data sets were not temporally shifted to reflect the optimum lag as determined by the cross-correlation analysis. In the second scenario the data sets were temporally shifted to account for the optimum lag as determined by the cross-correlation analysis, after 0.001 had been added to all the data records.

The results of this analysis indicated that accounting for the lag improved the goodness-of-fit statistics as compared to simply adding 0.001 to all values without accounting for lag. Table 5-29 provides an example of this. The goodness-of-fit statistics calculated using equations derived for the storm on August 13, 2006, at rain gage 5 in pixel 1 using radar scan elevation 3 are presented. Accounting for the lag in this instance decreased the standard error ratio by approximately 2%, while increasing the coefficient of determination by approximately 4%. This represents a slight improvement in goodness-of-fit statistics, which may not be significant, when equations are developed after accounting for the optimum lag. The purpose of determining the optimum lag was to determine whether or not a temporal shift in the data sets improved the prediction accuracy between the two. Therefore, accounting for the optimum lag in these situations strengthened the correlation between the radar data and rain gage data as expected. If a stronger relationship between the two data sets used to develop a linear regression equation existed, it would have been logical that the regression equation should better explain the variance in the data set, and therefore should have better goodness-of-fit statistics.

**Table 5-29: Goodness-of-Fit Statistics When Accounting for Lag vs. Not Accounting for Lag**

|        | Se/Sy | R     | $R^2$ | A              | b     |
|--------|-------|-------|-------|----------------|-------|
| No Lag | 1.151 | 0.000 | 0.000 | 0.001          | 0.865 |
| Lag    | 0.771 | 0.658 | 0.434 | $8.715*10^{-5}$ | 1.126 |

## *5.3.7.5. Evaluation of Rainfall Prediction Errors Made by Calibrated Z-R Equations Using Hypothesis Tests*

### 5.3.7.5.1. Methods

Several hypothesis tests were used to assess the errors in predictions made by the Z-R equations calibrated in this analysis. First, the errors made by the four equations corresponding to the four radar scan elevation levels, as compared to the rain gage measurements, were compared using an ANOVA single-factor test. This test compared the mean values of each of the four sets of errors. Then a two-sample t-test assuming equal variances was used to compare the means of the errors of the calibrated equation and the standard equation for a given scan elevation level for one pixel and rain gage combination. The final statistical test performed was a two-sample F-test on variance. This test was used to compare the standard deviations of the errors in rainfall predictions calculated using both the calibrated equation and the standard equation for a given radar elevation scan for each pixel and rain gage combination.

The null hypothesis for each of these tests would be that the means or the standard deviations of the prediction errors were not different between the equations being compared. If the null hypothesis was accepted for both the t-test and the F-test for the same radar scan elevation for a combination of radar and rain gage data sets, then this was assumed to indicate that a significant difference between the calibrated equation and the standard equation was not detected. If a statistical difference

between the two was not detected, then the calibrated equation does not provide improvement over the standard equation, and the effort and time required to calibrate specific Z-R relationships for a given location may not be necessary.

### 5.3.7.5.2. Results of ANOVA Single-Factor Test

The ANOVA Single-Factor test was used to compare the means of all errors in rainfall predictions made by the equations calibrated for all four scan elevation levels for a given pixel and rain gage combination. A 5% level of significance was chosen for this analysis. The null hypothesis for the analysis of each set of errors was that the means of each of the four sets of errors were equal to each other. If the null hypothesis was accepted and the means were nearly zero, then this would imply that the models were either unbiased or equally biased. Tables 5-30 and 5-31 provide the calculated F values and the calculated critical values of F used to make decisions in the ANOVA Single-Factor tests for both of the storm events. In none of the analyses was the null hypothesis rejected. This implies that the means of the errors calculated using the predicted equations for the four radar scan elevations were equal. The means of each of the equations were also noted to be very close to zero. For instance, the mean value of the errors calculated for pixel 1 and rain gage 1, using the second scan level for the storm event on August 13, 2006, was $7.369*10^{-7}$. This value is not significantly different from zero, and thus it can be determined that the errors calculated using each of the Z-R equations for pixel 1 and rain gage 1 for the storm event on August 13, 2006, are unbiased. The means of errors for the other pixel and rain gage combinations for both storm events are of similar magnitude. Based on

118

these results, each of the four radar scan elevations produced an unbiased Z-R equation.

Table 5-30: F and Critical F Values for ANOVA Single-Factor Test for 8/13/06 Event

| Pixel | Rain Gage | $F_{critical}$ | F | Decision |
|-------|-----------|----------------|---|----------|
| 1 | 1 | 2.732 | $2.473*10^{-10}$ | accept $H_0$ |
| 1 | 5 | 2.751 | $3.805*10^{-11}$ | accept $H_0$ |
| 4 | 32 | 2.730 | $4.555*10^{-11}$ | accept $H_0$ |
| 4 | 38 | 2.766 | $1.467*10^{-10}$ | accept $H_0$ |
| 7 | 69 | 2.669 | $3.433*10^{-11}$ | accept $H_0$ |
| 7 | 70 | 2.669 | $1.913*10^{-11}$ | accept $H_0$ |
| 10 | 17 | 2.708 | 0.006 | accept $H_0$ |
| 10 | 24 | 2.690 | $4.755*10^{-11}$ | accept $H_0$ |
| 10 | 28 | 2.706 | $9.155*10^{-12}$ | accept $H_0$ |
| 10 | 29 | 2.688 | $5.168*10^{-11}$ | accept $H_0$ |
| 10 | 33 | 2.713 | $7.018*10^{-10}$ | accept $H_0$ |
| 10 | 34 | 2.692 | 2.440 | accept $H_0$ |
| 10 | 81 | 2.700 | $6.096*10^{-13}$ | accept $H_0$ |
| 10 | 399 | 2.711 | $9.357*10^{-10}$ | accept $H_0$ |
| 16 | 47 | 2.715 | $3.171*10^{-11}$ | accept $H_0$ |

Table 5-31: F and Critical F Values for ANOVA Single-Factor Test for 7/20/07 Event

| Pixel | Rain Gage | $F_{critical}$ | F | Decision |
|-------|-----------|----------------|---|----------|
| 1 | 1 | 2.651 | $2.346*10^{-11}$ | accept $H_0$ |
| 1 | 5 | 2.650 | $2.281*10^{-6}$ | accept $H_0$ |
| 4 | 32 | 2.655 | $2.048*10^{-11}$ | accept $H_0$ |
| 4 | 38 | 2.652 | 0.014 | accept $H_0$ |
| 7 | 69 | 2.644 | 0.025 | accept $H_0$ |
| 7 | 70 | 2.642 | $3.490*10^{-12}$ | accept $H_0$ |
| 10 | 17 | 2.656 | $3.733*10^{-10}$ | accept $H_0$ |
| 10 | 24 | 2.652 | $5.250*10^{-11}$ | accept $H_0$ |
| 10 | 28 | 2.648 | $5.527*10^{-6}$ | accept $H_0$ |
| 10 | 29 | 2.649 | $1.138*10^{-10}$ | accept $H_0$ |
| 10 | 33 | 2.650 | $6.048*10^{-4}$ | accept $H_0$ |
| 10 | 34 | 2.650 | $9.927*10^{-11}$ | accept $H_0$ |
| 10 | 81 | 2.650 | $4.790*10^{-11}$ | accept $H_0$ |
| 10 | 399 | 2.646 | 0.530 | accept $H_0$ |
| 16 | 47 | 2.659 | $2.955*10^{-11}$ | accept $H_0$ |

**5.3.7.5.3. Results of t-Test for Two Samples Assuming Equal Variances**

A two-sided two-sample t-test that assumes equal variances was used to compare the means of the errors calculated using a specific calibrated Z-R equation to the means of the prediction errors calculated by the standard equation used by the

National Weather Service.  The null hypothesis for these tests was again that the means of the two error sets were equal.  If the null hypothesis was accepted based on the results of this analysis, the difference between the means of the prediction errors of the calibrated and standard equations was not significant.  If this was the case, it could indicate that the time and effort that went into calibrating Z-R equations for a specific location did not produce a significant improvement in rainfall predictions, and therefore were not necessary.  Conversely, if the null hypothesis was rejected, a significant difference between the means of the prediction errors made by the standard equation and the calibrated equation did exist.  Such a result would provide evidence that calibration of Z-R equations is a useful step when using radar data as input for hydrologic models.

Tables 5-32 and 5-33 provide samples of the calculated t values and critical t values used for making decisions for the two storm events.  The null hypothesis was accepted for at least one radar scan elevation for every single pixel and rain gage combination tested.  Which scan levels had the null hypothesis accepted for each rain gage in the pixel was seen to be reasonably consistent.  While the same scan levels did not necessarily accept the null hypothesis for every single rain gage within a pixel, the same scan levels did have the null hypothesis accepted frequently.  Similarly, reasonable consistency was seen between the two storm events analyzed in which scan elevations had the null hypothesis accepted.  In general, it seemed that the scan that had the null hypothesis accepted corresponded to the scan that had the best goodness-of-fit statistics for the Z-R equation calibrated.  This might suggest that poor goodness of fit at any scan level indicate that the measured data does not reflect

the physical processes. The scan elevations that had the best goodness-of-fit statistics

should provide the most accurate rainfall estimates. These results may indicate that

calibration of Z-R equations is not necessary. If the errors in the rainfall predictions

calculated by the calibrated Z-R equation with the best goodness-of-fit statistics do

not significantly differ in means from the errors in rainfall predictions calculated by

the standard equation, then the calibrated equations may not improve the predictions

compared to the standard equation. This may mean that the effort that is necessary to

calibrate Z-R equations is not necessary. However, the results of the t-test alone are

not sufficient to draw conclusions about the usefulness of calibrating Z-R equations

for specific locations because these results are only relevant to the means of the

prediction errors.

**Table 5-32: Sample of t and Critical t Values for 8/13/06 Event**

| Pixel | Rain Gage | Scan Level | $t_{critical}$ | t | Decision | Rejection Probability |
|---|---|---|---|---|---|---|
| 1 | 1 | 2 | 2.064 | 0.916 | accept $H_0$ | 0.369 |
| 1 | 1 | 3 | 2.021 | -2.605 | reject $H_0$ | 0.013 |
| 1 | 1 | 4 | 2.021 | -1.979 | accept $H_0$ | 0.055 |
| 1 | 1 | 5 | 2.021 | -1.731 | accept $H_0$ | 0.091 |

**Table 5-33: Sample of t and Critical t Values for 7/20/07 Event**

| Pixel | Rain Gage | Scan Level | $t_{critical}$ | t | Decision | Rejection Probability |
|---|---|---|---|---|---|---|
| 1 | 1 | 2 | 1.989 | 3.954 | reject $H_0$ | 0.0002 |
| 1 | 1 | 3 | 1.984 | 1.670 | accept $H_0$ | 0.098 |
| 1 | 1 | 4 | 1.984 | -1.779 | | 0.078 |
| 1 | 1 | 5 | 1.983 | -3.211 | reject $H_0$ | 0.002 |

**5.3.7.5.4. Results of Two-Sample F-Test on Variance**

The standard deviation of a set of errors is the standard error, which is a

measure of the accuracy of a statistic. The standard deviations of the errors made in

calculating rainfall predictions using the calibrated Z-R equations and the prediction

errors made by the standard equation were compared using a two-sided two-sample

F-test on variance. The null hypothesis for these analyses was that the standard

deviations of the two sample sets were equal.  Similar to the t-test, if the null

hypothesis was accepted for a given scan elevation level for a pixel and rain gage

combination, then the standard deviations of the errors made when using the

calibrated equation and the standard equation were not significantly different.  If the

null hypothesis was rejected, then the differences in the standard deviations of the

errors in rainfall predictions were significant.  This could provide evidence that the

calibration of Z-R equations for specific locations could be a valuable tool to

hydrologic analyses using radar data.

Tables 5-34 and 5-35 provide a sample of the calculated F values and the

critical F values used to make decisions in this analysis.  With one exception, the

storm event on August 13, 2006, for rain gage 399 in pixel 10, at least one scan

elevation level had the null hypothesis accepted for every scenario modeled.  These

results may indicate that, for these scan elevation levels at least, calibration of Z-R

equations for specific locations does not significantly improve the rainfall predictions.

However, the scan elevation levels that had the null hypothesis accepted for the F-test

were not necessarily the same scans that had the null hypothesis accepted for the t-

test.  They also did not correspond to the scans with the best goodness-of-fit statistics

for the Z-R equations as well as the results of the t-test did.  In order to draw

conclusions about the necessity of calibrating Z-R equations, the comparison of the

results of the t-test and the F-test need to be coordinated for each radar scan elevation

level for each pixel and rain gage combination.

**Table 5-34: Sample of F and Critical F values for 8/13/06 Event**

| Pixel | Rain Gage | Scan Level | $F_{critical}$ | F | Decision |
|-------|-----------|------------|----------------|---|----------|
| 1 | 1 | 2 | 3.277 | 2.476 | accept $H_0$ |
| 1 | 1 | 3 | 2.465 | 545.356 | reject $H_0$ |
| 1 | 1 | 4 | 2.465 | 4156.837 | reject $H_0$ |
| 1 | 1 | 5 | 4.464 | 4324.728 | reject $H_0$ |

**Table 5-35: Sample of F and Critical F Values for 7/20/07 Event**

| Pixel | Rain Gage | Scan Level | $F_{critical}$ | F | Decision |
|-------|-----------|------------|----------------|---|----------|
| 1 | 1 | 2 | 1.870 | 1.056 | accept $H_0$ |
| 1 | 1 | 3 | 1.770 | 1.053 | accept $H_0$ |
| 1 | 1 | 4 | 1.770 | 3.648 | reject $H_0$ |
| 1 | 1 | 5 | 1.780 | 4.003 | reject $H_0$ |

### 5.3.7.5.5. Conclusions Based on Results of t-Test and F-Test

If the null hypothesis was accepted for the t-test and the F-test for the same scan elevation for the same pixel and rain gage combination, then neither the means nor the standard deviations of the errors in predictions from the calibrated equation and the standard equation were significantly different. This gives a strong indication that calibration of Z-R equations does not significantly improve the rainfall predictions, which makes a strong argument for simply using the standard equation rather than calibrating equations for specific locations. Unfortunately, when comparing the results of these two analyses for all of the scenarios modeled, trends were not found to indicate that calibration was unnecessary. While the null hypothesis was accepted for both tests for several scenarios, there were at least an equal number of scenarios in which the null hypothesis was rejected for one or both of the tests. This indicates that in many of the modeled scenarios, significant differences do exist in either the mean, standard deviation, or both between the errors in rainfall prediction made by the calibrated equation versus the standard equation. The lack of strong, consistent evidence of a lack of difference is evidence that calibration of the Z-R relationships for a specific location could be useful, and

possibly even necessary, if using radar data as input to hydrologic models. In order to draw firmer conclusions, the effect that calibration of equations has on the goodness-of-fit statistics and overall accuracy of the predictions must be examined.

### 5.3.7.6. Evaluation of "Averaged Coefficient" Z-R Equations

**5.3.7.6.1. Methods**

Finally, the variation in the Z-R equation coefficients between storm events was investigated. A Z-R equation was calibrated for each radar pixel and rain gage combination for two separate storms. The *A* and *b* coefficients from the two equations calibrated for the same radar pixel and rain gage combination for two storm events were averaged, resulting in a new Z-R equation for each radar pixel and rain gage combination. The goodness-of-fit statistics for rainfall predictions made using these equations with average coefficient values were calculated and compared to those calculated using the two Z-R equations calibrated for each of the two storm events for the given radar pixel and rain gage data set combination. Rainfall intensity predictions were made using the Z-R equations with the average coefficient values as described previously. Then the errors in predictions were calculated for the average equations, and these were compared to the errors made using both of the calibrated equations as well as the standard equation for the given pixel and rain gage combination. This analysis investigated the sensitivity of the rainfall predictions to the coefficients of the Z-R equation.

**5.3.7.6.2. Results of "Averaged Coefficient" Z-R Equations**

When comparing the Z-R equation coefficients calibrated for a given rain gage between the two storm events used in these analyses more similarity in

coefficients than expected was observed. Therefore, to evaluate how sensitive the rainfall predictions were to the coefficients of the Z-R equation, the average values of the *A* and *b* coefficients for the same pixel and rain gage combination were calculated based on the calibrated coefficients for both storm events. Rainfall predictions were made for both storms using these Z-R equations with average coefficients, and the errors in rainfall rate predictions, as compared to the rain gage measurements, were calculated. The goodness-of-fit statistics for these equations with average coefficients were also calculated and compared to those of the calibrated equations for each storm. Then the accuracy of predictions and goodness-of-fit statistics for the calibrated equation, standard equation, and average equation for a given radar and rain gage combination could be evaluated.

The results of this analysis led to several interesting conclusions. A clear trend in the effects of the average coefficients on the goodness-of-fit statistics was not observed. In some cases, when the average coefficients were used to predict rainfall the goodness-of-fit statistics were seen to significantly worsen, but in many cases a significant change was not observed in the goodness-of-fit statistics with the use of average coefficient values. The means and standard deviations of the standard equation prediction errors, the calibrated equation prediction errors, and the average equation prediction errors were all calculated and compared. Wide variation was seen in the mean values of the errors; however, significant variation in standard deviation values was not always observed. The observations suggest that only calibrated equations typically provide unbiased rainfall predictions; however, the bias seen in the standard equation and average equation prediction errors, while sometimes

quite significant, does not necessarily significantly influence the accuracy of the rainfall estimates.

### *5.3.7.7. Conclusions*

The results observed made it difficult to reach conclusions regarding the necessity of location-specific calibration of Z-R equations. In general, an unbiased model is desirable, however the rainfall predictions made using the standard Z-R equation tended to be biased while the predictions made using the calibrated equations tended no to be biased. However, the goodness-of-fit statistics calculated in this analysis suggest that calibration of a Z-R equation for a location is not guaranteed to improve the rainfall estimates calculated as compared to the standard equation. Significant improvements in goodness-of-fit statistics for the rainfall predictions made using the standard equation and the calibrated equation were not consistently observed.

The process of calibrating Z-R equations for a given set of radar and rain gage data is a fairly time- and labor-intensive task. Therefore, the decision of whether or not to calibrate Z-R equations for a specific location when using radar data in a hydrologic model may need to be made on a case-by-case basis. If corresponding radar and rain gage data sets are readily available for the location, then perhaps calibration of equations would be wise. On the other hand, if rain gage and radar data that correspond well are not easily available, using the standard Z-R equation should suffice for most hydrologic analyses. The specific analyses to be conducted should also be considered. If, for instance, high accuracy and confidence in the results of an analysis are desired calibration of Z-R equations would likely be advisable. If the aim of the analysis is only to determine a general estimate, and high accuracy is not

necessarily needed, the standard equation would more than likely provide acceptable

results.

# CHAPTER 6

# ANALYSIS OF FACTORS AFFECTING THE

# SEMIVARIOGRAM

## *6.1. INTRODUCTION*

Semivariograms are often used in hydrological analysis as they can illustrate spatial or temporal variance in sample data.  Semivariograms are easiest to evaluate when measurements are made on a grid, where the grid lines are a distance h apart. In these experiments a square or rectangular grid was used with synthetic rainfall data to model a watershed.  The notation $\gamma(h)$ is used to represent the semivariogram for a separation distance h, and they are often plotted as $\gamma(h)$ versus h, where h is the separation distance between the grid points.  This graph will pass through the origin, and then it will gradually increase as the separation distance increases, up until a certain point, after which it will not increase further.  It is possible, in some cases, for a  $\gamma(h)$ to decrease as the separation distance increases, but this usually only happens when the sample size is small and the separation distance is large.  As far as the shape of the semivariogram is concerned, two characteristics are particularly important. The separation distance where the semivariogram begins to approach a constant value is called the radius of influence.  This value occurs when a semivariogram approaches the sample variance.  The second characteristic is known as the sill.  The sill is the portion of the semivariogram where $\gamma(h)$ is approximately the sample variance (Hromadka *et al.*, 1993).

128

Semivariograms are a commonly used analysis tool used in hydrological modeling. They serve as an input to the kriging method, which is used to interpolate rainfall values in areas where no data exists. Kriging is often used to predict rainfall at points where no rain gage exists or where data is missing for a time period. Semivariograms are also used to evaluate the accuracy of gage data. Therefore a semivariogram is an intermediate step to evaluating the spatial variability of rainfall based on data from a gage network (Cheng *et al.*, 2007). Because dense gage networks are very rare and many watersheds do not even have one rain gage, another method of computing semivariograms in order to predict rainfall would be desirable. Radar data may one day be able to fill this gap and provide input to the kriging method for the purpose of predicting rainfall at any point on a watershed.

The objective of these semivariogram studies was to determine the effect that various storm characteristics could have on the calculated semivariogram. Semivariograms are often used to estimate rainfall when data are not available, so it is important to understand how characteristics of the rainfall itself could influence those estimates. The results of this research could then be compared to future studies using other methods rainfall data sources, such as radar data.

## 6.2. COMPUTER PROGRAMS USED IN ANALYSES

Several computer programs, referred to as the RADARXX programs, were developed for the semivariogram analyses. Though each program had its own specific purpose, they all required the same general input data, and they all gave the same general output. The general input data required by each program included information about the study watershed and storm. In order to construct the

watershed, each program needed information about the length and width of the watershed, which was assumed to be rectangular in order to relate the results of these studies to potential future studies involving radar data, as well as the spacing between nodes of the watershed grid, with each node representing a rain gage. A variety of information relating to the size, shape, and movement of the storm was also required by each program. Because each storm was modeled as a series of concentric ellipses, the program required information about the length of the major axis of each ellipse and the ratio of the major axis to the minor axis, which was assumed to be the uniform across the ellipses of each storm. The program also required the rainfall depth that each ellipse boundary represented. Finally, in order to simulate a moving storm, each program required information about the velocity of the storm, the direction in which the storm was moving, and the number of time periods for which the storm should be simulated. Each of the programs allowed the user to choose from several possible semivariogram models. The spherical model, which is the most commonly used of the semivariogram models, was utilized in these studies.

## 6.3. EFFECT OF STORM SHAPE

### 6.3.1. Introduction

Real storms have many different shapes and sizes. In an attempt to identify the effect of storm shape on storm semivariograms, the shape of a storm was modified over a variety of modeling runs. To do this, synthetic elliptical storms were created, and then the ratio of the major axis to the minor axis of the ellipse was changed so that the storm varied in shape from circular to elliptical. While most true storms are neither perfectly circular nor elliptical, this experiment did provide some

130

insight into how the changing of the shape of a storm could change the semivariogram calculated for that storm. This study was also used to evaluate the possibility of assuming storm isotropy, by comparing the East-West, North-South, and nondirectional semivariograms.

## 6.3.2. Methods and Materials

To examine the effects of storm shape on the semivariogram the ratio of the lengths of the major to minor axes of the storm ellipses was varied. A program was developed to create a storm and a watershed. The grid, which will be referred to as watershed 1 for future use, was 60-km long and 48-km wide, and it had 208 nodes, or gages spaced 4-km apart. The storm that was created, which will be referred to as storm 1 for future use, contained five ellipses each representing different rainfall values. The ellipses each had an *a*-to-*b* ratio of 1.25, and the major axes were 0-km for the center of the storm, then 6-km, 15-km, 27-km, and 38-km. The inner ellipse represented a total rainfall depth of 11 mm, then 9 mm, 7 mm, 4 mm, and finally 2 mm. For this particular research objective watershed 1 was used with storm 1; however, the ratio of *a*-to-*b* was changed in each program run. A velocity of 5 km/hr was chosen for the storm velocity. This watershed and storm information was input into the program multiple times, each time changing the value of the *a*-to-*b* ratio. Values of 1.0, 1.1, 1.2, 1.25, 1.3, 1.4, and 1.5 were chosen, and the program was run using each of these ratios.

The output file for each of these runs was examined, and it was determined due to the level of variation in data that the values of 1.0, 1.25, and 1.5 should be further examined. The trends for the other ratios were very similar. The output files

for each of these ratios contained a semivariogram for each storm movement. The most representative semivariogram values were chosen for each ratio, and then those semivariograms were further evaluated. For each separate storm the relative bias, the standard error ratio, the correlation coefficient R, and the final estimates of the sill and radius of influence were recorded for comparison.

## 6.3.3. Results and Discussion

The results of this study, shown in Tables 6-1 and 6-2, show that the choice of the storm shape has little, if any, influence on the calculated semivariogram. The fitted semivariogram in the East-West direction did not show significant difference in values of the sill or radius of influence for the ratios of 1.0, 1.25, or 1.5. The fitted semivariogram in the North-South direction did show some significant change in the sill, though a change was not detected in the radius of influence. It is believed, however, that any change seen in the sill values in the North-South direction is due to the storm overhanging the edge of the watershed, rather than a direct effect of the change in the *a*-to-*b* ratio. The radius of influence of the semivariograms in the North-South direction are much smaller than the East-West direction because the major axis of the storm was oriented in the East-West direction. This means that the storm was longer than it was wide, and the storm affected a smaller distance in the North-South direction than it did in the East-West direction.

**Table 6-1: E-W Semivariograms for Storms of Varying Shapes**

| *a*-to-*b* Ratio | Sill (mm$^2$) | Radius of Influence (km) | Relative Bias | Standard Error Ratio | R |
|---|---|---|---|---|---|
| 1.0 | 5.8 | 40 | 0.033 | 0.256 | 0.962 |
| 1.25 | 5.6 | 40 | 0.035 | 0.270 | 0.967 |
| 1.5 | 5.7 | 40 | 0.028 | 0.235 | 0.975 |
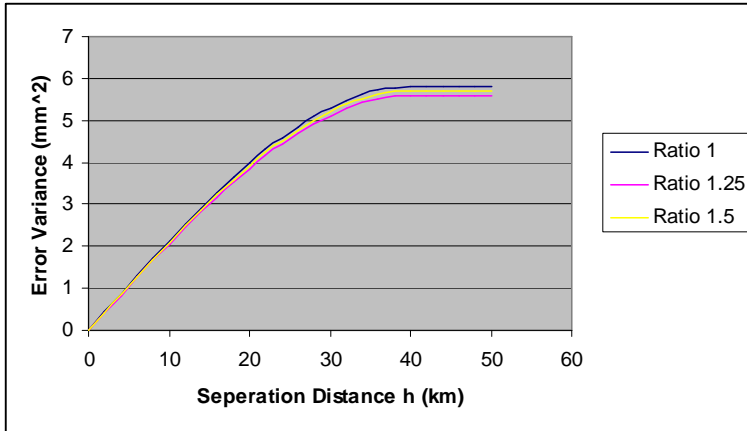
**Figure 6-1: E-W Semivariograms Where Ratio 1, Ratio 1.25, and Ratio 1.5 Denote Differing Storm Shapes**

**Table 6-2: N-S Semivariograms for Storms of Varying Shapes**

| *a*-to-*b* Ratio | Sill (mm²) | Radius of Influence (km) | Relative Bias | Standard Error Ratio | R |
|---|---|---|---|---|---|
| 1.0 | 3.0 | 28.8 | 0.034 | 0.383 | 0.933 |
| 1.25 | 4.5 | 27.0 | 0.033 | 0.443 | 0.910 |
| 1.5 | 5.8 | 26.3 | 0.041 | 0.036 | 0.943 |
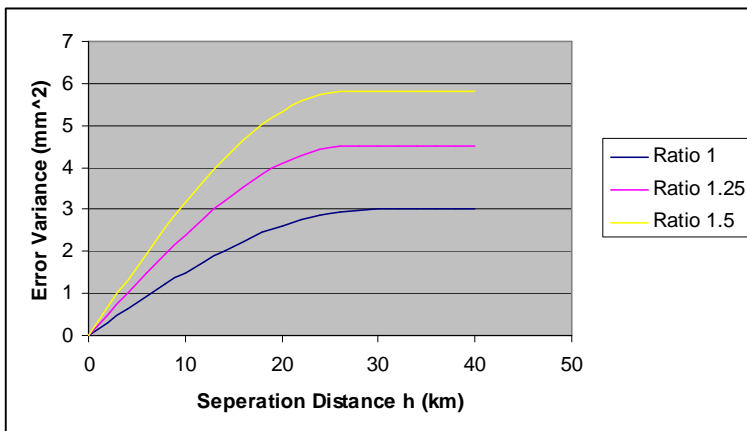


**Figure 6-2: N-S Semivariograms Where Ratio 1, Ratio 1.25, and Ratio 1.5 Denote Differing Storm Shapes**

The possibility of assuming storm anisotropy was also considered during this study. The East-West, North-South, and nondirectional semivariograms output by the program were compared for each storm computed. If the values of the semivariograms were similar between the three, and if the general patterns of ascending and descending values had been the same, the assumption of isotropy would have been declared acceptable. However, despite the fact that the values of

each semivariogram were all of the same magnitude, the variation in the data was considered excessive. Therefore, it was determined that the storms should be treated as anisotropic events, rather than as isotropic events.

## 6.4. EFFECT OF STORM SIZE COMPARED TO WATERSHED

### 6.4.1. Introduction

The first synthetic storm created to evaluate these questions of interest was a spatially large storm in comparison to the watershed. The variability of the semivariogram for the storm discussed in section 6.3 was less than expected. A possible explanation put forth for that result was that, because the storm was larger than the watershed, the rain gages were not experiencing the full variability of the storm. In order to evaluate the validity of this hypothesis a second, smaller storm, was created and studied.

### 6.4.2. Methods and Materials

To determine that the effect that the storm size had on the semivariogram, two different storms were simulated on the same watershed. Watershed 1 was used with both storms. The first step to providing answers to this question was to simulate storm 1 on the watershed. This served as the first case in which the storm was wider than the watershed. A semivariogram generated for this storm was chosen to be edited for further investigation. The relative bias, the standard error ratio, the correlation coefficient R, and the final estimates for the sill and radius of influence of the semivariogram were recorded.

The next step was to create a smaller storm that would not be wider than the watershed itself. For this storm, which will be referred to as storm 2 for future use, the *a*-to-*b* ratio of 1.25 was maintained, but smaller values for *a* were used. The largest value of *a* used in the storm was 28-km, then the smaller ellipses had values of 19-km, 12-km, 5-km, and 0-km, with the 0-km being the storm center. The rainfall values were also held constant from the first storm. Information about this storm was input into the program, and then a semivariogram was chosen for further use from the output of this program. All of the information that was recorded in the first storm was recorded for this storm. Comparisons between these values were made in order to determine the effect the storm-to-watershed width ratio had on the semivariogram.

### 6.4.3. Results and Discussion

The results of this study, shown in Tables 6-3 to 6-6, indicate that the size of the storm in comparison to the size of the watershed can have an effect on the semivariogram. In looking at the East-West semivariograms it is evident that for the smaller storm the radius of influence decreases while the sill increases. This increase in sill is due to the fact that the storm ellipses are closer together than those of the larger storm, so the watershed experiences a larger variation in rainfall. The decrease in radius of influence is due to the fact that the smaller storm is narrower than the larger storm. Therefore, the ellipses, which represent isohyets, are closer together and spatial correlation ends at a closer distance. Less effect is visible in the North-South semivariograms. This result was expected, and is caused by the storm moving in an East-West direction across the watershed.

**Table 6-3: Storm 1 E-W Semivariogram for Varying Storm Velocities**

| Velocity (km/hr) | Maximum Separation Distance (km) | Sill (mm$^2$) | Radius of Influence (km) | Relative Bias | Standard Error Ratio | R |
|---|---|---|---|---|---|---|
| 5 | 32 | 18.0 | 159 | 0.041 | 0.238 | 0.975 |
| 5 | 36 | 5.5 | 49 | 0.040 | 0.278 | 0.966 |
| 10 | 28 | 32.3 | 278 | 0.060 | 0.248 | 0.974 |
| 10 | 32 | 9.4 | 82 | 0.038 | 0.268 | 0.969 |
| 10 | 36 | 4.6 | 35 | 0.046 | 0.342 | 0.948 |
| 15 | 32 | 19.9 | 176 | 0.040 | 0.238 | 0.975 |
| 15 | 36 | 5.5 | 45 | 0.040 | 0.278 | 0.967 |
| 20 | 28 | 29.8 | 243 | 0.057 | 0.233 | 0.977 |
| 20 | 32 | 27.5 | 224 | 0.045 | 0.196 | 0.983 |
| 20 | 36 | 13.5 | 111 | 0.030 | 0.203 | 0.982 |
| 20 | 40 | 6.1 | 45 | 0.036 | 0.251 | 0.972 |

**Table 6-4: 2 E-W Semivariogram for Varying Storm Velocities**

| Velocity (km/hr) | Maximum Separation Distance (km) | Sill (mm$^2$) | Radius of Influence (km) | Relative Bias | Standard Error Ratio | R |
|---|---|---|---|---|---|---|
| 5 | 24 | 43.6 | 206 | 0.063 | 0.270 | 0.970 |
| 5 | 28 | 11.0 | 52 | 0.041 | 0.305 | 0.960 |
| 5 | 32 | 6.9 | 29 | 0.045 | 0.399 | 0.929 |
| 10 | 24 | 54.3 | 251 | 0.033 | 0.278 | 0.969 |
| 10 | 28 | 12.7 | 60 | 0.041 | 0.302 | 0.961 |
| 10 | 32 | 7.2 | 30 | 0.046 | 0.392 | 0.932 |
| 15 | 24 | 43.6 | 206 | 0.063 | 0.270 | 0.970 |
| 15 | 28 | 11.0 | 52 | 0.041 | 0.305 | 0.960 |
| 15 | 32 | 6.9 | 29 | 0.045 | 0.399 | 0.929 |
| 20 | 20 | 38.6 | 187 | 0.059 | 0.269 | 0.972 |
| 20 | 24 | 10.4 | 51 | 0.034 | 0.280 | 0.968 |
| 20 | 28 | 6.2 | 27 | 0.0396 | 0.321 | 0.956 |

**Table 6-5: Storm 1 N-S Semivariogram for Varying Storm Velocities**

| Velocity (km/hr) | Maximum Separation Distance (km) | Sill (mm$^2$) | Radius of Influence (km) | Relative Bias | Standard Error Ratio | R |
|---|---|---|---|---|---|---|
| 5 | 24 | 22.9 | 154 | 0.049 | 0.249 | 0.975 |
| 5 | 28 | 6.5 | 43 | 0.037 | 0.277 | 0.967 |
| 10 | 24 | 25.6 | 177 | 0.050 | 0.245 | 0.976 |
| 10 | 28 | 6.6 | 44 | 0.037 | 0.268 | 0.970 |
| 10 | 32 | 4.9 | 30 | 0.039 | 0.326 | 0.953 |
| 15 | 24 | 24.1 | 163 | 0.049 | 0.248 | 0.975 |
| 15 | 28 | 6.4 | 42 | 0.037 | 0.277 | 0.968 |
| 20 | 24 | 25.1 | 170 | 0.050 | 0.248 | 0.975 |
| 20 | 28 | 6.6 | 43 | 0.037 | 0.275 | 0.968 |

**Table 6-6: Storm 2 N-S Semivariogram for Varying Storm Velocities**

| Velocity (km/hr) | Maximum Separation Distance (km) | Sill (mm$^2$) | Radius of Influence (km) | Relative Bias | Standard Error Ratio | R |
|---|---|---|---|---|---|---|
| 5 | 20 | 34.2 | 133 | 0.048 | 0.271 | 0.972 |
| 5 | 24 | 6.90 | 24 | 0.045 | 0.386 | 0.939 |
| 10 | 20 | 41.6 | 164 | 0.050 | 0.269 | 0.973 |
| 10 | 24 | 6.90 | 24 | 0.045 | 0.383 | 0.939 |
| 15 | 20 | 34.2 | 133 | 0.048 | 0.271 | 0.972 |
| 15 | 24 | 6.90 | 24 | 0.045 | 0.386 | 0.939 |
| 20 | 20 | 46.3 | 171 | 0.054 | 0.270 | 0.972 |
| 20 | 24 | 8.50 | 30 | 0.041 | 0.335 | 0.954 |

## *6.5. EFFECT OF STORM VELOCITY*

## 6.5.1. Introduction

Actual rain storms can travel at many different velocities. The velocity of a storm is a function of the storm type and the climate conditions at the time. It was hypothesized that differences in velocity could impact the semivariogram for the storm. To evaluate this hypothesis the same storm was simulated over a watershed while moving at several different velocities, and then the computed semivariograms were compared.

## 6.5.2. Trial 1

### *6.5.2.1. Methods and Materials*

In order to determine the effect of storm velocity on the semivariogram, watershed 1 and storm 1 were utilized, with a slight modification. While most of the information from storm 1 was utilized, the velocity of the storm was varied in each simulation. This storm information was input to the program four separate times, with the velocities of 5 km/hr, 10 km/hr, 15 km/hr, and finally 20 km/hr. The semivariograms output from this program were examined, and then one was selected

from each velocity simulation to be further evaluated.  Several statistics of the fitted

semivariogram were recorded for future comparison and analysis.

### 6.5.2.2. Results and Discussion

The results of this trial, which are shown in Tables 6-7 and 6-8, indicated that

the velocity of the storm had very little effect on the fitted semivariogram.  The

values for the sill oscillated between 6.4 mm$^2$ and 6.6 mm$^2$, while the values for the

radius of influence fluctuated between 41 and 44 km.  It was interesting to note that

the semivariograms computed by the program for the storms with velocities of 5

km/hr and 15 km/hr were exactly identical.  This fact, coupled with the lack of

significant difference between the calculated parameters for each storm velocity led

to an unexpected conclusion.  Based on these facts it was determined that the velocity

of the storm was less important than where the storm center landed in relation to the

rain gages.  A storm traveling at a relatively constant speed over a watershed with

gages spaced uniformly over the watershed can be responsible for showing that storm

velocity does not influence semivariogram characteristics.  This indicates that the

semivariogram would be more impacted by the rain gage density and rain gage

locations, as well as the storm size than it would by the actual velocity of the storm.

It is expected that when the storm center lands relatively near a rain gage and the

storm is sized so that the watershed experiences the full range of rainfall contained by

the storm a higher variation in the semivariogram will result.  Conversely, if the

center of the storm lands relatively distant from any gage and the storm is large

enough that the full variation is not felt by the watershed little variation will show in

the semivariogram.

**Table 6-7: E-W Semivariogram for Varying Storm Velocities**

| Velocity (km/hr) | Sill (mm$^2$) | Radius of Influence (km) | Relative Bias | Standard Error Ratio | R |
|---|---|---|---|---|---|
| 5 | 4.1 | 32 | 0.031 | 0.513 | 0.872 |
| 10 | 3.5 | 28 | 0.028 | 0.706 | 0.740 |
| 15 | 4.1 | 32 | 0.031 | 0.513 | 0.872 |
| 20 | 5.6 | 40 | 0.035 | 0.270 | 0.967 |

**Table 6-8: N-S Semivariogram for Varying Storm Velocities**

| Velocity (km/hr) | Sill (mm$^2$) | Radius of Influence (km) | Relative Bias | Standard Error Ratio | R |
|---|---|---|---|---|---|
| 5 | 4.1 | 25 | 0.029 | 0.587 | 0.833 |
| 10 | 4.2 | 25 | 0.029 | 0.557 | 0.851 |
| 15 | 4.1 | 25 | 0.028 | 0.587 | 0.833 |
| 20 | 4.2 | 25 | 0.029 | 0.580 | 0.837 |

## 6.5.3. Trial 2

### 6.5.3.1. Methods and Materials

After examining the results of Trial 1 a potential source of problems in the data was discovered. The large size of the storm could be preventing the watershed from experiencing the full variation of the storm. For this second trial, therefore, storm 2, which is smaller than storm 1, was used for the purposes of comparison.

After information about storm 2 was input to the program four times, with velocities of 5 km/hr, 10 km/hr, 15 km/hr, and 20 km/hr, the semivariograms output by the program were examined. A semivariogram was chosen to represent each velocity simulation in further investigation. In order to compare results, the relative bias, standard error ratio, correlation coefficient R, and the final estimates of the sill and radius of influence were recorded for each velocity.

### 6.5.3.2. Results and Discussion

The results of this study into the effect of storm velocity on the semivariogram, shown in Tables 6-9 to 6-12, did not significantly differ from the results of the first study examining this particular research question, with one

exception. The final estimates of the sill and radius of influence were significantly

different for a velocity of 20 km/hr, though not for the other three velocities. Though

this difference was significant it is not considered to truly be the effect of the storm

velocity, because the first three velocity values did not show any significant

difference in sill or radius of influence. It is believed instead that this difference in

sill and radius of influence was due to the storm traveling off the watershed to some

degree during the course of the simulation. Despite the anomaly at a velocity of 20

km/hr, this smaller storm again indicates that it is not the velocity of the storm, but

where it falls in relation to the rain gages that truly impacts the storm semivariogram.

**Table 6-9: Storm 1 E-W Semivariogram for Varying Storm Velocities**

| Velocity (km/hr) | Maximum Separation Distance (km) | Sill (mm$^2$) | Radius of Influence (km) | Relative Bias | Standard Error Ratio | R |
|---|---|---|---|---|---|---|
| 5 | 32 | 18.0 | 159 | 0.041 | 0.238 | 0.975 |
| 5 | 36 | 5.5 | 45 | 0.040 | 0.278 | 0.966 |
| 10 | 28 | 32.3 | 278 | 0.060 | 0.248 | 0.974 |
| 10 | 32 | 9.4 | 82 | 0.038 | 0.267 | 0.969 |
| 10 | 36 | 4.6 | 35 | 0.046 | 0.342 | 0.948 |
| 15 | 32 | 19.9 | 176 | 0.040 | 0.238 | 0.975 |
| 15 | 36 | 5.5 | 45 | 0.040 | 0.278 | 0.966 |
| 20 | 28 | 29.7 | 243 | 0.057 | 0.233 | 0.977 |
| 20 | 32 | 27.5 | 224 | 0.045 | 0.196 | 0.983 |
| 20 | 36 | 13.5 | 111 | 0.030 | 0.203 | 0.982 |
| 20 | 40 | 6.1 | 45 | 0.036 | 0.251 | 0.971 |
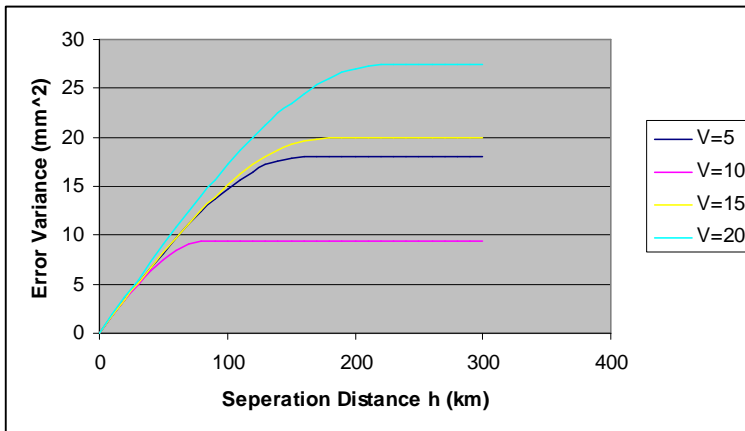


**Figure 6-3: E-W Semivariograms for Different Storm Velocities**

140

**Table 6-10: Storm 2 N-S Semivariogram for Varying Storm Velocities**

| Velocity (km/hr) | Maximum Separation Distance (km) | Sill (mm$^2$) | Radius of Influence (km) | Relative Bias | Standard Error Ratio | R |
|---|---|---|---|---|---|---|
| 5 | 24 | 43.6 | 206 | 0.063 | 0.270 | 0.970 |
| 5 | 28 | 11.0 | 52 | 0.041 | 0.305 | 0.960 |
| 5 | 32 | 6.9 | 29 | 0.045 | 0.399 | 0.929 |
| 10 | 24 | 54.3 | 251 | 0.066 | 0.278 | 0.969 |
| 10 | 28 | 12.7 | 60 | 0.041 | 0.302 | 0.961 |
| 10 | 32 | 7.2 | 30 | 0.046 | 0.392 | 0.932 |
| 15 | 24 | 43.6 | 206 | 0.063 | 0.270 | 0.970 |
| 15 | 28 | 11.0 | 52 | 0.041 | 0.305 | 0.960 |
| 15 | 32 | 6.9 | 29 | 0.045 | 0.399 | 0.929 |
| 20 | 20 | 38.6 | 187 | 0.059 | 0.269 | 0.972 |
| 20 | 24 | 10.4 | 51 | 0.034 | 0.280 | 0.968 |
| 20 | 28 | 6.2 | 27 | 0.039 | 0.321 | 0.956 |
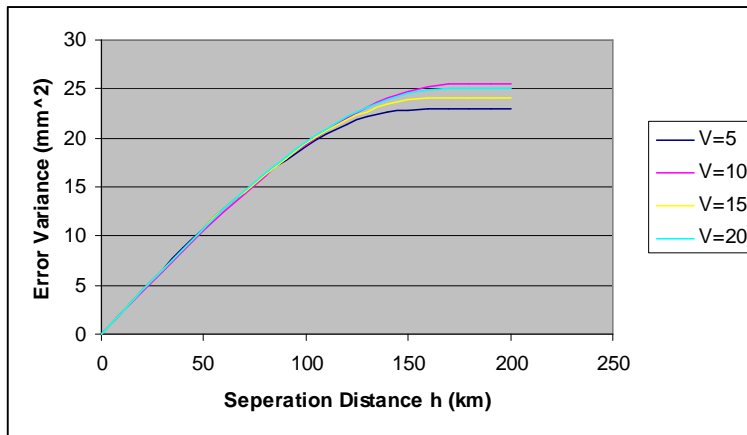


**Figure 6-4: N-S Semivariograms for Different Storm Velocities**

**Table 6-11: Storm 1 N-S Semivariogram for Varying Storm Velocities**

| Velocity (km/hr) | Maximum Separation Distance (km) | Sill (mm$^2$) | Radius of Influence (km) | Relative Bias | Standard Error Ratio | R |
|---|---|---|---|---|---|---|
| 5 | 24 | 22.9 | 154 | 0.049 | 0.249 | 0.975 |
| 5 | 28 | 6.5 | 43 | 0.037 | 0.277 | 0.967 |
| 10 | 24 | 25.6 | 177 | 0.050 | 0.245 | 0.976 |
| 10 | 28 | 6.6 | 44 | 0.037 | 0.268 | 0.970 |
| 10 | 32 | 4.9 | 30 | 0.039 | 0.326 | 0.953 |
| 15 | 24 | 24.1 | 163 | 0.049 | 0.248 | 0.975 |
| 15 | 28 | 6.4 | 42 | 0.037 | 0.277 | 0.968 |
| 20 | 24 | 25.1 | 170 | 0.050 | 0.245 | 0.975 |
| 20 | 28 | 6.6 | 43 | 0.037 | 0.275 | 0.968 |

**Table 6-12: Storm 2 N-S Semivariogram for Varying Storm Velocities**

| Velocity (km/hr) | Maximum Separation Distance (km) | Sill (mm$^2$) | Radius of Influence (km) | Relative Bias | Standard Error Ratio | R |
|---|---|---|---|---|---|---|
| 5 | 20 | 34.2 | 133 | 0.048 | 0.271 | 0.972 |
| 5 | 24 | 6.9 | 24 | 0.045 | 0.386 | 0.939 |
| 10 | 20 | 41.6 | 164 | 0.050 | 0.269 | 0.973 |
| 10 | 24 | 6.9 | 24 | 0.045 | 0.383 | 0.939 |
| 15 | 20 | 34.2 | 133 | 0.048 | 0.271 | 0.972 |
| 15 | 24 | 6.9 | 24 | 0.045 | 0.386 | 0.939 |
| 20 | 20 | 46.3 | 171 | 0.054 | 0.270 | 0.972 |
| 20 | 24 | 8.5 | 30 | 0.041 | 0.335 | 0.954 |

## 6.5.4. Trial 3

### 6.5.4.1. Methods and Materials

A final attempt to identify the effect of storm velocity on the semivariogram utilized a new program that calculated cumulative storm semivariograms. Watershed 1 was again used; however, a new storm was created to completely fill this watershed. The major axes of this storm were 0-km at the center, then 6-km, 13-km, 21-km, and 30-km. All other storm parameters, including the storm velocities, were the same as those used in storm 2. Because this program calculates cumulative semivariograms the storms were allowed to travel entirely over the watershed. The storm center was started 30-km to the left of the watershed, and it was allowed to travel 120-km, until the storm center was 30-km to the right of the watershed. This allowed the entire storm variation to contribute to the semivariogram calculations.

### 6.5.4.2. Results and Discussion

The results of trial 3, which investigated the effects of storm velocity on a cumulative storm semivariogram, shown in Tables 6-13 and 6-14, were much different from the results of trials 1 and 2. Less variation was seen in the East-West direction than in the North-South direction. This is due to the fact that the storm is moving from West to East across the watershed. Therefore, each point on the

watershed in the East-West direction should ultimately receive approximately the same amount of rainfall.  Because of the elliptical nature of the synthetic storms, more variation in rainfall was found in the North-South direction.  This was shown by the higher semivariogram parameters (e.g. the sill and radius of influence) for the North-South direction.  This demonstrates that the direction that the storm travels in can have significant impact on semivariograms.  When a cumulative semivariogram is computed after a storm has traveled over an entire watershed there will be little variation in the semivariogram in the direction that the storm traveled; however, there could be a significant amount of variation in the other direction, depending on the nature of the storm.

**Table 6-13: E-W Cumulative Semivariogram for Varying Storm Velocities**

| Velocity (km/hr) | Maximum Separation Distance (km) | Sill (mm$^2$) | Radius of Influence (km) | Relative Bias | Standard Error Ratio | R |
|---|---|---|---|---|---|---|
| 5 | 16 | 167.3 | 1 | 0.000 | 1.224 | 0.000 |
| 5 | 20 | 166.7 | 1.5 | 0.000 | 1.155 | 0.000 |
| 5 | 40 | 164.7 | 0 | 0.000 | 1.061 | 0.000 |
| 5 | 48 | 164.1 | 1 | 0.000 | 1.049 | 0.000 |
| 10 | 16 | 45.8 | 4 | 0.000 | 1.225 | 0.000 |
| 10 | 20 | 45.5 | 4 | 0.000 | 1.155 | 0.000 |
| 10 | 40 | 44.3 | 4 | 0.000 | 1.061 | 0.000 |
| 10 | 48 | 44.0 | 4 | 0.000 | 1.049 | 0.000 |
| 15 | 16 | 18.7 | 4 | 0.000 | 1.225 | 0.000 |
| 15 | 20 | 18.6 | 4 | 0.000 | 1.155 | 0.000 |
| 15 | 40 | 18.0 | 4 | 0.000 | 1.061 | 0.000 |
| 15 | 48 | 17.7 | 2 | 0.000 | 1.049 | 0.000 |
| 20 | 16 | 12.2 | 4 | 0.000 | 1.225 | 0.000 |
| 20 | 20 | 12.0 | 4 | 0.000 | 1.155 | 0.000 |
| 20 | 40 | 11.3 | 4 | 0.000 | 1.061 | 0.000 |
| 20 | 48 | 11.1 | 4 | 0.000 | 1.488 | 0.000 |

**Table 6-14: N-S Cumulative Semivariogram for Varying Storm Velocities**

| Velocity (km/hr) | Maximum Separation Distance (km) | Sill (mm²) | Radius of Influence (km) | Relative Bias | Standard Error Ratio | R |
|---|---|---|---|---|---|---|
| 5 | 16 | 366.8 | 4.2 | 0.000 | 1.170 | 0.000 |
| 5 | 20 | 368.3 | 4.3 | 0.000 | 1.078 | 0.000 |
| 5 | 40 | 374.4 | 4.6 | 0.000 | 0.961 | 0.434 |
| 5 | 48 | 375.4 | 4.6 | 0.000 | 0.942 | 0.440 |
| 10 | 16 | 90.1 | 4.3 | 0.000 | 1.150 | 0.000 |
| 10 | 20 | 91.0 | 4.5 | 0.000 | 1.067 | 0.000 |
| 10 | 40 | 94.6 | 5.0 | 0.000 | 0.955 | 0.434 |
| 10 | 48 | 95.1 | 5.1 | 0.000 | 0.937 | 0.450 |
| 15 | 16 | 42.2 | 4.4 | 0.000 | 1.171 | 0.000 |
| 15 | 20 | 42.8 | 4.6 | 0.000 | 1.078 | 0.000 |
| 15 | 40 | 44.8 | 5.1 | 0.000 | 0.959 | 0.427 |
| 15 | 48 | 45.1 | 5.2 | 0.000 | 0.940 | 0.443 |
| 20 | 16 | 22.0 | 4.6 | 0.000 | 1.130 | 0.000 |
| 20 | 20 | 22.5 | 4.9 | 0.000 | 1.054 | 0.000 |
| 20 | 40 | 24.4 | 5.7 | 0.000 | 0.949 | 0.447 |
| 20 | 48 | 24.7 | 5.8 | 0.000 | 0.930 | 0.462 |

The velocity of the storm was found to have some effect on the sill values in this trial. As the storm velocity increased, the sill values of both the East-West and the North-South semivariograms decreased. When a storm is moving with a higher velocity the watershed will actually experience less total rainfall. This is responsible for the decreasing sill values as the velocity increased. The velocity of the storm does not seem to have an impact on the radius of influence in either the East-West or the North-South direction, however. There is very little variation in the radius of influence as the velocity changes. The conclusion to be drawn from this is that the radius of influence is impacted more by the spacing of the ellipses used to simulate the storms than it is by the storm velocities.

In further examining these semivariograms it was noted that the semivariograms changed significantly as the storm progressed across the watershed. The increase in rainfall depths can obviously be attributed to the accumulation of

rainfall over the course of the storm. However, several interesting changes in the semivariograms were evident. For instance, for each of the storm velocities simulated, the initial semivariograms showed higher values for the East-West semivariogram, while the final semivariograms showed higher values for the North-South semivariogram. Also, the semivariograms in the East-West direction generally started out with increasing values, but in the final semivariograms the values were decreasing, while the values in the North-South semivariograms remained in an increasing pattern throughout the storm. This indicates that the point in the storm at which a semivariogram is being calculated can have a significant influence on that semivariogram. A semivariogram calculated at the beginning of a storm could be quite different from a semivariogram calculated at the end of the same storm.

## 6.6. EFFECT OF STORM TYPE

### 6.6.1. Introduction

Another research question for this preliminary study evaluated the effect that the type of storm could have on the semivariogram. A summer thunderstorm, for instance, has very different characteristics than a winter rainstorm. A summer thunderstorm is generally very short, very localized, and very intense, whereas a winter storm generally has a longer rainfall duration, is less intense and has a more spatially uniform rainfall duration, and the storm cell is generally larger. The purpose of this research question was to determine whether or not differences existed in the calculated semivariograms when various types of storms were applied to the same watershed.

## 6.6.2. Methods and Materials

In evaluating the effect that storm type has on the calculated semivariogram, three different storms were created for use with watershed 1.  The first storm, which was fairly uniform in space, was modeled after a winter storm.  The second storm was moderately peaked in space, and the third storm was severely peaked in space and was modeled after a summer thunderstorm.  Each storm had the same rainfall values, ratio of *a*-to-*b*, and velocity.  The only difference between the storms was in the *a* values for the ellipses.  The rainfall values used by each storm were 6 mm in the inner ellipse, then 5 mm, 4 mm, 2 mm, and finally 1 mm in the outer ellipse.

The uniform storm used *a* values of 0-km, 6-km, 14-km, 23-km, and 35-km.  This storm provided a gradual change in rainfall over the watershed.  The moderately peaked storm had *a* values of 0-km, 4-km, 12-km, 22-km, and 35-km.  In this storm more of the rainfall was located toward the intense center of the storm, but it was not a severely peaked storm.  The severely peaked storm had *a* values of 0-km, 2-km, 5-km, 21-km, and 35-km.  These values led to nearly all of the rain being deposited near the center of the storm, with only a very small amount of rain falling in areas far from the center of the storm.

These storms were input to the original program.  From that output a semivariogram was chosen to represent each storm.  For each storm semivariogram the relative bias, the standard error ratio, and the correlation coefficient R, as well as the final estimates for the sill and radius of influence of the semivariogram were recorded for comparison.

## 6.6.3. Results and Discussion

The results of this experiment are shown in Tables 6-15 and 6-16. As the peakedness of the storm increased, the sill decreased somewhat, and the radius of influence also decreased. Though these decreases are not necessarily significant decreases, a steady trend is evident. These results would imply that, as the peakedness of the storm increased, the variation in the rainfall decreased. This decrease can be explained by storm type. The more peaked storms have smaller inner ellipses; however, their outer ellipses are the same size as the uniform storms. This means that the watershed is experiencing more rainfall from the outer ellipses during more peaked storms, and therefore is experiencing less variation in rainfall than it would if the storm were spatially uniform. The more peaked storms actually have a larger area of low, uniform rainfall than the uniform storms did, and the small peaks of the peaked storms had little influence on the storm variance. The radius of influence can similarly be explained by the increasing area of the watershed receiving approximately the same rainfall by the peaked storms.

**Table 6-15: E-W Semivariogram for Varying Storm Types**

| Storm Type | Maximum Separation Distance (km) | Sill (mm$^2$) | Radius of Influence (km) | Relative Bias | Standard Error Ratio | R |
|---|---|---|---|---|---|---|
| Uniform | 28 | 8.5 | 166 | 0.051 | 0.245 | 0.975 |
| Uniform | 32 | 2.7 | 51 | 0.039 | 0.274 | 0.967 |
| Moderately Peaked | 28 | 6.1 | 138 | 0.052 | 0.256 | 0.972 |
| Moderately Peaked | 32 | 2.2 | 47 | 0.041 | 0.291 | 0.963 |
| Severely Peaked | 28 | 3.9 | 159 | 0.049 | 0.252 | 0.973 |
| Severely Peaked | 32 | 1.1 | 44 | 0.040 | 0.292 | 0.963 |
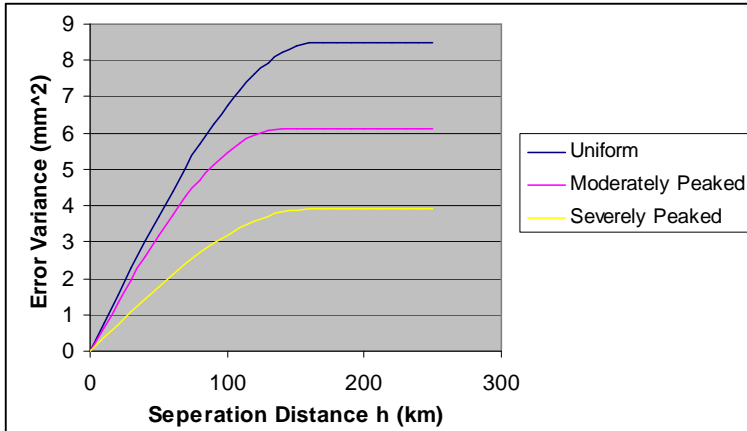
**Figure 6-5: E-W Semivariograms for Varying Storm Types**

**Table 6-16: N-S Semivariogram for Varying Storm Types**

| Storm Type | Maximum Separation Distance (km) | Sill (mm$^2$) | Radius of Influence (km) | Relative Bias | Standard Error Ratio | R |
|---|---|---|---|---|---|---|
| Uniform | 20 | 8.7 | 136 | 0.060 | 0.278 | 0.971 |
| Uniform | 24 | 3.1 | 49 | 0.037 | 0.284 | 0.967 |
| Uniform | 28 | 1.9 | 26 | 0.040 | 0.364 | 0.943 |
| Moderately Peaked | 20 | 7.2 | 128 | 0.062 | 0.287 | 0.969 |
| Moderately Peaked | 24 | 2.7 | 49 | 0.036 | 0.302 | 0.963 |
| Severely Peaked | 20 | 3.5 | 111 | 0.060 | 0.278 | 0.970 |
| Severely Peaked | 24 | 1.2 | 39 | 0.037 | 0.315 | 0.959 |
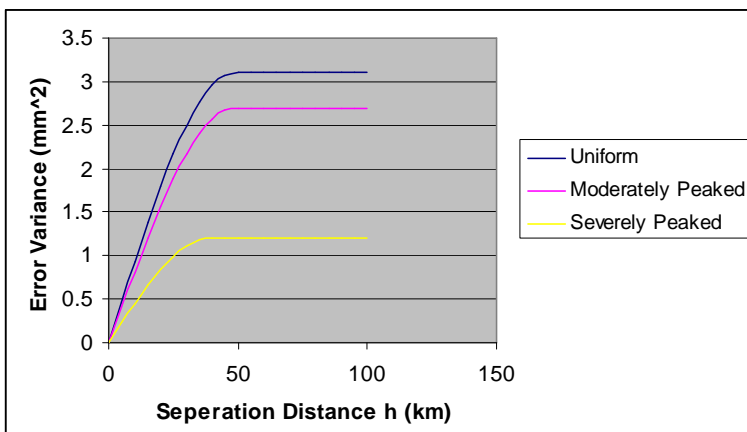


**Figure 6-6: N-S Semivariograms for Varying Storm Types**

## *6.7. CONCLUSIONS*

A variety of analyses were performed to evaluate factors that influenced the calculation of storm semivariograms. The factors examined included the shape of the storm, the size of the storm compared to the size of the watershed, the velocity of the storm, and the type of storm. Of these factors, the storm shape appeared to have the least impact on the calculated semivariogram. While no significant difference was found between semivariograms calculated for storms of different shapes, the importance of evaluating storms as anisotropic events, rather than isotropic, was identified. The size of the storm compared to the watershed and the type of storm were both found to have some effect on the semivariogram. Smaller storms were observed to result in a smaller radius of influence and a higher sill value; however, how the storm moved across the watershed was determined to play some role in these results. Particularly peaked storms were observed to decrease the sill value of the semivariogram somewhat, due to the fact that more of the watershed was experiencing either light or no rainfall, as compared to a less peaked storm.

The analysis of the velocity of the storm produced interesting results. For individual time periods during the storm the velocity of the storm was not seen to produce significant differences in the storm semivariogram. The location of the storm in relation to the location of the rain gages at the time of the measurement was actually found to be more influential than the velocity itself. This led to the conclusion that the density of rain gages within a watershed was more important than the velocity of the storm in determining the characteristics of the storm semivariogram. Cumulative storm semivariograms were also computed, and within

these semivariograms significant differences were observed.  The largest differences were observed in the direction perpendicular to the storm movement, again providing evidence that how the storm moves across the watershed can influence the semivariogram calculated.  Differences were also observed in semivariograms calculated at the beginning of the storm versus at the end of the storm.  This leads to the conclusion when the semivariogram is computed can significantly influence the semivariogram parameters.

# CHAPTER 7

# RAIN GAGE DENSITY ANALYSES

## *7.1. INTRODUCTION*

The accuracy of rainfall measurements for a given watershed will depend on the number of rain gages available to measure the rainfall. Each rain gage only measures rainfall at one point, so multiple rain gages are necessary to obtain a representative estimate of rainfall. A variety of potential errors, such as wind drift, blockage caused by trees, or mechanical failure, could also influence an individual rain gage, resulting in inaccurate measurements. For these reasons multiple rain gages within a watershed are ideal. Several studies were conducted to investigate the effect of rain gage density on hydrologic applications. First, the effect of rain gage density on storm semivariograms was investigated. Then the effect of rainfall averaging methods was investigated. The Thiessen polygon average and the arithmetic average rainfall estimates were compared, to determine which average resulted in less smoothing of the observed rainfall. Then the rainfall averages computed using two rain gages were compared to rainfall estimates made using only one rain gage, to evaluate the effect of an additional rain gage.

## *7.2. SEMIVARIOGRAM ANALYSES*

### 7.2.1. Introduction

A standard density of rain gages in gage networks does not exist across the country. A few watersheds, mostly experimental watersheds such as the Walnut

Gulch Experimental Watershed in Arizona, are heavily gaged; however, even most large watersheds contain only a small number of rain gages. This is due in part to the expense associated with installing, monitoring, and maintaining rain gages. Therefore, one aim of this study was to examine the effect of rain gage density on a storm semivariogram. The objectives of this experiment were to determine how the accuracy of a semivariogram varies with the rain gage density, and to evaluate the effects on the semivariogram if a lower density were used on a watershed.

### 7.2.2. Trial 1

#### 7.2.2.1. Methods and Materials

In order to determine the effect that gage density had on the semivariogram watershed 1 and storm 1 were simulated using a program that allowed the user to choose a percentage of rain gages within the grid to be removed from calculations. This program was utilized multiple times during a storm, each time removing a different percentage of gages. The first run with this program removed 0% of the gages, which served as a baseline for comparison. On the next simulation 10% of the gages were randomly removed, and then 20%, etc. During the final run with 97% of the gages were removed, in order to obtain a realistic number of gages for a watershed. A semivariogram was chosen from the output of each simulation for use in further evaluations. As in all previous experiments the relative bias, the standard error ratio, the correlation coefficient R, and the final estimates of the sill and radius of influence of the semivariogram were computed and compared.

#### 7.2.2.2. Results and Discussion

The results of this study, shown in Tables 7-1 and 7-2, are somewhat inconclusive. It is apparent that at lower gage densities the spread of the data is

greater because of random variation and a smaller number of gages. Despite this fact, when 80% of all gages were not recording the estimates of the sill and radius of influence were not terribly different from the estimates when all of the gages were used in calculations. However, when only 20% of the gages were removed from calculations the sill and radius of influence were quite different from the estimates when all gages were used. As shown in Table 7-1, when all gages were recording during the storm the sill was 5.5 mm$^2$ and the radius of influence was 45-km, whereas when 20% of the gages were removed the sill was 5.9 mm$^2$ and the radius of influence was 54-km. A measure of caution should be used, however, when considering the accuracy of a semivariogram computed with only a few gages, such as when 80% or 90% of the gages were removed. In these cases there are so few gages that the semivariograms are based on only a few data points. Such a small data sample must call the accuracy of the resultant semivariogram into question. Also, at a certain point so few data points remain that a semivariogram cannot even be computed. In order to compute a semivariogram at least two data points must be available. This occurred when 97% of the gages were removed in this experiment. The semivariograms computed contained only one point in both the East-West and the North-South directions, which is not enough to compute the sill and radius of influence of the population semivariogram.

The results of this study indicated that an accurate semivariogram was computed when 10%, 30%, 40%, 70%, and 80% of the gages were removed from calculations, while accurate semivariograms were not computed when 20%, 50%, 60%, or 90% of the gages were removed from calculations. This indicates that a

highly dense gage network is not necessarily required to obtain an accurate

semivariogram; however there does appear to be a great deal of randomness to these

results, as evidenced by acceptable results when 80% of gages were removed and yet

unacceptable results when only 20% of gages were removed.  As Table 7-1 shows,

the sill was 5.5 mm$^2$ when all gages were recording, 5.9 mm$^2$ when 20% of gages

were not recording, 4.6 mm$^2$ when 30% were removed and 5.3 mm$^2$ when 40% of

gages were not recording.  Corresponding radius of influence values were 45-km, 54-

km, 42-km, and 55-km.  It is believed that this experiment demonstrates that when a

low density gage network is used random chance determines whether or not an

accurate semivariogram is obtained.  This finding points to the potential value of

supplementing rain gage data with radar data as even though it can be possible to

obtain an acceptable semivariogram with a low number of gages.

**Table 7-1: E-W Semivariogram for Varying Gage Network Densities**

| % of Gages Removed | Maximum Separation Distance (km) | Sill (mm$^2$) | Radius of Influence (km) | Relative Bias | Standard Error Ratio | R |
|---|---|---|---|---|---|---|
| 0 | 32 | 18.0 | 159 | 0.040 | 0.238 | 0.975 |
| 0 | 36 | 5.5 | 45 | 0.040 | 0.278 | 0.966 |
| 10 | 32 | 17.4 | 153 | 0.041 | 0.237 | 0.976 |
| 10 | 36 | 5.5 | 45 | 0.040 | 0.279 | 0.965 |
| 20 | 32 | 22.8 | 216 | 0.047 | 0.216 | 0.980 |
| 20 | 36 | 5.9 | 54 | 0.038 | 0.270 | 0.968 |
| 30 | 32 | 19.0 | 188 | 0.045 | 0.239 | 0.975 |
| 30 | 36 | 4.6 | 42 | 0.043 | 0.325 | 0.953 |
| 40 | 28 | 23.6 | 246 | 0.065 | 0.275 | 0.968 |
| 40 | 32 | 10.4 | 111 | 0.041 | 0.281 | 0.965 |
| 40 | 36 | 5.3 | 55 | 0.035 | 0.278 | 0.965 |
| 50 | 20 | 19.9 | 226 | 0.083 | 0.392 | 0.940 |
| 50 | 24 | 12.3 | 143 | 0.052 | 0.333 | 0.955 |
| 50 | 28 | 20.5 | 223 | 0.056 | 0.297 | 0.962 |
| 50 | 32 | 6.3 | 69 | 0.034 | 0.332 | 0.952 |
| 60 | 28 | 30.0 | 297 | 0.075 | 0.359 | 0.945 |
| 60 | 32 | 8.7 | 93 | 0.036 | 0.451 | 0.909 |
| 60 | 36 | 4.0 | 36 | 0.020 | 0.020 | 0.891 |
| 70 | 20 | 22.3 | 191 | 0.076 | 0.076 | 0.933 |
| 70 | 24 | 5.2 | 46 | 0.042 | 0.042 | 0.923 |
| 80 | 28 | 50.1 | 361 | 0.087 | 0.327 | 0.954 |
| 80 | 32 | 119.0 | 864 | 0.061 | 0.292 | 0.963 |
| 80 | 36 | 5.5 | 35 | 0.057 | 0.492 | 0.888 |
| 90 | 28 | 82.0 | 431 | 0.140 | 0.745 | 0.733 |
| 90 | 32 | 85.4 | 428 | 0.117 | 0.655 | 0.795 |
| 90 | 36 | 8.9 | 50 | 0.046 | 0.853 | 0.594 |

**Table 7-2: N-S Semivariogram for Varying Gage Network Densities**

| % of Gages Removed | Maximum Separation Distance (km) | Sill (mm$^2$) | Radius of Influence (km) | Relative Bias | Standard Error Ratio | R |
|---|---|---|---|---|---|---|
| 0 | 24 | 22.9 | 154 | 0.049 | 0.249 | 0.975 |
| 0 | 28 | 6.5 | 43 | 0.037 | 0.277 | 0.967 |
| 10 | 24 | 22.8 | 157 | 0.047 | 0.241 | 0.977 |
| 10 | 28 | 5.8 | 338 | 0.037 | 0.284 | 0.967 |
| 20 | 24 | 14.0 | 100 | 0.037 | 0.236 | 0.977 |
| 20 | 28 | 4.7 | 30 | 0.039 | 0.304 | 0.961 |
| 30 | 20 | 24.5 | 166 | 0.062 | 0.291 | 0.967 |
| 30 | 24 | 6.7 | 46 | 0.038 | 0.304 | 0.962 |
| 40 | 20 | 27.0 | 183 | 0.063 | 0.289 | 0.968 |
| 40 | 24 | 5.3 | 35 | 0.042 | 0.335 | 0.954 |
| 50 | 20 | 30.1 | 223 | 0.070 | 0.301 | 0.965 |
| 50 | 24 | 7.2 | 54 | 0.040 | 0.316 | 0.959 |
| 60 | 20 | 30.9 | 213 | 0.077 | 0.339 | 0.956 |
| 60 | 24 | 6.1 | 43 | 0.044 | 0.376 | 0.942 |
| 70 | 16 | 33.9 | 215 | 0.127 | 0.624 | 0.861 |
| 70 | 20 | 25.0 | 156 | 0.084 | 0.484 | 0.908 |
| 80 | 20 | 48.0 | 263 | 0.161 | 0.604 | 0.852 |
| 80 | 24 | 35.9 | 201 | 0.105 | 0.524 | 0.884 |
| 80 | 28 | 75.9 | 341 | 0.128 | 0.530 | 0.875 |
| 80 | 32 | 6.9 | 31 | 0.082 | 0.799 | 0.673 |
| 90 | 20 | 71.1 | 324 | 0.322 | 0.943 | 0.577 |
| 90 | 28 | 112.6 | 460 | 0.211 | 0.885 | 0.590 |

## 7.2.3. Trial 2

### 7.2.3.1. Methods and Materials

After examining the results of Trial 1 it was determined that a second trial

would be necessary to confirm the results.  For this second trial two new storms were

created.  In evaluating the results of trial 1 it was realized that storm 1 was

significantly larger than watershed 1, which meant that the full variability of storm

was not falling on the watershed.  Therefore two new storms were created that would

be large enough to cover most of the watershed, but not be larger than the watershed.

Two storms and two watersheds were created to evaluate the case of an elliptical

storm on a rectangular watershed and the case of a circular storm on a square

watershed. Each storm was evaluated using two distinctly different random number seeds. This considered the question of whether or not the specific gages removed from calculations had any effect on the semivariogram.

The first storm created, referred to as storm A, was an ellipse with an *a*-to-*b* ratio of 1.25. The *a* values of the ellipses were 0-km, 6-km, 15-km, 27-km, and 38-km. The ellipses represented rainfall depths of 1.1 cm, 0.9 cm, 0.7 cm, 0.4 cm, and 0.2 cm. This storm traveled at a velocity of 5 km/hr, it had an orientation of $0^{o}$, and the storm was allowed to make three storm movements. The watershed used for this storm was 76-km long and 60-km wide, with gages spaced 4-km apart. This storm was simulated using both RADAR06-1 and RADAR06-2 several times. The first simulation included all of the rain gages, and each of the following simulations removed a larger percentage of the rain gages. First 10% of the gages were removed, then 20%, 30%, 40%, 50%, 60%, and finally 70% of the gages were removed. A representative semivariogram was chosen for each simulation from each program. For purposes of data analysis and comparison the relative bias, the standard error ratio, the correlation coefficient, the final estimate of the sill, and the final estimate of the radius of influence were computed.

The second storm, referred to as storm B, was a circular storm. With the exception of the ratio of *a*-to-*b* all storm parameters used for storm A were used for storm B. The watershed was assumed to be a square, 76-km by 76-km. Again the gages were 4-km apart. This storm was simulated with two versions of the program for each fraction of removed gages mentioned in storm A, and representative semivariograms were chosen from the output. The second version of the program

allowed the user to input a seed which was used to determine which rain gages were

removed from calculations during each simulation.  The parameters recorded for

storm A were also recorded for storm B for the purpose of comparison.

### 7.2.3.2. Results and Discussion

This trial considered whether or not the gage network density had any effect

on the semivariogram, and it also considered whether or not the specific gages

removed had any effect.  The results of this trial, which are shown in Tables 7-3

through 7-10, showed a large amount of variability in the data, but without trends.

Storm A showed a difference in sill and radius of influence in the North-South

direction as gage density decreased, but a trend in the East-West direction was not

evident.  Storm B, however, did not show any trend in the sill or radius of influence in

either semivariogram direction.  For both storms it was noted that the goodness of fit

statistics consistently decreased as the gage density decreased.

**Table 7-3: Storm A Seed 1 E-W Semivariogram for Varying Gage Network Densities**

| % of Gages Removed | Maximum Separation Distance (km) | Sill (mm$^2$) | Radius of Influence (km) | Relative Bias | Standard Error Ratio | R |
|---|---|---|---|---|---|---|
| 0 | 32 | 44.6 | 329 | 0.068 | 0.262 | 0.970 |
| 0 | 36 | 24.8 | 187 | 0.047 | 0.253 | 0.972 |
| 0 | 40 | 6.9 | 78 | 0.046 | 0.319 | 0.954 |
| 10 | 32 | 46.0 | 311 | 0.074 | 0.275 | 0.967 |
| 10 | 36 | 41.6 | 287 | 0.053 | 0.254 | 0.971 |
| 10 | 40 | 7.7 | 49 | 0.048 | 0.344 | 0.946 |
| 10 | 44 | 6.4 | 39 | 0.048 | 0.418 | 0.918 |
| 20 | 32 | 40.4 | 300 | 0.065 | 0.267 | 0.969 |
| 20 | 36 | 14.9 | 113 | 0.044 | 0.276 | 0.966 |
| 20 | 40 | 7.0 | 49 | 0.044 | 0.301 | 0.959 |
| 20 | 44 | 6.1 | 41 | 0.044 | 0.332 | 0.949 |
| 30 | 32 | 35.3 | 265 | 0.064 | 0.262 | 0.970 |
| 30 | 36 | 15.4 | 118 | 0.042 | 0.274 | 0.967 |
| 30 | 40 | 7.2 | 52 | 0.042 | 0.288 | 0.962 |
| 30 | 44 | 6.1 | 41 | 0.042 | 0.321 | 0.953 |
| 40 | 32 | 31.7 | 246 | 0.059 | 0.262 | 0.970 |
| 40 | 36 | 12.1 | 96 | 0.038 | 0.292 | 0.962 |
| 40 | 40 | 6.2 | 45 | 0.042 | 0.317 | 0.954 |
| 50 | 32 | 44.3 | 298 | 0.081 | 0.337 | 0.950 |
| 50 | 36 | 36.6 | 251 | 0.059 | 0.307 | 0.958 |
| 50 | 40 | 9.8 | 66 | 0.045 | 0.350 | 0.944 |
| 50 | 44 | 7.4 | 47 | 0.047 | 0.357 | 0.941 |
| 50 | 48 | 7.0 | 43 | 0.043 | 0.366 | 0.937 |
| 60 | 32 | 47.1 | 304 | 0.077 | 0.353 | 0.945 |
| 60 | 36 | 27.4 | 184 | 0.049 | 0.361 | 0.941 |
| 60 | 40 | 7.2 | 43 | 0.052 | 0.421 | 0.918 |
| 60 | 44 | 7.4 | 47 | 0.047 | 0.357 | 0.941 |
| 70 | 36 | 27.2 | 168 | 0.047 | 0.369 | 0.939 |
| 70 | 40 | 7.1 | 38 | 0.054 | 0.492 | 0.886 |

**Table 7-4: Storm A Seed 2 E-W Semivariogram with Varying Gage Network Densities**

| % of Gages Removed | Maximum Separation Distance (km) | Sill (mm$^2$) | Radius of Influence (km) | Relative Bias | Standard Error Ratio | R |
|---|---|---|---|---|---|---|
| 0 | 32 | 44.6 | 329 | 0.068 | 0.262 | 0.970 |
| 0 | 36 | 24.8 | 187 | 0.047 | 0.253 | 0.971 |
| 0 | 40 | 6.9 | 48 | 0.046 | 0.319 | 0.954 |
| 10 | 36 | 27.6 | 211 | 0.047 | 0.226 | 0.977 |
| 10 | 40 | 7.1 | 50 | 0.044 | 0.304 | 0.958 |
| 10 | 44 | 5.9 | 40 | 0.044 | 0.367 | 0.937 |
| 20 | 32 | 36.6 | 267 | 0.064 | 0.250 | 0.973 |
| 20 | 36 | 23.8 | 177 | 0.044 | 0.239 | 0.975 |
| 20 | 40 | 6.1 | 40 | 0.051 | 0.379 | 0.934 |
| 30 | 28 | 42.90 | 314 | 0.083 | 0.306 | 0.960 |
| 30 | 32 | 29.7 | 220 | 0.060 | 0.272 | 0.968 |
| 30 | 36 | 8.2 | 60 | 0.045 | 0.308 | 0.958 |
| 30 | 40 | 5.8 | 39 | 0.049 | 0.357 | 0.941 |
| 40 | 28 | 43. | 319 | 0.094 | 0.331 | 0.953 |
| 40 | 32 | 32.3 | 245 | 0.063 | 0.303 | 0.960 |
| 40 | 36 | 8.2 | 61 | 0.047 | 0.330 | 0.951 |
| 40 | 40 | 5.8 | 39 | 0.051 | 0.366 | 0.939 |
| 50 | 28 | 44.7 | 328 | 0.096 | 0.349 | 0.948 |
| 50 | 32 | 26.8 | 203 | 0.063 | 0.336 | 0.951 |
| 50 | 36 | 12.7 | 98 | 0.044 | 0.325 | 0.953 |
| 50 | 40 | 6.1 | 42 | 0.050 | 0.361 | 0.940 |
| 60 | 28 | 48.0 | 306 | 0.108 | 0.385 | 0.936 |
| 60 | 32 | 22.8 | 156 | 0.063 | 0.427 | 0.919 |
| 60 | 36 | 18.8 | 128 | 0.049 | 0.377 | 0.936 |
| 60 | 40 | 7.5 | 47 | 0.050 | 0.399 | 0.927 |
| 60 | 44 | 6.3 | 38 | 0.049 | 0.485 | 0.888 |
| 70 | 36 | 48.5 | 348 | 0.058 | 0.239 | 0.975 |
| 70 | 40 | 13.2 | 96 | 0.039 | 0.289 | 0.962 |
| 70 | 44 | 6.3 | 40 | 0.047 | 0.459 | 0.900 |

**Table 7-5: Storm B Seed 1 E-W Semivariogram for Varying Storm Velocities**

| % of Gages Removed | Maximum Separation Distance (km) | Sill (mm$^2$) | Radius of Influence (km) | Relative Bias | Standard Error Ratio | R |
|---|---|---|---|---|---|---|
| 0 | 32 | 42.9 | 312 | 0.069 | 0.265 | 0.970 |
| 0 | 36 | 32.6 | 242 | 0.049 | 0.249 | 0.972 |
| 0 | 40 | 7.4 | 52 | 0.045 | 0.308 | 0.966 |
| 0 | 44 | 6.1 | 40 | 0.046 | 0.371 | 0.936 |
| 10 | 36 | 29.4 | 204 | 0.050 | 0.259 | 0.970 |
| 10 | 40 | 7.3 | 46 | 0.049 | 0.345 | 0.946 |
| 10 | 44 | 6.4 | 39 | 0.047 | 0.401 | 0.925 |
| 20 | 36 | 28.8 | 205 | 0.047 | 0.258 | 0.970 |
| 20 | 40 | 7.2 | 46 | 0.048 | 0.332 | 0.950 |
| 20 | 44 | 6.3 | 40 | 0.046 | 0.378 | 0.933 |
| 30 | 36 | 18.2 | 137 | 0.042 | 0.269 | 0.968 |
| 30 | 40 | 6.8 | 46 | 0.045 | 0.310 | 0.956 |
| 30 | 44 | 6.0 | 39 | 0.044 | 0.355 | 0.942 |
| 40 | 32 | 29.2 | 219 | 0.059 | 0.280 | 0.967 |
| 40 | 36 | 9.8 | 74 | 0.042 | 0.300 | 0.960 |
| 40 | 40 | 6.5 | 46 | 0.043 | 0.305 | 0.958 |
| 40 | 44 | 6.0 | 41 | 0.04 | 0.312 | 0.955 |
| 50 | 36 | 24.0 | 168 | 0.048 | 0.271 | 0.967 |
| 50 | 40 | 8.2 | 54 | 0.044 | 0.303 | 0.958 |
| 50 | 44 | 7.2 | 46 | 0.043 | 0.299 | 0.959 |
| 50 | 48 | 6.8 | 42 | 0.040 | 0.322 | 0.952 |
| 60 | 32 | 38.8 | 249 | 0.059 | 0.300 | 0.961 |
| 60 | 36 | 8.4 | 52 | 0.048 | 0.344 | 0.947 |
| 60 | 40 | 7.7 | 46 | 0.042 | 0.322 | 0.953 |
| 60 | 44 | 7.4 | 44 | 0.039 | 0.309 | 0.956 |
| 60 | 48 | 7.1 | 42 | 0.035 | 0.311 | 0.955 |
| 70 | 36 | 14.0 | 82 | 0.041 | 0.501 | 0.883 |
| 70 | 40 | 7.6 | 40 | 0.048 | 0.524 | 0.869 |

**Table 7-6: Storm B Seed 2 E-W Semivariogram for Varying Gage Network Densities**

| % of Gages Removed | Maximum Separation Distance (km) | Sill (mm$^2$) | Radius of Influence (km) | Relative Bias | Standard Error Ratio | R |
|---|---|---|---|---|---|---|
| 0 | 32 | 42.9 | 312 | 0.069 | 0.265 | 0.970 |
| 0 | 36 | 32.6 | 242 | 0.049 | 0.249 | 0.973 |
| 0 | 40 | 7.4 | 52 | 0.045 | 0.308 | 0.957 |
| 0 | 44 | 6.1 | 40 | 0.046 | 0.371 | 0.936 |
| 10 | 36 | 32.7 | 243 | 0.051 | 0.237 | 0.975 |
| 10 | 40 | 7.7 | 54 | 0.044 | 0.307 | 0.957 |
| 10 | 44 | 6.2 | 41 | 0.046 | 0.366 | 0.938 |
| 20 | 32 | 45.2 | 324 | 0.072 | 0.278 | 0.966 |
| 20 | 36 | 27.8 | 206 | 0.049 | 0.279 | 0.965 |
| 20 | 40 | 6.1 | 39 | 0.054 | 0.413 | 0.921 |
| 30 | 28 | 45.1 | 328 | 0.095 | 0.347 | 0.949 |
| 30 | 32 | 41.0 | 298 | 0.071 | 0.230 | 0.961 |
| 30 | 36 | 10.2 | 76 | 0.048 | 0.343 | 0.947 |
| 30 | 40 | 5.8 | 38 | 0.054 | 0.419 | 0.919 |
| 40 | 28 | 39.8 | 282 | 0.096 | 0.353 | 0.947 |
| 40 | 32 | 41.4 | 304 | 0.072 | 0.304 | 0.959 |
| 40 | 36 | 7.9 | 58 | 0.050 | 0.385 | 0.933 |
| 40 | 40 | 5.5 | 37 | 0.054 | 0.453 | 0.904 |
| 50 | 28 | 59.3 | 399 | 0.100 | 0.367 | 0.942 |
| 50 | 32 | 44.7 | 299 | 0.077 | 0.315 | 0.957 |
| 50 | 36 | 9.9 | 68 | 0.050 | 0.391 | 0.961 |
| 50 | 40 | 6.0 | 37 | 0.056 | 0.482 | 0.891 |
| 60 | 28 | 59.7 | 365 | 0.114 | 0.421 | 0.923 |
| 60 | 32 | 47.3 | 297 | 0.080 | 0.385 | 0.934 |
| 60 | 36 | 13.2 | 86 | 0.052 | 0.412 | 0.923 |
| 60 | 40 | 6.6 | 37 | 0.059 | 0.450 | 0.882 |
| 70 | 28 | 64.5 | 381 | 0.100 | 0.359 | 0.945 |
| 70 | 32 | 59.9 | 354 | 0.076 | 0.310 | 0.958 |
| 70 | 36 | 8.3 | 47 | 0.057 | 0.423 | 0.918 |

**Table 7-7: Storm A Seed 1 N-S Semivariogram for Varying Gage Network Densities**

| % of Gages Removed | Maximum Separation Distance (km) | Sill (mm$^2$) | Radius of Influence (km) | Relative Bias | Standard Error Ratio | R |
|---|---|---|---|---|---|---|
| 0 | 28 | 32.8 | 194 | 0.049 | 0.253 | 0.973 |
| 0 | 32 | 6.7 | 36 | 0.046 | 0.338 | 0.950 |
| 10 | 28 | 26.5 | 164 | 0.047 | 0.245 | 0.975 |
| 10 | 32 | 6.3 | 35 | 0.045 | 0.336 | 0.950 |
| 20 | 32 | 6.8 | 44 | 0.037 | 0.267 | 0.969 |
| 20 | 36 | 5.7 | 34 | 0.037 | 0.293 | 0.962 |
| 30 | 32 | 6.6 | 44 | 0.034 | 0.272 | 0.968 |
| 30 | 36 | 5.2 | 32 | 0.036 | 0.383 | 0.933 |
| 40 | 28 | 20.8 | 143 | 0.043 | 0.257 | 0.972 |
| 40 | 32 | 5.7 | 35 | 0.043 | 0.331 | 0.952 |
| 50 | 28 | 36.8 | 239 | 0.055 | 0.256 | 0.972 |
| 50 | 32 | 12.1 | 79 | 0.036 | 0.267 | 0.969 |
| 50 | 36 | 6.1 | 35 | 0.044 | 0.340 | 0.948 |
| 60 | 32 | 30.4 | 189 | 0.045 | 0.243 | 0.974 |
| 60 | 36 | 8.2 | 48 | 0.040 | 0.291 | 0.962 |
| 60 | 40 | 6.1 | 33 | 0.041 | 0.543 | 0.859 |
| 70 | 32 | 39.8 | 257 | 0.066 | 0.469 | 0.901 |
| 70 | 36 | 24.5 | 164 | 0.042 | 0.452 | 0.906 |
| 70 | 40 | 6.2 | 36 | 0.051 | 0.624 | 0.809 |

**Table 7-8: Storm A Seed 2 N-S Semivariogram with Varying Gage Network Densities**

| % of Gages Removed | Maximum Separation Distance (km) | Sill (mm$^2$) | Radius of Influence (km) | Relative Bias | Standard Error Ratio | R |
|---|---|---|---|---|---|---|
| 0 | 28 | 32.8 | 194 | 0.049 | 0.253 | 0.973 |
| 0 | 32 | 6.7 | 36.4 | 0.046 | 0.338 | 0.950 |
| 10 | 28 | 31.2 | 185.0 | 0.050 | 0.236 | 0.977 |
| 10 | 32 | 6.8 | 37.4 | 0.044 | 0.331 | 0.951 |
| 20 | 28 | 27.3 | 168 | 0.047 | 0.247 | 0.974 |
| 20 | 32 | 6.7 | 37.7 | 0.043 | 0.318 | 0.956 |
| 30 | 28 | 30.4 | 180.8 | 0.049 | 0.244 | 0.975 |
| 30 | 32 | 6.8 | 37.4 | 0.023 | 0.343 | 0.948 |
| 40 | 28 | 42.6 | 244 | 0.050 | 0.309 | 0.959 |
| 40 | 32 | 9.5 | 53 | 0.038 | 0.318 | 0.956 |
| 40 | 36 | 8.2 | 61 | 0.047 | 0.330 | 0.951 |
| 40 | 40 | 5.8 | 30 | 0.036 | 0.61 | 0.817 |
| 50 | 28 | 34.1 | 193 | 0.054 | 0.304 | 0.961 |
| 50 | 32 | 8.8 | 48 | 0.041 | 0.336 | 0.950 |
| 50 | 36 | 6.6 | 33 | 0.044 | 0.390 | 0.931 |
| 60 | 28 | 52.0 | 259 | 0.077 | 0.319 | 0.957 |
| 60 | 32 | 10.0 | 49 | 0.052 | 0.394 | 0.931 |
| 60 | 36 | 7.0 | 31.8 | 0.054 | 0.489 | 0.889 |
| 70 | 32 | 9.2 | 48.3 | 0.048 | 0.348 | 0.947 |
| 70 | 36 | 6.7 | 32.3 | 0.050 | 0.436 | .913 |

**Table 7-9: Storm B Seed 1 N-S Semivariogram for Varying Gage Network Densities**

| % of Gages Removed | Maximum Separation Distance (km) | Sill (mm$^2$) | Radius of Influence (km) | Relative Bias | Standard Error Ratio | R |
|---|---|---|---|---|---|---|
| 0 | 32 | 41.0 | 298 | 0.069 | 0.265 | 0.970 |
| 0 | 36 | 30.5 | 226 | 0.049 | 0.248 | 0.973 |
| 0 | 40 | 7.4 | 51 | 0.045 | 0.312 | 0.956 |
| 0 | 44 | 6.1 | 40 | 0.046 | 0.372 | 0.936 |
| 10 | 36 | 33.4 | 253 | 0.055 | 0.240 | 0.974 |
| 10 | 40 | 7.6 | 55 | 0.046 | 0.322 | 0.953 |
| 10 | 44 | 6.0 | 40 | 0.048 | 0.394 | 0.928 |
| 20 | 36 | 44.7 | 326 | 0.065 | 0.245 | 0.973 |
| 20 | 40 | 8.0 | 57 | 0.048 | 0.369 | 0.938 |
| 20 | 44 | 6.0 | 39 | 0.051 | 0.472 | 0.894 |
| 30 | 36 | 29.5 | 228 | 0.054 | 0.260 | 0.970 |
| 30 | 40 | 6.7 | 48 | 0.049 | 0.358 | 0.941 |
| 30 | 44 | 5.7 | 39 | 0.048 | 0.433 | 0.912 |
| 40 | 36 | 43.4 | 312 | 0.064 | 0.268 | 0.968 |
| 40 | 40 | 7.7 | 53 | 0.051 | 0.372 | 0.936 |
| 40 | 44 | 6.1 | 40 | 0.052 | 0.452 | 0.903 |
| 50 | 36 | 39.8 | 273 | 0.072 | 0.299 | 0.960 |
| 50 | 40 | 26.3 | 188 | 0.046 | 0.320 | 0.953 |
| 50 | 44 | 6.6 | 41 | 0.056 | 0.487 | 0.887 |
| 50 | 48 | 6.0 | 38 | 0.048 | 0.581 | 0.833 |
| 60 | 36 | 61.9 | 395 | 0.092 | 0.344 | 0.947 |
| 60 | 40 | 37.7 | 253 | 0.060 | 0.365 | 0.939 |
| 60 | 44 | 7.3 | 43 | 0.063 | 0.505 | 0.878 |
| 60 | 48 | 6.8 | 41 | 0.054 | 0.553 | 0.849 |
| 70 | 40 | 59.4 | 376 | 0.096 | 0.612 | 0.817 |
| 70 | 44 | 24.1 | 161 | 0.061 | 0.632 | 0.800 |
| 70 | 48 | 7.7 | 45 | 0.071 | 0.699 | 0.746 |

**Table 7-10: B Seed 2 N-S Semivariogram with Varying Gage Network Densities**

| % of Gages Removed | Maximum Separation Distance (km) | Sill ($mm^2$) | Radius of Influence (km) | Relative Bias | Standard Error Ratio | R |
|---|---|---|---|---|---|---|
| 0 | 32 | 41.0 | 298 | 0.069 | 0.265 | 0.000 |
| 0 | 36 | 30.5 | 226 | 0.049 | 0.248 | 0.000 |
| 0 | 40 | 7.4 | 51 | 0.045 | 0.312 | 0.000 |
| 0 | 44 | 6.1 | 40 | 0.046 | 0.372 | 0.000 |
| 10 | 36 | 30.7 | 228 | 0.048 | 0.228 | 0.000 |
| 10 | 40 | 7.3 | 50 | 0.044 | 0.307 | 0.000 |
| 10 | 44 | 5.9 | 39 | 0.044 | 0.424 | 0.000 |
| 20 | 36 | 35.4 | 267 | 0.048 | 0.210 | 0.000 |
| 20 | 40 | 7.2 | 51 | 0.043 | 0.308 | 0.000 |
| 20 | 44 | 6.1 | 40 | 0.044 | 0.355 | 0.000 |
| 30 | 36 | 19.1 | 145 | 0.039 | 0.220 | 0.000 |
| 30 | 40 | 6.2 | 24 | 0.044 | 0.336 | 0.000 |
| 30 | 44 | 5.8 | 39 | 0.040 | 0.358 | 0.000 |
| 40 | 36 | 28.1 | 214 | 0.062 | 0.266 | 0.000 |
| 40 | 40 | 6.1 | 42 | 0.041 | 0.335 | 0.000 |
| 40 | 44 | 5.7 | 39 | 0.037 | 0.352 | 0.000 |
| 50 | 36 | 30.4 | 235 | 0.048 | 0.245 | 0.000 |
| 50 | 40 | 5.8 | 40 | 0.049 | 0.457 | 0.000 |
| 60 | 36 | 35.9 | 268 | 0.053 | 0.292 | 0.000 |
| 60 | 40 | 5.5 | 37 | 0.048 | 0.626 | 0.000 |
| 70 | 36 | 48.6 | 360 | 0.071 | 0.361 | 0.000 |
| 70 | 40 | 5.3 | 37 | 0.051 | 0.753 | 0.000 |

The results presented in Tables 7-3 through 7-10 indicated that the rain gage network density did not have a significant impact on the semivariogram calculations. Based on comparisons between the simulations using different seeds of the random number generator it did not appear that which specific gages were removed had an effect on the semivariogram. The trends in the data actually indicate that the most important factor influencing the semivariogram parameters is the number of data pairs used to form the original semivariogram. This factor seemed to have much more impact on the data variation than either the seed or the gage density.

### 7.2.4.4. Conclusions

The effect of rain gage density on calculated storm semivariograms was evaluated using two studies. The results of the rain gage density analysis proved somewhat inconclusive. While this was expected to have a very significant effect on the semivariogram, this was not always seen to be the case. In fact, the conclusion drawn from this analysis was that a very dense rain gage network is not absolutely necessary in order to compute an accurate semivariogram.

## 7.3. EFFECT OF AVERAGING METHODS ON RAINFALL ESTIMATES

### 7.3.1. Introduction

The accuracy of rainfall estimates for a watershed can be improved by increasing the number of rain gages within the pixel, but the level of improvement has not been quantified; therefore, it is unknown how significant the density of the rain gage network is to the accuracy of rainfall estimates for a watershed. The purpose of this research was to determine whether increasing the number of rain gages in a watershed from one to two significantly improved the accuracy of rainfall estimates calculated for the watershed. This is one step in understanding the value of spatial estimates of rainfall made from radar measurements.

When rainfall estimates are calculated for a watershed, some method of averaging the rain gage measurements is necessary. Two possible methods are the Thiessen polygon method and the arithmetic averaging method. The Thiessen polygon method takes a weighted average of all of the gages weighted on the portion of the watershed area that each gage represents. To form the polygons each pair of

rain gages are connected by a line, and the perpendicular bisectors of these connecting lines are drawn. The perpendicular bisectors are connected to define polygons around each gage. These polygons represent the area of the watershed represented by each rain gage. To calculate the average rainfall for the watershed each rain gage measurement is multiplied by the area of its corresponding area, these are added together, and the sum is divided by the total area of the watershed.

The arithmetic averaging method assumes a weighting factor equal to the reciprocal of the number of gages, which weights each rain gage equally. To calculate the average rainfall for the watershed using this method the rainfall measured by each rain gage is summed, and then the sum is divided by the total number of rain gages. For cases of an inhomogeneous distribution of gages, this method can give an estimate that is quite different from the Thiessen method.

## 7.3.2. Spatially Distributed Storm Surfaces

Three storm surfaces were created using quadratic equations. These surfaces modeled different rainfall characteristics, such as rainfall depth and the spatial spread of the storm in order to characterize the effects of the storm characteristics. The different storm surfaces represented different levels of uniformity of rainfall intensity. To create these rainfall scenarios an intensity-duration-frequency curve was used to determine rainfall amounts for a storm of constant duration and various return periods. A multiple regression program was used to fit quadratic polynomials to represent rainfall surfaces described by these rainfall amounts.

To visualize these surfaces and confirm their suitability the three-dimensional plotting tools of Matlab were used to produce graphs of each equation. Figure 7-1

167

provides a three-dimensional plot of the quadratic surface representing rainfall

scenario 1. The equation for this surface is:

$$Z = 39.45321 + 7.228134x - 0.7372159y$$
$$-0.0566769x^2 + 0.2652926y^2 - 0.0028013xy$$

(7-1)

This rainfall surface is fairly linear, and the rainfall values vary from 38.83 mm at the

lowest point to 133.2 mm at the highest point. Figure 7-2 illustrates rainfall scenario

2 with a three-dimensional plot. The equation describing this surface is:

$$Z = 121.0983 - 5.262119x - 4.188004y$$
$$-0.204217x^2 + 1.047001y^2 + 0.0000004xy$$

(7-2)

This surface is also fairly linear, but the rainfall amounts clearly vary much more

widely than in rainfall scenario 1. The minimum rainfall amount in this scenario is

33.07 mm and the maximum rainfall amount is 447.8 mm. In both rainfall scenarios

1 and 2, the maximum amount of rainfall is near the pixel edges. Figure 7-3

illustrates rainfall scenario 3. The equation describing this surface is:

$$Z = 19.82887 + 41.92591x + 1.965484y$$
$$-8.509185x^2 - 0.4913644y^2 - 0.0000107xy$$

(7-3)

Unlike rainfall scenarios 1 and 2 this surface peaks near the center of the pixel. The

magnitude of the rainfall for this scenario is lower than the other two scenarios,

ranging from 19.83 mm to 71.61 mm, but the quadratic shape of the surface results in

a higher degree of variation of rainfall experienced across the synthetic pixel. The

maximum rainfall is experienced near the center of the pixel, while the edges of the

pixel experience less rainfall. In summary, the following describe the characteristics

of the three scenarios:

- Scenario 1: nearly linear, moderate depths, maximum at edge

- Scenario 2: nearly linear, high depths, maximum at edge

- Scenario 3: quadratic, low depths, maximum at center

The three quadratic surfaces are assumed to represent the rainfall as measured by the radar. The value of the surface at a given location represents the true rainfall, as measured by the radar. It is very rare, though, for radar data and rain gage data to correlate perfectly for a variety of reasons. For example, mountains or buildings could partially block the radar beam, resulting in an inaccurate radar measurement for a given location, or wind could cause rain drops to drift significantly in the horizontal direction between the time that they are measured by the radar in the atmosphere and the time that they fall to the ground surface. To account for this, some amount of random variation was added to the rain gage measurements. The rain gage measurements were calculated as a function of the height of the rainfall surface at the location of the gage plus or minus some random variation to account for the potential lack of correlation between the radar and rain gage measurements. Several possible distribution functions were available to describe this random error. Z-R relationships have shown that such error exists in radar rainfall measurements. The program to calculate the rainfall estimates for the pixel was used three times, using each of the storm surfaces once.

A variety of storm parameters, rain gage parameters, and rainfall characteristics were calculated. The volume of rainfall occurring over the pixel, the average depth of rainfall over the pixel, and the variation in reflectance were calculated. The mean and standard deviation of the rain gage measurements were calculated for each scenario. Also, the bias, the relative bias, the standard error, and

the relative standard error were calculated for the rainfall estimates.  These statistics

allowed the accuracy of the estimates to be assessed.
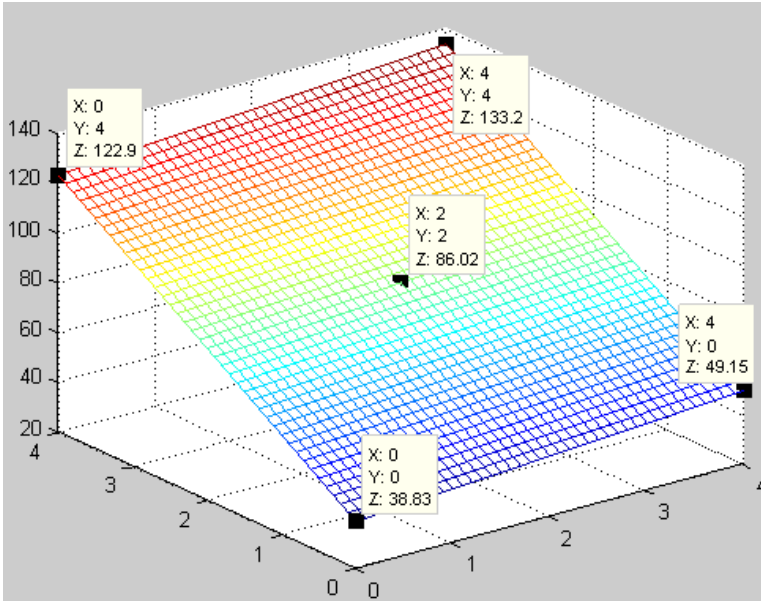


**Figure 7-1: Three-Dimensional Quadratic Surface Representing Rainfall Scenario 1**
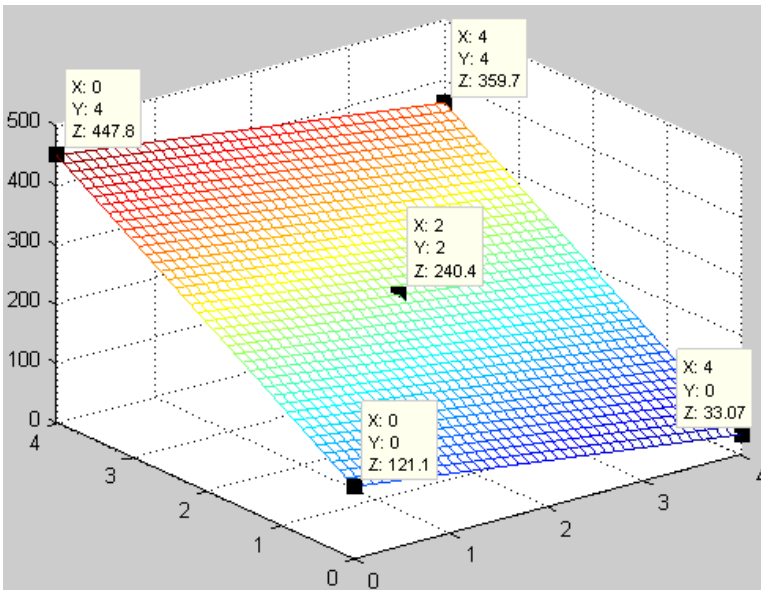


**Figure 7-2: Three-Dimensional Quadratic Surface Representing Rainfall Scenario 2**
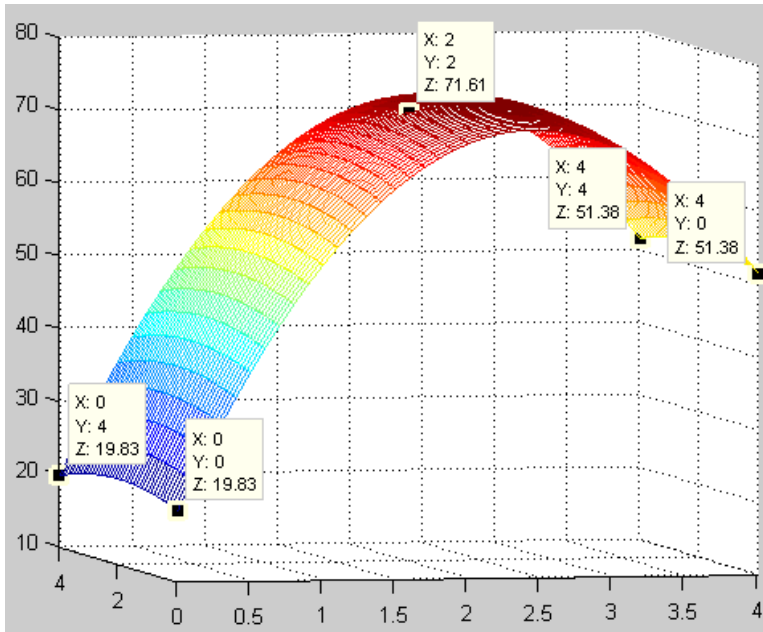
**Figure 7-3: Three-Dimensional Quadratic Surface Representing Rainfall Scenario 3**

## 7.3.3. One Rain Gage Randomly Located

### *7.3.3.1. Introduction*

A computer program was developed to simulate a spatially varying storm depth in three dimensions and to calculate the depth and volume of rain that would fall over the pixel from that storm. The first scenario modeled had one rain gage. The program randomly located the rain gage at some point in the watershed for every simulation. Since the rainfall surface was known, the true amount of rain was known and could be used as the basis for comparison. The rainfall estimates calculated from that rain gage could then be compared to the true rainfall values to determine the accuracy of estimates from one rain gage.

The first set of results to be calculated were storm characteristics, including the volume under the rainfall surface, the average depth of rainfall over the pixel, and the standard deviation of the rainfall surface values. The latter reflects the variation

171

in intensity over the pixel. These results for each of the three storm surfaces are presented in Table 7-11. These values were constant for all four of the experiments.

Table 7-11: Storm Characteristics for Each of the Three Rainfall Surfaces

|  | Rainfall Scenario 1 | Rainfall Scenario 2 | Rainfall Scenario 3 |
|---|---|---|---|
| Volume (km$^2$*mm) | 856.58 | 1691.08 | 953.90 |
| Average depth (mm) | 53.54 | 105.69 | 59.62 |
| Standard Deviation of Surface Values | 8.50 | 7.53 | 14.69 |

### 7.3.3.2. Methods and Materials

The program described above was used to simulate rainfall catches at one rain gage located randomly in the pixel. The number of simulations desired, the size of the watershed, and the probability density function of the random error associated with the rain gage measurements were specified as input to the program. For these models 10,000 simulations were run for each scenario, the pixel was specified to be a square, 4-kilometers by 4-kilometers, and a normal probability density function was assigned to the quadratic surface value at the location of the rain gage to introduce some random error. The location of the rain gage was chosen randomly for each of the 10,000 simulations.

### 7.3.3.3. Results and Discussion

This program randomly located a single rain gage at points within the pixel for each simulation in a given scenario. For each scenario the mean and standard deviation of the rain gage measurements for all simulations were calculated. For rainfall scenario 1 the mean rainfall captured at the gage was 55.46 mm with a standard deviation of 8.145 mm. For rainfall scenario 2 the mean rainfall was 107.76 mm with a standard deviation of 7.207 mm. Finally, for rainfall scenario 3 the mean

rainfall captured at the rain gage was 61.40 mm and the standard deviation was 13.81 mm.

To assess the accuracy of rainfall estimates made using only one rain gage the rain gage measurements were compared to the average rainfall surface value from simulation at the location corresponding to the location of the rain gage (see Table 7-11 for the storm characteristics). The relative bias and relative standard error values were noted for comparison with the two-rain gage model that will be discussed. These values, along with the bias and standard error values, are presented in Table 7-12 for each rainfall scenario. The relative biases ranged from 2% to 4% for the different rainfall surfaces, which indicates that the gage measurements for one rain gage are fairly free from bias. The relative standard error, though, ranges from 95% to 100%. In most cases, the relative standard error would be a reflection of the accuracy of the measurements. In the case of one rain gage being randomly located around the simulated pixel, the rain gage measurements are reproducing the rainfall surface, and any variation seen in the results is due to the random variation added. Therefore the relative standard error makes no statement about the accuracy of the rainfall estimates. The results that were observed, relative biases approximately equal to zero and relative standard error values close to 1, are the expected results, because the rainfall surface is being sampled as the rain gage is randomly located around the pixel.

**Table 7-12: Bias, Relative Bias, Standard Error, and Relative Standard Error for Each Rainfall Scenario with One Rain Gage Compared to True Rainfall Surface Values**

|  | Rainfall Scenario 1 | Rainfall Scenario 2 | Rainfall Scenario 3 |
|---|---|---|---|
| Bias | 1.929 | 2.068 | 1.785 |
| Relative Bias | 0.036 | 0.020 | 0.030 |
| Standard Error | 8.370 | 7.500 | 13.927 |
| Relative Standard Error | 0.985 | 0.997 | 0.948 |

## 7.3.4. Two Rain Gages Randomly Located

### 7.3.4.1. Introduction

To determine the effect that gage density had on the rainfall estimates calculated for the watershed a second program, which randomly located two rain gages around the watershed, was utilized. This program again simulated rainfall over the watershed using the three quadratic surfaces to represent rainfall. The rainfall catch was simulated for both rain gages in each simulation, and then the two averaging methods, Thiessen polygon and arithmetic, were used to calculate an average rainfall for the watershed. These calculations could then be compared to the known rainfall values to determine the accuracy of rainfall estimates derived from two rain gages.

### 7.3.4.2. Methods and Materials

The only difference between this experiment and the previous experiment was that two rain gages were randomly located around the pixel for each simulation. Again the number of simulations desired, the size of the watershed, and the probability density function of the random error used in calculating the rain gage measurements were specified. As was done in the previous experiment, 10,000 simulations were chosen to model each scenario, the pixel was set to be square, four kilometers by four kilometers, and a normal probability density function was chosen to introduce variation into the rain gage measurements. The three rainfall surfaces

described above were again used, and the program was run using each rainfall surface once. The same parameters were calculated by this program as by the last. In this case both the Thiessen polygon average and the arithmetic average were calculated from the rain gage measurements, then the bias, the relative bias, the standard error, and the relative standard error were calculated by comparing them to the reflectance estimates.

### 7.3.4.3. Results and Discussion

When two rain gages were randomly located within the pixel, both the Thiessen polygon and the arithmetic averaging methods were used to calculate rainfall estimates. Both averages were then compared to the average rainfall surface value for the location corresponding to the rain gage location. The averages and standard deviations of both averaging methods are presented in Table 7-13 for all three rainfall scenarios.

**Table 7-13: Averages and Standard Deviations of Thiessen Polygon Averaging Method and Arithmetic Averaging Method for Each Rainfall Scenario**

|  | Rainfall Scenario 1 | Rainfall Scenario 2 | Rainfall Scenario 3 |
|---|---|---|---|
| Thiessen Polygon Method Average | 55.28 | 107.71 | 62.48 |
| Arithmetic Method Average | 55.47 | 107.76 | 61.50 |
| Thiessen Polygon Method Standard Deviation | 5.48 | 4.88 | 9.80 |
| Arithmetic Method Standard Deviation | 5.76 | 5.12 | 9.65 |

In order to assess the accuracy of these estimates, it was necessary to compare the estimates to the known values of the rainfall surfaces, which are intended to reflect the reflectance rainfall. The relative bias and relative standard error were

again used to assess to accuracy of the rainfall estimates. For the Thiessen polygon

averaging method, these values, along with the bias and standard error values, are

presented in Table 7-14 for each rainfall scenario. The same values are presented for

the arithmetic averaging method in Table 7-15. In examining the relative biases

presented in these tables, it is evident that the Thiessen polygon averaging method

provides slightly lower, but not significantly lower, relative biases for rainfall

scenarios 1 and 2, indicating that this method results in less systematic error in the

estimates than the arithmetic average in these scenarios. The same trend can be seen

in comparing the relative standard errors. For rainfall scenarios 1 and 2 the Thiessen

polygon averaging method results in slightly lower, though not significantly lower,

errors than the arithmetic averaging method. For these rainfall scenarios at least, it

would appear that the Thiessen polygon and arithmetic averaging methods provide

equally good rainfall estimates.

**Table 7-14: Bias, Relative Bias, Standard Error, and Relative Standard Error for Thiessen Polygon Averaging Method Compared to True Rainfall Surface Values**

|  | **Rainfall Scenario 1** | **Rainfall Scenario 2** | **Rainfall Scenario 3** |
|---|---|---|---|
| Bias | 1.743 | 2.020 | 2.861 |
| Relative Bias | 0.033 | 0.019 | 0.048 |
| Standard Error | 5.477 | 4.882 | 9.804 |
| Relative Standard Error | 0.645 | 0.649 | 0.667 |

**Table 7-15: Bias, Relative Bias, Standard Error, and Relative Standard Error for Arithmetic Averaging Method Compared to True Rainfall Surface Values**

|  | **Rainfall Scenario 1** | **Rainfall Scenario 2** | **Rainfall Scenario 3** |
|---|---|---|---|
| Bias | 1.934 | 2.066 | 1.881 |
| Relative Bias | 0.036 | 0.020 | 0.032 |
| Standard Error | 5.760 | 5.114 | 9.652 |
| Relative Standard Error | 0.678 | 0.680 | 0.657 |

**7.3.5. Comparison of Results of One and Two Randomly Located Rain Gages**

In order to determine whether the addition of a second rain gage improves the accuracy of the rainfall estimates calculated for the synthetic pixel the results of the one-gage and two-gage programs discussed previously needed to be compared. Specifically, the relative bias and relative standard error were compared among the modeling scenarios. The relative bias and relative standard error compare the rainfall estimate derived for the pixel from the radar reflectance measurement, which is represented by the quadratic rainfall surface, to the rain gage rainfall measurement. A summary of the results of interest in this comparison are presented in Table 7-16, which shows that the difference in the relative bias of the rainfall estimates for one rain gage versus two rain gages is not significant. Regardless of the number of rain gages, the relative bias of the rain gage estimates is quite low, ranging from about 2% to 4%.

The relative standard error does experience significant decreases when a second rain gage is added to the watershed. When there is only one rain gage the relative standard error values are high, between 0.95 and 1.00. These values indicate that rainfall estimates made from only one rain gage are not very accurate. When the rainfall estimates are based on two rain gages, however, the relative standard error values range from 0.65 to 0.68. Adding the second rain gage appears to result in a 30% decrease in error in the rainfall estimates, which is quite significant. The rainfall estimates calculated from two rain gages under these scenarios can be expected to be much more accurate than rainfall estimates based on only one rain gage. The decrease in relative standard error can be attributed to the fact that two points located

177

on a specific surface will better represent the variation of the surface than one point

on that surface.

An important conclusion can be drawn from comparing the results of these

two experiments.  For one instant in time one rain gage will likely give a poor

estimate of rainfall.  However, over the course of a storm one rain gage may provide

acceptable results, due to the law of averages.  At some points in time the rain gage

will under-predict the instantaneous rainfall, while at other points in time it will over-

predict rainfall.  These under-predictions and over-predictions may ultimately provide

a reasonable average for the entire storm.  For any single point in time, two rain gages

will more likely represent the true average rainfall than one rain gage could.  This

illustrates the importance of spatial data in improving hydrologic models.

**Table 7-16: Comparison of Relative Bias and Relative Standard Error for Each Rainfall Scenario for One Gage and Two Gage Rainfall Estimates**

|  | **Rainfall Scenario 1** | **Rainfall Scenario 2** | **Rainfall Scenario 3** |
|---|---|---|---|
| One Gage Relative Bias | 0.036 | 0.020 | 0.030 |
| One Gage Relative Standard Error | 0.985 | 0.997 | 0.948 |
| Thiessen Average Relative Bias | 0.033 | 0.019 | 0.048 |
| Thiessen Average Relative Standard Error | 0.645 | 0.649 | 0.667 |
| Arithmetic Average Relative Bias | 0.036 | 0.02 | 0.032 |
| Arithmetic Average Relative Standard Error | 0.678 | 0.68 | 0.657 |

## 7.3.6. One Rain Gage in a Fixed Location

### *7.3.6.1. Introduction*

It was believed that randomly locating the rain gages within the pixel with

every simulation would force the rainfall estimates calculated to be fairly close to the

mean values for the watershed.  Therefore, the one-gage and two-gage experiments

were repeated with computer programs that allowed the user to set the rain gages at a fixed location within the pixel for the duration of the modeling scenario. The first program again simulated rainfall over the entire pixel based on a quadratic surface representing the rainfall surface. One rain gage was set in a fixed location, and the depth of rainfall caught by the gage in each simulation was calculated. The amount of rainfall caught by the rain gage for each simulation was a function of the value of the rainfall surface at the location of the rain gage as well as some amount of random error. As mentioned previously, random error was added to reflect the fact that, for a variety of reasons, radar measurements and rain gage measurements are not perfectly correlated. This calculation could then be compared to the known rainfall values for the pixel in order to draw conclusions about the accuracy of the rainfall estimates.

### 7.3.6.2. Methods and Materials

As with the one-gage experiment described previously, the number of simulations, the size of the watershed, and the probability distribution function of the random error in the rain gage measurements were specified as input. For all of the modeling scenarios described here, 10,000 simulations were used, the pixel was a square with sides of 4-kilometers, and a normal rainfall probability distribution function was chosen to introduce variation in the rain gage measurements. Despite the fact that the rain gage remained stationary throughout the simulations and the rainfall surface did not change between simulations, some variation in rainfall measurements between each simulation did occur due to the probability distribution function used to add random variation to the rainfall measurements to account for the typical disagreement between radar data and rain gage data. Also like the previous experiment, three quadratic surfaces were used to represent radar rainfall surfaces

179

over the pixel.  However, this program also allowed the user to specify a location in

the pixel for the rain gage, and the gage remained at that location for all simulations.

For each storm surface the program was run seven times, placing the rain gage in

seven distinct locations across the watershed.  A diagram of the possible rain gage

locations within the pixel is presented in Figure 7-4, with the coordinate locations of

the gages presented in Table 7-17.  This allowed the full variability of the storm

surface to be examined more clearly than the previous experiment with randomly

located rain gages did.  The same storm, rain gage, and rainfall estimate parameters as

discussed previously were calculated for these simulations.
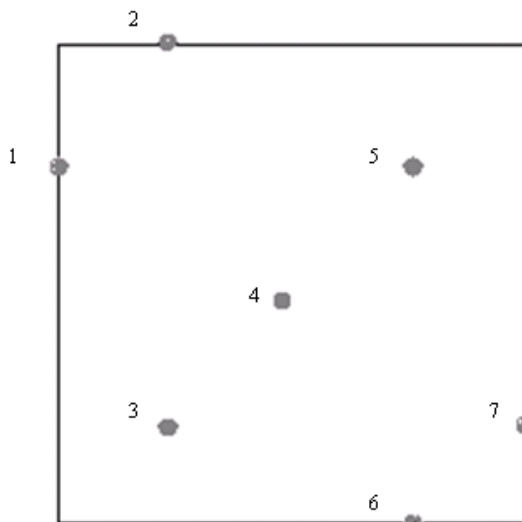


**Figure 7-4: Possible Locations of Fixed Rain Gages Within Pixel**

**Table 7-17: X and Y Coordinates of Possible Locations for Fixed Rain Gages**

| Gage ID | X Coordinate | Y Coordinate |
|---------|--------------|--------------|
| 1 | 0 | 3 |
| 2 | 1 | 4 |
| 3 | 1 | 1 |
| 4 | 2 | 2 |
| 5 | 3 | 3 |
| 6 | 3 | 0 |
| 7 | 4 | 1 |

### 7.3.6.3. Results and Discussion

The programs holding rain gages in a fixed location for the duration of the individual scenarios provide for a much more realistic examination of the rainfall estimates calculated based on one rainfall gage versus two rainfall gages. For each modeling scenario, 10,000 rain storms were simulated, and rainfall accumulation at the rain gage was measured. For each modeling scenario the program provided a mean rainfall measurement and a standard deviation for the group of simulations. When only one rain gage was present, the mean and standard deviations of the amount of rainfall caught by the gage varied widely, depending on the position of the gages.

To better evaluate the accuracy of rainfall estimates made using one rain gage in a fixed location, the mean amount of rainfall caught by the gage for each modeling scenario was examined. Table 7-18 presents the minimum of the mean rainfall depths at the rain gage, the maximum of the mean values, and the average of the mean values for each of the three rainfall scenarios. The relative biases and relative standard error values were also examined to assess the accuracy of the rainfall estimates. For rainfall scenario 1, the relative biases ranged from -0.223 to 0.228, and the relative standard error values ranged from 0.207 to 1.817. For rainfall scenario 2, the relative biases ranged from -0.1 to 0.121, while the relative standard errors ranged from 0.061 to 1.696. For rainfall scenario 3, the relative biases ranged from -0.609 to 0.235, and the relative standard errors ranged from 0.199 to 2.479. In considering the mean rainfall depths caught by the rain gage as well as the relative biases and relative standard errors, it is apparent that wide variation is possible in rainfall predictions when there is only one rain gage within the pixel.

**Table 7-18: Maximum and Average of Mean Values of Rainfall Caught by the Rain Gage for Each Rainfall Scenario**

| Rainfall Scenario | Minimum Mean (mm) | Maximum Mean (mm) | Average Mean (mm) | True Value (mm) |
|---|---|---|---|---|
| 1 | 41.62 | 68.97 | 55.61 | 53.54 |
| 2 | 95.13 | 118.45 | 108.00 | 105.70 |
| 3 | 23.31 | 73.61 | 58.18 | 59.62 |

To determine under what conditions the most accurate rainfall estimates could be obtained using one rain gage the gages were classified for each storm as experiencing low, moderate, or high rainfall. The rain gages that had experienced low rainfall conditions were compared among themselves, then compared to rain gages that had experienced a moderate amount of rainfall, and finally compared to rain gages that had experienced a high amount of rainfall. Similar comparisons were made for all rain gages that experienced moderate amounts of rainfall, and all rain gages that experienced high amounts of rainfall. The relative biases and relative standard errors for the gages after they had been classified into groups were compared to assess the accuracy of predictions. Both statistics were found to be generally the lowest for rain gages experiencing moderate rainfall, regardless of the rainfall scenario, and higher for both low and high rainfall. This leads to the conclusion that, when only one rain gage is located in a pixel, the best rainfall estimates can be made when that gage experiences moderate rainfall. This is likely because a moderate amount of rainfall is likely close to average rainfall experienced over the watershed, unless a particularly peaked storm were to occur. In the simulated pixel used for this experiment, all three storms resulted in a moderate amount of rainfall occurring in the area nearest the center of the pixel. Further conclusions cannot really be drawn as to the effect of the location of the rain gage in the watershed without respect to the storm

event; however, logic would indicate that, in general, the closer a rain gage is to the center of the storm, the more likely it is to experience a rainfall representative of the entire watershed. This further reinforces the conclusion that one rain gage can provide misleading results for any one instant in time and that spatially distributed rainfall from radar measurements can potentially improve predictions.

### 7.3.7. Two Rain Gages in Fixed Locations

#### 7.3.7.1. Introduction

Finally, an experiment was devised in which two rain gages were placed in fixed locations within the pixel for a series of simulations. As with all previous examples, the number of simulations, the size of the pixel, and the probability distribution function for the random error associated with the rain gage measurements were specified. The three storm surfaces were utilized to examine the variability of rainfall estimates under different rainfall conditions. The amount of rainfall measured at each rain gage for each simulation was calculated, and two averaging methods, the Thiessen polygon method and the arithmetic averaging method, were used to calculate rainfall averages for the pixel. These average values were used to assess the accuracy of the rainfall estimates by comparing them to the known rainfall values for the pixel.

#### 7.3.7.2. Methods and Materials

As with the previous examples the number of simulations, the size of the pixel, and the rainfall probability distribution were specified. Again 10,000 simulations were chosen, the pixel was set to be a square with sides of four kilometers, and a normal probability distribution was selected to provide some amount of random variation to the rainfall estimates to account for the common

183

disagreement between radar and rain gage data sets.  The seven possible rain gage

locations devised for the experiment in which one rain gage was set at a fixed

location, as shown in Figure 7-4, were again used.  Because using every possible

combination of two gages at these seven locations would have required a large

number of modeling scenarios, and a large investment of time to complete, fourteen

combinations of two rain gages were chosen to give a good amount of variety in gage

arrangement.  These were chosen in order to examine the effect when the rain gages

were located close to each other, far away, on the same side of the watershed, an on

opposite sides of the watershed.  These fourteen gage location combinations were run

for each of the three rainfall surfaces, with one additional combination run for rainfall

scenario 2, resulting in a total of 43 modeling scenarios.  The goal of this was to

clearly assess the effect that variability of the storm had on the rainfall estimates

calculated for the watershed.  The same parameters as discussed previously were

calculated by this program.  The Thiessen polygon and arithmetic averages were

calculated, and then the bias, the relative bias, the standard error, and the relative

standard error were for the averages were used to assess the accuracy of the rainfall

estimates.

### 7.3.7.3. Results and Discussion

In examining the results of the 43 scenarios modeled for two rain gages in

fixed locations, several important, and in some cases surprising, observations were

made.  When the relative standard errors of the various scenarios were compared,

very little variation was evident.  Regardless of the rainfall scenario, the averaging

method used, or the position of the rain gages relative to each other, the relative

standard error ranged between 0.019 and 0.054.  Clear trends could not be identified

in the variation of relative standard error, and the differences were so small that they could simply be due to random chance.

Despite the lack of variation in the relative standard error values, significant variation was seen in the relative biases. The relative biases were seen to be both positive and negative. For rainfall scenario 1 the relative bias ranged from 0.013 to 0.285 for the Thiessen polygon estimates, and from -0.018 to 0.229 for the arithmetic average estimates. For rainfall scenario 2, the relative biases ranged from -0.002 to 0.121 for Thiessen polygon estimates and from 0.01 to 0.10 for arithmetic average estimates. Rainfall scenario 3 experienced the most variation in bias, because this storm surface was more variable than the other two. For the Thiessen polygon estimates, the relative biases ranged from -0.609 to 0.023, and for the arithmetic average estimates the range was from -0.344 to 0.059.

Several interesting trends with respect to the gages locations relative to each other were noted. First, the closer to two gages were to each other, the more likely the mean rainfall depths were to be similar. For instance, in one scenario gages as coordinates (1,4) and (3,0) were used. The distance between these gages was 4.472 km. The mean rainfall depths caught at these rain gages for rainfall scenario 1 were 49.91 mm and 62.63 mm, respectively. In comparison, the gages located at coordinates (3,3) and (2,2), located a distance of only 1.414 km apart, were also used. The rainfall means for rainfall scenario 1 at these gages were 55.25 mm and 62.78 mm, respectively. Similar trends were observed in both the Thiessen polygon averages and the arithmetic averages. Generally, it was found that when the two gages were farther apart from each other the relative biases and relative standard error

values improved, compared to when the two gages were located close to each other.

For instance, for rainfall scenario 1, rain gages located at (4,1) and (3,0) were used to

calculate averages. These gages were located a distance of 1.414 km apart. The

relative bias for this rainfall average was 0.285, and the relative standard error was

0.046. Similarly, the gages located at coordinates (3,0) and (3,3), with a distance of 3

km between them, were used to calculate averages. The relative bias of this estimate

was 0.172, while the relative standard error was 0.035. It was also noted that the

relative bias seemed to generally improve when the two rain gages experienced

different rainfall amounts. For rainfall scenarios 1 and 2 this meant that, when the

rain gages were not located close to each other, the rainfall estimates they provided

were the most accurate. Logic does seem to support this finding, as two rain gages

located in different parts of the watershed would most likely experience rainfall that

better represents the rain falling over the entire watershed. From a statistics

standpoint, gages located near each other are less likely to be independent

measurements and, thus, the effective sample size is less than the number of gages.

In general, for all three rainfall scenarios, when one rain gage was experiencing high

rainfall while the other experienced moderate rainfall the estimates were the least

biased.

### 7.3.8. Comparison of Results of One and Two Rain Gages in Fixed Locations

To determine whether or not an additional rain gage improved the accuracy of

rainfall estimates for the pixel the relative biases and standard errors of the various

modeling scenarios were compared. The rain gages were grouped as being in a

position to experience low rainfall, moderate rainfall, or high rainfall.  For the two rain gage case, scenarios in which both rain gages experienced similar rainfall and in which the rain gages experienced different rainfall were considered.  Specifically, the following scenarios were tested: (1) both rain gages experienced low rainfall, (2) one rain gage experienced low rainfall and one experienced moderate rainfall, and (3) one rain gage experienced low rainfall while the other experienced high rainfall, were examined.  Each of these scenarios was compared to the scenario in which one rain gage experienced low rainfall.  Corresponding comparisons were made for moderate and high rainfall scenarios.

The comparison of relative bias and relative standard error for these cases led to the general conclusion that two rain gages provided more accurate rainfall estimates than one rain gage.  An overall trend of decreasing relative biases and relative standard errors between compared scenarios with one and two rain gages resulted in this conclusion.  The decrease in relative standard error when a second rain gage was added was often quite significant.  For instance, in many cases the relative standard error was between 1.0 and 2.0 when only one rain gage was present; however, when there were two rain gages, regardless of rainfall scenario, averaging method, and gage location, the relative standard error was between 0.02 and 0.06.  This would indicate that the addition of the second rain gage significantly improves the accuracy of the rainfall estimates calculated for the pixel.

The change in relative bias when a second rain gage is added was not so consistent.  Generally speaking, the addition of a rain gage resulted in some improvement in relative bias; however it is evident that the rainfall scenario and

locations of the rain gages relative to each other influences the bias. For low to moderate rainfall at the rain gage the relative bias was more likely to be negative, indicating that in these situations the rainfall estimates are likely to under predict the amount of rainfall. Under high rainfall conditions the relative bias was most likely to be positive, indicating an over prediction in the pixel rainfall. When one rain gage experienced high rainfall while the other experienced low rainfall, the relative bias decreased dramatically, compared to a similar scenario with only one rain gage. This general statement is applicable to rainfall scenarios 1 and 2, though it is not necessarily true for the more variable rainfall scenario 3. In considering the rainfall scenarios used in these experiments, it is most likely that for two rain gages, with one experiencing high and one experiencing low rainfall, that these rain gages would not be located close to each other. Therefore it would be expected that two rain gages in this scenario would be able to fairly well represent the average rainfall being experienced over the entire watershed. Also, from a mathematical standpoint, it is reasonable to expect that two values, one particularly high and one particularly low, would average out to a reasonable representation of the sample as a whole. The best improvement in relative bias most often occurred with rainfall scenario 2. This rainfall surface had the least variation of the three surfaces tested, so this finding is expected. Conversely, the least improvement in relative bias often occurred with rainfall scenario 3. This rainfall surface was highly variable, so again, this finding was not unexpected.

### 7.3.9. Conclusions

The effects of using an averaging method such as the Thiessen polygon method of the arithmetic averaging method on rainfall estimates calculated for a watershed were investigated. This analysis also further investigated the importance of rain gage density in a watershed. The results of this study illustrate that for any one time period one rain gage will likely give a poor estimate of rainfall for the entire watershed, but due to the law of averages one rain gage may give a reasonably accurate rainfall estimate for an entire storm. Similarly, for any one time period, two rain gages are likely to better represent the rainfall surface over the entire watershed than one rain gage. This proves the importance of using spatial data to make rainfall estimates. An overall trend of decreasing relative biases and relative standard errors with the addition of a second rain gage within a watershed were observed, proving that two rain gages could provide more accurate watershed rainfall averages than one rain gage. However, the location of the two rain gages relative to each other played a key role in determining the level of improvement the second rain gage provided. Two rain gages located relatively far from each other were found to have better relative bias and relative standard error values than two rain gages located close to each other.

The results of this study indicate that increased spatial data about rainfall can improve the accuracy of rainfall predictions. However, few dense rain gage networks currently exist, limiting the amount of improvement in accuracy possible. Radar data may be a suitable substitute for rain gage data, as it provides more detailed spatial information about rainfall at a reasonable time step. The use of radar data as input to

hydrologic models and analyses should be investigated with the goal of improving the

accuracy of the results of those models and analyses.

# CHAPTER 8

# UNIT HYDROGRAPH ANALYSES: POINT VS. SPATIAL RAINFALL INPUT DATA

## *8.1. INTRODUCTION*

Unit hydrographs (UHs) are frequently used in hydrologic design. A UH is a system transfer function that is used to transform precipitation excess (PE) into direct runoff (DRO). The exact definition of a UH is a hydrograph that results from exactly one inch of precipitation that falls in a uniform manner and at a uniform rate over a watershed during a specified time interval. Several portions of this definition are particularly important. First, a UH must have exactly one inch of PE. Second, the precipitation must have a uniform spatial distribution over the watershed. Except for very small watersheds this condition rarely occurs, so this portion of the definition must often be applied loosely in order to use the unit hydrograph procedure. Third, PE must be constant in time. This is also not a realistic requirement, so it must be interpreted loosely in the application of the unit hydrograph process. Finally, the PE must occur over a specific time interval. In unit hydrograph analyses, this rule is met by selecting short duration storms.

The extent to which these assumptions are met in either analysis or design has not received the attention that it deserves, given the extent to which unit hydrographs are used, such as in the HEC and USDA programs. The degree to which failure to meet these assumptions influences a design is not known. In the case of unit

hydrograph analysis, the uncertainty of spatial variation of rainfall over the watershed on the fitted UH needs to be investigated, as UHs are often fitted using data from a single rain gage. Rainfall characteristics are not constant over time except for very small watersheds and short duration, intense storms. This lack of temporal homogeneity also introduces inaccuracy into a fitted UH. The objectives of this research were to determine the degree to which spatial characteristics of rainfall influenced the fitted UH, and to determine whether UHs could be improved by using spatial rainfall data such as radar data.

In developing a unit hydrograph, the first step is to obtain rainfall and runoff data for a storm in a given watershed. Then baseflow, which is the flow that would occur in a channel when there had been no precipitation, must be separated from the DRO. This is not necessary in arid and semi-arid regions where channels tend to be ephemeral. Next losses, including the initial abstraction, need to be separated from the rainfall in order to determine the PE. Precipitation that infiltrates into the subsurface, or is stored in some sort of surface detention would be considered losses. These separation analyses are done in order to identify the transfer function, which will be used with a synthetic design storm to determine a design runoff hydrograph. The process in which the design storm and the transfer function (UH) are combined to produce DRO is called convolution. Convolution, also known as the theory of linear superpositioning, is a process that combines multiplication, translation with time, and addition. The ordinates of the design storm are convolved with the ordinates of the transfer function to calculate the ordinates of the design runoff hydrograph. Equation

8-1 is used to determine the number of ordinates on the direct runoff hydrograph the formula:

$$n_{DRO} = n_{PE} + n_{UH} - 1 \qquad\qquad (8\text{-}1)$$

where n is the number of ordinates.

### 8.1.1. UH Derivation

Two methods by which a unit hydrograph can be derived are the rainfall-excess reciprocal method and least-squares analysis. The rainfall-excess reciprocal method is a very computationally simple method that can be used for fairly simple storm events. Each ordinate of the DRO hydrograph is multiplied by the reciprocal of the depth of the PE (which is equal to the depth of the DRO). This results in a UH with a depth of one inch, as required by the definition of the UH.

A second option for deriving a unit hydrograph is least squares analysis. This method can be used on more complex storm events. When using nonlinear least squares analysis to determine a UH, the PE is the predictor variable while the DRO is the dependent variable. This is a convenient method for deriving UHs; however, some limitations exist. It will also be necessary to ensure that the UH ordinates sum to one area-inch, as the least squares method does not necessarily force this result as the rainfall-excess reciprocal method does (McCuen, 2005).

In the nonlinear least squares (NLLS) procedure used herein, the precipitation excess and direct runoff distribution are determined external to the analysis and used as input to develop the UH. A UH model is assumed, with the model being a function of parameters (i.e., coefficients) that need to be calibrated (i.e., fitted via least squares). In the analyses reported herein, a Weibull distribution is used as the

UH, with the Weibull being a function of two parameters (one shape and one scale).

Estimates of the two parameters are assumed and used to fit the Weibull function,

which is then convolved with the rainfall excess to get a computed distribution of

direct runoff.  The computed and measured direct runoff distributions are compared

statistically, with the two parameters adjusted until the computed DRO(t) provides the

best possible fit to the observed DRO(t).

## 8.1.2. Transmission Losses

In arid regions, transmission loss (TL), which is the infiltration of flow into

the channel bed, can be a significant factor in hydrological modeling.  The result of

TL is a decrease in both flow volume and peak discharge as the flood wave moves

downstream (Jordan, 1977).  Normally, the peak discharge is expected to increase as

the flood wave moves downstream because of local inflow, but where transmission

losses are significant, they can cause a decrease as the flood moves downstream.

The hydrographs shown in Figure 8-1 are for gages in the Walnut Gulch Watershed,

Arizona.  The hydrographs show the flow moving downstream during the storm event

of July 31, 2007, and demonstrate that transmission losses offset local inflow rates.

Flow gage 11 is the most upstream flow gage, and it clearly has the highest peak

discharge (2.899 mm/hr).  The peak flows decrease at flow gages 6 (1.201 mm/hr)

and 2 (0.980 mm/hr), which are downstream of flow gage 11.  Finally, the flow

measured at flow gage 1, the watershed outlet, is seen to have the lowest peak flow

(0.615 mm/hr).  A trend of decreasing area under the hydrograph is also seen as the

flood wave moves downstream.

It is also interesting to note that, as the flood wave travels downstream, the rising limb of the hydrograph becomes steeper, to the point that at flow gage 1, the outlet, the rising limb is almost an instantaneous rise to the peak flow rate. Transmission losses can be responsible for the steep rising limbs of hydrographs that are characteristic of arid regions. This occurs because much of the initial flood waters infiltrate into the dry channel bed as the flood wave travels downstream. The rate of streamflow exceeds the transmission loss rate only when the rainfall intensity is high. Thus, runoff appears in the form of a hydrograph with a steep rising limb. This phenomenon will be significant in the development of unit hydrographs from data influenced by transmission losses.
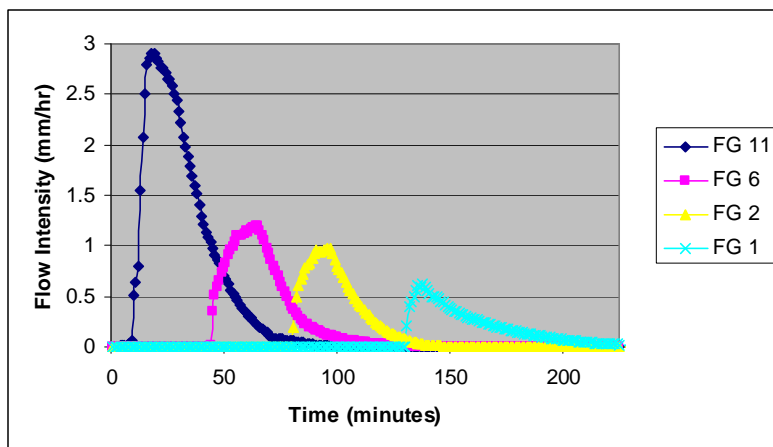


**Figure 8-1: Flow Records Measured At Different Flow Gages as Flood Wave Moves Downstream for Storm on 7/31/07**

### 8.1.3. Weibull Distribution as a UH

Unit hydrographs are often represented with a scaled gamma distribution (Dooge, 1973; Nash, 1958). The gamma distribution is not sufficiently flexible to represent the steeply sloped UHs analyzed for Walnut Gulch. Therefore, the Weibull distribution, which is more flexible than the Gamma distribution, was selected as a

UH model.  The Weibull distribution is an extreme value type III distribution.  The

Weibull distribution is defined by the equation:

$$f(t) = \frac{c}{b^c}(t^{c-1})e^{-(\frac{t}{b})^c}$$ (8-2)

where t must be ≥0, and *b* and *c* must be >0.  The *b* value is the Weibull scale

parameter, while the *c* is the Weibull shape parameter.  Several different shapes are

possible for this distribution, depending on the shape parameter (*c*).  When *c* is less

than 1.0, a reverse-J shape occurs.  When *c* equals 1.0, an exponential shape occurs.

When *c* increases above 1.0, a skewed bell shape curve that starts at f(x=0)=0 occurs

(Haan, 1977).  This is demonstrated in Figure 8-2, which plots three Weibull

distributions, where the Weibull *b* value is set equal to three and the Weibull *c* value

is varied.  A typical unit hydrograph would be expected to have a somewhat skewed

distribution, so when using this distribution to fit unit hydrographs, Weibull *c* values

greater than 1.0 would be expected.
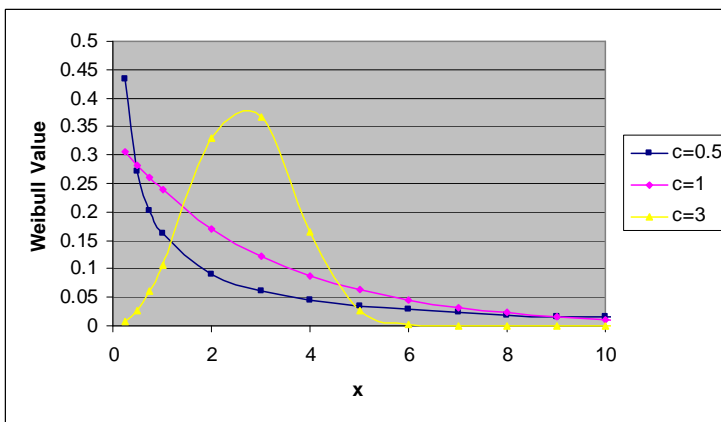


**Figure 8-2: Weibull Distribution for Various c Values, While b=3**

Bhunya *et al.* (2007) evaluated four probability distribution functions (pdfs) to

determine which could best be used to develop synthetic unit hydrographs.  The pdfs

under consideration were the two-parameter Gamma, the three-parameter Beta, the

196

two parameter Weibull, and the one-parameter Chi-square.  The results of that study

indicate that, because the Beta and Weibull distributions have both positive and

negative skew, they were more flexible, and thus were better able to fit UHs from

observed data.  Because of this extra flexibility the Beta and Weibull distributions

were found to more accurately predict unit hydrographs than the Gamma and Chi-

square distributions (Bhunya *et al.*, 2007).  The Weibull distribution was chosen over

the Beta distribution for this research because the Weibull distribution has only two

parameters to be fit, while the Beta distribution has three parameters.

### 8.1.4. Applications of UHs

Unit hydrographs have a variety of uses in hydrologic design.  Currently, peak

discharge methods are widely used for analyses that involve small watersheds, such

as highway drainage and urban watershed drainage, to name a few; however, peak

discharge methods are not considered accurate enough for many other applications.

Computer models using hydrograph methods are widely considered to be more

accurate than peak discharge methods and are becoming more popular for many

applications.  Hydrograph methods are frequently used for moderate to large

watershed analyses.  They are also used when significant amounts of natural storage

exist within the watershed being analyzed.  If significant variations exist in either the

watershed itself or the hydrometeorologic conditions, then hydrograph methods are

preferred over peak discharge methods.  Also, if subdivision of the watershed will be

necessary, or if any constraints to the principal flow paths within the watershed exist,

hydrograph methods should be used.  The following list from McCuen (2005)

describes the procedure for using unit hydrographs for hydrologic design:

1.  Choose a design storm and a return period.

2.  If a large watershed is being analyzed make appropriate depth-area
    adjustments.

3.  Calculate the initial abstractions and losses in order to separate the PE
    from the chosen design storm.

4.  Choose a unit hydrograph model and obtain the necessary inputs to put
    it in dimensional form.  Ensure that the unit hydrograph volume is
    equal to one area-inch.

5.  Convolve the PE hyetograph and the unit hydrograph to determine the
    DRO hydrograph.

6.  Add baseflow, if applicable, to the DRO hydrograph to compute the
    total runoff hydrograph.

7.  If necessary, route the total runoff hydrograph through the channel
    system.

## 8.1.5. Potential Problems in UH Derivation

Traditionally, the rainfall record used to determine the PE for the UH

procedure is obtained from a rain gage located within, or close to, the watershed

being analyzed.  Two problems immediately arise with this.  First, a rain gage only

measures point rainfall, which may not be representative of the rain on other portions

of the watershed either in total storm depth or in intensity over the duration of the

event.  This is especially true when larger watersheds are being analyzed.  Second,

not all watersheds have even one rain gage located within the boundaries.  In such

cases, the rainfall record from the rain gage located nearest to the watershed must be

used, but again, this may not be representative of the rainfall experienced on the watershed.

The temporal distribution of rainfall is critical to the development of a watershed unit hydrograph. Several possible methods for obtaining a representative rainfall record for the unit hydrograph procedure can be used. If multiple rain gages are located within one watershed, then the rainfall records from these gages may be averaged in some way, such as the Thiessen polygon method, to develop one rainfall record. It is rare, however, for a watershed to have more than one rain gage located within its boundaries, so this solution is generally not feasible. An alternative method of developing a representative rainfall record is to use radar data. Radar data essentially measure an average rainfall rate for a given radar pixel, which is often a square measuring approximately 4-km by 4-km. Because radar data are available for most of the United States, it would eliminate the problem of not having representative rainfall data. If a radar rainfall record were substituted for a rain gage rainfall record, it would be expected to provide a unit hydrograph that better accounted for spatial variability in rainfall over the radar pixel area.

## 8.2. UH DERIVATION PROCESS

### 8.2.1. Rainfall and Flow Data Preparation

Rain gage and flow gage data were obtained from the United States Department of Agriculture (USDA) Agricultural Research Service (ARS) Southwestern Watershed Research Center's website for the Walnut Gulch Experimental Watershed. Both datasets included the date of the event, the start time for rainfall or runoff for each gage, the number of minutes elapsed from the start time

for each individual reading, as well as the rainfall rate and accumulated depth, or the runoff rate and accumulated volume.  The information related to the event start time, the time elapsed, and the rainfall or runoff rate was extracted for use in the unit hydrograph derivation process.  Neither dataset had readings that occurred on a constant time interval, which would be required for the unit hydrograph analyses, so an interpolation program was used to create records that were on a constant time interval of one-minute.

Radar data were obtained from an internet service known as Hydro-NEXRAD (The University of Iowa, 2008).  This is a service operated and supported primarily by researchers at the University of Iowa, along with several other partners, that aims to make radar data more accessible for use in hydrologic applications.  It provides an easy-to-use method for downloading radar data for a particular watershed or radar station.  Radar data for the desired storm events were obtained for the San Pedro River Basin, which is the larger watershed that contains the Walnut Gulch Experimental Watershed.  Data could be obtained either as files that were viewable in ArcGIS, or as text files.  Using a file visualized in ArcGIS, along with a shapefile showing the boundaries of Walnut Gulch the radar pixels that covered the watershed of interest were identified.  Then the necessary radar data could be extracted from the downloaded files.  The radar data files are not recorded on a constant time interval, so they too needed to be interpolated.  Due to the slightly different format of the data files as compared to the rain and flow gage data files, a separate interpolation program was created for use with these files.  The result of this interpolation was radar hyetographs on a one-minute time increment.  Figure 8-3 shows the Walnut

Gulch Experimental Watershed, along with the locations of rain gages. The squares of varying colors also shown in this figure are the radar pixels that correspond to the Walnut Gulch area.
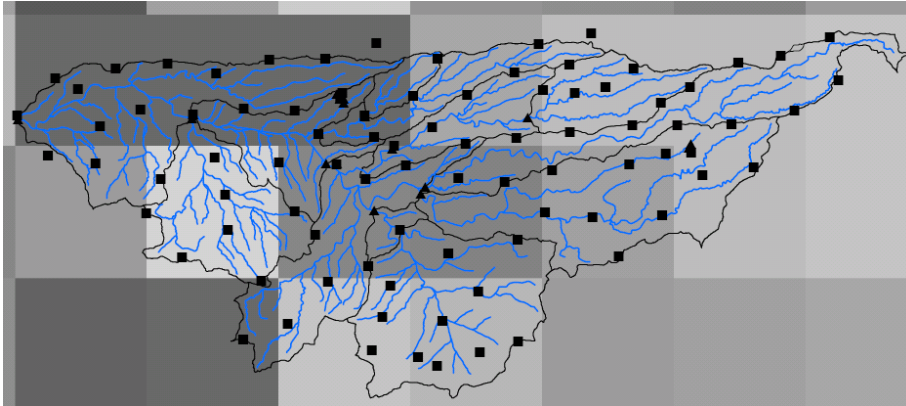


**Figure 8-3: Walnut Gulch Map with Corresponding Rain Gage (black squares), Flow Gage (black triangles), and Radar Data (large, gray-scale squares) (http://www.tucson.ars.ag.gov/dap/images/WalnutGulch_map.jpg)**

## 8.2.2. Separation of Losses

Once acceptable rainfall and runoff data files had been developed, the first step was to create precipitation excess hyetographs (PE) and direct runoff hydrographs (DRO). Because Walnut Gulch is located in an arid region and the streams are ephemeral, it was assumed that baseflow did not exist. Therefore, all of the runoff measured by the flow gages was considered DRO.

The next step was to separate losses from the rainfall hyetograph to determine the PE hyetograph. The first assumption made in this process was that all rainfall prior to the start of runoff was lost as initial abstraction. The initial abstraction is rainfall that occurs near the beginning of the storm that is not available to runoff, normally because it is intercepted by the vegetation or infiltrates into the watershed subsurface. After the initial abstraction was removed from the rainfall data, the constant percentage method was used to separate losses from the PE. In using the constant percentage method, losses are assumed to be proportional to the rainfall rate

such that the volumes of PE and DRO are equal.  Therefore, some percentage of rainfall was removed from every rainfall data record that remained after the initial abstraction had been removed, with the remaining rainfall considered to be the PE responsible for the DRO.  Using the φ-index method to separate losses would have been preferable; however, this method eliminated too many ordinates of the hyetograph, thus leaving only a few very intense ordinates.  With so few hyetograph ordinates a rational hyetograph, and therefore a rational UH, could not be derived.

A program that would delete all rainfall records prior to the start of runoff and then use the constant percentage method to separate losses from the PE was developed.  This program also used the drainage area of the flow gage to convert the runoff from intensity measurements to volume measurements.  As a final step, the program confirmed that the volume of PE was equal to the volume of DRO.  The output from this program provided the PE hyetograph and DRO hydrograph that would be used to determine the optimum UH parameters for that event.

## 8.2.3. Nonlinear Least Squares Analysis of UH Parameters

The PE hyetograph and the DRO hydrograph calculated previously were used in a least squares analysis to determine the optimum Weibull UH parameters for each storm event.  Based on work done by the Stone *et al.* (2008), it was known that runoff in Walnut Gulch peaked very quickly after the runoff began, and it typically did not have a long duration.  It was believed that this could result in UHs that differed somewhat in shape from the commonly seen hydrograph shape.  Hydrographs with particularly steep rising limbs with shorter than normal recessions have also been seen in arid regions by Peebles *et al.* (1981) and Sen (2007 and 2008).  Peebles *et al.*

(1981) attribute these particular characteristics to transmission losses in the channel. The nonlinear least squares analysis determined the best-fit values of the Weibull shape (*c*) and scale (*b*) parameters. Then the UH and PE(t) were convolved to calculate a predicted DRO hydrograph. Goodness-of-fit statistics including the standard error ratio, the correlation coefficient, and the coefficient of determination were evaluated using the calculated and measured DRO hydrographs.

## *8.3. ANALYSIS OF UHS*

### 8.3.1. UHs Derived from Rain Gage Data

To compare unit hydrographs derived for different rain gages the first step was to identify the rain gages located within the boundaries of specific radar pixels. This was done for ease in later comparing UHs derived with rain gages to those derived with radar rainfall data. Then the downstream flow gage located nearest to this radar pixel was identified. Unit hydrographs were derived using each individual rain gage located within the pixel for four storm events, and the variation between these UHs was assessed. This analysis procedure was then used on two radar pixels within the Walnut Gulch watershed. The results of the two pixels analyzed for the same storm event were compared to evaluate the variability of unit hydrographs derived for different portions of the watershed. The goodness-of-fit statistics derived using the rain gages in the different pixels were compared to evaluate the accuracies of the runoff predictions made from rainfall and flow data for difference portions of the watershed. Then the unit hydrographs derived for the different pixels were

plotted and compared to visually detect differences caused by location within the

watershed.

### 8.3.1.1. Comparison of UHs Derived from Rain Gages Within One Pixel

Given that unit hydrographs are commonly developed using data from one

rain gage, it was of interest to assess the potential uncertainty that this limitation

might have on developing a representative watershed UH.  Therefore, one objective

was to evaluate the variability of Weibull UHs derived using different rain gages

located within the boundaries of one radar pixel.  Two pixels were used for this

analysis for each of four different storm events.  Figure 8-4 provides the unit

hydrographs derived for seven rain gages located within pixel 12 for the storm event

on August 13, 2006.  Table 8-1 provides a summary of the Weibull distribution shape

and scale parameters used to fit the unit hydrographs and the goodness-of-fit statistics

calculated for the resulting predicted runoff hydrographs.

In examining both the plot of the UHs (Figure 8-4) and the parameter values

presented in Table 8-1, it is evident that significant variation in the UHs is possible

depending on the rain gage used.  The peak ordinates of the UHs vary significantly,

from a minimum of approximately 10 to a maximum of approximately 40 cms/mm.

The shapes of the UHs also vary significantly.  The greatest difference is in the UH

rising limbs.  In some cases there is no rising limb (see RG 61), in which case the

Weibull shape parameter ($c$) is less than 1.0 leading to an exponential UH, while in

other cases a slight rising limb is visible (see RG 58).  Potential explanations for

exponentially shaped UHs can be provided, from both a modeling and a physical

standpoint, and will be provided at a later point in this discussion.  The present

purpose is only to point out the level of variation that is possible in fitted unit hydrographs depending on the rain gage used to provide rainfall information.
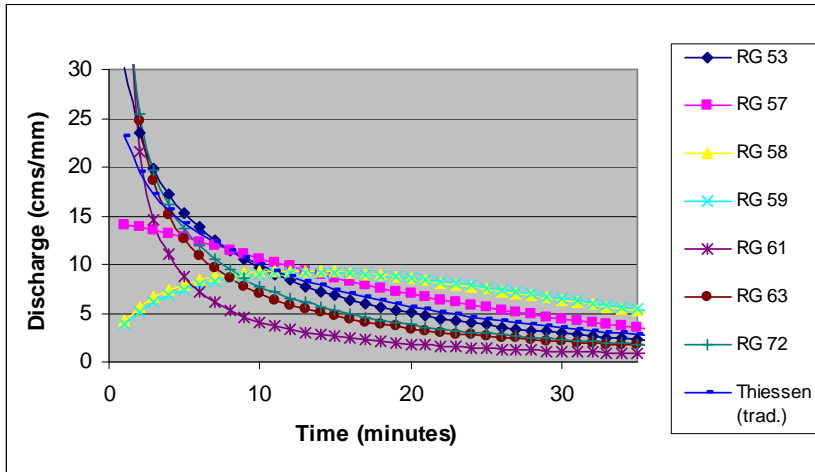


**Figure 8-4: Rain Gage and Thiessen (traditional method) Rainfall UHs Derived for Storm on 8/13/06 Pixel 12**

**Table 8-1: Rain Gage Unit Hydrograph Parameter and Goodness of Fit Statistics for Storm on 8/13/06 Pixel 12**

|                        | b    | c    | Se/Sy | R    | R$^2$ |
|------------------------|------|------|-------|------|-------|
| RG 53                  | 15.5 | 0.77 | 0.37  | 0.93 | 0.86  |
| RG 57                  | 22.5 | 1.05 | 0.45  | 0.90 | 0.80  |
| RG 58                  | 28.5 | 1.43 | 0.44  | 0.90 | 0.81  |
| RG 59                  | 29.3 | 1.46 | 0.43  | 0.90 | 0.82  |
| RG 61                  | 3.5  | 0.33 | 0.27  | 0.96 | 0.93  |
| RG 63                  | 12.7 | 0.53 | 0.42  | 0.91 | 0.82  |
| RG 72                  | 13.1 | 0.59 | 0.32  | 0.95 | 0.90  |
| Thiessen (traditional) | 19.2 | 0.85 | 0.40  | 0.92 | 0.84  |

This level of variation in unit hydrographs derived using different rain gages was not always seen.  Figure 8-5 presents a comparison of unit hydrographs derived for the six rain gages located within pixel 1 for the storm event on August 17, 2006. Table 8-2 presents the optimum Weibull parameter values determined for these unit hydrographs, along with the goodness-of-fit statistics calculated for the predicted runoff calculated using these UHs.  From these results (Figure 8-5 and Table 8-2) it is evident that the UHs derived for these six rain gages are essentially identical.  These

UHs are quite different from those presented in Figure 8-4 in that they have little variation between them and in that they have a typical UH shape. For this particular event all of the unit hydrographs were found to have a common UH shape, as opposed to the exponential unit hydrographs seen in Figure 8-4. The likely explanation for this will be provided later in the discussion; for now the important points are (1) there is a lack of variation in the unit hydrographs derived from these particular rain gages, and (2) storm characteristics can vary the degree of variation between UHs for the same storm. For this storm event, the hyetographs obtained from the individual rain gages were very similar to each other. Since the same flow record was used to derive each of the UHs and the rainfall hyetographs were similar, the UHs (shown in Figure 8-5) also were very similar to each other.
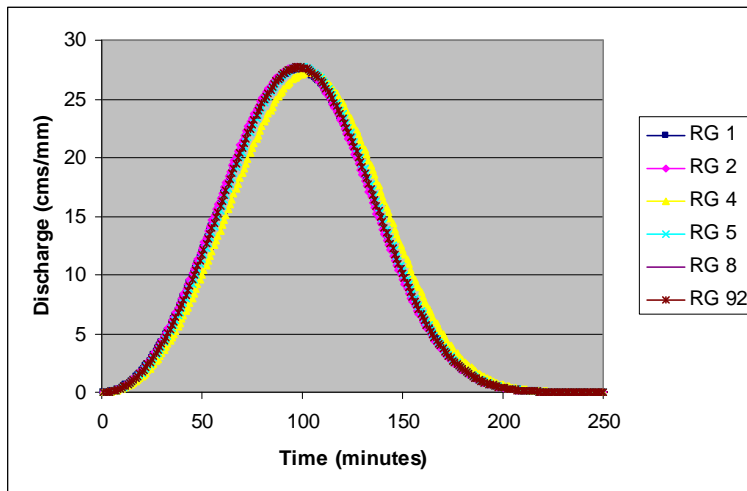


**Figure 8-5: Comparison of Unit Hydrographs Derived from Different Rain Gages for the Storm on 8/17/06 Pixel 1**

**Table 8-2: Rain Gage Unit Hydrograph Parameter and Goodness of Fit Statistics for Storm on 8/17/06 Pixel 1**

|  | b | c | Se/Sy | R | $R^2$ |
|---|---|---|---|---|---|
| RG 1 | 110.8 | 3.13 | 0.33 | 0.94 | 0.89 |
| RG 2 | 109.5 | 3.13 | 0.33 | 0.94 | 0.89 |
| RG 4 | 115.5 | 3.26 | 0.34 | 0.94 | 0.89 |
| RG 5 | 111.5 | 3.20 | 0.33 | 0.94 | 0.89 |
| RG 8 | 115.7 | 3.25 | 0.34 | 0.94 | 0.89 |
| RG 92 | 110.8 | 3.17 | 0.33 | 0.94 | 0.89 |

The variation, or lack of variation as the case may be, between UHs derived from different rain gages within one pixel appears to be related to the length of time between the center of mass (CM) of the PE and the CM of the DRO. This factor appears to control the Weibull *c* values fit to the UHs. For the storm event on August 13, 2006, the hyetographs for the individual gages differed and thus produced differences in the time of the center of mass of the PE. Therefore, the centers of masses for the PE and DRO were different. Conversely, the storm occurring over pixel 1 on August 17, 2006, was very short at all of the rain gages, but it resulted in a very long runoff record. Therefore, little variation in the timing of the PE CM was evident between the rain gages, because the storm was so short, and a long period of time was also evident between the PE centers of mass and the DRO center of mass. Collectively, these factors likely forced the normal shape of the unit hydrographs for these rain gages and resulted in the small amount of variation between them (see Figure 8-5). The shorter difference in centers of mass of the PE and the DRO for the storm on August 13, 2006, forced lower Weibull c values, which caused the exponential unit hydrographs (see Figure 8-4) seen for some of the rain gages.

### *8.3.1.2. Comparison of UHs Derived for Different Subareas*

For many analyses and designs, a watershed is subdivided because of differences in land use or storage. The general practice is to use the same unit hydrograph model for the analysis of each subarea, with variation only dependent on the area, depth of runoff, and time of concentration. This practice can be questioned if the shape of the unit hydrograph is believed to vary over the subwatersheds.

Preliminary indications suggest that transmission losses and variation in timing influence the UH shape. Therefore, it seemed reasonable to study whether or

not the UHs for different subareas of the Walnut Gulch watershed were different.

While UHs are known to vary from storm to storm, within-watershed variation of unit

hydrographs needed to be investigated.

Unit hydrographs were derived for all of the rain gages located within the

boundaries of two different pixels for the same storm event.  Figure 8-3 provides a

map of the Walnut Gulch Experimental Watershed and the corresponding radar

pixels.  The pixels used in this evaluation are pixel 1 (first row, left-most cell) and

pixel 10 (second row, third cell from the left).  The unit hydrographs derived for the

rain gages located within pixel 1 (see Figure 8-6) are compared to those located

within pixel 10 (see Figure 8-7) for the storm on July 31, 2007.  Table 8-3 provides

the UH parameters and the predicted runoff goodness-of-fit statistics for pixel 1.

Table 8-3 can be compared to Table 8-4, which provides this information for pixel 10.

The first thing to note in comparing these plots is the differences in scales.

The maximum unit hydrograph value for pixel 1 is slightly under 250 cms/mm, while

the maximum value for pixel 10 is approximately 200 cms/mm.  This is a significant

difference between the two pixels, which is caused by differences in the drainage area

of the flow gages used to derive the UHs for each rain gage.  The flow gage used to

derive UHs for pixel 1 drained approximately 14,933 ha, while the flow gage used to

drive UHs for pixel 10 drained 9510 ha.  The difference in scales is not larger than

this because significant amounts of flow are lost to the channel bed as the flood wave

moves downstream, as illustrated in Figure 8-1.  The UH derived for pixel 1 will

produce a much different direct runoff prediction for a storm event than the UH

derived for pixel 10 would due to this difference in peak ordinates.  If one of these

UHs were to be applied to the entire watershed for the purpose of design work, significantly inaccurate runoff predictions could result.  Inaccurate runoff predictions will likely result in either an inadequate design for the true hydrologic conditions, or an excessive design for the hydrologic conditions, each of which presents its own set of problems.

The differences in shape should also be noted between Figures 8-6 and 8-7. None of the UHs in Figure 8-6 have a Weibull scale parameter greater than 1.0; thus, they are all exponentially shaped.  Figure 8-7 has six of eight unit hydrographs with shape parameters greater than 1.0, producing UHs that are not exponential.  In general, the unit hydrographs derived for pixel 1 are steeper than the unit hydrographs derived for pixel 10.  One potential explanation for this is the presence of transmission losses in arid watersheds.  Pixel 1 is located downstream of pixel 10, so transmission losses would be expected to cause the runoff hydrograph associated with pixel 1 be to steeper than the hydrograph associated with pixel 10.  The decrease in flow volume as the flood wave moves downstream was illustrated for this storm event in Figure 8-1.  This steeper runoff hydrograph causes the difference in the steepness of the rising limbs of the UHs between the pixels.  This provides evidence that transmission losses could be responsible for variation in the UHs derived for different areas of a watershed.

Overall there would appear to be more variation in the unit hydrographs for pixel 10 than for pixel 1.  The scale parameters for the unit hydrographs in pixel 10 ranged from 6.5 to 15.3, while the shape parameters ranged from $1.4*10^{-6}$ to 2.17.  If data from rain gage 33, which appears to be an outlier, are removed, the scale

parameter ranged from 7.7 to 15.6 and the shape parameter ranged from 0.88 to 2.17.

The results obtained for rain gage 33 were obviously widely different from results

obtained for the other results in this pixel.  These results were further investigated in

an attempt to provide some explanation.  The $c$ value was set, and held constant, at

higher values that were similar to those found for the other rain gages, which had

been found to improve the results in other scenarios where one of the rain gages

produced unusual results.  However, in this case absolutely no improvement was seen

with changes in the parameter values.  The goodness-of-fit statistics did not improve

at all, leading to the conclusion that a data error must somehow exist to explain the

poor results.

For the UHs in pixel 1 the scale parameters ranged from 15.6 to 31.8, which is

a larger range that what was seen in pixel 10; however, the shape parameters only

range from 0.36 to 0.68.  This small range in shape parameters forced all the UHs

derived from rain gages in Pixel 1 to be exponential in shape, and to be very similar,

though a difference in scales, caused by the variation in the $b$ parameters, is visible.

The large range in shape parameters for UHs from pixel 10 resulted in much more

varied UHs.  It is also interesting to note, in regards to pixel 10, that two of the UHs,

those derived from rain gages 28 and 33, did not result in acceptable goodness-of-fit

statistics.  If either of these UHs were used to predict runoff for the watershed, it

would be impossible to have any confidence in the results, due to the poor goodness-

of-fit statistics.

Generally, UHs are attributed to characteristics of the watershed.  Factors such

as the land use, including the runoff curve number, drainage area or length, and slope

are used to scale a UH.  For the analyses reported herein, it is evident that

transmission losses are a major factor governing the shape and scale of the UHs.

Transmission losses are generally associated with the channel (Lane *et al.*, 2007), but

they are also likely associated with infiltration rates over the entire watershed.  Thus,

the UHs appear to reflect channel processes as much as watershed processes.

The results of this analysis indicate that the portion of the watershed in which

the unit hydrograph was derived should be an important consideration.  The

conclusion to be reached from this is that if a derived UH is used for design work in

the future, the location of the rain gage within the watershed could be very important

to the final result.  If the UH was derived for a portion of the watershed other than

where the design work was being done, it is possible that the UH will not be accurate,

which could result in a poor design.  If the differences between the different areas of

the watershed were severe enough, a poor design based on an inaccurate unit

hydrograph could result in negative safety and health consequences.
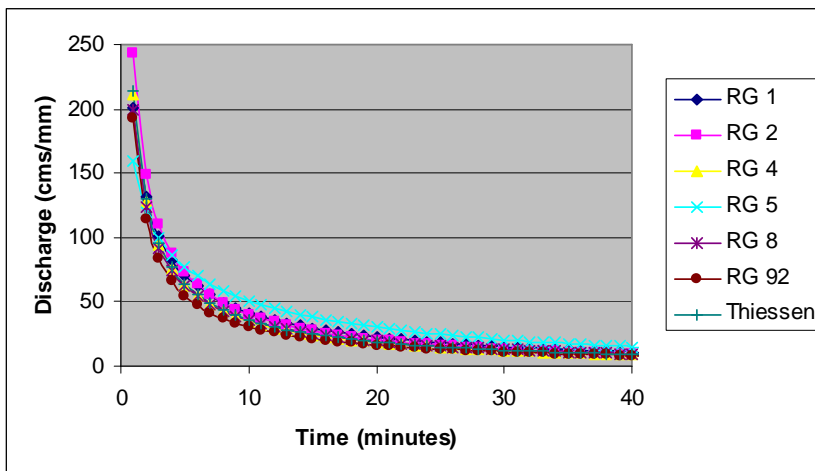


**Figure 8-6: Comparison of Unit Hydrographs Derived Using Rain Gages in Pixel 1 for the Storm on 7/31/07**

211
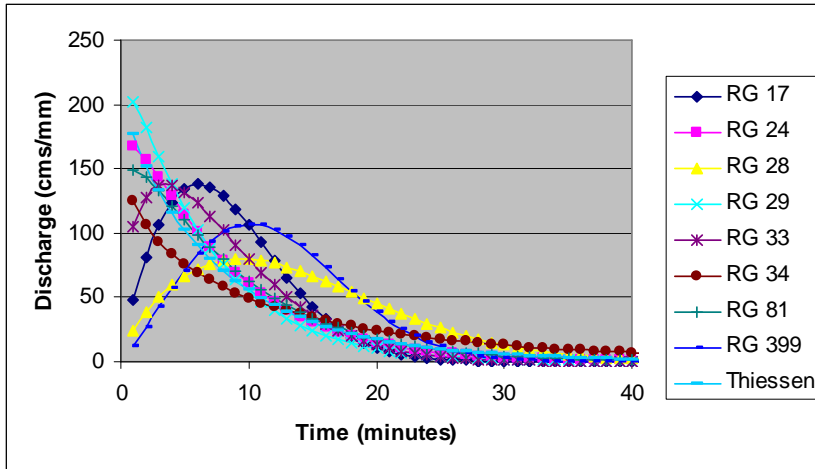
**Figure 8-7: Rain Gages and Thiessen (traditional method) Rainfall UHs in Pixel 10 for the Storm on 7/31/07**

**Table 8-3: Rain Gage Unit Hydrograph Parameters and Goodness-of-Fit Statistics for Storm on 7/31/07 Pixel 1**

|       | b    | c    | Se/Sy | R    | $R^2$ |
|-------|------|------|-------|------|------|
| RG 1  | 25.7 | 0.50 | 0.34  | 0.94 | 0.89 |
| RG 2  | 15.6 | 0.45 | 0.42  | 0.91 | 0.82 |
| RG 4  | 23.9 | 0.40 | 0.40  | 0.92 | 0.84 |
| RG 5  | 27.7 | 0.68 | 0.31  | 0.95 | 0.90 |
| RG 8  | 28.9 | 0.43 | 0.39  | 0.92 | 0.85 |
| RG 92 | 31.8 | 0.36 | 0.55  | 0.84 | 0.70 |

**Table 8-4: Rain Gage and Thiessen Rainfall Unit Hydrograph Parameters and Goodness-of-Fit Statistics for Storm on 7/31/07 Pixel 10**

|                        | b    | c    | Se/Sy | R    | $R^2$ |
|------------------------|------|------|-------|------|------|
| RG 17                  | 9.3  | 1.84 | 0.57  | 0.82 | 0.68 |
| RG 24                  | 7.7  | 1.08 | 0.65  | 0.76 | 0.58 |
| RG 28                  | 15.6 | 1.72 | 1.03  | 0.00 | 0.00 |
| RG 29                  | 6.5  | 1.06 | 0.58  | 0.81 | 0.66 |
| RG 33                  | 8.5  | 1.41 | 1.07  | 0.00 | 0.00 |
| RG 34                  | 13.8 | 0.88 | 0.41  | 0.91 | 0.84 |
| RG 81                  | 8.6  | 1.09 | 0.64  | 0.77 | 0.59 |
| RG 399                 | 13.5 | 2.17 | 0.82  | 0.57 | 0.33 |
| Thiessen (traditional) | 8.2  | 0.97 | 0.50  | 0.87 | 0.76 |

## 8.3.2. UHs Derived from the Traditional Thiessen Average Rainfall Data

Rain gage measurements reflect rainfall over the area local to the gage. The degree to which the rain gage measurements reflect rainfall at a point removed from the gage depends partly on the distance between the gage and the point. The extent to which a gage measurement reflects the size of the pixel is in doubt given the variation

in UHs in Figures 8-6 and 8-7. Therefore, it was of interest to assess if the average rainfall from the gages within a pixel would provide a realistic assessment of the accuracy of UHs derived from radar data. The Thiessen polygon averaging method was used to spatially average rainfall data to derive a UH. Using this method an average rainfall record was calculated based on measurements at the rain gages located within the borders of each radar pixel.

The first step to completing this analysis was to calculate Thiessen weights for each rain gage within the pixel using areas obtained with a planimeter. For pixel 10 the Thiessen weights were determined to be as follows: for rain gage 17 a weight of 0.068, for rain gage 24 a weight of 0.070, for rain gage 28 a weight of 0.068, for rain gage 29 a weight of 0.117, for rain gage 33 a weight of 0.144, for rain gage 34 a weight of 0.234, for rain gage 81 a weight of 0.174, and for rain gage 399 a weight of 0.125. For pixel 12 the Thiessen weights were determined to be as follows: for rain gage 53 a weight of 0.155, for rain gage 57 a weight of 0.150, for rain gage 58 a weight of 0.060, for rain gage 59 a weight of 0.243, for rain gage 61 a weight of 0.095, for rain gage 63 a weight of 0.104, and for rain gage 72 a weight of 0.193. Then an average rainfall hyetograph was created using the Thiessen weights and the 1-minute rainfall depths. From this point the standard procedure described previously was used to derive the UH and calculate runoff predictions. The goodness-of-fit statistics for the predictions were compared to those calculated using the rain gages. The UH was plotted using the optimum parameters identified, and then it too could be compared to the UHs derived using the rain gages. This comparison would indicate

whether or not spatially averaged rainfall data could provide any benefit to UH analyses.

### 8.3.2.1. UH Results Using Traditional Thiessen Calculations

Figure 8-4 compares the Thiessen average rainfall unit hydrograph to the individual rain gage unit hydrographs for pixel 12 for the storm event occurring on August 13, 2006.  The rain gage unit hydrograph parameters and goodness-of-fit statistics were presented previously in Table 8-1.  Both the $b$ and $c$ values for the Thiessen averaged rainfall and the goodness-of-fit statistics fall well into the ranges provided by the rain gages, resulting in a UH that compares well to the rain gage UHs.

Similarly good unit hydrographs derived from Thiessen average rainfall datasets for several other storm events.  For instance, Figure 8-7 shows the UHs of the rain gages in Pixel 10 as well as the Thiessen average rainfall for the storm event on July 31, 2007.  Table 8-4 provides the corresponding unit hydrograph parameters, as well as the goodness-of-fit statistics for the predicted runoff calculated using the derived unit hydrographs.  In this case, the Thiessen rainfall UH falls approximately in the middle of the exponential UHs derived from rain gages.  Because the Thiessen rainfall is an average of the rainfall measured by the individual rain gages, this was the expected outcome.  The goodness-of-fit statistics for the Thiessen rainfall UH also fall into the range of those calculated from the rain gage UHs.

The goodness-of-fit statistics of the predicted runoff hydrographs indicate that the Thiessen average rainfall can be used to derive an acceptable unit hydrograph. The purpose of the UH is often to do design work within the watershed, so the main objective of the UH is to be able to accurately predict runoff based on rainfall over

214

the watershed.  In comparing the goodness-of-fit statistics for the predicted runoff for both of the storm events evaluated here, it is obvious that the Thiessen rainfall UH is able to predict runoff at least as accurately as the rain gage UHs.  The Thiessen rainfall for pixel 12 for the storm occurring on August 13, 2006, has better goodness-of-fit statistics than four of the seven rain gages, while the Thiessen rainfall for pixel 10 for the storm occurring on July 31, 2007, has better goodness-of-fit statistics than seven of the eight rain gages.  This provides further evidence that the Thiessen average rainfall can produce an accurate unit hydrograph and an accurate prediction of runoff.

For the storm events occurring on August 13, 2006, and August 17, 2006, only slight variation was seen in the individual rain gage hyetographs.  Between the rain gages there was high similarity in both hyetograph shape and magnitude.  Therefore the traditional Thiessen analysis was able to retain the appropriate hyetograph shape, and was truly representative of the rainfall experienced on the pixel.  The storm event on July 20, 2007, did not have such strong similarities between the individual rain gage hyetographs for pixel 12.  High variability was seen especially in the shape of the hyetographs, so the traditional Thiessen calculation was not able to represent the average rainfall over the pixel.  Therefore the UH derived from this average hyetograph did not compare well to the UHs derived for the individual rain gages, as seen in Figure 8-8 and Table 8-5.  The lower UH parameters determined for the Thiessen UH result in a UH (shown in Figure 8-8) that is steeper than any of the individual rain gage UHs, whereas the expected result would be a UH falling in the middle of the rain gage UHs, as seen in Figure 8-4.

**Table 8-5: Rain Gage and Thiessen UH Parameters and Goodness-of-Fit Statistics for Storm Even on 7/20/07 Pixel 12**

|                       | b   | c    | Se/Sy | R    | R²   |
|-----------------------|-----|------|-------|------|------|
| RG 53                 | 2.2 | 0.97 | 0.57  | 0.82 | 0.67 |
| RG 57                 | 1.8 | 0.83 | 0.56  | 0.83 | 0.69 |
| RG 58                 | 2.7 | 1.10 | 0.53  | 0.85 | 0.72 |
| RG 59                 | 7.3 | 1.23 | 0.55  | 0.83 | 0.70 |
| RG 61                 | 7.2 | 1.24 | 0.51  | 0.86 | 0.74 |
| RG 63                 | 4.2 | 1.06 | 0.53  | 0.85 | 0.72 |
| RG 72                 | 3.3 | 1.06 | 0.49  | 0.87 | 0.76 |
| Thiessen (traditional) | 0.9 | 0.77 | 0.46  | 0.89 | 0.79 |



**Figure 8-8: Rain Gage and Thiessen (traditional method) UHs for Storm Event on 7/20/07 Pixel 12**

## 8.3.3. UHs Derived from the Pattern-Preserving Thiessen Average Rainfall Data

The traditional method of calculating a Thiessen average rainfall record applies Thiessen weights to each ordinate in each individual rainfall hyetograph. Aron *et al.* (1979) found that this method can result in severe attenuation of the hyetograph. This would result in an average hyetograph that is not actually representative of the individual rainfall hyetographs on which it is based. Aron e*t al.* (1979) did find that the traditional Thiessen averaging method could be applied to storm totals, just not to individual hyetograph ordinates. To determine whether this

affected the UHs derived based on Thiessen average rainfall a second averaging method, the pattern-preserving Thiessen method, was used to derive UHs.

The pattern-preserving Thiessen method, which uses some of the comments identified by Aron *et al.* (1979), was based on the Thiessen method, but the Thiessen weights were not applied to each hyetograph ordinate. Instead, the average peak intensity was calculated based on the Thiessen weights, as were the average time to peak and the average hyetograph duration. The formula used to calculate the average peak intensity is:

$$i_{pm} = \sum_{j=1}^{n} i_{pj} * w_j \qquad (8\text{-}3)$$

Where $i_{pm}$ is the average peak intensity, $i_{pj}$ is the individual hyetograph peak intensity, and $w_j$ is the Thiessen weighting factor assigned to each hyetograph. The average time to peak was then calculated using:

$$t_{pm} = \sum_{j=1}^{n} t_{pj} * w_j \qquad (8\text{-}4)$$

where $t_{pm}$ is the average time to peak, and $_{pj}$ is the time to each individual hyetograph peak. Finally the average hyetograph duration was calculated using the equation:

$$D_m = \sum_{j=1}^{n} D_j * w_j \qquad (8\text{-}5)$$

where $D_m$ represents the average hyetograph duration, and Dj represents the duration of the individual hyetographs. After the average hyetograph peak and duration were calculated the rest of the average hyetograph was filled in to maintain the general shape characteristics of the individual hyetographs. The average hyetograph ordinates were determined based on the individual rain gage hyetographs and their corresponding Thiessen weights.

### 8.3.3.1. UH Results Using Pattern-Preserving Thiessen Calculations

Thiessen average rainfall records were calculated using the pattern-preserving Thiessen averaging method for the storm events for August 13, 2006, and July 20, 2007. As seen in Figure 8-4 and Table 8-1, the agreement between the Thiessen UH parameters and the original UH parameters and the goodness-of-fit statistics calculated for the Thiessen UHs indicated that the traditional Thiessen averaging method was quite successful. The results seen in Figure 8-4 and Table 8-1 can be compared to Figure 8-9 and Table 8-6, which provide the UH results obtained for the same storm event (August 13, 2006) and pixel (pixel 12) using the pattern-preserving Thiessen rainfall hyetograph. In this scenario, using the pattern-preserving Thiessen method did not provide an improvement in results as compared to the traditional Thiessen method. The individual rain gage hyetographs used to calculate the two Thiessen hyetographs did not show significant variation for the storm on August 13, 2006, so the rain gage hyetographs had similar magnitudes and shapes. Because the individual hyetographs had similar magnitudes and shapes the traditional Thiessen averaging method was able to provide a representative average hyetograph. Both of the UHs derived using rainfall from the different Thiessen calculation methods fall into the range of values found for the individual rain gage UHs; however, the parameters derived using the traditional method seem more representative of the individual rain gages than the parameters derived using the pattern-preserving Thiessen method. For instance, the rain gage Weibull $b$ values range from 3.5 to 29.3, but four of the seven values are less than 20, making the traditional Thiessen $b$ value of 19.2 seem like the better average value than the alternative Thiessen $b$ value of 25.0. A similar statement can be made for the Weibull $c$ values. In Figure 8-9 the

shape of the UH derived using the traditional Thiessen method is more similar to the

individual rain gage UH shapes than the UH derived using the pattern-preserving

Thiessen approach.

**Table 8-6: Rain Gage, Thiessen (traditional) and Thiessen (pattern-preserving) Rainfall UH Parameters and Goodness-of-Fit Statistics for Storm Event on 8/13/06 Pixel 12**

|  | b | c | Se/Sy | R | $R^2$ |
|---|---|---|---|---|---|
| RG 53 | 15.5 | 0.77 | 0.37 | 0.93 | 0.86 |
| RG 57 | 22.5 | 1.05 | 0.45 | 0.90 | 0.80 |
| RG 58 | 28.5 | 1.43 | 0.44 | 0.90 | 0.81 |
| RG 59 | 29.3 | 1.46 | 0.43 | 0.90 | 0.82 |
| RG 61 | 3.5 | 0.33 | 0.27 | 0.96 | 0.93 |
| RG 63 | 12.7 | 0.53 | 0.42 | 0.91 | 0.82 |
| RG 72 | 13.1 | 0.59 | 0.32 | 0.95 | 0.90 |
| Thiessen (traditional) | 19.2 | 0.85 | 0.40 | 0.92 | 0.84 |
| Thiessen (pat. pres.) | 25.0 | 1.31 | 0.38 | 0.93 | 0.86 |
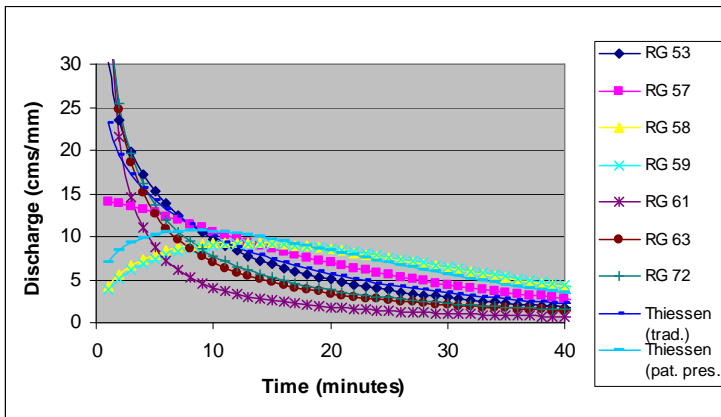


**Figure 8-9: Rain Gage, Thiessen (traditional), and Thiessen (pattern preserving) Rainfall UHs for Storm Event on 8/13/06 Pixel 12**

Table 8-6 and Figure 8-9 illustrate an example in which the traditional

Thiessen method can be used to create a representative average rainfall hyetograph,

and using the pattern-preserving Thiessen method did not offer any improvement in

the final UH results.  For the storm event on July 20, 2007, in pixel 12, the traditional

Thiessen method was shown, in Table 8-5 and Figure 8-8, to be unable to create a

representative average rainfall hyetograph from the individual rain gage hyetographs.

In examining Figure 8-8 and Table 8-5 it becomes evident that the UH derived using

the Thiessen hyetograph does not agree with the individual rain gage UHs.  Both the

$b$ and $c$ parameter values for the Thiessen UH are lower than any of the parameters

for the UHs derived from rain gages.  When using an averaging method, it would be

expected that the UH parameters would fall within the range of parameters found for

the individual rain gages.  Because the UH results using the traditional Thiessen

hyetograph did not seem logical, the pattern-preserving Thiessen method was used to

compute an average hyetograph for comparison.

The UH results using the pattern-preserving Thiessen method, which can be

compared to Figure   8-8 and Table 8-5, are presented in Figure 8-10 and Table 8-7.

In comparing the UH parameters derived using the traditional and pattern-preserving

Thiessen methods a significant difference is observed.  The UH parameters derived

using the pattern-preserving Thiessen method are within the range of parameters

derived using the individual rain gage hyetographs.  The pattern-preserving Thiessen

calculation method is obviously able to produce a representative average rainfall

hyetograph in this scenario, where the traditional method could not.  In examining

Figure 8-10, the UH derived using the pattern-preserving Thiessen method to

calculate the average rainfall is observed to fall in the middle of the rain gage UHs,

where the UH derived using the traditional Thiessen method falls below all the rain

gage UHs.  The pattern-preserving Thiessen method results in the UH that was

expected for an average rainfall hyetograph, a UH that is representative of all of the

rain gages used in its derivation.  The conclusion to be drawn from this is that, when

using an averaging method on individual hyetographs, care should be taken to ensure

that the hyetograph shape and magnitude are maintained.  When significant variation

exists in either magnitude or shape between the individual hyetographs, the traditional

Thiessen averaging method will not be able to produce a representative average

hyetograph.

**Table 8-7: Rain Gage and Thiessen UH Parameters and Goodness-of-Fit Statistics for Storm Event on 7/20/07 Pixel 12**

|                        | b   | c    | Se/Sy | R    | R$^2$ |
|------------------------|-----|------|-------|------|------|
| RG 53                  | 2.2 | 0.97 | 0.57  | 0.82 | 0.67 |
| RG 57                  | 1.8 | 0.83 | 0.56  | 0.83 | 0.69 |
| RG 58                  | 2.7 | 1.10 | 0.53  | 0.85 | 0.72 |
| RG 59                  | 7.3 | 1.23 | 0.55  | 0.83 | 0.70 |
| RG 61                  | 7.2 | 1.24 | 0.51  | 0.86 | 0.74 |
| RG 63                  | 4.2 | 1.06 | 0.53  | 0.85 | 0.72 |
| RG 72                  | 3.3 | 1.06 | 0.49  | 0.87 | 0.76 |
| Thiessen (traditional) | 0.9 | 0.77 | 0.46  | 0.89 | 0.79 |
| Thiessen (pat. pres.)  | 2.6 | 0.91 | 0.47  | 0.88 | 0.78 |
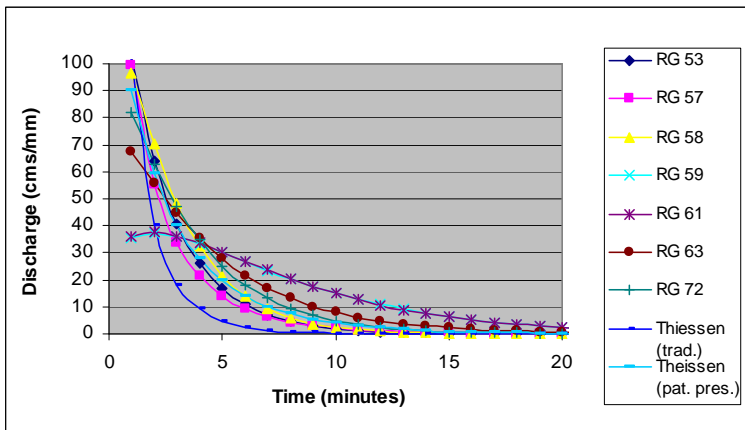


**Figure 8-10: Rain Gage, Thiessen (traditional method), and Thiessen (alternate method) Rainfall UHs for Storm Event on 7/20/07 Pixel 12**

## 8.3.4. UHs Derived from Radar Data

Several objectives were examined when UHs were derived using radar rainfall

data. The first objective was to compare the performance of various radar scan

elevation levels in developing UHs and predicting runoff. The second objective was

to evaluate whether using a calibrated Z-R equation to transform raw radar data from

decibels of reflectance (mm$^6$/m$^3$) to rainfall rate (mm/hr) resulted in more accurate

UHs and runoff predictions than using the standard Z-R equation used by the

National Weather Service (Ulbrich and Miller, 2001):

$$Z = 300R^{1.4} \qquad\qquad (8\text{-}6)$$

in which Z is reflectance ($mm^6/m^3$) and R is rainfall rate (mm/hr).  The final objective

was to compare the performance of radar data to the performance of another spatially

averaged rainfall record, the Thiessen polygon average rainfall, in creating UHs and

predicting runoff.

When previous analyses were conducted to determine whether there was any

benefit to calibrating location- and storm-specific Z-R transformation equations, firm

conclusions were not reached.  It was difficult to determine whether or not one of the

five radar scan elevations provided a more accurate picture of the rainfall over

Walnut Gulch than the other, while analyses comparing the performance of a

calibrated Z-R equation in predicting rainfall intensities to the performance of the

standard Z-R equation proved inconclusive.  To determine whether one radar scan

elevation was a more accurate representation than the other, radar scans 3 and 4,

which appeared to be the best based on previous studies, were used to derive UHs for

several pixels.  The goodness-of-fit statistics of the runoff predictions were compared,

as were the plots of the derived UHs.  To determine whether there was any benefit to

hydrologic modeling from calibrating location- and storm-specific Z-R

transformation equations several of the equations calibrated in a previous study

(presented in section 5.3.7.) were used in transforming raw radar data into rainfall rate

data prior to the derivation of pixel UHs.  The standard equation (Eq. 8-6) was also

used to transform the raw radar data to rainfall rate data for these pixels, and then the

UHs and runoff predictions were compared as discussed previously. These analyses thoroughly evaluated the ability of radar data to serve as PE input to the UH derivation process.

Unit hydrographs were computed for each rain gage, the Thiessen average rainfall, and the radar rainfall data using the procedure outlined previously. To compare UHs and runoff predictions made using radar data to those made using the Thiessen average rainfall the goodness-of-fit statistics computed for the Thiessen average rainfall based on all of the rain gages located within the boundaries of the radar pixel were compared to those computed for the radar data. The standard error ratio, the correlation coefficient, and the coefficient of variation were used to assess the accuracy of runoff predictions made using each unit hydrograph. The UHs that were derived for the Thiessen average and the radar rainfall data sets were plotted by inserting the optimum shape and scale parameters into the Weibull distribution equation. The UHs were then visually compared. Ideally the Thiessen average rainfall record and the radar rainfall record should represent similar rainfall, since both provide an average rainfall for the same area.

### 8.3.4.1. Comparison of Radar Scan Elevations

Radar measurements, or scans, are taken at several different beam orientations. These orientations are determined by the tilt angle of the radar beam. The radar data obtained for the Walnut Gulch region were available at five scan elevations. The scan with the lowest elevation angle is referred to as scan 1, while the scan with the highest elevation angle is referred to as scan 5. The scan elevation of the radar measurements is important because it dictates the height of the radar above the ground when it measures rainfall droplets in the air. Higher radar scan elevations

223

are less likely to be representative of the rainfall at the ground because factors such as wind drift or evaporation can change the rainfall profile between the point in the air at which the radar measured it and the point at which it reaches the ground. Lower radar scan elevations may also be inaccurate because they are more likely to be blocked by mountains and buildings located between the radar station and the watershed.

Figure 8-11 includes pixel 10 UHs derived for radar scans 3 and 4 using both the standard and calibrated Z-R transformation equations for the August 13, 2006, event. In comparing the UHs for scan 3 and scan 4 using the standard Z-R equation, very little difference is seen. The parameters given in Table 8-8 are very close, and a significant difference in goodness-of-fit statistics between the runoff predictions made using the two radar scans is not evident. Similar results are seen in comparing the unit hydrographs derived using the calibrated Z-R equations for both scans 3 and 4, though the change in standard error ratio between the two does indicate a slightly significant difference. The standard error ratio for scan 3 is 0.13, versus 0.16 for scan 4. An increase in standard error ratio of 3% (as seen here) is generally considered significant, indicating an improvement in accuracy when using scan 3 rather than scan 4.
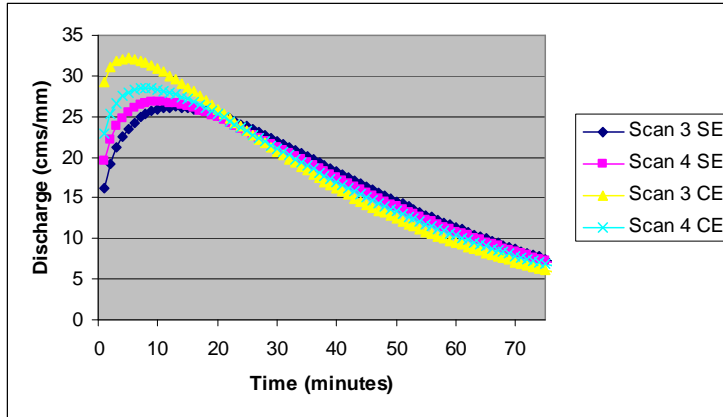
**Figure 8-11: Comparison of UHs Derived using the Standard (SE) and Calibrated (CE) Z-R Equations for Radar Scans 3 and 4 for Storm on 8/13/06 Pixel 10**

**Table 8-8: Comparison of Unit Hydrograph Parameters and Goodness-of-Fit Statistics for Radar Scans 3 and 4 Using the Standard and Calibrated Z-R Transformation Equations for the Storm on 8/13/06 Pixel 10**

|  | b | c | Se/Sy | R | $R^2$ |
|---|---|---|---|---|---|
| Scan 3 Standard Equation | 44.8 | 1.27 | 0.13 | 0.99 | 0.98 |
| Scan 3 Calibrated Equation | 39.4 | 1.11 | 0.11 | 0.99 | 0.99 |
| Scan 4 Standard Equation | 44.5 | 1.21 | 0.16 | 0.99 | 0.98 |
| Scan 4 Calibrated Equation | 42.6 | 1.17 | 0.15 | 0.99 | 0.98 |

A comparison of UHs derived using different radar scan elevations was also conducted using data from the July 20, 2007, storm for pixel 12. In this case slightly higher variation in the UHs was visible, as seen in Figure 8-12 and Table 8-9. While the shapes of the two UHs are similar, a slight difference in scales can be seen when comparing the peaks of the unit hydrographs. Table 8-9 shows that a difference in the *b* values between the two UHs is responsible for this and a comparison of goodness-of-fit statistics between the two illustrate that the difference in the characteristics of the unit hydrographs derived using different radar scans is possibly significant. Based on the comparisons of the goodness-of-fit statistics for runoff predictions made using the various UHs calculated using radar data for the storms on August 13, 2006, and July 20, 2007, the decision to use radar scan elevation 3 was made. While little difference between the two radar scan elevations in terms of the UH analysis was generally evident, scan elevation 3 usually provided more accurate goodness-of-fit

statistics, and in some of the analyses, the difference between the two was sufficiently

significant to justify this decision.

**Table 8-9: Unit Hydrograph Parameters and Goodness-of-Fit Statistics for Radar Rainfall Data for the 7/20/07 Storm Pixel 12**

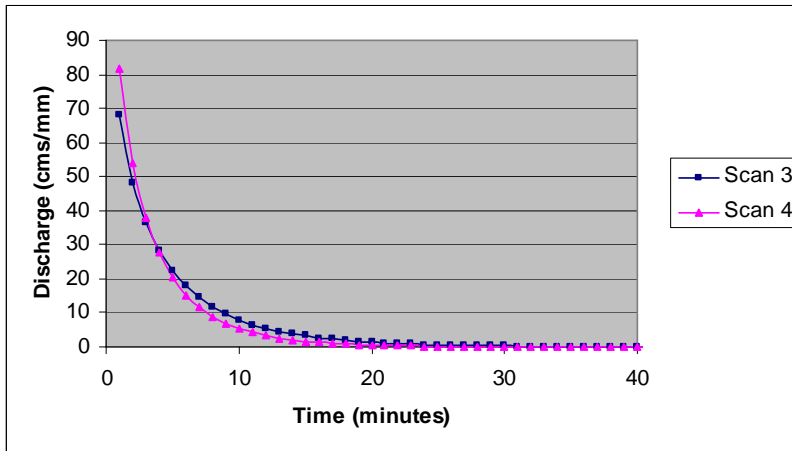|  | b | c | Se/Sy | R | $R^2$ |
|---|---|---|---|---|---|
| Scan 3 | 4.2 | 0.85 | 0.39 | 0.92 | 0.85 |
| Scan 4 | 3.0 | 0.85 | 0.45 | 0.89 | 0.80 |



**Figure 8-12: Comparison of Unit Hydrographs for Radar Scans 3 and 4 for the Storm on 7/20/07 Pixel 12**

### 8.3.4.2. Comparison of Calibrated and Standard Z-R Transformation Equations

The second analysis determined whether or not using a calibrated Z-R

transformation equation instead of the standard equation used by the National

Weather Service provided improved accuracy.  Figure 8-11 and Table 8-8 compare

the standard and calibrated Z-R equations for radar scans 3 and 4 for the August 13,

2006, storm for pixel 10.  Based on these results, there would appear to be some

difference between the unit hydrographs derived after using the standard and the

calibrated Z-R transformation equations to convert the radar data to rainfall intensity

data.  The shapes of the UHs derived for the standard and calibrated Z-R equations

are very similar; however, the hydrograph peaks are somewhat different.  In

comparing the goodness-of-fit statistics for the runoff predictions made using these

UHs, slightly better accuracy is seen in the UHs derived using a calibrated equation

226

than the standard equation. However, for scan 3, as seen in Table 8-8, the decrease in standard error ratio is only 2%, and there is no difference in the correlation coefficient, so the improvement seen is not statistically significant. Based on this conclusion, the decision to use the standard equation rather than a calibrated equation was made. The procedure to calibrate a Z-R equation for a pixel is a fairly complicated, time-intensive procedure, so if it does not provide a significant improvement in the unit hydrograph accuracy it does not seem to be worthwhile.

### *8.3.4.3. Comparison of Thiessen and Radar Rainfall UHs*

In most of these analyses, the UHs derived from individual rain gages within a pixel area showed considerable variation. Also, the Thiessen UH generally fell in the center of the rain gage generated UHs. Unit hydrographs derived from radar data were compared to UHs derived from Thiessen average rainfall to examine the usefulness of spatial data in hydrologic applications. The purpose of this was to compare methods of using spatially averaged rainfall data, rather than point rainfall data such as rain gage data, in the UH procedure. Figure 8-13 compares the UHs derived using Thiessen average rainfall to radar rainfall for the storm on August 13, 2006, for pixel 12, while Table 8-10 provides the corresponding UH parameters and goodness-of-fit statistics for those UHs. Reasonable agreement is observed between the Thiessen average and radar UHs, though differences in shape and scale are visible. For instance, the radar rainfall UH is slightly steeper than the Thiessen averaged rainfall UH. Based on the goodness-of-fit statistics, the radar UH appears to be slightly more accurate, when compared to the Thiessen UH.

As a second example, Figure 8-14 compares the UHs derived using Thiessen average and radar rainfall data for the August 17, 2006, storm event for pixel 1.

Table 8-10 also contains the parameters and goodness-of-fit statistics for these UHs. As seen earlier, the UHs derived for various rain gages within the pixel boundaries were very consistent for this storm event. The gage-to-gage consistency is evident in the Thiessen average and radar rainfall UHs. The Weibull parameters and the goodness-of-fit statistics of the runoff predictions made using these UHs are very similar for both the radar and the Thiessen average rainfall. They are also very similar to the values determined for the UHs derived using the rain gages in this pixel. The explanation for the shape and consistency of the UHs for this storm event discussed previously, the long amount of time between the centers of mass of the PE and the DRO, as well as the lack of variation in the centers of mass of the PE between the gages, are also responsible for the shape and similarity of the Thiessen and radar unit hydrographs. Both precipitation excess records were quite short, as were the rain gage PE records, so the PE CM did not vary significantly in time between the different PE records for the individual rain gages. Also, the time base of the DRO for this storm event was long, which resulted in a large difference in the time of occurrence of the PE CM and the DRO CM. This reflects considerable watershed smoothing of the rainfall hyetograph. These factors have resulted in Thiessen and radar UHs that are very similar to each other and very similar to the UHs derived from the rain gages in the pixel.
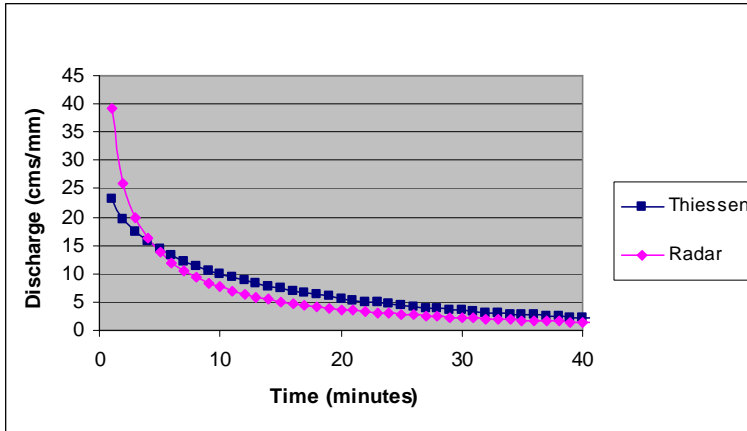
**Figure 8-13: Comparison of Thiessen and Radar Unit Hydrographs for the Storm on 8/13/06 Pixel 12**

**Table 8-10: Comparison of Thiessen Averaged and Radar Rainfall UH Parameters and Goodness-of-Fit Statistics for Storms on 8/13/06 Pixel 12 and 8/17/06 Pixel 1**

|                  | b     | c    | Se/Sy | R    | $R^2$ |
|------------------|-------|------|-------|------|-------|
| 8/13/06 Thiessen | 19.2  | 0.85 | 0.40  | 0.92 | 0.84  |
| 8/13/06 Radar    | 12.1  | 0.57 | 0.26  | 0.97 | 0.93  |
| 8/17/06 Thiessen | 112.5 | 3.20 | 0.33  | 0.94 | 0.89  |
| 8/17/06 Radar    | 116.3 | 3.30 | 0.33  | 0.94 | 0.89  |
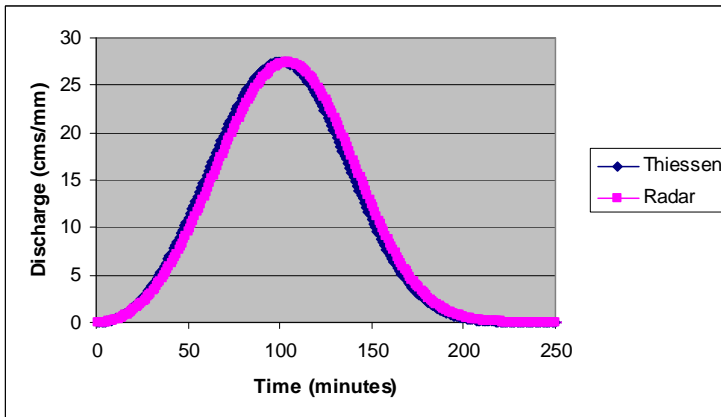


**Figure 8-14: Comparison of Thiessen Average and Radar Rainfall Unit Hydrographs for Storm on 8/17/06 Pixel 1**

## 8.3.5. Effect of Transmission Loss

### 8.3.5.1. Methods of Analysis

Transmission losses are hypothesized to be responsible for the exponential UHs that have resulted from these analyses. The cause of the exponential unit hydrographs was previously explained, from a modeling stand point, to be the length of time between the CM of the PE and the CM of the DRO. The differences in timing

229

of the PE CM and the DRO CM have been shown to influence the Weibull shape parameter. From the standpoint of physical processes, however, it would appear that transmission losses are responsible for the exponential unit hydrographs. As already mentioned, transmission losses result in much steeper hydrographs. The steeper rising limbs of hydrographs where transmission losses are experienced also result in earlier DRO centers of mass. Therefore, transmission losses serve to decrease the length of time between the occurrence of the PE center of mass and the DRO center of mass. An analysis was conducted to attempt to verify these hypotheses.

To verify the effect of TL on a UH, a flow record was altered in such a way as to simulate a higher degree of TL. To do this several values from the rising limb of the hydrograph were moved to the falling limb of the hydrograph. This steepened the rising limb of the hydrograph, but also conserved the flow volume, which was necessary to develop UHs that could be compared. Then UHs were derived using data from one rain gage and both the original and the altered flow records. To determine the effect of simulation of additional TL, the final Weibull parameters for both UHs were compared, and the UHs were plotted for comparison.

The difference between the time of occurrence of the PE CM and the DRO CM has been hypothesized to have some influence on the Weibull $c$ values. Transmission losses would be one factor that influences the time of occurrence of the center of mass of the DRO. Therefore, the difference in CM can be considered to be an effect of the physical processes occurring in the watershed. The relationship between the Weibull $c$ value and the differences in centers of mass needed to be confirmed to support this hypothesis. To do this the centers of mass of the PE and the

DRO were calculated for every PE dataset and DRO dataset used to calculate unit hydrographs. By examining trends in the difference in time between the centers of mass and the *c* values, it was possible to determine the relationship between the two.

### 8.3.5.2. *Effect of Transmission Loss on UHs*

The effects of TL on a UH are illustrated in Figure 8-15 and Table 8-11. Figure 8-15 provides the UHs derived from this analysis, while Table 8-11 provides the Weibull parameters and the goodness-of-fit statistics calculated for each of the unit hydrographs. Figure 8-15 illustrates the differences between the two, including the fact that the UH with greater transmission losses is steeper than the UH without additional transmission losses. In Table 8-11 the effect that the additional transmission losses had on the *c* value are particularly of interest, as the exponential UHs are caused by a Weibull *c* values being decreased to a value below 1.0. In this study, the additional transmission losses were found to decrease the Weibull *c* value from 0.77 to 0.67. This indicates that transmission losses are able to force a decrease in the *c* value, and therefore may be responsible for the *c* values below 1.0 which result in exponential unit hydrographs.
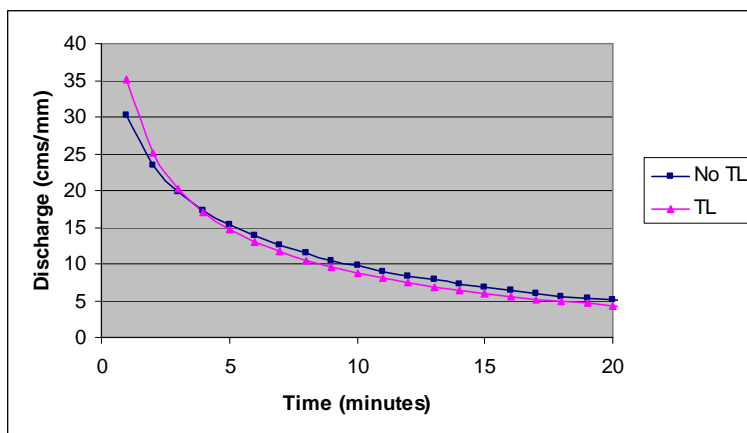


**Figure 8-15: Comparison of Unit Hydrographs With and Without Additional Transmission Losses for Storm on 8/13/06 Rain Gage 53**

**Table 8-11: Comparison of Parameters and Goodness-of-Fit Statistics for Unit Hydrographs With and Without Additional Transmission Losses for Storm on 8/13/06 Rain Gage 53**

|       | b    | c    | Se/Sy | R    | $R^2$ |
|-------|------|------|-------|------|------|
| No TL | 15.5 | 0.77 | 0.37  | 0.93 | 0.86 |
| TL    | 13.9 | 0.67 | 0.46  | 0.89 | 0.79 |

### *8.3.5.3. Effect of Center of Mass on Weibull Shape Parameter*

The first step to explain the exponential UHs was to examine the relationship between the Weibull $c$ values to the difference between the time of occurrence of the PE CM and the DRO CM. Table 8-12 provides the time of the occurrence of the PE CM and the DRO CM (in minutes), the difference between the two (in minutes), and the Weibull $c$ value calculated for that UH for the rain gages in pixel 1 for the storm event on July 31, 2007. With the exception of the UH derived for rain gage 2, there is a clear direct trend, as the difference between the two centers of mass increases, the Weibull $c$ value also increases. The precipitation excess measured at rain gage 2 had somewhat different characteristics as the PE measured at the other rain gages within pixel 1, which may explain why the unit hydrograph derived for rain gage 2 does not follow trend observed in the other unit hydrographs.

**Table 8-12: Comparison of Differences in Time of Occurrence of PE and DRO Centers of Mass and Weibull c for Unit Hydrographs Derived from Storm on 7/31/07 Pixel 1**

| Rain Gage | Time of PE CM | Time of DRO CM | Difference | Weibull c |
|-----------|---------------|----------------|------------|-----------|
| 92        | 12            | 21             | 9          | 0.36      |
| 4         | 10            | 21             | 11         | 0.41      |
| 8         | 9             | 21             | 12         | 0.43      |
| 2         | 11            | 21             | 10         | 0.45      |
| 1         | 8             | 21             | 13         | 0.50      |
| 5         | 7             | 21             | 14         | 0.68      |

## 8.3.6. Artifacts of the Modeling Technique

Some of the results alluded to or discussed in previous sections can be attributed to the modeling technique used in this analysis. For instance, in some cases differences in the UHs between rain gages, Thiessen average rainfall, and radar

rainfall data appeared to be related to the number of PE ordinates in each data set. A very good example of this was evident in comparing the rain gage UHs to the radar unit hydrographs for pixel 10 for the storm event on August 13, 2006. The rain gage UHs for this event, shown in Figure 8-16, were seen to have a higher peak value than the UHs derived using radar data (shown in Figure 8-17). Upon examining the PE data for the rain gages and radar rainfall, it was seen that the number of PE ordinates for the rain gages ranged from 41 to 63, with all but two of three of the rain gage PE records having more than 50 ordinates. The radar data only had 47 PE ordinates. The differences often seen in UH peaks between the rain gage data, Thiessen average rainfall data, and the radar data was therefore attributed, at least in part, to the number of PE ordinates in each data set. With fewer PE ordinates, the number of UH ordinates increases (see Equation 8-1), which forces the UH to be spread over a longer time period. This forces the $c$ value to be larger.
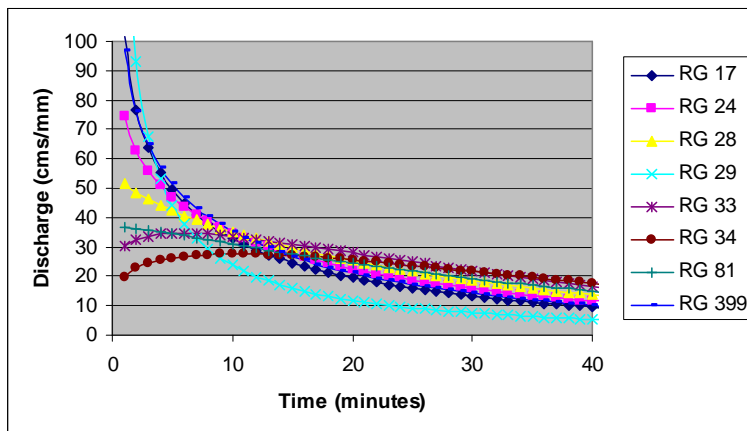


Figure 8-16: Comparison of Rain Gage Unit Hydrographs for Storm on 8/13/06 for Pixel 10
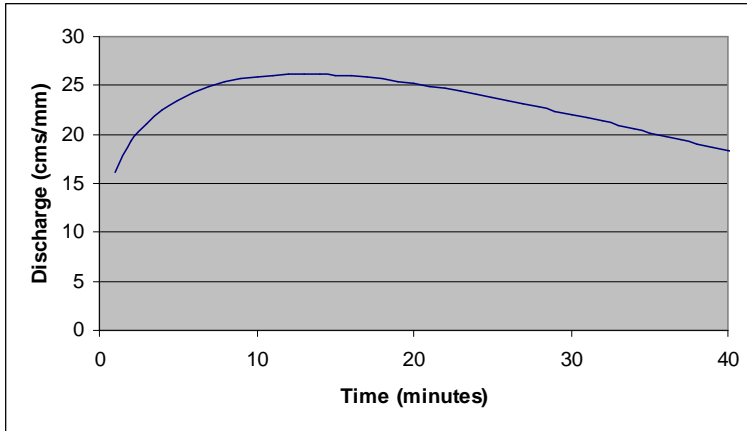
**Figure 8-17: Radar Rainfall Unit Hydrograph for Storm on 8/13/06 for Pixel 10**

The differences in centers of mass of the PE and the DRO, which appears to be strongly linked to the Weibull $c$ values determined for the UH, may also be an artifact of the modeling technique used to some extent. It is true that transmission losses result in steeper hydrographs, as mentioned earlier, which has some influence on the timing of the DRO center of mass. Storm movement may also play some role in the location of the PE CM, so physical explanations for this phenomenon are possible. However, the modeling assumptions made in separating losses from PE also likely influence this. In separating losses from PE, all rainfall that occurred prior to the start of runoff was assumed to be initial abstraction, which is a loss. This is a common assumption; however, this assumption is influencing the results of the analyses conducted. Assuming that all rainfall prior to the beginning of runoff is a loss influences the amount of PE that will be used to derive the unit hydrograph, and it therefore influences the time when the PE CM occurs. If a different assumption had been used to separate the initial abstraction from the PE the volume of PE and the distribution of it in time would have been different. This would affect the PE CM, the difference in centers of mass of the PE and the DRO, and it would affect the final $c$ value determined for the unit hydrograph.

234

An example of this can be seen in the storm event occurring on July 31, 2007. For rain gage 8, located in pixel 1, there are originally 68 rainfall ordinates, as shown in Figure 8-18. After initial abstraction and losses were separated, the hyetograph only included 22 PE ordinates, as shown in Figure 8-19. The PE CM occurred after only 9 minutes, while the DRO CM, seen in Figure 8-20, occurred after 21 minutes. The difference of only 12 minutes between the PE and DRO centers of mass resulted in a $c$ value of 0.43. As discussed above, though the assumption that all precipitation prior to the start of direct runoff is commonly used in UH analyses, using a different assumption to identify initial abstraction may have resulted in a longer PE record, which would have resulted in a higher $c$ value. Transmission losses also play a role here, in that they cause DRO to start later, because initial runoff is being lost to channel infiltration.
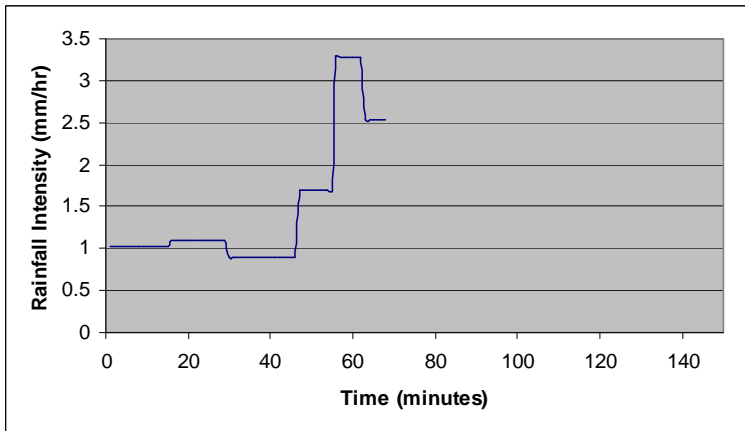


**Figure 8-18: Rainfall Collected at Rain Gage 8 in Pixel 1 During Storm on 7/31/07**
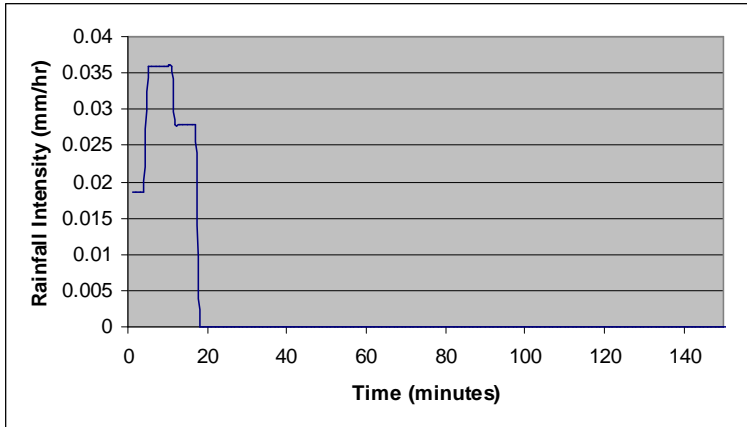
**Figure 8-19: PE Calculated for Rain Gage 8 in Pixel 1 for Storm on 7/31/07**
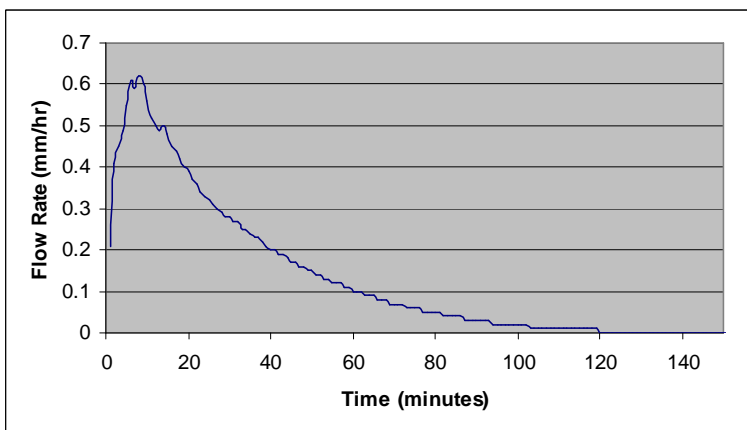


**Figure 8-20: DRO Calculated for Flow Gage 1 in Pixel 1 During Storm on 7/31/07**

## *8.4. IMPLICATIONS OF UH VARIATION ON DESIGN*

In examining the variation in unit hydrographs derived using different rain

gages, Thiessen average rainfall, and radar rainfall, potentially significant variation

was evident. It appears that the rain gage used in deriving a UH could significantly

impact the result. This suggests that it could be difficult to obtain a UH that was

representative of the watershed using just a single rain gage. Ultimately, the effect of

this variation on an engineering design is the criterion used to judge the significance

of the variation. Because the ultimate goal of the UH procedure is to predict runoff

from given storm events, in order to properly design storage facilities, conduits,

levees, etc., a UH that is not actually representative of the watershed could cause significant design error.

The purpose of this part of the study was to show the potential impact of the variations in UHs derived using different rain gages on predicted peak discharge rates. Peak discharge estimates are used in the design of pipe systems and levees. Knowledge of these quantities is vital for ensuring that designs for storing and controlling runoff are sufficient.

### 8.4.1. Methods of Analysis

The Weibull UH parameters calculated for each of the rain gages located within two pixels, the Thiessen average rainfall for each of those pixels, and the radar rainfall for each of those pixels, were convolved with a 24-hour Type II design storm to obtain a predicted runoff hydrograph. The NRCS (previously SCS) method was used in this process. Data from Walnut Gulch pixels 10 and 12 for the storm on August 13, 2006, were used. Data from pixel 12 for the storm event on July 20, 2007, were also used. A generic watershed of 64 acres and a curve number of 75 were used for this analysis. The analysis was repeated three times for each unit hydrograph, once for a 2-year design storm (3.2 inches of rainfall), once for a 10-year design storm (4.8 inches of rainfall), and once for a 100-year design storm (7.2 inches of rainfall).

To more closely evaluate the differences in peak flows a frequency analysis was conducted. Using logarithms of the discharges, frequency curves were plotted for each of the rain gages located within a given radar pixel for each return period, the Thiessen average rainfall, and the radar rainfall. This visualized the variation

possible in designs made based on varying UHs.  Ideally, the Thiessen average

rainfall and the radar rainfall should measure similar rainfall, and therefore should not

result in significant differences in UHs or in designs.  Thus, the frequency curves for

the Thiessen average and radar rainfall datasets should be fairly close together, and

they should fall near the middle of the spread seen between the rain gages.

## 8.4.2. Peak Discharge Analysis for August 13, 2006, Storm Event

For the storm event occurring on August 13, 2006, the UHs derived for pixels

10 and 12 were used in frequency analyses.  The figures developed from these

frequency analyses are presented in Figures 8-21 and 8-22.  Tables 8-13 and 8-14

present calculated peak discharges using the different UHs derived for each pixel.

### *8.4.2.1. Peak Discharge Frequency Analysis for Pixel 10*

In pixel 10, a spread of slightly more than 0.3 log cycles, resulting in

differences in discharges that ranged from 6 cfs for a 2-year storm to 120 cfs for a

100-year storm, resulted between the peak flows for the lowest and highest rain

gages.  These differences result in peak flows doubling between the lowest and

highest rain gages.  For instance, for the 2-year storm event for this group of UHs, the

lowest possible peak flow is 6.47 cfs and the highest possible peak flow is 12.41 cfs.

For the 100-year storm event the lowest peak flow is 108 cfs and the highest peak

flow is 227 cfs.  Table 8-13 presents the peak flows calculated using each UH, as well

as ratios of the rain gage or radar peak discharge values to the Thiessen peak

discharge.  Figure 8-21 presents the log frequency curve developed based on these

analyses.  A pipe system or levee designed using one of the lower rain gage UHs,

such as the UH for rain gage 34, may not be capable of handling the amount of runoff

produced if one of the higher rain gage UHs, such as rain gage 17, were the more accurate UH for the watershed, and may result in flooding of the area. This is an especially significant problem for larger return periods, such as the 100-year event, where the difference in peak discharges for rain gage 34 and rain gage 17 is nearly 120 cfs. Conversely, if a design was based on the larger discharge but in reality the lower discharge more accurately reflected rainfall over the watershed, then the larger design would be wasting money, with a certain opportunity cost lost, i.e., the money that could have been spent on other projects.

**Table 8-13: Peak Discharge Rates (cfs) Calculated for 2 ($Q_2$)-, 10 ($Q_{10}$)-, and 100 ($Q_{100}$)-year return periods (T) Using UHs Derived for Storm Event 8/13/06 Pixel 10, where $Q_p$ is the gage peak discharge, and $Q_{pT}$ is the Thiessen peak discharge**

|  | $Q_2$ | $Q_p/Q_{pT}$ | $Q_{10}$ | $Q_p/Q_{pT}$ | $Q_{100}$ | $Q_p/Q_{pT}$ |
|---|---|---|---|---|---|---|
| RG 17 | 12.41 | 1.677 | 60.26 | 1.755 | 226.53 | 1.781 |
| RG 24 | 9.32 | 1.259 | 45.41 | 1.323 | 172.76 | 1.358 |
| RG 28 | 9.93 | 1.342 | 46.93 | 1.367 | 176.14 | 1.385 |
| RG 29 | 7.57 | 1.023 | 35.31 | 1.029 | 131.17 | 1.031 |
| RG 33 | 7.13 | 0.964 | 32.78 | 0.955 | 120.77 | 0.950 |
| RG 34 | 6.47 | 0.874 | 29.48 | 0.859 | 108.14 | 0.850 |
| RG 81 | 7.00 | 0.946 | 32.44 | 0.945 | 120.14 | 0.945 |
| RG 399 | 11.52 | 1.557 | 56.23 | 1.638 | 212.14 | 1.668 |
| Thiessen | 7.40 | --- | 34.33 | --- | 127.18 | --- |
| Radar | 6.38 | 0.862 | 28.95 | 0.843 | 105.92 | 0.833 |



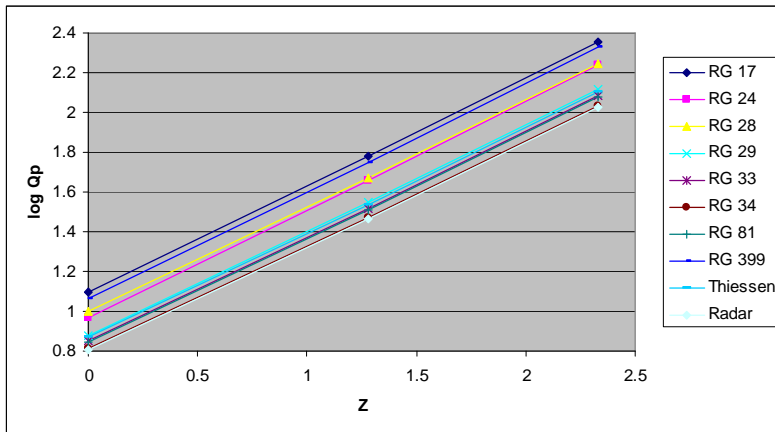**Figure 8-21: Log Frequency Curve of Peak Discharge for Storm on 8/13/06 Pixel 10 based on 2-year (Z=0), 10-year (Z=1.282) and 100-year (Z=2.327), where Z is the standard normal deviate.**

The peak flows calculated for the Thiessen average rainfall for this storm event fall roughly in the middle of the peak flows calculated using the individual rain gage hyetographs. This is the expected and desired outcome when using an average rainfall hyetograph. Based on these results combined with the previous results comparing UHs derived using the Thiessen average rainfall and individual rain gages, it would appear that the Thiessen rainfall hyetograph is representative of the rainfall being experienced on the watershed. If the Thiessen average rainfall is likely to be representative of the rainfall being experienced on the watershed, then it is likely to result in an adequate engineering design such as a storage or transportation facility. Therefore, when multiple rain gages are available and provide wide variation in measured rainfall hyetographs, the Thiessen average rainfall should be considered for use in design work. In the absence of enough rain gages to develop a Thiessen UH, the closeness of the radar and Thiessen discharges indicates that a radar rainfall derived UH would be better than use of a single rain gage.

Ideally, radar rainfall should be similar to the Thiessen average rainfall, since both provide an average rainfall measurement over the watershed. This should mean that the Thiessen rainfall and the radar rainfall should result in similar designs, which then means that radar rainfall data could be used rather than Thiessen rainfall data in engineering design. This would be ideal because many watersheds do not have enough rain gages within their boundaries to calculate an accurate Thiessen average rainfall. For the storm event on August 13, 2006, over pixel 10 the magnitudes of peak flow do not differ greatly (6.4 cfs for radar rainfall vs. 7.4 cfs for Thiessen rainfall for the 2-year storm and 106 cfs for radar rainfall vs. 127 cfs for Thiessen

rainfall for the 100-year storm).  The frequency analysis indicates that the radar

rainfall results in a peak discharge approximately equivalent to that calculated for the

lowest rain gage.  This could be an anomaly, though, and should not automatically be

considered as evidence that the radar rainfall hyetograph cannot be used in the unit

hydrograph and design calculation procedures.  Because the rain gage and Thiessen

rainfall frequency analyses were consistent, the possibility of an error in the radar

rainfall data should be considered as a possible explanation for the lack of agreement

between the Thiessen and radar rainfall designs.

### 8.4.2.2. Peak Discharge Frequency Analysis for Pixel 12

The UHs derived for pixel 12 during the August 13, 2006, storm event were

also used in a peak discharge analysis of predicted storm runoff.  A log frequency

analysis was conducted using the peak discharges calculated based on each of the rain

gage UHs, the Thiessen average rainfall UH, and the radar rainfall UH, the results of

which can be seen in Figure 8-22.  For this storm event the differences between the

lowest and highest rain gages in the frequency analysis was nearly half a log cycle,

resulting in differences of nearly 20 cfs for a 2-year storm and 345 cfs for a 100-year

storm.  The peak discharges and ratios of rain gage or radar peak discharges to the

Thiessen peak discharge calculated for this pixel are presented in Table 8-14.  For the

2-year storm event the peak discharges ranged from a low value of 8.1 cfs to a high

value of 27.8 cfs, while for the 100-year storm event the peak discharges ranged from

136 cfs to 481 cfs.  An increase in peak discharge of nearly 350 cfs could

significantly overwhelm a facility designed using one of the lower rain gage UHs.

Serious flooding could be a problem in a case such as this.  This indicates that the use

241

of a UH that is not representative of the watershed in design work could have

significant safety and risk consequences.

**Table 8-14: Peak Discharge Rates (cfs) Calculated for 2 ($Q_2$)-, 10 ($Q_{10}$)-, and 100 ($Q_{100}$)-year return periods (T) Using UHs Derived for Storm Event 8/13/06 Pixel 12, where $Q_p$ is the gage peak discharge and $Q_{pT}$ is the Thiessen peak discharge**

|          | $Q_2$  | $Q_p/Q_{pT}$ | $Q_{10}$ | $Q_p/Q_{pT}$ | $Q_{100}$ | $Q_p/Q_{pT}$ |
|----------|--------|--------------|----------|--------------|-----------|--------------|
| RG 53    | 14.68  | 1.258        | 71.36    | 1.251        | 268.11    | 1.240        |
| RG 57    | 9.50   | 0.814        | 44.47    | 0.780        | 165.53    | 0.766        |
| RG 58    | 8.22   | 0.704        | 37.68    | 0.661        | 138.31    | 0.640        |
| RG 59    | 8.12   | 0.696        | 37.17    | 0.652        | 136.16    | 0.630        |
| RG 61    | 27.84  | 2.386        | 131.18   | 2.300        | 481.48    | 2.228        |
| RG 63    | 19.87  | 1.703        | 94.89    | 1.664        | 351.85    | 1.628        |
| RG 72    | 18.81  | 1.612        | 90.15    | 1.580        | 335.11    | 1.550        |
| Thiessen | 11.67  | ---          | 57.04    | ---          | 216.14    | ---          |
| Radar    | 19.69  | 1.687        | 94.20    | 1.651        | 349.65    | 1.618        |



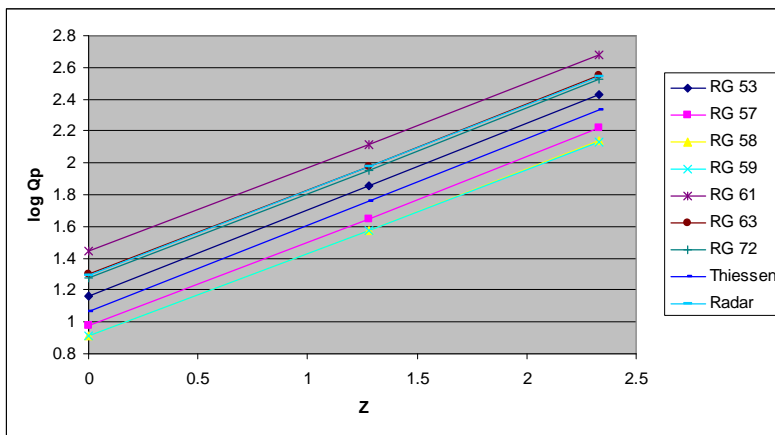**Figure 8-22: Log Frequency Curve for Storm on 8/13/06 Pixel 12 based on 2-year (Z=0), 10-year (Z=1.282), and 100-year (Z=2.327), where Z is the standard normal deviate.**

The Thiessen rainfall hyetograph calculated for this pixel again appears to be

fairly representative of the rainfall over the watershed and it results in an accurate

UH. The frequency analysis conducted illustrates that the peak discharges calculated

using the Thiessen average UH fall in the middle of the range of peak discharges

calculated using the individual rain gages. Therefore, using the Thiessen average

rainfall hyetograph rather than one of the individual rain gage hyetographs should

produce a more adequate runoff storage or transport design.

The Thiessen average rainfall peak discharge and the radar rainfall (presented in Table 8-14) peak discharge were again compared. Unfortunately, a lack of similarity between the two designs was again seen. Based on differences in the UH parameters for each, the radar peak discharge was seen to be 0.2 log cycles above the Thiessen average peak discharge. For the 2-year storm event the peak discharge calculated using the Thiessen rainfall was 11.7 cfs vs. 19.7 cfs calculated using the radar rainfall. For the 100-year storm the peak discharges were 216 cfs using the Thiessen rainfall vs. 350 cfs using the radar rainfall. These differences do seem to be significant. Because the Thiessen average rainfall UH and peak discharge calculation seem accurate based on the individual rain gage results, this casts some doubt on the radar rainfall data. Compared to the relative similarity seen between the Thiessen and radar rainfall designs seen in pixel 10, the differences seen in pixel 12 seem quite large. However, the possibility of an error in the radar data should still be considered as a possible explanation, due to the fact that Thiessen rainfall results seem appropriate.

### 8.4.3. Peak Discharge Analysis for July 20, 2007, Storm Event

To confirm the findings of the analysis of the storm event on August 13, 2006, a peak discharge analysis was also completed for the storm event on July 20, 2007, over pixel 12. The results of this analysis are presented in Table 8-15. The spread seen between the peak flows calculated using the individual rain gage UHs was nearly 0.4 log cycles, as seen in Figure 8-23, with a minimum peak flow of 5.5 cfs for the 2-year storm and a maximum peak flow of 17.5 cfs. For the 100-year storm the peak flows ranged from 395 cfs to 939 cfs. The peak discharges and ratios of rain

gage or radar peak discharges to Thiessen peak discharges calculated for the storm

event on July 20, 2007, for pixel 12 are presented in Table 8-15.

**Table 8-15: Peak Discharge Rates (cfs) Calculated for 2 ($Q_2$)-, 10 ($Q_{10}$)-, and 100 ($Q_{100}$)-year return periods (T) Using UHs Derived for Storm Event 7/20/07 Pixel 12, where $Q_p$ is the gage peak discharge and $Q_{pT}$ is the Thiessen peak discharge**

|          | $Q_2$ | $Q_p/Q_{pT}$ | $Q_{10}$ | $Q_p/Q_{pT}$ | $Q_{100}$ | $Q_p/Q_{pT}$ |
|----------|-------|--------------|----------|--------------|-----------|--------------|
| RG 53    | 54.76 | 1.148        | 255.15   | 1.140        | 927.53    | 1.136        |
| RG 57    | 55.63 | 1.166        | 258.58   | 1.156        | 938.63    | 1.150        |
| RG 58    | 50.32 | 1.054        | 235.95   | 1.055        | 860.95    | 1.054        |
| RG 59    | 22.45 | 0.470        | 106.95   | 0.478        | 395.26    | 0.484        |
| RG 61    | 22.76 | 0.477        | 108.38   | 0.484        | 400.41    | 0.490        |
| RG 63    | 35.08 | 0.735        | 167.44   | 0.748        | 617.98    | 0.757        |
| RG 72    | 42.59 | 0.892        | 201.34   | 0.900        | 738.47    | 0.904        |
| Thiessen | 47.72 | ---          | 223.74   | ---          | 816.53    | ---          |
| Radar    | 34.37 | 0.720        | 163.29   | 0.730        | 601.38    | 0.737        |



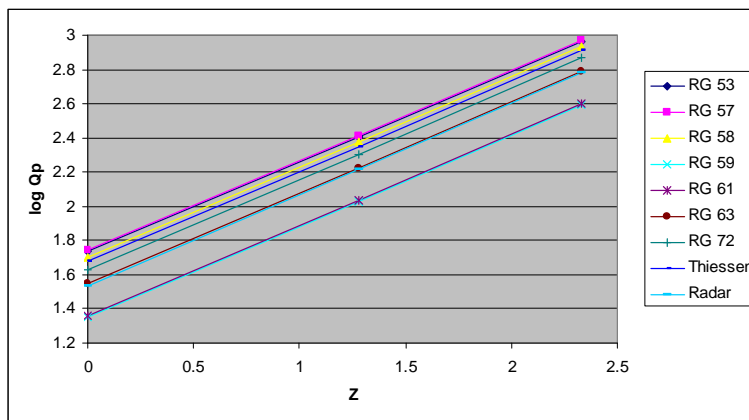**Figure 8-23: Frequency Curve Developed for Storm on 7/20/07 Pixel 12 based on 2-year (Z=0), 10-year (Z=1.282), and 100-year (Z=2.327), where Z is the standard normal deviate.**

Based on the results presented for the storm event on August 13, 2006, the

peak flows calculated using the Thiessen average UH were expected to fall within

this range, which was observed. The Thiessen peak discharges calculated for the 2-

year storm event was 47.7 cfs and for the 100-year storm the peak flow was 817 cfs.

These values obviously fall into the range of values calculated using each of the

individual rain gages. The Thiessen design calculations are overall comparable to the

individual rain gage calculations, indicating that the Thiessen average UH could be

successful in calculating a reasonable peak discharge for storm runoff in the watershed. The Thiessen hyetograph should be more representative of the rainfall being experienced over the watershed than any one of the individual rain gage hyetographs, so the facility being designed (e.g. pipe system, levee) should stand a better chance of being adequate to manage the storm runoff if designed using the Thiessen average UH than one of the individual rainfall UHs.

The peak discharges calculated using the Thiessen average hyetograph are also moderately close to the radar to the peak flows calculated using the radar rainfall (34.4 cfs for a 2-year storm event and 601 cfs for a 100-year storm event). Based on the reasonable similarity between the Thiessen peak discharges and the radar rainfall peak discharges, it would appear that the radar rainfall hyetograph may ultimately be able to provide a reasonably accurate UH that can be safely used in design calculations. This is further reinforced by the fact that the frequency analysis results indicate that the radar rainfall provides a better average than the Thiessen average. In this scenario, it is the radar rainfall UH that produces peak flows that fall in the middle of the rain gages, more so than it is the Thiessen average hyetograph, as seen in previous analyses. The conclusion to be drawn from this is that radar rainfall may provide a viable method of calculating and using unit hydrographs, which is encouraging for watersheds without rain gage networks able to provide a spatially representative rainfall hyetograph.

## 8.5. CONCLUSIONS

Several conclusions are evident from this examination of the variability in UHs derived using different rain gages, different storm events, and from different

areas of the watershed; additionally, examining the ability of spatially averaged data to yield reliable UH was investigated. It is generally believed that UHs reflect the response of a watershed, not the rainfall. The results of this research indicate that UHs do reflect rainfall, though they are intended to only represent watershed processes, and this is why they are averaged over different storm events. When deriving UHs using rainfall records from different rain gages and storm events, significant variation was found in both the shape and the scale of the unit hydrographs. This is not to say that significant variation was always found, as under certain circumstances, nearly no variation was seen between UH derived using measurements from different rain gages. The majority of this variation was seen in the rising limbs of the UHs, and some of the UHs did not even exhibit a rising limb. Similarly, significant variation in UH shape and scale was seen to be possible when the UHs were derived from rain gages located in different portions of the watershed. This provides an understanding that the location of the rain gage can influence the UH derived, which is important because it is very unusual for a watershed to have multiple rain gages. The engineer must use the data that are available, but he or she must also understand the potential inaccuracy of that data. Considerable uncertainty can be inherent to any UH, and this variation will be transferred to designs based on the UH. Unit hydrographs based on spatially averaged data could be used to limit this uncertainty.

Unit hydrographs derived from Thiessen average rainfall data were compared to both the rain gage UHs and to UHs derived using radar data. The Thiessen average UHs were not always a perfect fit to the rain gage UHs; however, the average rainfall

246

was seen to provide acceptably accurate UHs that were comparable to the rain gage UHs. In fact, under some circumstances the Thiessen average rainfall appeared to provide a more accurate UH, based on goodness-of-fit statistics, than the rain gages did.

In deriving UHs using radar data, two preliminary questions first needed to be answered. Little difference between UHs was usually seen when they were derived with different radar scans; however, the third scan elevation generally appeared to provide the most accurate goodness-of-fit statistics. This scan elevation is not too low that it is blocked by mountains and buildings on the ground, but it is also not so high that it is not representative of the rainfall on the ground. When comparing calibrated Z-R transformation equations to the standard equation, the calibrated equations were generally seen to perform better in UH derivation; however, the improvement was not sufficiently significant to justify the Z-R equation calibration procedure. After these questions had been answered the radar rainfall UHs were compared to the Thiessen average rainfall UHs. They were not usually seen to agree perfectly; however, they were usually fairly comparable in shape and scale. Both average rainfall methods were clearly able to provide a reasonable UH that performed comparably to the traditional rain gage unit hydrographs, and both seemed able to make reasonably accurate runoff predictions. Since Thiessen UHs are generally not available, the agreement indicates that the radar UHs accurately reflect the rainfall over a watershed.

Transmission losses were shown to be a concern in developing unit hydrographs for data from the Walnut Gulch Experimental Watershed, resulting in

decreased flow volumes and peak flows as the flood wave moved downstream. Transmission losses cut off much of the initial part of the hydrograph, which causes a significant difference in time of occurrence of the centers of mass of the PE and the DRO. This difference in CMs of the PE and DRO is evident in the steepening of the rising limb of the hydrograph. This change in the timing of the centers of mass in relation to each other was shown to influence the Weibull shape parameter. Therefore, it was concluded that transmission losses were likely responsible for the exponential UHs that occurred in some cases. This leads to the interesting conclusion that the presence of transmission losses causes the UH to reflect channel properties as much as they reflect watershed properties.

Several of the results observed can be attributed to the modeling technique used in these analyses. First, the number of PE ordinates may influence the peakedness and the steepness of the UHs. Using Equation 8-1, it can be determined that longer PE records result in fewer UH ordinates, thus forcing a steeper, more peaked UH. The length of time between the PE CM and the DRO CM may also be to some degree a result of the modeling assumptions made. The assumption made in specifying the initial abstraction controls the amount of PE available for derivation of the UH. Therefore, the assumption used in specifying the initial abstractions influences the time of occurrence of the PE CM. The time of occurrence of the PE CM influences the final parameter values; therefore, the modeling assumption used in this analysis has influenced the results of the analysis.

Three conclusions can be drawn from the analysis of the effect of the UH variation on design calculations. First, significant variation in runoff peak flow rate is

248

possible depending on the UH used in calculations.  Unit hydrographs are typically

derived using only one rain gage hyetograph.  If several rain gages are available for

use within a watershed, the rain gage used to derive the UH may make a difference in

ultimate designs.  The variation in UHs resulting from use of different rain gage

hyetographs is also evident in design calculations made using the different UHs.

Depending on the level of variation seen in the individual rain gage hyetographs,

these differences can be quite significant.

Second, the Thiessen average UH, which typically is based on a more

representative rainfall hyetograph than a UH derived from one rain gage, can also

produce designs more likely to be sufficient to handle the runoff from a storm event.

The variation in UHs from different rain gages leaves much room for errors in design,

which can be minimized by using the more representative Thiessen UH.  Third, radar

rainfall data, while still experiencing many problems, can be used to calculate

reasonable designs based on peak flow rates.  The radar rainfall UH showed promise

in producing designs that were similar to the Thiessen average design or otherwise

representative of the individual rain gage designs.  It has been shown in this study that

more representative rainfall data, such as Thiessen average rainfall, can improve upon

the accuracy of the derived UH and the storage and transport designs developed based

on that UH.  Unfortunately not every watershed has a sufficient number of rain gages

to calculate a Thiessen average and develop a representative rainfall hyetograph.

Radar rainfall data could fill that gap in many scenarios, if it is found to be accurate

and representative.  This research has taken the first step in finding that radar data can

be representative of the Thiessen average rainfall and the individual rain gage

rainfalls, in both derivation of the UH and design work using the rain gage.

# CHAPTER 9

# CONCLUSIONS AND RECOMMENDATIONS

## *9.1. CONCLUSIONS*

### 9.1.1. Transmission Loss

A model, the Spatio-Temporal Transmission Loss (STTL) model, was developed herein to estimate transmission losses along a channel. This model estimated transmission losses while routing the floodwave through the channel. The transmission losses themselves were modeled based on Hortonian infiltration. The STTL model is an improvement over existing TL models because it allows for estimating transmission losses (TL) based on the hydrograph, rather than the total flow volume; therefore, it is more sensitive to changes in depth and storage along the channel than other models used for this purpose. Both storm-to-storm and site-to-site variation were examined, in hopes of determining a set of average parameters that could be used to predict transmission losses over the watershed. Due to high variability in conditions over the watershed, average parameters were not found to be able to accurately predict transmission losses. However, when appropriate parameter values were determined for each storm event and for each stream reach, the model was seen to perform well, with acceptable bias and goodness-of-fit statistics in nearly all of the test cases.

### 9.1.2. Analyses That Involve Radar Rainfall

#### *9.1.2.1. Analysis of Spatial Data Problems Using Synthetic Data*

In this investigation, two rainfall averaging methods, the Thiessen polygon and the arithmetic averaging method, were compared. The ability of each to estimate rainfall over a watershed without resulting in excessive smoothing was evaluated. The influence of the following four factors on this loss of variation in rainfall estimates was also studied: storm variability, amount of the watershed represented by each of two rain gages, varying amounts of rainfall, and varying the probability distribution functions (pdfs) used to add random variation to the rainfall estimates. Overall, average rainfall estimates made using the Thiessen polygon method were found to result in lower loss of variation than were arithmetic averages. This means that the Thiessen polygon estimate is a better representation of the rainfall over the watershed than is the arithmetic average. The level of storm variability and the amount of the watershed being represented by each rain gage were found to have the biggest influence on the loss of rainfall variation in rainfall average estimates, while the amount of rainfall and the pdf chosen did not have as significant effects. This conclusion led to using the Thiessen method in averaging unit hydrographs from individual rain gages to compare with unit hydrographs based on radar data in a later study.

#### *9.1.2.2. Z-R Transformation Equations*

When using radar data, an equation, known as a Z-R transformation equation, is necessary to convert the radar data (in units of reflectance $mm^6/m^3$) to rainfall rate (in mm/hr). Several studies were conducted to determine the effect that using a calibrated Z-R equation versus a standard Z-R equation had in hydrologic

applications. First, two studies were conducted to determine the effect of using radar

data with different Z-R equations rather than rain gage data on the calculation of

storm semivariograms. The Z-R equation parameters affected the semivariogram sill

more than the radius of influence; however, it was determined that in order to

calculate an accurate storm semivariogram using radar data, the Z-R equation should

either be calibrated or at least carefully chosen. Finally, research into the effect of

calibrating Z-R equations on rainfall predictions was conducted. Corresponding radar

and rain gage data were used in this experiment, where log-transformed linear

regression was used to fit a power model Z-R transformation equation to the data.

The calibrated and standard Z-R equations were used to predict rainfall rates,

which were compared to the observed rainfall rates obtained from rain gage data. In

some cases, significant improvements in rainfall predictions were achieved when

using the calibrated equation, but in other cases a significant difference was not

evident between predictions made with the two equations. From this research it is

difficult to recommend the calibration process because it was a time-intensive process

and did not always result in a significant improvement in prediction accuracy.

### 9.1.3. Analysis of Factors Affecting the Semivariogram

Several studies were used to evaluate the effect of several factors on the

calculated storm semivariogram. The factors of interest were the storm shape (i.e.,

circular vs. elliptical), the storm size, the storm velocity, and the storm type (i.e.,

peaked vs. uniform). Of these factors, the storm shape was found to have the least

influence on the semivariogram. While a significant difference in computed

semivariograms was not evident based on varying the storm shape, it was determined

that storms ought to be analyzed as anisotropic events. The size of the storm in comparison to the size of the watershed and the type of storm were both found to have significant effects on the semivariogram. The results of the storm velocity study were not what was expected, but in retrospect they are rational. The results indicated that the storm velocity did not influence the semivariogram as much as the location of the storm in comparison to the location of the rain gages. This indicates that storm movement across the watershed is a more important factor than storm velocity on the calculated semivariogram. If the path of the storm across the watershed puts the intense center of the storm in close contact with the rain gages the semivariogram will be different than if the path across the watershed results in only the low intensity edge of the storm contacting the rain gages. The storm velocity may influence the total depth of rainfall at the rain gages, as a storm moving slowly may result in a higher depth of rainfall at each gage as it moves over the watershed than a storm having the same intensity but a higher velocity, but the effect on the gage-to-gage variability is minimal.

### 9.1.4. Rain Gage Density

Several studies were conducted to evaluate the effect of rain gage density on estimates of areal averaged rainfall. The first of these studies considered the effect of rain gage density on computed storm semivariograms, while the second study compared the potential of one rain gage versus two rain gages to give reasonable watershed rainfall averages.

### 9.1.4.1. Semivariogram Analyses

Two studies were conducted to evaluate the effect of the density of the rain gage network on the calculated storm semivariogram. These studies calculated semivariograms as the density of the rain gage network was decreased. The results of this study indicated that the density of rain gages in a watershed was not a significant factor influencing the calculated semivariogram. Specific trends were not identified in the semivariograms as the rain gage density was decreased. These results were not expected, because it was believed that a higher density of rain gages should provide more accurate rainfall data, and thus should be able to provide a more accurate semivariogram. The density of the rain gage data did not have a significant effect on the variance of the catches.

### 9.1.4.2. Effect of Averaging Methods on Rainfall Estimates

This study evaluated both the effect of rain gage density and the type of rainfall averaging method used when multiple rain gages were present. When two rain gages were present, both the Thiessen polygon and the arithmetic averaging methods were used to compute rainfall averages for the watershed. These estimates were compared to rainfall estimates made when only one rain gage was present in the watershed. Based on the results of this study, it was determined that one rain gage would not likely provide an accurate estimate of watershed rainfall for any given time period; however, due to the law of averages one rain gage could give a reasonable rainfall estimate for the entire storm volume. Two rain gages gave more reasonable watershed rainfall estimates for any given time period. It is important to note; however, that this research assumed that rain gages were completely accurate, which is not true. Rainfall estimates made using rain gage data in a real watershed would

also be influenced by any rain gage error (e.g. wind effects, poor gage placement, and improper calibration of a recording rain gage), which was not accounted for in this study.

The location of the two rain gages in relation to each other proved to be an important factor in determining how accurate the rainfall estimates would be. Two rain gages located in the immediate vicinity of each other were not able to capture spatial variability in the rainfall as well as two rain gages located in different areas of the watershed. The implication of these results is that spatial data, such as rainfall estimates made from multiple rain gages or radar data, could be very useful in hydrologic analyses requiring rainfall data as input. These conclusions are further supported by the successful application of radar data in the unit hydrograph procedure.

### 9.1.5. Unit Hydrograph Analyses: Point vs. Spatial Rainfall Input Data

The analyses of unit hydrographs (UHs) resulted in several interesting conclusions. First, unit hydrographs derived from different rain gages, even rain gages located physically close to each other, can have very different characteristics. When a storm is characterized by considerable spatial variation in depth and timing, the individual rain gage hyetographs will differ considerably, which leads to UHs that have significantly different shapes. Similarly, unit hydrographs derived from rain gages located within different portions of the watershed can also have significantly different characteristics. Not all of the unit hydrographs will be equally accurate, with the accuracy depending on the apparent temporal randomness of the hyetograph. Because unit hydrographs are used in design work this is an important point to

understand.  The inaccuracy of a UH will likely result in inaccuracy in a final design.  The analyses and results presented herein show that the design accuracy can be substantial.  The true unit hydrograph for a storm in not known, so this study was comparing computed UH values to other computed UH values based on different data sets.

Unit hydrographs derived from spatially averaged rainfall data such as Thiessen polygons and radar pixels were found to be, generally speaking, at least as accurate to potentially more accurate than those UHs derived from individual rain gage data.  This indicates that spatial data can be used in deriving unit hydrographs, and could even be an improvement over the one-gage method of derivation.

Many of the unit hydrographs derived in this study had an exponential shape.  While this is not typical of a unit hydrograph, a potential explanation that involved the physical processes of transmission losses was offered.  Transmission losses cause a decrease in flow volume, most of which comes at the beginning of the floodwave when the dry channel beds of the ephemeral streams characteristic of arid and semi-arid regions have some infiltration demand.  Then when the intense portion of the storm occurs, the channel can not infiltrate the large volume of water, so the runoff hydrograph is characterized by a very steep rising limb of a hydrograph.  Fitting this steep rising limb of the hydrograph appears to be responsible for the exponential unit hydrographs, as greater accuracy results from the exponential UH than from a UH with the traditional shape.

### 9.1.6. Effect of Unit Hydrograph Variation on Design

The implication of unit hydrograph variation on design calculations was also investigated. Unit hydrographs derived using different rainfall inputs were used to calculate storm runoff peak discharge rates. Significant variations in the peak discharge rates were seen in this analysis, as illustrated by a frequency analysis. This confirms that the variation seen in unit hydrographs derived from different rain gages will affect any design calculations based on them. Peak discharge rates calculated based on the Thiessen average unit hydrograph and the radar rainfall unit hydrograph were typically seen to agree fairly well, especially compared to variation in unit hydrographs derived from individual rain gages. This reinforces the conclusion reached earlier, that spatially averaged rainfall data should be used in unit hydrograph analysis and design. Because these unit hydrographs were based on a more representative rainfall hyetograph, designs based on these unit hydrographs should be better able to represent runoff over the watershed from a given storm event.

## 9.2. RECOMMENDATIONS

### 9.2.1. Transmission Loss

There is still much work to be done in the area of transmission losses. The STTL model had the ability to model lateral inflow to the channel; however, a method of estimating the appropriate amount of lateral inflow for given conditions is currently needed. A method of estimating lateral inflow would significantly improve the usefulness and accuracy of model results. Similarly, methods to estimate channel soil properties such as antecedent moisture condition and porosity would be useful.

These properties are vital to determining the ability of water to infiltrate into the channel bed, so an estimation method for both would improve prediction accuracy.

### 9.2.2. Analyses That Involve Radar Rainfall

The various studies conducted to evaluate radar rainfall data leave room for future research. The evaluation of rainfall averaging methods, which compared the loss of true rainfall variation when using Thiessen polygon and arithmetic averages to estimate watershed rainfall, was conducted entirely with synthetic data. These studies should also be conducted using observed rainfall data to ensure that the conclusions reached are applicable to observed data. The two studies conducted to determine the effect of using radar data with different Z-R transformation equations on the calculation of storm semivariograms were also done using synthetic data. It would be interesting to conduct similar studies using observed data and verify that the trends observed held true in observed data as well. It could also be interesting to use studies like these to identify acceptable Z-R equations for various storm characteristics.

Firm conclusions as to whether calibration of Z-R transformation equations was necessary for hydrologic applications were not reached. To reach a better understanding of this problem more research should be done. Data should be obtained for more storms, preferably with different rainfall characteristics, if possible. Equations calibrated based on these datasets should be compared to the standard equation, as was done in this study. More research into this topic could lead to more decisive results. Similar research could also be conducted for other watersheds. The Walnut Gulch Experimental Watershed can not be considered representative of the country as a whole because it is located in an arid region and because it is surrounded

by mountainous terrain, which may have interfered with the radar beam.  Data from other parts of the country may also lead to more decisive results that could be used to make a final determination on the importance of calibrated Z-R equations in hydrologic applications.

### 9.2.3. Analysis of Factors Affecting the Semivariogram

The results of the semivariogram analyses leave several questions to be answered by future research.  First, the studies that led to inconclusive or unexpected results, such as the storm velocity evaluation, could be re-examined.  Further results may add weight to the evidence supporting these conclusions, or find some factor that explains the surprising results.  Also, based on the results of the storm velocity evaluation, perhaps the effect of storm movement needs to be specifically studied.  Finally, these analyses were conducted using synthetic data.  It would be interesting to repeat these exercises with observed data, to confirm the results observed.

### 9.2.4. Rain Gage Density

In two studies conducted to determine the effect of rain gage density on storm semivariograms, the results indicated that this was not an important factor influencing semivariogram accuracy.  Because this finding was somewhat surprising, further research into this topic is necessary.  Further studies using synthetic data should be conducted to attempt to identify trends in the data, though there appeared to be no trends based on the results of this research.  Then, the studies could be conducted using observed rainfall data rather than synthetic, in order to determine that the effects remain the same for observed and synthetic data.

The study that evaluated the averaging methods used with multiple rain gages found that increasing the rain gage density resulted in rainfall estimates for the watershed that were more representative of the actual rainfall experienced. This study was conducted with synthetic data though, so future research could verify these findings using observed data. The next step may then be to calculate rainfall estimates with truly spatial data, such as radar data, to compare to the rainfall estimates made using rain gages.

### 9.2.5. Unit Hydrograph Analyses: Point vs. Spatial Rainfall Input Data

An additional analysis of unit hydrographs derived from spatial data is needed. Further work to explain the differences between the Thiessen rainfall and radar rainfall unit hydrographs and the rain gage unit hydrographs is necessary. Also, much more investigation into the exponential unit hydrographs is needed. This does not appear to have been seen before, so verification of the proposed explanation will be important. Further studies into the implications on designs may also be useful. In this research peak discharge calculations were compared among the different unit hydrographs; however, there are many other design calculations that could be evaluated. Further examples of the design implications may further quantify the degree to which variation in unit hydrograph will effect any design calculations for which they are used.

Another interesting step for future research could be developing watershed unit hydrographs using radar data. The research conducted here only used one radar pixel at a time to develop unit hydrographs, which does incorporate more spatial information than a rain gage unit hydrograph, but further steps could be taken to

provide truly spatial information to the unit hydrograph procedure.  If the unit

hydrograph is meant to predict the watershed response to a given storm event, it

seems that calibrating the unit hydrograph with precipitation data from the entire

watershed could improve those predictions greatly.

# APPENDIX A: SPATIO-TEMPORAL TRANSMISSION LOSS MODEL OUTPUT

The following figures compared the observed downstream hydrograph to the predicted downstream hydrograph, as calculated by the STTL model, for three storm events and gage pairs.  Very good agreement is seen between the observed hydrograph and the model results for the August 17, 2007, event.  For the August 6, 2007, event moderate agreement is seen between the observed hydrograph and the model results.  Finally, for the August 4, 2007, event poor agreement is seen between the observed hydrograph and the model results.
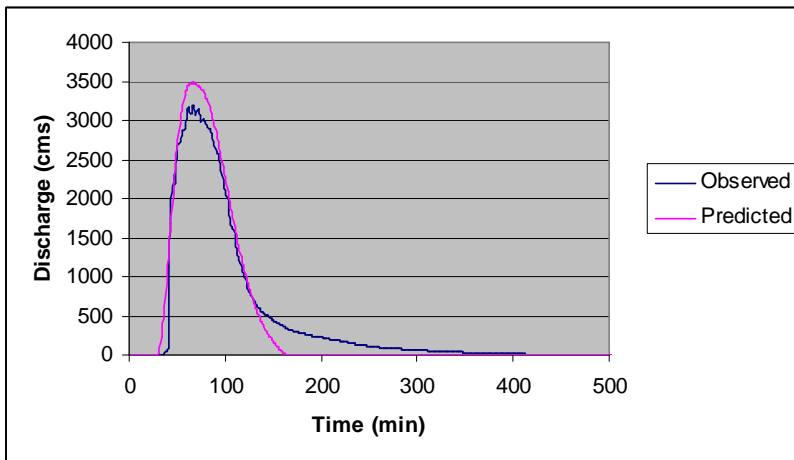


**Figure A-1: Observed Downstream Hydrograph vs. Predicted Downstream Hydrograph for 8/17/07 Storm Event Between Upstream Flow Gages 6 and 3 and Downstream Flow Gage 2**
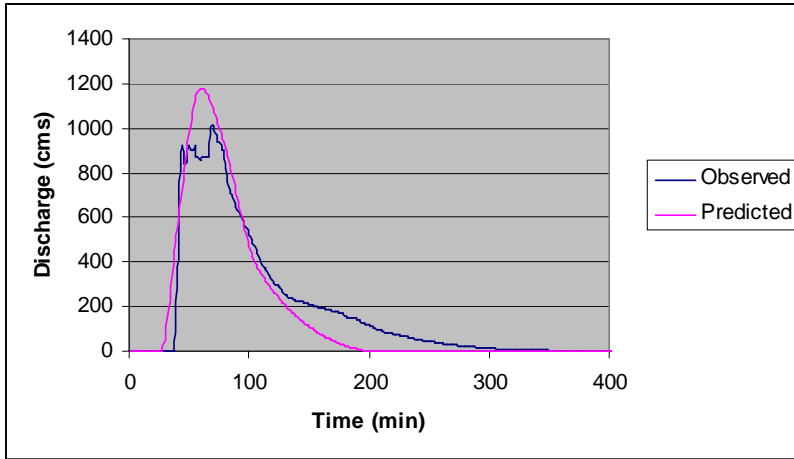
**Figure A-2: Observed Downstream Hydrograph vs. Predicted Downstream Hydrograph for 8/06/07 Storm Event Between Upstream Flow Gage 6 and Downstream Flow Gage 2**
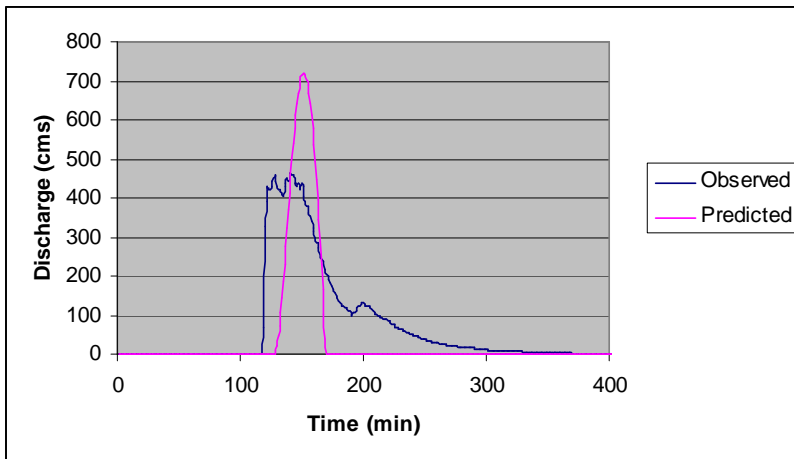


**Figure A-3: Observed Downstream Flow Hydrograph vs. Predicted Downstream Hydrograph for 8/04/07 Storm Event Between Upstream Flow Gages 6 and 3 and Downstream Flow Gage 2**

# APPENDIX B: UNIT HYDROGRAPH PREDICTED

# HYROGRAPHS VS. OBSERVED HYDROGRAPHS

The optimum unit hydrographs derived using non-linear least squares analysis
of the Weibull distribution parameters were used to predict flow hydrographs based
on rain gage rainfall measurements, then goodness-of-fit statistics were calculated for
the predicted runoff hydrographs.  The observed and predicted hydrographs are
compared in the following six figures, where rain gages which resulted in the best and
worst goodness-of-fit statistics for the storm event were chosen for illustration.
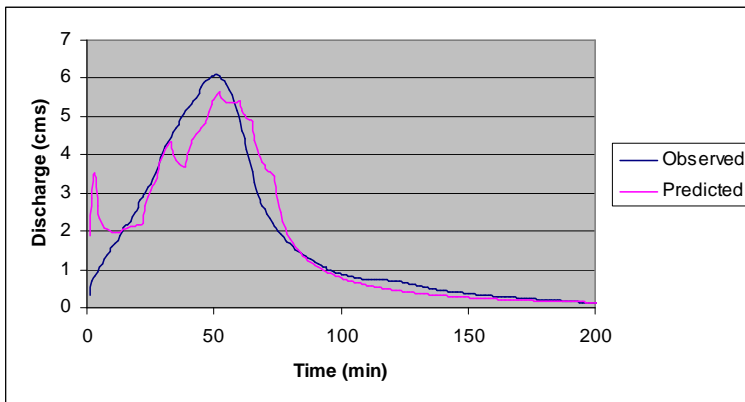


**Figure B-1: Observed Flow Hydrograph vs. Predicted Hydrograph for 8/13/06 Storm Event Rain Gage 61
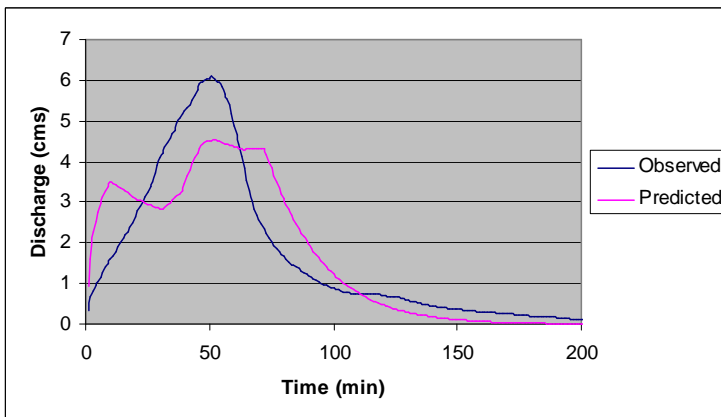(Best Goodness-of-Fit Statistics for the Event)**



**Figure B-2: Observed Flow Hydrograph vs. Predicted Hydrograph for 8/13/06 Storm Event Rain Gage 57
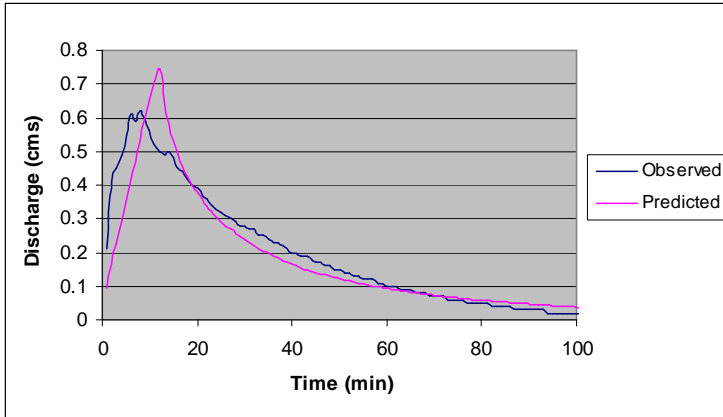(Worst Goodness-of-Fist Statistics for the Event)**

**Figure B-3: Observed Flow Hydrograph vs. Predicted Hydrograph for 7/31/07 Storm Event Rain Gage 5 (Best Goodness-of-Fit Statistics for the Event)**
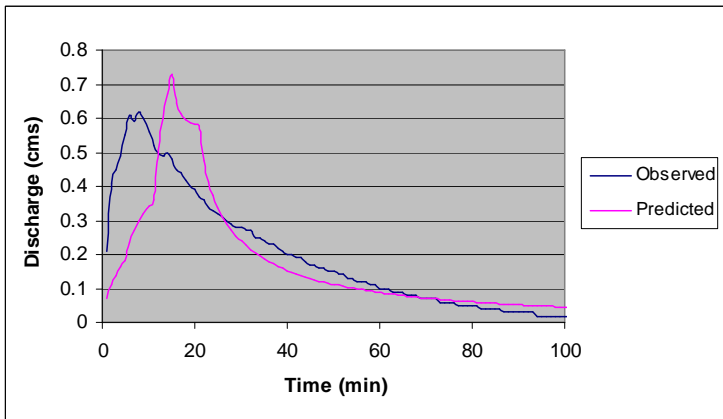


**Figure B-4: Observed Flow Hydrograph vs. Predicted Hydrograph for 7/31/07 Storm Event Rain Gage 92 (Worst Goodness-of-Fist Statistics for the Event)**
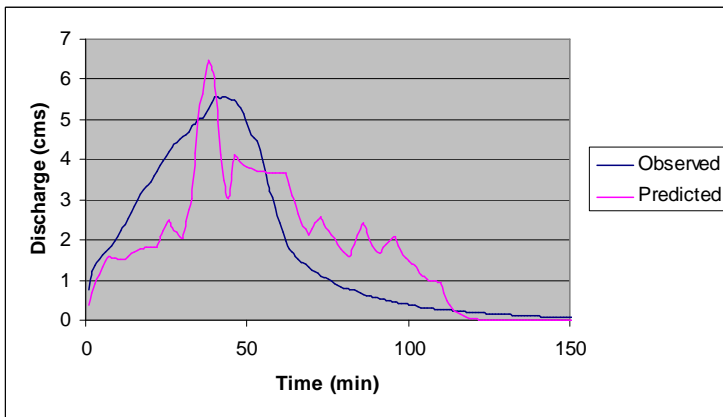


**Figure B-5: Observed Flow Hydrograph vs. Predicted Hydrograph for7/20/07 Storm Event Rain Gage 72 (Best Goodness-of-Fit Statistics for the Event)**
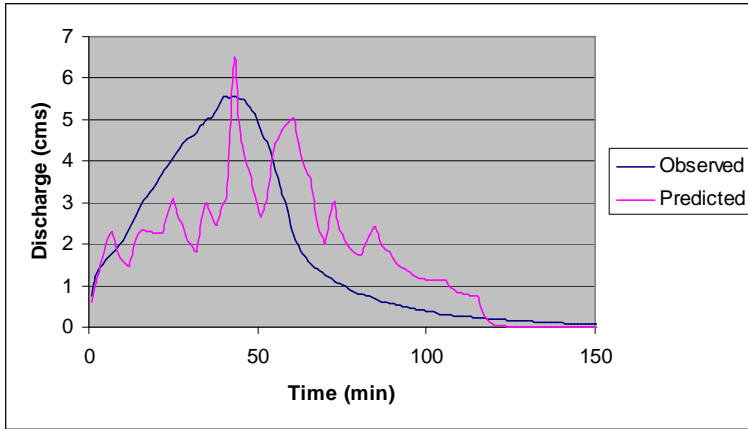
**Figure B-6: Observed Flow Hydrograph vs. Predicted Hydrograph for 7/20/07 Storm Event Rain Gage 53 (Worst Goodness-of-Fist Statistics for the Event)**

# REFERENCES

Anon. (2007). "Southwest Watershed Research Center and Walnut Gulch
    Experimental Watershed." USDA ARS SWRC. Walnut Gulch, AZ.

Aron, G., Collins, J.G., and Kibler, D.F. (1979). "Problems in Weighting of
    Hyetographs." *Water Resources Bulletin*, 15(6): 1556-1562.

Arunaud, P., Vouvier, C., Cisneros, L., and Dominguez, R. (2002). "Influence of
    rainfall spatial variability on flood prediction." *Journal of Hydrology,* 260:
    216-230.

Bedient,P.B., Huber, W.C., and Vieux, B.E. (2008). *Hydrology and Floodplain
    Analysis 4th ed*, Prentice Hall Publishing Co, New Jersey.

Ben-Hur, M., and Lado, M. (2008). "Effect of soil wetting conditions on seal
    formation, runoff, and soil loss in arid and semiarid soils – a review."
    *Australian Journal of Soil Research,* 46(3): 191-202.

Borga, M., Tonelli, F., Moore, R.J., and Andrieu, H. (2002). "Long-term assessment
    of bias adjustment in radar rainfall estimations." *Water Resources Research*,
    38(11): 8-1-8-10.

Bunya, P.K., Berndtsson, R., Ojha, C.S.P., and Mishra, S.K. (2007). "Suitability of
    Gamma, Chi-square, Weibull, and Beta distributions as synthetic unit
    hydrographs." *Journal of Hydrology*, 334(1-2): 28-38.

Carmi, G., and Berliner, P. (2008). "The effect of soil crust on the generation of
    runoff on small plots in an arid environment." *Catena,* 74: 37-42.

Cheng, S.J., Hseih, H.H., and Wang, Y.M. (2007). "Geostatistical interpolation of space-time rainfall on Tamshui River basin, Taiwan." *Hydrological Processes*, 21: 3136-3145.

Chumchean, S., Sharma, A., and Seed, A. (2006a). "An Integrated Approach to Error Correction for Real-Time Radar-Rainfall Estimation." *Journal of Atmospheric and Oceanic Technology*, 23: 67-79.

Chumchean, S., Seed, A., and Sharma, A. (2006b). "Correcting of real-time radar rainfall bias using a Kalman filtering approach." *Journal of Hydrology*, 317, 123-137.

Cleveland, T.G., Thompson, D.B., Fang, X., and He, X. (2008). "Synthesis of Unit Hydrographs from a Digital Elevation Model." *Journal of Irrigation and Drainage Engineering*, 134(2): 212-(?).

Collier, C.G. (1996). Applications of Weather Radar Systems: A Guide to Uses of Radar Data in Meteorology and Hydrology, 2nd ed. Praxis Publishing, Chinchester, England.

Cornish, J.H. (1961). "Flow Losses in Dry Sandy Channels." *Journal of Geophysical Research,* 66(6): 1845-1853.

Dooge, J.C.I. (1973). Linear Theory of Hydrologic Systems. Tech. Bull. No. 1468, USDA-ARS, USGPO, Washington, D.C.

Foote, G.B., and Du Toit, P.S. (1969). "Terminal Velocity of Raindrops Aloft." *Journal of Applied Meteorology,* 8: 249-253.

Gerstner, E. M., and Heinemann, G. (2008). "Real-time aerial precipitation determination from radar by means of statistical objective analysis." *Journal of Hydrology*, 352: 296-308.

Goodrich, D.C., Keefer, T.O., Unkrich, C.L., Nichols, M.H., Osborn, H.B., Stone, J. J., Smith, J.R. (2008). "Long-term precipitation database, Walnut Gulch Experimental Watershed, Arizona, United States." *Water Resources Research* 44 (5): 1-5.

Habib, E., Malakpet, C.G., Tokay, A., and Kucera, P.A. (2008). "Sensitivity of Streamflow Simulations to Temporal Variability and Estimation of Z-R Relationships." *Journal of Hydrologic Engineering,* 13(12): 1177-1186.

Haan, C.T. (1977). *Statistical Methods in Hydrology*. The Iowa State University Press, Ames.

Hastings, N.A., andPeacock, J.B. (1975). *Statistical Distributions*. John Wiley & Sons, Inc. NY.

Haws, N.W., Liu, B., Boast, C.W., Rao, P.S.C., Kladivko, E.J., and Franzmeier, D.P. (2004). "Spatial Variability and Measurement Scale of Infiltration Rate on an Agricultural Landscape." *Soil Science of America Journal,* 68(6): 1818-1826.

Hoblit, B.C., and Curtis, D.C. (2002). "Integration of Radar Rainfall into Hydrologic Models." Presented at 9th International Conference on Urban Drainage Global Solutions for Urban Drainage, Portland, Oregon, September 8-13, 2002.

Hoblit, B.C., Castello, C., Liu, L., and Curtis, D. (2003). "Creating a Seamless Map of Gage-Adjusted Radar Rainfall Estimates for the State of Florida." Presented at EWRI World Water and Environmental Congress, Philadelphia, Pennsylvania, June 23-26, 2003.

Hromadka, T.V., McCuen, R.H., DeVries, J.J., and Durbin, T.J. *Computer Methods in Environmental and Water Resources Engineering*. Lighthouse Publications.

Islam, R., and P.F. Rasmussen. (2008). "Improved High Resolution Radar-Based Rainfall Estimation." *Journal of Hydrologic Engineering*, 13(9): 910-913.

Jordan, P.R. (1977). "Streamflow Transmission Losses in Western Kansas." *Journal of the Hydraulics Division*, 103(HY8): 905-919.

Jordan, P., Seed, A., and Austin, G. (2000). "Sampling errors in radar estimates of rainfall." *Journal of Geophysical Research*, 105(D2): 2247-2257.

Keefer, T.O., Moran, M.S., and Paige, G.B. (2008). "Long-term meteorological and soil hydrology database, Walnut Gulch Experimental Watershed, Arizona, United States." *Water Resources Research*, 44: 1-8.

Keppel, R.V., and Renard, K.G. (1962). "Transmission Losses in Ephemeral Stream Beds." *Journal of the Hydraulics Division,* 8(HY3): 59-68.

Kull, D.W., and Feldman, A.D. (1998). "Evolution of Clark's Unit Graph Method to Spatially Distributed Runoff." *Journal of Hydrologic Engineering*, 3(1): 9-19.

Krajewskiw, W.F., and Smith, J.A. (2002). "Radar hydrology: rainfall estimation." Advances in Water Resources, 25(8-12): 1387-1394.

Lane, L.J. and eight others. (2007). "Transmission Losses." Chapter 19 National Engineering Handbook, NRCS, USDA. Washington, D.C.

Lee, K.T., and Huang, J.K. (2007). "Effect of moving storms on attainment of equilibrium discharge." *Hydrologic Processes*, 21: 3357-3366.

March, W.J., Wallace, J.R., and Swift, L.W., Jr. (1979). "An Investigation Into the Effect of Storm Type on Precipitation in a Small Mountain Watershed." *Water Resources Research,* 15(2): 298-304.

Marshall, J.S., Langille, R.C., and Palmer, W.M. (1947). "Measurement of Rainfall by Radar." *Journal of Meteorology,*4: 186-192.

Marshall, J.S., and Palmer, W.M. (1948). "The distribution of raindrops with size." *Journal of Meteorology*, 5: 165-166.

Meadows, D.G., Young, M.H., and McDonald, E.V. (2005). "A Laboratory Method for Determining the Unsaturated Hydraulic Properties of Soil Peds." *Soil Science of America Journal,* 69(3): 807-815.

Meselhe, E.A., Habib, E.H., Oche, O.C., and Gautam, S. (2009). "Sensitivity of Conceptual and Physically Based Hydrologic Models to Temporal and Spatial Rainfall Sampling." *Journal of Hydrologic Engineering,* 14(7): 711-720.

McCuen, R.H., Rawls, W.J., and Brakensiek, D.L. (1981) "Statistical Analysis of the Brooks-Corey and the Green-Ampt Parameters Across Soil Textures." *Water Resources Research,* 17(4): 1005-1013.

McCuen, R.H. (2005). *Hydrologic Analysis and Design 3$^{rd}$ ed.,* Pearson Prentice Hall, New Jersey.

Moench, A.F., Sauer, V.B., and Jennings, M.E. (1974). "Modification of Routed Streamflow by Channel Loss and Base Flow." *Water Resources Research,* 10(5):963-968.

Morin, E., Goodrich, D.C., Maddox, R.A., Gao, X., Gupta, H.V., and Sorooshian, S. (2006). "Spatial patterns in thunderstorm rainfall events and their coupling with watershed hydrological response." *Advances in Water Resources*, 29(6): 843-860.

Nash, J.E. (1958). "The Form of the Instantaneous Unit Hydrograph." General Assembly of Toronto, IASH, Publ. 42, Compt. Rend. 3:114-118.

Noto, L.V., and La Loggia, G. (2007). "Derivation of a Distributed Unit Hydrograph Integrating GIS and Remote Sensing." *Journal of Hydrologic Engineering*, 12(6): 639-650.

Peebles, R.W., Smith, R.E., and Yakowitz, S.J. (1981). "A Leaky Reservoir Model for Ephemeral Flow Recession." *Water Resources Research,* 17(3): 628-636.

Peters, J.C., and Easton, D.J. (1996). "Runoff Simulation Using Radar Rainfall Data." *Water Resources Bulletin*, 32(4): 753-760.

Sen, Z. (2007). "Hydrograph and unit hydrograph derivation in arid regions." *Hydrological Processes,* 21: 1006-1014.

Sen ,Z. (2008). "Modified hydrograph method for arid regions." *Hydrological Processes,* 22: 356-365.

Seo, D.J., Breidenbach, J.P., and Johnson, E.R. (1999). "Real-time estimation of mean field bias in radar rainfall data." *Journal of Hydrology*, 223(3-4): 131-147.

Sharif, H.O., Ogden, F.L., Krajewski, W.F., and Xue, M. (2002). "Numerical simulations of radar rainfall error propagation." *Water Resources Research*, 38(8): 15-1-15-13.

Sharif, H.O., Ogden, F.L., Krajewski, W.F., and Xue, M. (2004). "Statistical Analysis of Radar Rainfall Error Propagation." *Journal of Hydrometeorology*, 5(1): 199-212.

Sieck, L.C., Ruges, S.J., and Steiner, M. (2007). "Challenges in obtaining reliable measurements of point rainfall." *Water Resources Research*, 43(1): 1-23.

Stone, J.J., Nichols, M.H., Goodrich, D.C., Buono, J. (2008). "Long-term runoff database, Walnut Gulch Experimental Watershed, Arizona, United States." *Water Resources Research,* 44(4): 1-5.

Southwest Watershed Research Center. Online Data Access. Accessed 7/3/2008. http://www.tucson.ars.gov/dap/

The University of Iowa. NEXRAD Rainfall Data for Hydrology: An NSF-Sponsored Effort. Accessed 9/10/2008. http://hydro-nexrad.net/hydronexrad_v0.7/index.html

Ulbrich, C.W., and N.E. Miller. (2001). "Experimental Test of the Effects of the Z-R Law Variations on Comparison of WSR-88D Rainfall Amounts with Surface Rain Gauge and Disdrometer Data." *Weather and Forecasting*, 16: 369-374.

Vieux, B.E., Park, J-H., and Kang, B. (2009). "Distributed Hydrologic Prediction: Sensitivity to Accuracy of Initial Soil Moisture Conditions and Radar Rainfall Input." *Journal of Hydrologic Engineering,* 14(7): 671-689.

Walters, M.O. (1990). "Transmission Losses in Arid Region." *Journal of Hydraulic Engineering,* 116(1): 129-138.

Westcott, N.E., Knapp, H.V., and Hilberg, S.D. (2008). "Comparison of gage and
multi-sensor precipitation estimates over a range of spatial and temporal
scales in the Midwestern United States." *Journal of Hydrology*, 351: 1-12.

Wood, S.J., D.A. Jones, and R.J. Moore. (2000). "Static and dynamic calibration of
radar data for hydrological use." *Hydrology and Earth System Science*, 4(4):
545.

Young, C.B., and Brunsell, N.A. (2008). "Evaluating NEXRAD Estimates for the
Missouri River Basin: Analysis Using Daily Raingauge Data." 13(7):
549-553.